HYGROSCOPICITY OF PHARMACEUTICAL CRYSTALS

A DISSERTATION
SUBMITTED TO THE FACULTY OF GRADUATE SCHOOL
OF THE UNIVERSITY OF MINNESOTA
BY

DABING CHEN

IN PARTIAL FULFILLMENT OF THE REQUIREMENTS
FOR THE DEGREE OF
DOCTOR OF PHILOSOPHY

RAJ SURYANARAYANAN
(ADVISER)

JANUARY, 2009

ACKNOWLEDGEMENTS

I am very grateful to my thesis advisor, Prof. Raj Suryanarayanan, for his constant guidance, support, and encouragement throughout my research. Without his help, the completion of this thesis would be impossible. His friendship and advices are precious to my professional and personal growth and will help me overcome many difficulties in my future career.

I would like to take the opportunity to thank Prof. David J.W. Grant, who was my advisor during the first three years in graduate school and led me into the research area of physical pharmacy. It was my great honor to have worked for him, and he will always live as a role model in my life.

Many thanks to Dr. Zheng Jane Li at Boehringer Ingelheim Pharmaceuticals (BI) for her invaluable advice as an industrial mentor and also for agreeing to serve on my committee. I sincerely appreciate her helpful discussions, revision of the manuscripts, and supervision of my research. I also want to thank her for providing me the internship opportunity at BI.

I thank Dr. Timothy S. Wiedmann and Dr. Theodore P. Labuza for serving on my committee and for critically reviewing my thesis. I also want to thank Dr. Timothy S. Wiedmann for allowing me the use of the HPLC instruments in his lab and also for his advice as the Director of Graduate Studies.

I acknowledge a Fellowship in Graduate Research from Novartis Corporation, and the David J.W. Grant Fellowship in Physical Pharmacy. I thank Pfizer Inc. for financial support.

I particularly thank Dr. Bakul S. Bhatnagar, Ms. Paroma Chakravarty, Dr. Ramprakash Govindarajan, Dr. Sisir Bhattacharya, Dr. Xiangming Liao, Mr. Prakash Sundaramurthi, Dr. Nitin Tayade, Dr. Venu Vangala, and Dr. Aditya

Kaushal in the Sury lab for their friendship and for sharing their expertise and creating a jovial working environment. I want to thank Dr. Yuchuan Gong, Dr. Yuegang Zhang, Dr. Sharmistha Datta, Dr. Sachin Lohali, Dr. Agam Sheth, Dr. Enxian Lu, Dr. Yushi Feng, and Dr. Deliang Zhou - the former Grant lab members. I am very grateful to Ms. Paroma Chakravarty for reviewing my thesis. I want to thank all the faculty, and graduate students in the Department of Pharmaceutics, University of Minnesota, for their guidance and friendship. A big thank you goes out to Ms. Candice McDermott and Ms. Erica Flynn and Mrs. Sarah Sexton for making my graduate life easier with their help and smiles.

I want to thank Dr. Greg Haugstad and Dr. Jingping Dong in the characterization facility, institute of Technology in the University of Minnesota for the help and discussion on atomic force microscopy. I thank Dr. Guifang Zhang for the help with HPLC experiments. I also thank Dr. Gianluigi Veglia and Dr. Nathaniel J Traaseth at the Department of Chemistry, University of Minnesota, for the solid state NMR experiments.

The completion of my thesis would not have been possible without the unconditional love and blessings of my father, Mr. Changsong Chen, my mother, Mrs. Zhongfeng Zhang, and my sister, Ms. Yan Chen. I am ever indebted to them for their understanding, patience, and sacrifice; which will always inspire me.

Dedicated to

My family

And

Late Prof. David J.W. Grant

Dabing Chen

297 words

Abstract

The active pharmaceutical ingredients (APIs) as well as excipients in a solid dosage form can take up water vapor both during manufacture and subsequent storage of the product. Uptake of unacceptable amount of water can cause adverse effects on physical and chemical stability of APIs and functionality of excipients. It is prudent to select drug candidates with low hygroscopicity to minimize the development risk and time. The objectives of this study are: (i) to investigate the risk in predicting long-term water uptake from short-term water sorption studies, (ii) to understand the thermodynamic and kinetic factors that affect water uptake by pharmaceutical crystals. Automated sorption microbalance (ASM) is often used to determine the hygroscopicity, in which the small sample size and gas purge are believed to accelerate the water sorption process so that equilibrium could be attained in a short time period. However, caution must be exercised when the rates of water vapor diffusion or heat transfer at the solid-vapor interface are not the limiting factors. Four cases are discussed in this thesis, in which ASM failed to predict long-term water uptake. 1) Water vapor was believed to diffuse into the lattice of a metastable crystalline form and induced a polymorphic transformation. The crystallization of the stable form led to a decrease in water content. 2) Adsorbed water formed a surface solution and enhanced the mobility of surface molecules. Nucleation rate of hydrate could be the rate-limiting step. 3) Water sorption induced a crystal to liquid crystal transformation in a surface-active compound, where the latter retains orientational but lacks positional order of molecular packing. 4) The formation of a metastable liquid crystalline phase was kinetically favored for amorphous materials formed in surface-active compounds. The metastable liquid crystalline phase was stable for 3 months when stored under ambient conditions.

Table of Contents

List of Tables

List of Figures

Chapter 1

Introduction and Theoretical Background

1.1 Introduction

Many pharmaceutical crystalline solids sorb water vapor readily from the environment and are considered to be hygroscopic.[1] Water, when taken up by pharmaceutical solids, could alter their physicochemical properties.[2] Water sorption by solid formulations can adversely affect product performance.[3-5] The effect could be physical implications, such as decrease in dissolution,[6] variation in water content in the final product,[2] crystallization of formulation components,[7] and powder caking.[8] Chemical reactions, such as hydrolysis and oxidation, could also be accelerated by water sorption.[5, 9] Compounds with low hygroscopicity are desired during drug development to minimize the downstream development risk.[10] The objectives of this research are to understand the mechanism of water-solid interaction and to investigate the feasibility of predicting long-term water uptake of a pharmaceutical crystal from short-term sorption studies.

1.2 Motivation

Modern high-throughput technologies, such as combinatorial chemistry and pharmacological screening, have led to a tremendous increase in the number of new chemical entities for pre-clinical and clinical development.[11] In light of the pressure to reduce the development cycle times, the drug discovery groups in pharmaceutical companies are forced to make developability decisions on large number of compounds in a short time with limited resources. It is prudent to choose the compounds with desired physicochemical properties.

It is a generally accepted criterion that the drug candidate should not have a water uptake exceeding 2% w/w at 60% RH/25°C, and no more than 5% w/w water uptake at this condition (assuming that it does not form a stable hydrate).[10] Conventionally, the hygroscopicity of a drug is determined by storing the dry

powder to periodically weigh a sample stored under controlled temperature and relative humidity (RH). This RH chamber storage method usually requires long time to reach equilibrium, and relative large quantity of sample size (~ several hundred milligrams). Such a large amount of sample is usually not available in the early stage of drug development. Nowadays, an automated sorption microbalance (ASM) technique is being widely used in industry to evaluate the hygroscopicity of drug candidates. In an ASM, a small amount of drug (~ 5 mg) is purged with humid nitrogen, and the weight is recorded automatically by a microbalance. The equilibration time for water sorption in ASM is expected to be much shorter than that in RH chambers because of the small sample size and the gas purge. However, the reliability of ASM in predicting long term water uptake has not been systematically tested.

In Chapter 2, we evaluated the reliability in predicting the long-term water uptake from short-term sorption studies. Both RH chambers and ASM were used to determine the hygroscopicity of 40 compounds. The monographs of most of these compounds can be found in the United States Pharmacopoeia (USP). For majority of samples, the water uptake determined by the two method were in agreement, but a few showed difference. The cause of discrepancy were further investigated in the following chapters. The correlation between solubility and deliquescence RH was studied. The initial rate of water uptake during deliquescence was correlated to the environmental RH and critical RH (RH_0). The impact of crystal structure on their water sorption behavior was also demonstrated.

Chapter 3 examines the polymorphic transformation induced by water sorption, using homochlorcyclizine·2HCl (HCC) as the model compound. The lattice parameters of HCC form I and II were simulated from their synchrotron powder diffraction patterns. The structural similarity between form I and the desolvate of acetonitrile solvate were evaluated by Raman spectroscopy and X-ray

diffractometry (XRD). The polymorphic transformation was monitored by near infrared spectroscopy (NIR) and XRD.

Chapter 4 studies the surface properties at different RH values and the role of surface solution in theophylline hydrate formation in the solid state. The thickness of surface solution, surface adhesion and frictional properties, and surface mobility at different RH values were investigated by contact, pulse force, and AC mode atomic force microscopy. The effect of grinding and seeding on hydrate formation was examined.

Chapter 5 investigates the crystal → liquid crystal transformation induced by water sorption, using trifluoperazine·2HCl (TFP) as the model compound. The liquid crystal was characterized by XRD and PLM. The liquid crystal transition RH was determined from the phase transformations of amorphous and liquid crystalline TFP at different RH values. The crystal → liquid crystal formation was also monitored by NIR and XRD. Three structurally related compounds were also examined to study the influence of molecular structure on liquid crystal formation.

Chapter 6 describes the effect of preparation method on water sorption and phase transformations of amorphous materials. Amorphous TFP was prepared by freeze-drying and cryo-milling, and characterized by PLM and small angle X-ray scattering. The water sorption and crystallization behavior of different amorphous TFP phases were investigated at different RH values. The phase transformation of TFP during freeze-drying was monitored by *in situ* XRD.

Chapter 7 presents a summary of the thesis and suggestions for future work.

1.3 Hygroscopicity

The term, hygroscopicity, is widely used in the pharmaceutical community to describe the water vapor uptake behavior of solids.[1, 2, 12] However, there is no universally accepted definition of hygroscopicity in the pharmaceutical literature. The term 'hygroscopicity' describes the ability of a solid to take up and retain water.[2] Hygroscopicity could be defined as the rate and extent of water vapor uptake by a solid at certain RH values and temperatures..The water content in pharmaceutical solids can vary with water activity and temperature. Different physicochemical properties, such as morphology, crystallinity, specific surface area, crystal structure, and state of hydration (whether hydrate or anhydrate), would also affect the water uptake under different experimental conditions.[2] A substance is sometimes defined as hygroscopic without further details.[1] Water uptake by a hygroscopic material could lead to deliquescence, hydrate formation, or formation of mesophases.[13] Deliquescence or formation of mesophase could result in chemical instability[14] or increased dissolution rate,[15] while the same amount of water existing as a hydrate may pose no chemical stability issues and will usually result in lower aqueous dissolution rate compared to the corresponding anhydrate form.[16] Therefore, a mechanistic understanding of the interaction of water with the drug would be beneficial in drug product development.[17]

Pharmaceutical solids could be categorized into different groups according to the extent of water uptake. Callahan determined the equilibrium water content of a number of pharmaceutical excipients after storage at different RH values for one week.[18] The following classification was proposed based on the water uptake after storage for one week at different conditions: Class I, non-hygroscopic (no water sorption below 90% RH, and < 20% at 90% RH); Class II, slightly hygroscopic (no water sorption below 80% RH, and < 40% at 80% RH); Class III, moderately hygroscopic (< 5% below 60% RH, and < 50% at 80% RH); Class IV,

very hygroscopic (> 5% below 60% RH).[19] However, the above critera may not directly apply to our investigation, since most samples included in Callahan's study were substantially amorphous. Studies were also conducted on a number of pharmacopoeial substances, following storage at 79% RH (25°C) for one week.[1] Based on the water content after storage at 79% RH for 24 hours, the following classification of hygroscopicity was proposed: Class I, non-hygroscopic (< 0.2%, w/w); Class II, slightly hygroscopic (0.2 ~ 2%, w/w); Class III, hygroscopic (2 ~ 15%, w/w); Class IV, very hygroscopic (> 15%, w/w). The two criteria are compared in Table 1.1.

The rate and extent of water sorption depend on the mechanism of water-solid interactions.[17] Several mechanisms of solid-water interactions have been proposed: surface adsorption, capillary condensation, hydrate formation, deliquescence, and absorption into amorphous materials.[13, 17, 20-22] The amount of surface adsorption is determined by the surface area of the solid and is usually < 0.1% w/w.[22] Capillary condensation might occur in porous samples or the fissures in the crystals.[23] Water may interact with solids to form hydrates, in which water is incorporated in the crystal lattice.[24] Above RH_0, which is defined as the RH in the headspace over the saturated solution, a drug could dissolve in the adsorbed water, which leads to deliquescence.[25] Amorphous materials could absorb significant amount of water due to their high free volumes.[26] Milling and compaction can generate surface amorphization in crystalline materials which bring about significant change in water sorption behavior.[27] More than one mechanism could be involved in the water sorption process.[28] The different types of water-solid interactions are further discussed in the following section.

1.4 Water-solid Interactions

Water molecules can interact with the components of a dosage form by hydrogen bonding, van der Waals forces, and, if the solid is ionic, cation-water interactions

and anion-water interactions. Water can be associated with macromolecules in similar ways, which have been reviewed extensively in the food science literature,[29, 30] and will not be discussed in this chapter.

1.4.1 Surface Adsorption by Crystalline Solids

Adsorption is the process by which the components of one phase are accumulated in the interfacial region between two phases (the boundary), such as adsorption by activated carbon.[31] Adsorption can involve chemical bonding, which is usually referred to as chemisorption. Adsorption without chemical bonding is defined as physisorption. We will focus on physisorption, which is the case for water adsorption on pharmaceutical powders. The adsorption process is sometimes accompanied by absorption, i.e. the penetration of the adsorbent molecules into the bulk of the solid phase.[32] The term sorption is used to include both adsorption and absorption processes.

Experimental sorption isotherms, which determine the amount of adsorption at different relative pressures of the absorbent vapor, usually show distinct characteristics for different vapor-solid systems. The majority of the isotherms of physical adsorption may conveniently be categorized into six classes (Fig. 1.1).[23]

Type I isotherms are typical of microporous solids. In a Type I isotherm, the curve is concave to the relative pressure axis; the amount of vapor adorbed increases rapidly at low relative pressures and reaches a plateau as the relative pressure approaches 1. The low relative pressure necessary to attain the plateau is an indication of existence of micropores or strong vapor-solid interaction and the plateau afterwards indicates the negligible amount of physical adsorption on the solid surface.[33]

Type II isotherms are usually sigmoidal in shape. The amount of vapor adsorbed increases rapidly at lower relative pressures, showing a profile concave with respect to x-axis. At higher relative pressures, the curve assumes a shape convex with respect to x-axis. The turning point of the curve is usually considered as the completion of the monomolecular layer and the beginning of the formation of multi-molecular layers of adsorbate on the surface.[34]

In Type III isotherms, the amount of adsorption increases slowly as the relative pressure increases, and the curve is convex with respect to x-axis over the entire relative pressure range. This pattern indicates weak adsorbent-adsorbate interactions; in other words, the strength of vapor-substrate interactions is close to that of vapor-vapor interactions.[35] The adsorption sites on the solid surface tend to have different surface energies. At low relative pressures, vapor molecules prefer the high surface energy adsorption sites on the solid surface.[35] As the relative pressure is increased, more vapor molecules are adsorbed on the low surface energy sites. However, before the solid surface is covered, condensation of vapor molecules also occurs to form multi-layer adsorption at those high-energy sites on the solid surface since the heat of adsorption is close to the heat of condensation of water.[35, 36]

A Type IV isotherm is similar to the Type II isotherm at low relative pressures. At high relative pressures, the amount of adsorbed vapor levels off and exhibits a hysteresis loop as the relative pressure decreases. The hysteresis is usually associated with the “filling and emptying” of the mesopores by capillary condensation.[37]

In a Type V isotherm, the curve is initially convex and also levels off at high relative pressures. Similar to the type III isotherm, the convex curve indicates weak adsorbent-adsorbate interactions. Type V isotherm also exhibits hysteresis, which is attributed to pore filling and emptying.[38]

A Type VI isotherm is relatively rare and is associated with layer-by-layer adsorption on a highly uniform surface. The sharpness of the steps depends on the system and the temperature.[39]

Based on a number of assumptions, Brunauer, Emmett and Teller [34] extended the Langmuir single layer adsorption equation to describe multilayer adsorption. According to the BET model, the adsorbed molecules in one layer can act as adsorption sites for the molecules in the next layer. The associated equation for the BET model is:

$$W = \frac{W_m C_B (\frac{p}{p_0})}{\{1-(\frac{p}{p_0})\}\{(1-(\frac{p}{p_0}) + C_B(\frac{p}{p_0})\}} \qquad \text{Eq. 1.1}$$

where W is the weight of water adsorbed per unit weight of dry solid at the relative pressure of $\frac{p}{p_0}$, W_m is the weight of water adsorbed corresponding to monolayer coverage, the parameter C_B is related to the difference between heat of adsorption on the first layer and heat of water condensation.

Usually, the plot of W versus p/p_0 has a shape similar to that of a type II isotherm. However, when $C_B < 2$, which means that the interaction between water and solid surface is comparable to that between water molecules, the isotherm is convex over the entire relative pressure range, and loses its inflection point as in a Type III isotherm. It has been observed that water sorption isotherms of pharmaceutical crystals are usually Type III, which could be attributed to weak solid-water interactions.[2] The strength of the hydrogen bond in ice or liquid water has been estimated to be about 15 to 25 KJ per mole of hydrogen bonds.[32] For water adsorption on more polar surfaces, such as metals or metal oxides, overall binding energies are generally in the range of 40 – 60 KJ per mole.[32] Since the strengths of water-solid and water-water interactions are comparable, clustering

of water molecules can occur even before a complete monolayer has formed, leading to the formation of multilayer networks beyond the first layer. Such clustering before complete monolayer coverage also suggests that there is significant lateral diffusion along the surface despite the relatively strong hydrogen bonding with the adsorbent surface.

It is generally recognized that adsorption of water on a crystalline surface does not amount to more than 4-5 molecular layers below the deliquescence point.[40, 41] The water content resulting from surface adsorption could be negligible (< 0.1% w/w) for most pharmaceutical solids with a specific surface area of 5-10 m^2/g.[22] However, many crystalline pharmaceutical solids could sorb a much higher amount of water below their deliquescence points.[13] This higher water sorption could be attributed to amorphous regions, often resulting from pharmaceutical processes, such as grinding and compaction. The amorphous fraction is usually below the detection limit of routine analytical techniques, such as XRD, PLM, and FTIR. The presence of surface amorphous regions could significantly change the physicochemical properties of solids. For example, aspirin showed significantly higher water sorption after roller compaction.[42] Ball milled lactose exhibited high crystallinity by XRD, while the surface energy was higher than that of amorphous lactose prepared by spray-drying as indicated by inverse gas chromatography.[43] Water sorption into surface amorphous regions could also induce crystallization and cause powder caking and flow problems during storage and manufacture, as seen in spray-dried lactose.[44]

Surface amorphization could explain many effects of water sorption on physicochemical properties of the solids, such as decrease in specific surface area,[44] increase in surface conductivity,[45] and tendency to cake and flow.[8, 46] However, it is not clear how surface adsorption affects the properties of crystalline surfaces. From a thermodynamic point of view, it has been argued that surface dissolution of crystalline solids should not occur before deliquescence.[13]

Indeed, solid-state NMR studies on NaCl at different RH values did not show an increase in molecular mobility below its deliquescence point (76% RH/25°C).[44] However, because surface molecules are only a small fraction of the bulk, SS-NMR may not be able to detect an increase in surface mobility and therefore may not be a suitable tool to study surface properties. Since the invention of atomic force microscopy in 1986,[47] there have been many studies on the effect of water adsorption on the surface properties of solids.[48]

Atomic force microscopy (AFM) quantifies the force between a sharp tip and the substrate surface. AFM is very sensitive to changes in surface morphology and surface properties.[49] It has been shown by AFM studies that water adsorption on a crystalline surface has significant impact on the physicochemical properties of solids.[40, 50, 51] Water adsorbed on the surface could dissociate and induce corrosion or oxidation.[32] For example, it was observed that NO_2 can react with NaCl surfaces below its deliquescence point, which was proposed to be mediated by surface solution formed by adsorbed water. Another study also showed that surface steps flowed at 35% RH on crystalline NaCl surfaces, well below the deliquescence point of 75% RH, suggesting enhanced surface mobility.[52] Existence of surface solution on freshly cleaved NaCl surface was also proven at 40% RH using frictional force microscopy.[53] Infrared spectroscopy also revealed that the surface adsorbed water on NaCl crystalline surfaces showed liquid-like properties at 40% RH.[54] It was proposed that hydration of ions on the surface could increase molecular mobility and surface solution could exist below the deliquescence point to mediate potential chemical reactions or phase transformations.[52]

1.4.2 Capillary Condensation

Water can condense onto highly curved surfaces, such as pores and capillaries.[55, 56] For a pore or a capillary with a radius, r, the decrease in vapor

pressure of the pure solvent upon capillary condensation can be calculated using the Kelvin equation:[57]

$$\ln(\frac{p_r}{p_0}) = -\frac{2\gamma V_m}{rRT} \qquad \text{Eq. 1.2}$$

where γ is the surface tension of the liquid, V_m is the molar volume of the liquid, p_r is the vapor pressure of the liquid in the pore or capillary with radius *r*, p_0 is the vapor pressure of the liquid on flat surfaces.

Micropores, mesopores and macropores are defined to be pores of internal width < 2 nm, between 2 and 50 nm, and > 50 nm, respectively.[55] It is noteworthy that the surface tension of the liquid in micropores and mesopores will not be the same as that in the bulk liquid.[55]

1.4.3 Deliquescence

Deliquescence is defined as the process by which a substance sorbs water vapor from the environment and gradually dissolves in the sorbed water to form a solution.[58] The RH value at which the solid begins to deliquesce is defined as deliquescence RH (DRH). Another important term is critical RH (RH_0), which is defined as the RH value in the overhead space of the saturated solution.[59] For polycrystalline powders, DRH is very close to RH_0. At equilibrium, the water activity in the vapor phase is equal to that in the saturated solution, so that the RH_0 could be calculated from the solubility of the compound. Generally, compounds with high solubility may deliquesce at RH values lower than 100%.

Fig. 1.2 illustrates the water uptake of a crystalline sample at different RH values.[20] Below RH_0, water was adsorbed on the surface without bulk dissolution. At RH_0, molecules dissolved in the adsorbed water to form a saturated solution. Above RH_0, water was continuously sorbed to form an undersaturated solution.

The rate of water uptake during deliquescence would depend on the difference between the environment RH and RH_0, temperature, sample surface area, the flow rate of overhead humid air, and surface properties. Van Campen et al.[60] developed a model which predicted a linear relationship between rate of water uptake and environmental RH. The diffusion rate of water to the solid surface and the heat dissipation rate from the surface were found to be the main factors controlling the rate of water uptake during deliquescence.

For multi-component systems, the RH_0 of the mixture can be calculated from the RH_0 of individual component using the Ross equation,[61]

$$\frac{(RH_0)_{mix}}{100} = \frac{(RH_0)_1}{100} \bullet \frac{(RH_0)_2}{100} \bullet \frac{(RH_0)_3}{100} \ldots\ldots \qquad \text{Eq. 1.3}$$

where $(RH_0)_{mix}$ is the relative humidity above the saturated aqueous solution of the mixture. $(RH_0)_i$ is the deliquescence RH of an individual component.

The deliquescence point has historically been considered to be a thermodynamic parameter of a compound and is determined by its solubility.[62] However, some recent studies have revealed the kinetic aspect of deliquescence as well.[58, 63-66] Deliquescence of NaCl occurred at an RH almost 4% higher than RH_0, after the sample was pre-exposed to moisture.[58] It was believed that the deliquescence of the (001) face of the NaCl single crystals was controlled by nucleation of water droplets. The density of defects on the crystal surface can affect the value of DRH.[67]

It was also observed that the deliquescence of small NaCl particles occurred at a higher RH value than that of bigger particles.[68] The DRH of a 6 nm size NaCl particles was determined to be 87% RH, in contrast to 75% RH for particle size > 40 nm at 25°C.[69] The increase of DRH for small particles is very intriguing because the higher solubility of the small particles should result in lower DRH values. Russel and Ming proposed that the salt particles were actually coated by adsorbed water below the RH_0 and constructed a model based on

physicochemical properties of NaCl and $(NH_4)_2SO_4$,.[69] They showed that the change in the surface tension of the water coated particles led to the unusual increase in the deliquescence RH.[68]

The theory of deliquescence, proposed by Biskos, is as follows:[70] deliquescence will occur at the RH value at which the free energy of the solid particles equals that of the aqueous droplets.[71] Aqueous droplets form when crystalline salt particles deliquesce. The free energy (G) of a particle consists of volume (G_V) and surface terms (G_S).

$$G_c = G_{V,c} + G_{S,c} \quad \text{Eq. 1.4}$$

$$G_{aq} = G_{V,aq} + G_{S,aq} \quad \text{Eq. 1.5}$$

where c and aq represents crystalline solids and aqueous droplets, respectively.

$$G_{V,c} = \mu_c n_c + (\mu_w n_w)_{gas} \quad \text{Eq. 1.6}$$

$$G_{S,c} = \sigma_c A_c \quad \text{Eq. 1.7}$$

$$G_{V,aq} = \mu_{aq} n_c + \mu_w n_w \quad \text{Eq. 1.8}$$

$$G_{S,aq} = \sigma_{aq} A_{aq} \quad \text{Eq. 1.9}$$

where μ_c and μ_{aq} are the chemical potentials of the compound in solid and aqueous states, respectively. n_c and n_w are the number of moles of the compound and water molecules, respectively. σ is the surface tension, and A is the surface area.

For deliquescence to occur, the free energy of crystalline particles should be equal to that of aqueous droplets at DRH:

$$G_c - G_{aq} = (\mu_c - \mu_{aq}) n_c + (\sigma_c A_c - \sigma_{aq} A_{aq}) = 0 \quad \text{Eq. 1.10}$$

For large particles, the surface energy term is negligible compared with the volume energy term. For particles in the nanometer size range, the surface energy term could be quantitatively comparable to the volume term. The volume free energy term is zero at 75% RH (25°C) for NaCl because the RH_0 of NaCl is

75%. When the surface energy is higher for the crystalline particle compared to that of the liquid droplets, the DRH would shift to lower values. DRH increases when the surface energy of the solid particles is lower than that of the liquid particles. The relative magnitude of the surface tension of the crystalline and aqueous particles determines whether the DRH increases or decreases at different particle sizes.[69] It should be mentioned that the partial coverage of water molecules below DRH would lead to a surface tension different from that of dry particles.[66, 72]

1.4.4 Hydrate Formation

Many pharmaceutical compounds can exist as hydrates. It has been reported that 29% of the 808 solid organic compounds listed in the European Pharmacopoeia could exist as hydrates (Fig. 1.3).[16] This high incidence of hydrate formation in pharmaceuticals could be attributed to the hydrophilic and ionic nature of many drugs.[16] Water is incorporated into the crystal lattices of hydrates, where water may have different roles: (1) reduce the electrostatic repulsive forces between ions, (2) form hydrogen bonds with functional groups of the drug molecules and other water molecules, and (3) coordinates cations.[73] Single crystal X-ray diffractometry is the preferred technique to confirm the existence of a hydrate. When a crystal of suitable size is not attainable, powder XRD, thermal analysis, Karl Fischer titrimetry, polarized light microscopy, infrared spectroscopy, and solid-state NMR can also be used to identify hydrate phases. Hydrate formation could occur during many pharmaceutical processes such as wet granulation, lyophilization, crystallization, and also upon storage. Temperature and humidity fluctuations during manufacture might lead to partial hydration or dehydration, which can lead not only to variation in the water content of the final product but also potential decrease in dissolution rate and bioavailability.

According to the arrangement of water molecules in crystal lattice, hydrates can be categorized into three groups[74]: (1) water present at isolated lattice sites, (2) water existing in lattice channels, as in ampicillin trihydrate,[75] and (3) water coordinated with ions, as in nedocromil salts.[76] Hydrates can also be stoichiometric or, occasionally, nonstoichiometric.[77] In stoichiometric hydrates, the numbers of water and host molecules have a stoichiometric ratio, while the amount of water in non-stoichiometric hydrates depends on the RH of the environment.

Stoichiometric hydrates have a constant mole ratio of water to drug over a range of water activities. Stoichiometric hydrates often show step-wise water sorption isotherms (Fig. 1.4). Hydrate formation is a water activity controlled process. The thermodynamically stable phase would change from anhydrate to hydrate when water activity exceeds the transitional/critical value. The physical stability of hydrates usually depend on the packing efficiency of water molecules and the strength of the host-water interactions in the crystal.[78-81]

Nonstoichiometric hydrates are a type of inclusion compound.[16] Water could enter or leave the lattice without causing significant changes to the lattice structure.[82] However, some anisotropic lattice expansion or contraction may occur.[83] Cromolyn sodium showed a continuous and reversible water sorption isotherm, forming a continuous range of nonstoichiometric hydrates (Fig. 1.5),[84] with lattice expansion along c axis. The flexibility of the drug molecule and disorder of the sodium ion contributed to the reversible water uptake and the formation of nonstoichiometric hydrate between 10 and 93% RH (25°C). LY297892 tartarate, a muscarinic agonist, also exhibits reversible water uptake with water content up to 0.5 moles per mole of drug.[82] Powder X-ray diffractometry revealed that the anhydrous and the hydrated forms of the drug had similar crystal structures. Solid-state NMR (SS-NMR) indicated that water molecules were very mobile and could hop rapidly between the hydrogen binding

sites in the crystal lattice. The rates of hydration and dehydration are determined by the size of the water channels and the strength of the drug-water interactions. A similar phenomenon was also observed in sildenafil citrate.[85] Thiamine HCl can also form a nonstoichiometric hydrate,[86] which can convert to a more stable stoichiometric hemihydrate.[87]

L-lysine hydrochloride (LH) was found to form a dihydrate or a mono-methanol solvate at different water activities in methanol-water mixture.[88] The LH hydrate and methanol solvate had similar structure, and therefore the same PXRD pattern, but different crystal habit. During dehydration in methanol-water mixture, water in the crystal lattice can be gradually replaced by methanol without disrupting the crystal structure.

Another interesting phenomenon is the formation of an isomorphic desolvate. When water in a hydrate is removed from the lattice, the resulting lattice could either undergo a phase change (polymorphic transition or formation of amorphous materials) or remain unchanged with some anisotropic lattice contraction.[16] The latter phase is known as an isomorphic desolvate; the PXRD pattern of the dehydrated product is similar to that of the parent solid with minor shifts in the position of a few peaks. This may pose difficulties in characterizing the solid phase in the final product. Many pharmaceuticals are known to form isomorphic desolvates, including erythromycin, cephalexin, ampicillin, cromolyn sodium, caffeine, theophylline, thiamine hydrochloride (vitamin B1) and sildenafil citrate.[85, 86, 89-94] Vacancy in the lattice, resulting from the removal of water, renders the isomorphic desolvate in a higher energy state. Higher water sorption and chemical degradation rate would be expected in isomorphic desolvates.[95]

Thermodynamic Considerations in Hydrate Formation

Different hydration states of a compound exhibit different physicochemical properties.[96, 97] The incorporation of water molecules into crystal lattice changes the interactions and packing of molecules, which changes the enthalpy and entropy of the crystal.[98] Therefore, the hydrate and anhydrate phases usually have different solubility values in water. The quick way to identify the stable form (with lower solubility) is to perform a slurry experiment, in which the anhydrate and the hydrate are suspended together in water.[99] The unstable form will eventually convert to the stable form.

Consider the following equilibrium:

A (anhydrate) + $m$$H_2O$ ↔ A.$m$$H_2O$ (hydrate)

The equilibrium constant of hydrate formation can be written as

$$K_{hydration} = \frac{a[A.mH_2O(hydrate)]}{a[A(anhydrate)] \times a[H_2O]^m} \qquad \text{Eq. 1.11}$$

Since the thermodynamic activity of each pure solid phase is a constant, which is usually set equal to unity:

$$K_{\text{hydration}} = a[H_2O]^{1/m} \qquad \text{Eq. 1.12}$$

Therefore, hydrate formation is influenced by water activity of the solvent system. Zhu et al.[100] investigated the influence of water activity on the stability of anhydrous phase using organic solvent - water mixture. It was concluded that if a drug can form a hydrate, the water activity is the main factor determining whether anhydrate or hydrate will crystallize. When the hydration and dehydration processes of theophylline in methanol-water mixtures were separately investigated, the transition water activities for anhydrate and hydrate were found to be 0.25 without any hysteresis.

Kinetic Considerations in Hydrate Formation in the Solid State

Hydrate formation could be affected by surface properties of the anhydrate crystals. When carbamazepine was subjected to dissolution studies, a supersaturated solution (with respect to carbamzepine dihydrate) could be obtained since nucleation of the stable hydrate was the rate limiting step in the anhydrate → hydrate transformation. Grinding of crystalline anhydrous carbamazepine created lattice defects and amorphous regions on the crystal surface, thereby eliminating the induction time.[101,102] Modification of surface properties can also be achieved by surface adsorption of organic solvents.[103] The hydrate formation of carbamazepine at 97% RH was inhibited in the first 10 hours after exposure to n-butanol vapor, while the 'as is' anhydrous carbamazepine transformed readily without an induction period. N-butanol also lowered the hydrophobicity of the carbamazepine surface and thereby enhanced the dissolution rate of carbamazepine.

Additives in solution can also change the kinetics of hydrate formation.[104] Sodium lauryl sulfate was found to promote the formation of dihydrate on the surface of carbamazepine crystals,[105] while non-ionic polymers, such as Tween 80, HPMC, and poloxamer inhibited the phase transition in solution.[106, 107] The possible interaction between the hydroxyl group and the drug hindered water binding, thereby retarding dihydrate formation.[107] α-lactose was found to facilitate the formation of theophylline monohydrate, while silicified microcrystalline cellulose (SMCC) inhibited theophylline monohydrate formation.[108]

1.4.5 Water Uptake by Amorphous materials

Many processes, such as grinding, spray drying, wet granulation, and thermal treatments, may introduce significant amorphous fractions to pharmaceutical crystals.[109] Most pharmaceutical polymer excipients, such as starches, cellulose

derivatives, proteins, and synthetic hydrogels, are substantially amorphous.[26] The amount of water sorbed into amorphous materials is usually proportional to the volume/weight of the amorphous solid and independent of the surface area of the solid. Amorphous materials take up significantly higher amount of water than their crystalline counterparts, which could cause physicochemical instability in their formulations.[2] Therefore, it is very important to study the water sorption by amorphous materials.

The sorption of water causes a lowering in the T_g of the amorphous materials, and the T_g of the mixture could be calculated from the T_g of individual components using the Gordon-Taylor equation:[110]

$$\frac{1}{T_g} = \frac{1}{T_{g_1}} - w_2\{\frac{T_{g_1}T_{g_2}}{T_{g_1}+T_{g_2}}\} \qquad \text{Eq. 1.13}$$

where T_{g1}, T_{g2}, and T_g are the glass transition temperatures, of the amorphous drug, water, and mixture, respectively, and w_2 is the weight fraction of water in the amorphous drug. Andronis and Zografi[111] observed that the T_g of amorphous indomethacin decreased as storage RH increased. When the T_g is below the environmental temperature, the solid enters the rubbery or supercooled liquid state (Fig. 1.6). Fitzpatrick[112] showed that PVP transformed from glassy to rubber state at high temperature and humidity conditions. However, the conversion did not occur at lower temperatures, at which long term stability was tested. The result showed that the glass transition must be considered when accelerated stability tests are designed. The mobility of drug molecules would increase and the viscosity would decrease above the glass transition, which could lead to significant increase in the crystallization rate. A well known example is the crystallization of spray-dried lactose induced by water uptake.[113] The crystallization of amorphous lamotrigine mesylate was also accelerated by water sorption.[7] The crystallization of amorphous sucrose showed different induction times at different RH values.[114]

The water vapor sorption isotherms of amorphous materials can be fitted reasonably well to some gas adsorption equations,[115] such as the Guggenheim-Anderson-de Boer (GAB) equation which is an extension of the BET equation. [116] Although the GAB equation may yield a good fit to the water sorption isotherm, it does not provide a mechanistic understanding of the water uptake process at the molecular level.[117] For example, the amount of water corresponding to monolayer coverage, W_m, could be calculated using the GAB equation. However, the physical meaning of this term is not clear for water sorption into amorphous materials. It has been considered to be the amount of water directly bound to the anhydroglucose units in the solid.[22] The W_m values of various starch and cellulose derivatives were determined to be 0.8 to 1.0 mole of water per mole of anhydroglucose unit.[115] Although the physical meaning of W_m is still under debate, significant change in the physiochemical properties of the amorphous materials has been observed at water contents above W_m. The MCC tablets with different water contents showed different tensile strengths.[118] W_m of MCC was determined to be 3.3% (w/w).[119] When water content was below the W_m, the presence of water increased the contact area of polymer chains and the interaction forces between them. At higher water contents, water molecules were able to cluster and began to exhibit solvent-like behavior which decreased the bonding strength, leading to decrease in tablet tensile strength.

The water content above the W_m could also cause chemical instability. Li[120] found that the dissolution rate of benazepril hydrochloride tablets was highly correlated with the water content. When the water content was < 3.4%, it did not seem to influence the dissolution rate. At water content > 3.4%, the dissolution rate decreased linearly with increasing water content. Similarly, the disintegration time also increased as a function of water content. The “pre-activation” of crospovidone, a disintegration agent, was identified to be responsible for the reduction in dissolution rate above the critical water content. Rohrs found that, following storage at high humidity, delevirdine mesylate tablet exhibited

incomplete dissolution.[6] ^{13}C CP/MAS NMR detected that 30% of the salt converted to its free base, which resulted in a significant decrease in dissolution rate. FT-IR further confirmed that a solid-state reaction occurred between the API and the carboxyl group of the croscarmellose sodium.

To provide a mechanistic understanding of water sorption by amorphous materials, the Flory-Huggins solution theory[121] was used to model and predict the water sorption behavior of a model amorphous excipient (PVP).[122] According to this model, the sorbed water dissolves in the polymer to form a solid solution. The amount of water sorbed into the amorphous solid could be reasonably predicted when the experimental temperature was higher than the glass transition temperature, but significant deviation arose where the system was in the glassy state.[123]

It is well known that water sorption can have a significant plasticizing effect and could cause structural changes in amorphous materials.[124, 125] To account for this, Vrentas and co-workers used the free volume theory[126] to describe the diffusion of small solvent molecules in glassy polymers. The authors also proposed that the local rearrangement of the polymer molecules, upon entry of the solvent, would cause a net loss in free volume. The microscopic free volume change was correlated with the macroscopic volume change. Using the parameters for PVP-water system, Hancock and Zografi[123] successfully used the Vrentas model to describe the entire water sorption isotherm curve of PVP.

1.5 Investigation of Water-Solid Interactions using Different Techniques

Pharmaceutical scientists have several techniques at their disposal to investigate water-solid interactions. Presence of water in the solid brings about changes in the physicochemical properties of the solid. Therefore, any technique that measures the properties of a solid material may in principle be used to study

water-solid interactions. The intent of this section is to briefly survey the most commonly used techniques. Since every technique has its own limitations, it is very important to use a wide variety of techniques to investigate water-solid interactions. The established and frequently-used techniques include hot-stage microscopy, powder X-ray diffractometry, differential scanning calorimetry, thermogravimetric analysis, Karl Fischer titrimetry, infrared spectroscopy, single crystal X-ray analysis, and solution calorimetry. Only the most relevant methods will be discussed here.

1.5.1 Water Vapor Sorption Analysis

Water vapor sorption isotherms, which indicate the water uptake by the sample at different RH values but at a fixed temperature, are widely used to evaluate the hygroscopicity of pharmaceutical solids. The sorption/desorption isotherms can be obtained based on the weight change after storage at a fixed RH, usually inside a closed chamber containing saturated salt solutions. It is necessary to use several RH chambers to cover a wide RH range. An advantage of RH chamber storage is that the sample at each RH value could be further characterized by other techniques, such as vibrational spectroscopy, DSC, SS-NMR and XRD. The RH chamber storage method is labor intensive and time consuming. Nowadays, automated sorption microbalances (ASM) have replaced the RH chambers (Fig. 1.10). The attainment of equilibrium can be accelerated by (i) the small sample size, and (ii) the dynamic environment provided by the gas (humidified nitrogen) purge.

Differences in water content are often observed between the sorption and desorption cycles, which is referred to as hysteresis.[2] Fig. 1.8 shows several common water sorption isotherms of pharmaceutical solids.[2] Although the major cause of hysteresis is the slow water sorption kinetics, there could be intrinsic differences between the sorption and desorption curves even under “equilibrium” conditions. The different possible situations are as follows. 1. Deliquescence.

During the desorption stage, the drug does not crystallize from the supersaturated solution or crystallizes at a much lower RH value than the RH_0. This was reported in NaCl.[69] 2. Capillary condensation. Pore sizes "encountered" during sorption and desorption stages could be different. This is referred to as the ink-bottle effect (Fig. 1.9).[23] 3. Amorphous materials. Polymers or proteins could undergo conformational change during water uptake.[127, 128] 4. Stoichiometric hydrates. The high energy barrier for hydrate nucleation in the solid state leads to hydrate formation at RH values much higher than the "true" transition RH.[16]

The experimental setup in the ASM could accelerate water sorption if the rate limiting step is the diffusion of water in the gas phase or the heat transfer at the gas-solid interface. Discrepancy between the RH chamber storage method and ASM can be expected when the induction time for nucleation is the rate limiting step. The water sorption induced nucleation can lead to polymorphic transformation, anhydrate → hydrate conversion, and mesophase formation.

1.5.2 Atomic Force Microscopy

Surface properties significantly affect the water sorption behavior and subsequent phase transformations in pharmaceutical solids.[103, 129] Atomic force microscopy (AFM) can be used to characterize the surface properties of solids at a nanometer resolution. Unlike electron microscopy, AFM requires no sample pretreatment, and high resolution images can be obtained under a variety of experimental conditions.[51,130]. AFM determines the forces between the substrate surface and the AFM tip, providing a digital map of surface morphology as well as surface properties, such as surface energy,[131] frictional properties,[132, 133] and surface rheology[134-136] (Fig. 1.10). AFM can be used in different modes: contact, AC, and pulse force mode. The tip of the AFM probe can also be modified to investigate drug-excipient interactions. In general, AFM can provide a very flexible and versatile platform for various applications. For example, protein or

DNA unfolding was studied by force-distance curve;[137] AFM was also used in biological imaging to investigate the interaction sites of drug on proteins under physiological conditions.[138]

To study water-solid interactions, AFM could be housed in an enclosed chamber with controlled humidity and temperature. Humidity controlled AFM has been used to investigate the water adsorption on the sample surface,[40, 139] deliquescence,[67] and the moisture induced crystallization of amorphous materials.[140] At high RH values, the intrinsic problem with AFM studies is the capillary condensation between the AFM tip and substrate.[141] A meniscus could form between the tip and substrate and move with tip during the scanning process, which could potentially change surface properties and cause surface dissolution (Fig. 1.11).[142] Scanning polarization force microscopy was developed to overcome this shortcoming by scanning in noncontact mode. This technique allows imaging the liquid structures on the sample surface, including very thin films, layers, and droplets etc. The structure of water films on different surfaces, such as mica and NaCl, has been studied.[41]

The direct assessment of particle-particle and particle-device interactions could be achieved by replacing the normal AFM tip with drug particles and determining the adhesion force between drug particles and substrate using contact mode AFM (Fig. 1.12).[143] It has been shown that the particle-particle adhesion increases at higher RH values for some materials but decreases for others. This was attributed to the long-range attractive electrostatic interactions.[144] The particle-particle interactions are affected by many factors, such as surface morphology, surface roughness, exposed chemical moieties and thermodynamic properties.[145] The direct measurement of the adhesive force between drug and excipient could be misleading in predicting the drug-excipient interactions and may vary from experiment to experiment. However, the ratios of cohesive and adhesive forces could be used to determine the de-aggregation mechanism of

particles in dry powder formulations.[146] The heterogeneity of the substrate surface could be characterized by pulse force mode AFM, which could generate a surface map of the adhesion force along with surface topography.[147] This technique has been successfully used to detect high energy spots on polystyrene surface.[148]

1.5.3 Near and Middle Infrared Spectroscopy

Near infrared spectroscopy (NIR) covers the wavelength range between visible and mid-infrared (800–2500 nm, respectively 1282–4000 cm^{-1}). NIR peaks originate from vibrations of –CH, –OH, –SH and –NH bonds. All the absorption bands are the results of overtones or combinations of the fundamental mid-infrared vibrations.[149] The low absorbance coefficient permits direct analysis of strongly absorbing and highly scattering samples without sample treatment.[149] NIR is a fast, non-destructive method, which could determine both physical and chemical properties simultaneously.[150-152] The major disadvantage of NIR analysis is the dependence on time-consuming and laborious calibration procedures and the data pretreatment for quantitative analysis. The transfer of calibration model could be difficult due to the difference in optics between instruments.[153] In industry, NIR probes are widely used to provide fast and nondestructive analysis for raw material testing, product quality control, and process monitoring.[154-156]

The near-infrared (NIR) bands at about 1930 and 1440 nm are suited for rapid non-destructive water determination, and are assigned to the combination of the OH stretching and bending and the first overtone of OH stretching, respectively.[157] The water peak would shift to longer wavelength (lower frequency) with strengthening hydrogen bonding.[158] Ions, organic solvents, and polymers have strong effect on the near infrared spectrum. By using the NIR bands of water, the hydrogen bonds and the hydration of water in aqueous solution were investigated.[152] NIR spectroscopy combined with chemometric

methods is very sensitive and able to detect electrolytes in water as low as 10 mmol/L.[159] Water content in hygroscopic drugs was determined by NIR spectroscopy.[160] NIR spectroscopy was used to distinguish the different states of water, such as free and lattice water, in solids.[161, 162] The vibration of OH bonds in the lattice water occurred at a lower frequency than that in free water because the lattice water forms stronger hydrogen bonds with the drug lattice. The water peak around 1950 nm was deconvoluted into two peaks, corresponding to hydrate and surface water. A NIR model was constructed using TGA and KFT techniques as the validation methods.[162]

Infrared spectroscopy is very sensitive to vibrations of water O-H bond, and the OH stretching vibration band systems are particularly sensitive probes of hydrogen bonding networks.[163-165] The IR spectrum of adsorbed water on NaCl crystal surface below the deliquescence point was compared to that of pure water and dilute salt solution at 25°C.[54] It was found that the surface adsorbed water had properties similar to that of bulk water (Fig. 1.13). The water adsorption on different surfaces has been recently studied using FT-IR.[41] The aggregation of water in some polymers was also investigated by FT-IR.[164, 166-168] The O-H stretch peak around 3500 cm^{-1} was deconvoluted into five Gaussian components, which correspond to different states of water in the poly (ethylene glycol) film, such as bound water, dimeric water, and bridging water. The state of water during its penetration through poly (ethylene glycol) polymer film was also investigated based on the change in water stretching peaks.[167] Two-dimensional ATR-FTIR was also used to investigate the water diffusion in polypropylene film using the bending vibration bands of water (around 1640 cm^{-1}).[166, 169] This approach avoids the complication of symmetric and asymmetric coupling in the stretching vibration range (3900-2800 cm^{-1}). However, the bending vibrations tend to be weak and may also be complicated by overlapping of peaks of other constituents. The peaks at 1592, 1645, and 1676 cm^{-1} were respectively assigned to aggregated water with strong hydrogen bonds, aggregated water

with moderate hydrogen bonds, and free water. Using FTIR imaging system, the water sorption into different areas in the solid dispersion could be visualized.[170]

The vibrational spectrum of water has been studied extensively.[157, 171, 172] In the gaseous state, the vibrations of water molecules involve combinations of symmetric stretching (v_1), asymmetric stretching (v_3) and bending (v_2) of the H-O bonds.[171] Water molecules have a very small moment of inertia of rotation which causes tens of thousands to millions of absorption lines to be attributed to the combination of stretching and rotating modes. In the liquid state, rotation tends to be restricted by hydrogen bonds between water molecules. The spectral peaks are broader and many of them overlap. Variations in the environment around each liquid water molecule give rise to considerable vibration shifts in liquid water.[173] The strength of the hydrogen bonding depends on the nature of the surrounding hydrogen bonds with the strongest hydrogen bonds giving the lowest vibrational frequencies.[174] In hexagonal ice, these water bands were observed at 3085 cm^{-1}, 1650 cm^{-1}, and 3220 cm^{-1}.[175] In supercooled water, the spectrum is shifted to a lower wavenumber (by 70 cm^{-1}) with a 30% increase in its intensity between 298 K and 238 K.[176] In liquid water, the molecular stretch vibrations shift to higher frequencies on raising the temperature, which is attributed to the weaker hydrogen bonding with higher vibration frequencies.[175] However, the intramolecular vibrations shift to lower frequencies and the molecular bend vibration peak shifts to lower frequencies and becomes narrower and stronger.[177]

1.5.4 Solid State Nuclear Magnetic Resonance Spectroscopy

Solid state NMR (SS-NMR) dates back to 1976, when three techniques, magic-angle spinning, proton-to-carbon cross polarization, and high-power proton decoupling, were used to produce high-resolution NMR spectra for ^{13}C and some other nuclei in solids.[178] The popularity of this technique has increased tremendously in the last decade.[179, 180] SS-NMR is very sensitive to the local chemical environment of the corresponding nuclei in the molecule. Due to fast

exchange rate of proton in the system, ^{1}H and ^{17}O NMR spectroscopy have difficulties in provide structural information of the solids.[181] ^{13}C CP/MAS NMR spectroscopy is widely used to indirectly observe the effect of water.[179, 182] NMR, along with X-ray crystallography and vibrational spectroscopy, can provide in-depth understanding of hydration and dehydration processes.[180, 183]

Pulsed field gradient NMR measurements has been used to study the self diffusion of water in porous inorganic materials.[184, 185] It was found that the diffusion coefficient increased after complete monolayer coverage. The self-diffusion coefficient of water in partially filled pores was found to be 4 times lower than that of bulk water. Deuterium (^{2}H) has a large quadrupolar interaction and the observed ^{2}H spectral frequency could be used to determine the orientation of the covalent bond relative to the ^{2}H nucleus. The room temperature ^{2}H NMR quadrupole echo spectra and T_1 relaxation times showed that the surface adsorbed water on porous solid silicate surfaces is in the solid state, which agreed with the heat evolution determined by calorimetric methods.[186]

The spin-spin relaxation times (T_2) of water for 11 API hydrates listed in the Japanese Pharmacopoeia were determined using pulsed ^{1}H-NMR.[187] The water in different hydrates showed significant differences in molecular mobility and the free induction decay also exhibited different patterns, which could be described by Gaussian or Lorentzian model.[188] The T_2 of proton in the hydrates which showed Lorentzian decay showed good correlation with the dehydration tendency of water determined by DSC and water sorption isotherms. However, the proton T_2 for the hydrates showed Gaussian decay, which was not related to the tendency of dehydration.[188]

SS-NMR was used to study the molecular mobility of water in different types of hydrates.[180, 187] ^{2}H and ^{17}O NMR quadrupole line shape analysis was used to study the exchange between the hydrate and isotopically labeled water. It was

found that the water associated with ions in the larger tunnel were more mobile than the hydrogen-bonded water.[189, 190] The mobility of water in different gelling macromolecules were also quantified by their spin lattice relaxation times. The reduced mobility of water was attributed to the change in the hydrogen binding of water.[191]

SS-NMR was also applied to study the physicochemical properties of water as well as the drug in non-stoichiometric hydrate systems. LY297802 showed no peak splitting and a gradual shift of ^{13}C NMR peaks during water sorption into crystal lattice.[82] It was proposed that water molecules were highly mobile and disordered, with a kinetic equilibrium with the hydrogen bonding sites along the zig-zag channels in the crystal lattice. ^{13}C and ^{15}N NMR were used to study the water vapor sorption of sildenafil citrate, a non-stoichiometric hydrate, in the solid state.[85] It was found that water formed hydrogen bonds with the carboxyl group of the citrate anion, which caused a shift in the chemical resonance of citrate carbons. NMR spectra obtained at different RH values showed that water molecules in the lattice were very mobile and exchanged rapidly among the interaction sites. The ^{13}C relaxation time of hydroxyethyl functional group in thiamine HCl monohydrate was found to decrease after dehydration.[86] The increase in molecular mobility was attributed to an increase in the free volume after water removal.

SS-NMR was also used to investigate the physicochemical properties of amorphous materials in presence of water and excipients.[192, 193] NMR relaxation time can be a direct and specific measurement of the molecular mobility of water as well as drug molecules.[181] ^{2}H-NMR has been used to determine the spin-lattice relaxation time of isotopically label water in the amorphous matrix.[194] The crystallization rates of nifedipine with different excipient levels could be explained by the decrease in the molecular mobility of both drug and excipient due to hydrogen-bonding interactions.[195] A ^{13}C-NMR relaxation experiment showed an

increase in the molecular mobility of PVP as the water content increased.[196, 197] However, PVP colyophilized with sucrose did not show any increase in molecular mobility at higher water contents, which was explained by the interaction between the carbonyl group in PVP and the hydroxyl group in sucrose.[198]

1.6 Thesis overview and hypotheses

Chapter 2

We had earlier pointed out the importance of evaluation of hygroscopicity of drug candidates in the early stages of drug development. The objective of this study is to investigate the risk in predicting long-term water uptake of pharmaceutical crystals from short-term sorption studies and to study the physicochemical properties that may affect their hygroscopicity.

> Working hypothesis: The long-term water uptake of crystalline pharmaceuticals can be predicted from short-term experiments.

The hygroscopicity of 40 APIs was investigated by both RH chamber storage and ASM. Discrepancy between the RH chamber storage method and ASM was observed when the induction time for nucleation is the rate limiting step. The water sorption induced nucleation led to polymorphic transformation, anhydrate → hydrate conversion, and mesophase formation. The deliquescence RH values of 19 compounds were correlated with their solubilities. Different polymorphs of carbamazepine and indomethacin were prepared, and the impact of crystal structure on their hygroscopicity was discussed.

Chapter 3

Polymorphic transformation during processing and storage of dosage form could affect product performance including bioavailability. However, water sorption induced polymorphic transition of pharmaceuticals in the solid state is rare. Polymorphic transformation of homochlorcyclizine·2HCl (HCC) occurred at 75% RH (25°C) but not at lower RH values. The polymorphic transformation caused,

first an increase, then a decrease in water content. Polymorphic transformations in the solid state could be surface solution mediated or solid-state processes. The objective is to determine the mechanism of the polymorphic transformation in the solid state.

Working hypothesis: Water sorption into the crystal lattice of the metastable anhydrate leads to structural rearrangement and eventual crystallization of the stable anhydrate.

The lattice parameters of the HCC form I and II were simulated from their synchrotron powder diffraction patterns. The crystal structure of acetonitrile solvate was determined by X-ray crystallography. The structures of desolvate and form I were compared by Raman spectroscopy and XRD. NIR spectroscopy and XRD were used to investigate the water-solid interaction and the structural change during the polymorphic transformation.

Chapter 4

Many active pharmaceutical ingredients can exist as hydrates. Phase transformations between anhydrate and hydrate are of great importance in pharmaceutical industry, because such transformations could lead to complications during manufacture and can compromise product quality. Hydrates usually have lower aqueous solubility compared to corresponding anhydrous phases, which can lead to lower dissolution rate and potentially lower bioavailability.. We have examined the surface properties of anhydrous theophylline exposed to different RH values.

Working hypothesis: Above the anhydrate → hydrate transition RH, there is a formation of “surface solution” on anhydrous crystal surface, which eventually leads to hydrate formation.

The thickness of surface solution, surface frictional and adhesion properties, and surface mobility of theophylline anhydrate was investigated by atomic force microscopy. The theophylline hydrate formation was also observed using PLM.

Chapter 5

It is well accepted that water sorption can induce phase transformations, such as hydrate formation and deliquescence. Water sorption caused the transformation of crystalline trifluoperazine·2HCl (TFP) into a liquid crystalline form at RH > 75% (25°C). The objective of this chapter is to understand the mechanism of liquid crystal formation in the solid state and the effect of molecular structure on this unique phase transformation.

Working hypothesis: The crystal → liquid crystal transformation is an enthalpically driven process.

The liquid crystal was characterized by XRD and polarized light microscopy. The phase transformation was monitored by NIR spectroscopy and powder XRD. The thermodynamics of liquid crystal formation was studied by isothermal calorimetry.

Chapter 6

The physicochemical properties of amorphous materials depend on their preparation method and thermal history. Amorphous materials usually show local or short-range order and lack long-range order in their molecular packing. The local structure in amorphous materials could significantly affect their

crystallization and water sorption behavior. The preparation method is one of the most important factors that affect the local structures in amorphous materials. The structural memory of the starting or intermediate states in amorphous materials would significantly affect their physical stability. The objective of this chapter is to study the influence of preparation method and local structure on the physical stability of amorphous materials.

Working hypotheses:

1. The physicochemical properties of amorphous TFP are determined by their processing history.

2. The local structures of amorphous TFP arise from the structural memories of the starting or intermediate states during preparation.

Amorphous trifluoperazine·2HCl (TFP) was prepared by freeze-drying and cryo-milling. Small angle X-ray scattering and DSC were used to confirm the amorphous nature of both samples. PLM showed that freeze-dried TFP exhibited some structural order in molecular orientation. An intermediate state of TFP during freeze-drying was detected using *in situ* XRD.

Table 1.1 Classification of hygroscopicity by Callahan [19] and European Pharmacopeia [1] (reprinted from ref[17]).

Classification	Criteria per Callahan et al.[1]	Criteria per European Pharmacopeia[a]
Nonhygroscopic	Class I: essentially no moisture increase below 90% RH; less than 20% increase in moisture content above 90% RH in 1 week	0–0.12% (w/w)
Slightly hygroscopic	Class II: essentially no moisture increase below 80% RH; less than 40% (w/w) increase in moisture content above 80% RH in 1 week	0.2–2% (w/w)
Moderately hygroscopic	Class III: moisture content does not increase >5% (w/w) below 60% RH; less than 50% (w/w) increase in moisture content above 80% RH in 1 week	2–15% (w/w)
Very hygroscopic	Class IV: moisture content will increase as low as 40–50% RH; greater than 20% (w/w) increase in moisture content above 90% RH in 1 week	>15% (w/w)

[a]Percent water uptake at 25°C/80% RH.

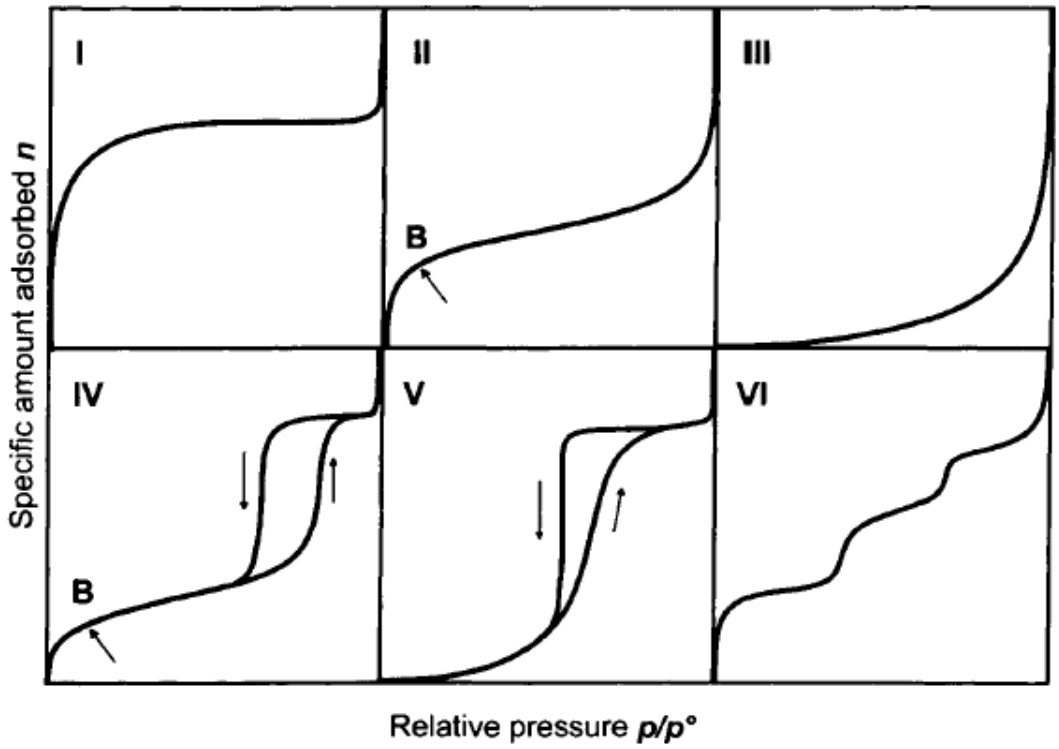

Fig. 1.1 Six main types of gas sorption isotherms, according to the IUPAC classification (reprinted from refence[31]).

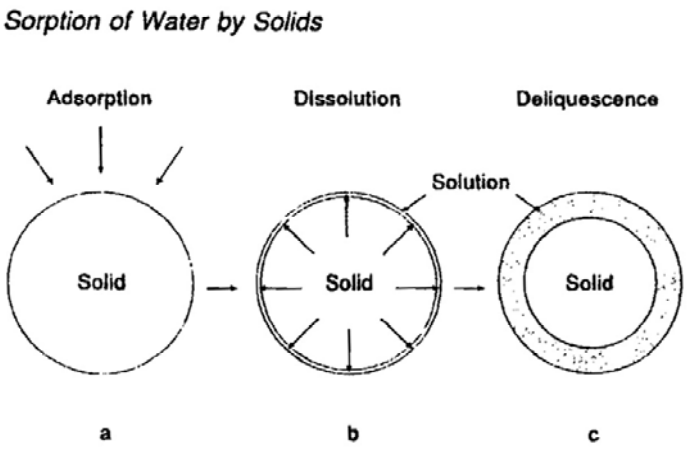

Fig. 1.2 Water vapor sorption and deliquescence of a water-soluble solid: (a) atmosphere RH, $RH_i < RH_0$; (b) $RH_i = RH_0$; (c) $RH_i > RH_0$ (reprinted from reference[20]).

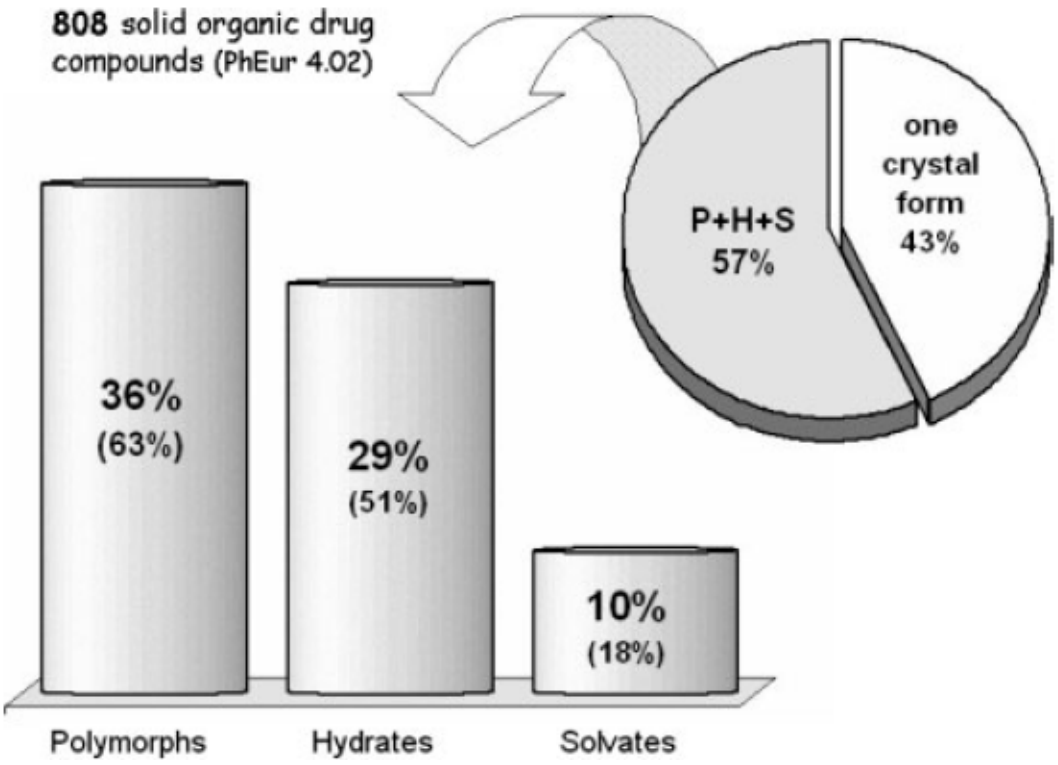

Fig. 1.3 Percentages of compounds listed in Pharmacopoea Europaea that can exist as polymorphs (P), hydrates (H) and solvates containing organic solvents (S). The total number of compounds is 808. The pie chart shows that 57% of substances can exist in more than one solid form. Some substances can exist in different solid-state species which lead to the total percentage exceeds 100% (reprinted from reference[16]).

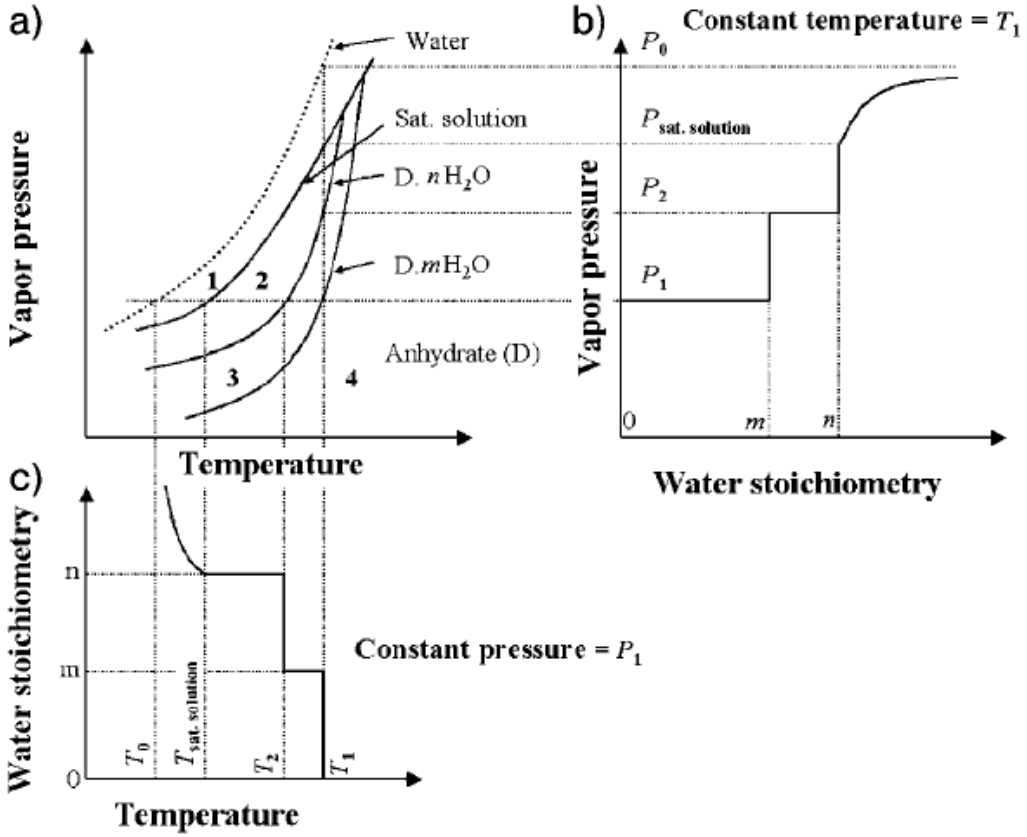

Fig. 1.4 (a) Vapor pressure of water versus temperature diagram of a hypothetical drug D, existing as two stoichiometric hydrates. The dotted line represents the vapor pressure–temperature curve for pure water. The solid lines 1–4 represent the pressure–temperature values for D.nH2O, D.mH2O, and D, respectively (n>m). (b) Plot of vapor pressure versus water stoichiometry at constant temperature, T1. (c) Plot of water stoichiometry versus temperature at constant pressure, P1 (reprinted from reference[199]).

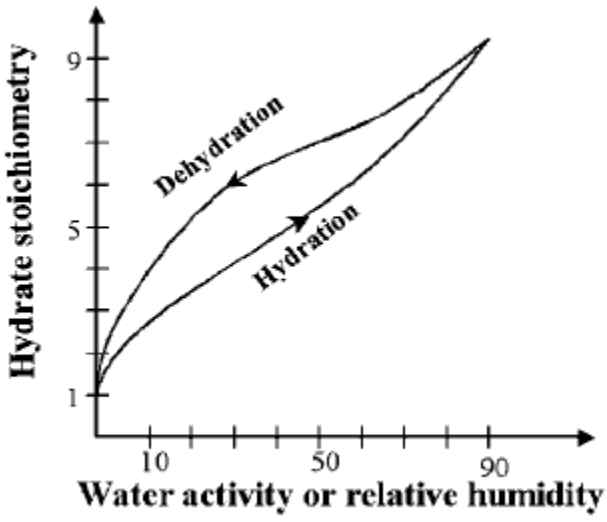

Fig. 1.5 Water sorption isotherm of a non-stoichiometric hydrate, cromolyn sodium (reprinted from reference[84]).

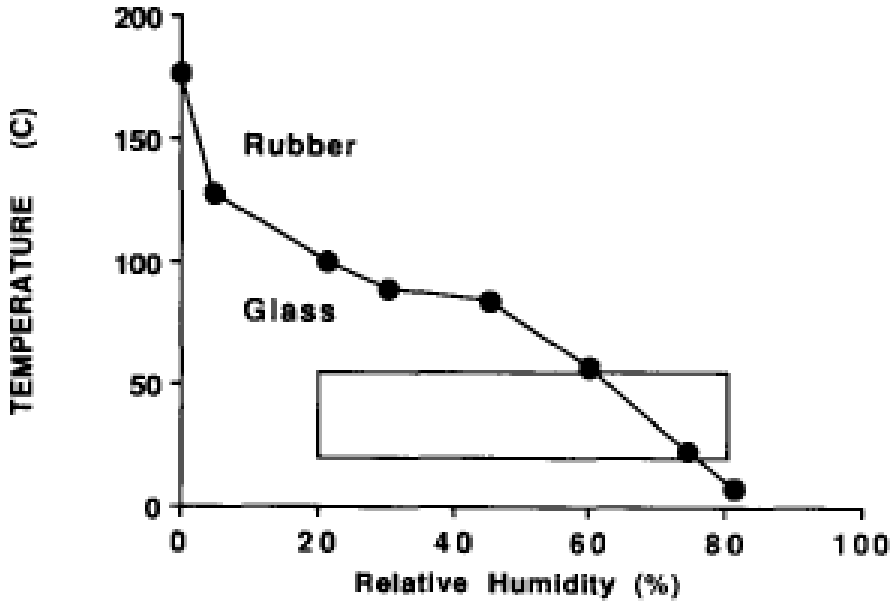

Fig. 1.6 Effect of water sorption at different RH values on the glass transition temperature of PVP K30. The box illustrates conditions normally in use during accelerated storage testing (reprinted from referece[22]).

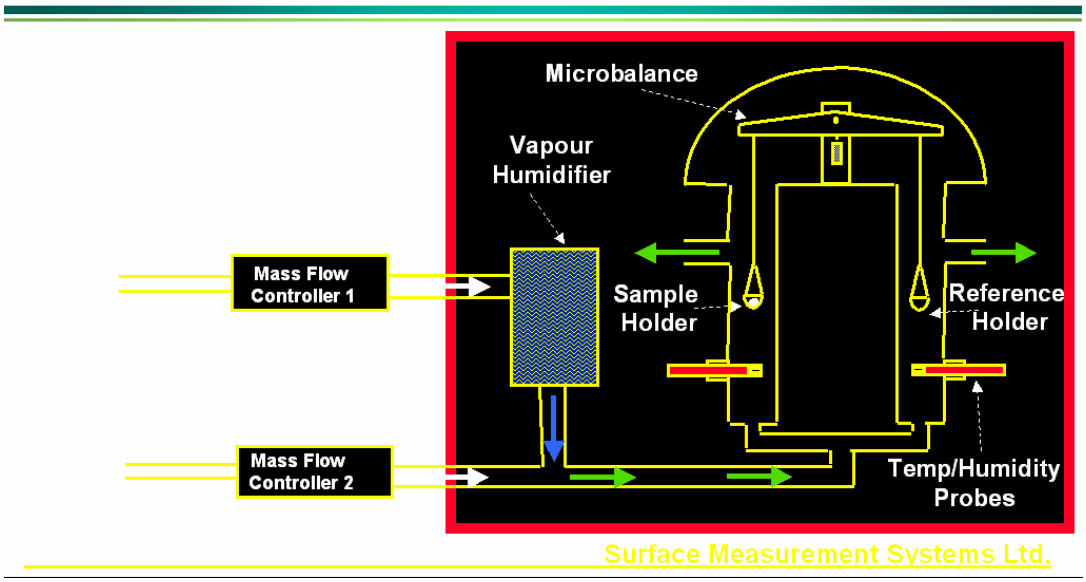

Fig. 1.7 Schematic diagram of an automated sorption microbalance (reprinted from presentation slides of Surface measurement Systems Ltd. London, UK).

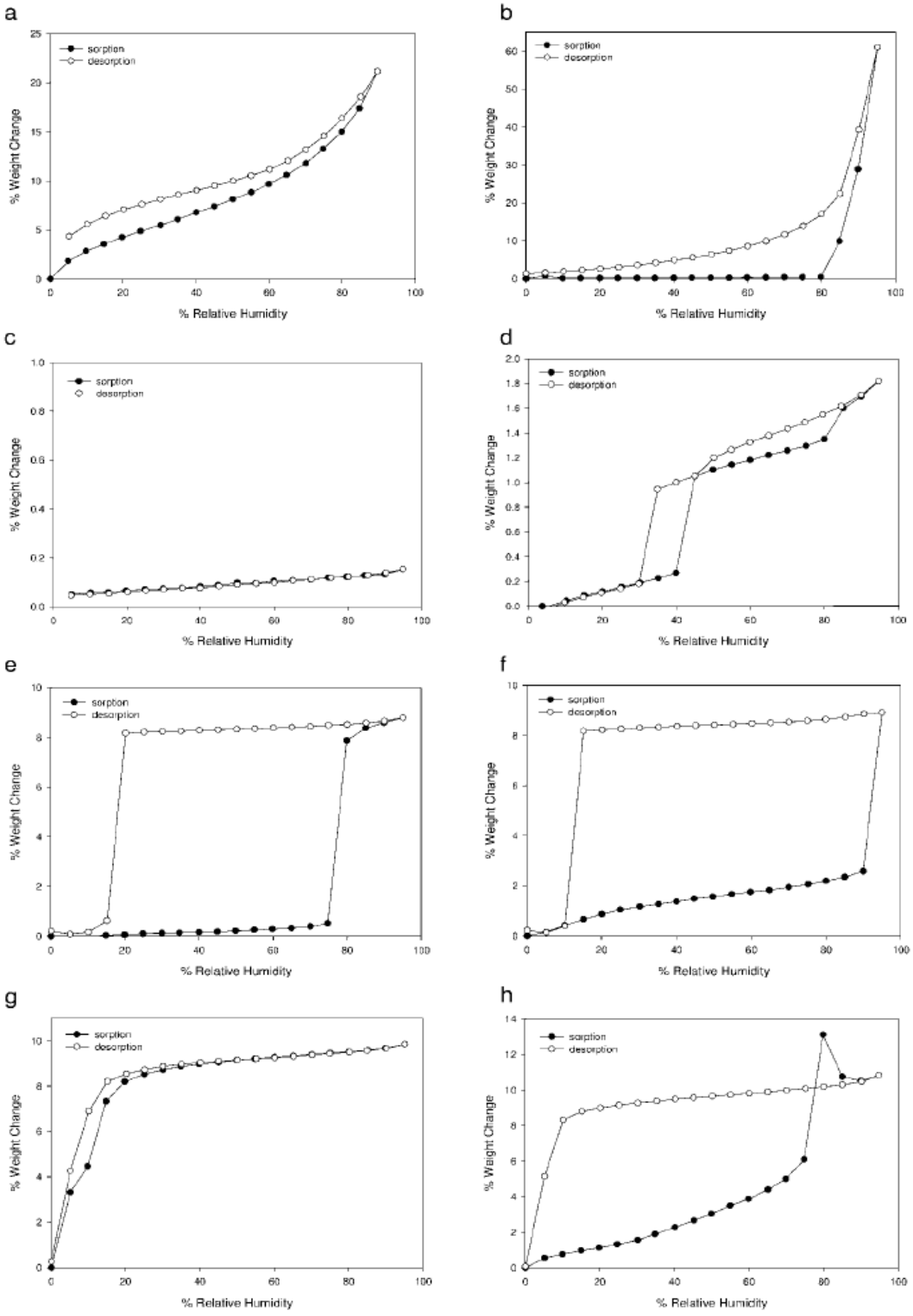

Fig. 1.8 Water sorption/desorption isotherms of pharmaceutical solids (reprinted from reference[2]).

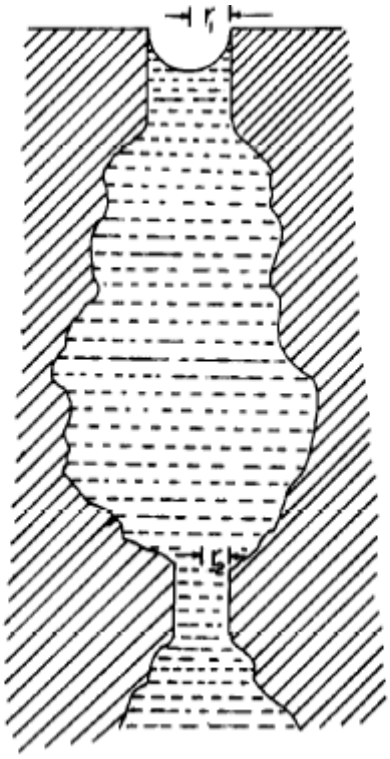

Fig. 1.9 Illustration of ink-bottle effect (reprinted from reference[23]).

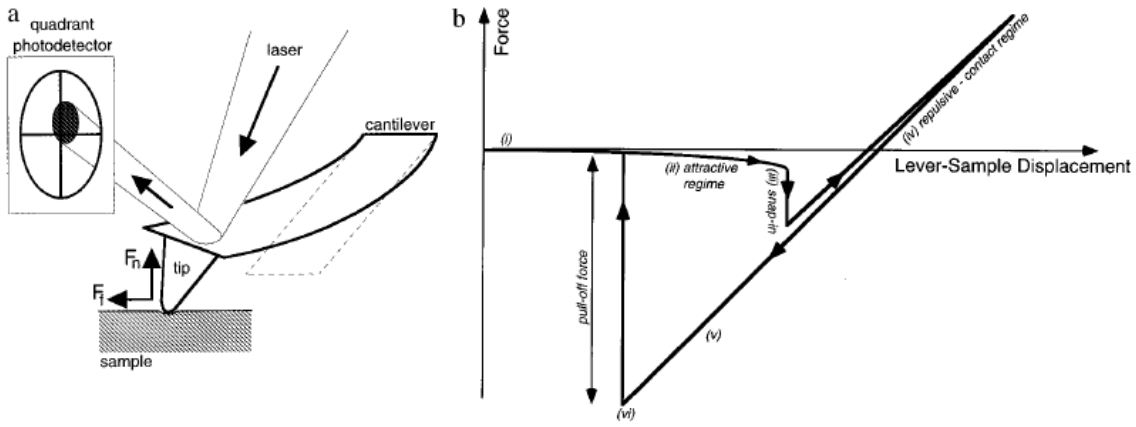

Fig. 1.10 (a) Schematic diagram of the atomic force microscopy (AFM). (b) A force-distance curve displays the vertical cantilever displacement vs lever-sample distance. (reprinted from reference[200]).

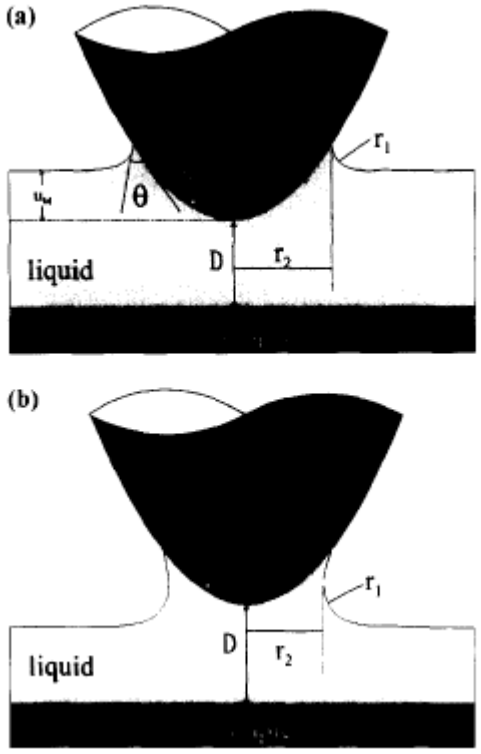

Fig. 1.11 The meniscus of liquid water between the sample surface and a paraboidal tip, during approach (panel a) and retraction (panel b). R is the radius of curvature of the tip, D is the distance from the sample, U_M is the penetration depth in the liquid layer, r_l and r_2 the two radii that define the liquid meniscus, θ is the contact angle the liquid contacts with the tip, and d is the height of the meniscus relative to the end of the tip (reprinted from reference[201]).

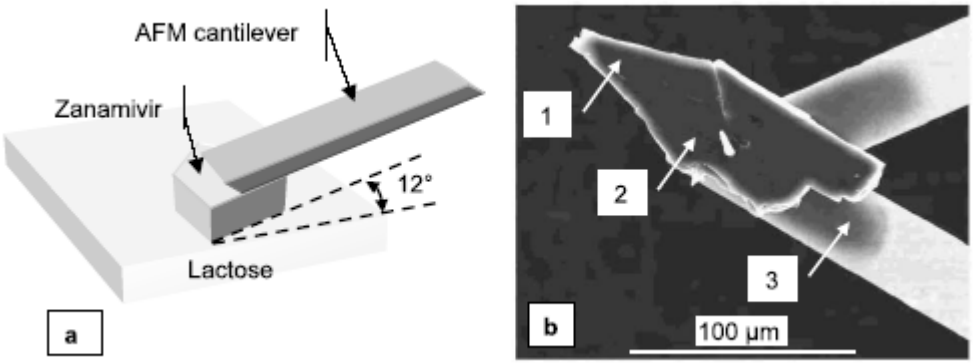

Fig. 1.12 (a) Schematic depiction of the contact between the zanamivir crystal and the compact lactose. (b) SEM image of zanamivir crystal fixed at the free end of a V-shaped AFM cantilever (reprinted from reference[202]).

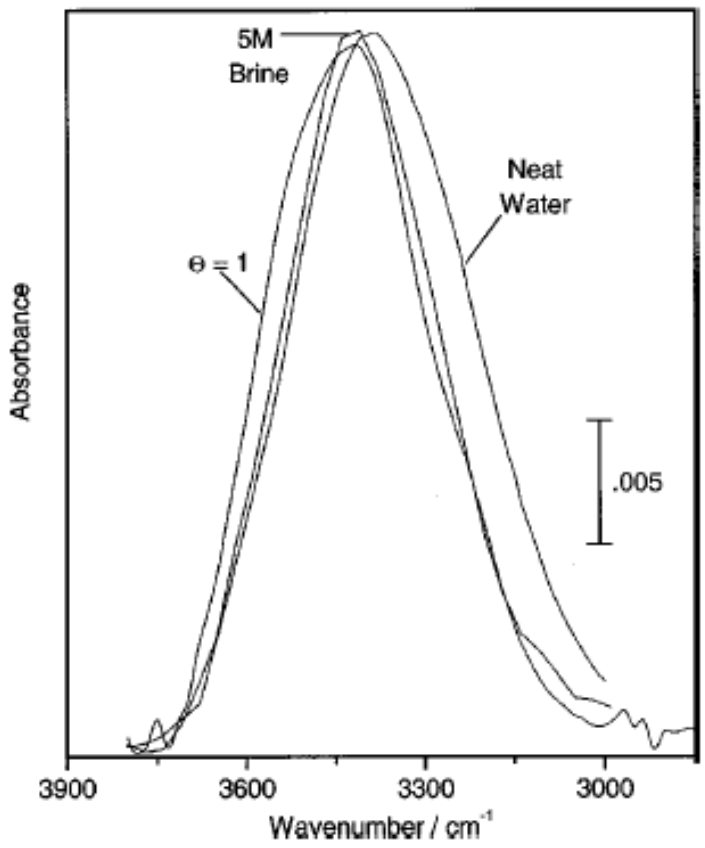

Fig. 1.13 FT-IR spectra of water in solutions of different NaCl concentrations and water adsorption on NaCl crystal at 50% RH (25°C). (reprinted from reference[67]).

1.7 References

1. *Survey hygroscopicity*. Pharmeuropa. Vol. 4. 1992.
2. Reutzel-Edens, S.M. and Newman, A.W., *Physical characterization of hygroscopicity in pharmaceutical solids*, in *Polymorphism in the Pharmaceutical Industry*, R. Hilfiker, Editor. 2006, Wiley-VCH: Weinheim, Germany. pp. 235-258.
3. Labuza, T.P. and Altunakar, B., *Water activity prediction and moisture sorption isotherm*, in *Water Activity in Foods*, Gustavo V. Barbosa-Cánovas, et al., Editors. 2007, IFT Press: Ames, Iowa. pp. 109-154.
4. Labuza, T.P. 1980. The effect of water activity on reaction kinetics of food deterioration. *Food Technology (Chicago, IL, United States)*, **34**: 36-41.
5. Nelson, K.A. and Labuza, T.P. 1992. Relationship between water and lipid oxidation rates. Water activity and glass transition theory. *ACS Symposium Series*, **500**: 93-103.
6. Rohrs, B.R.T., T.J.; Gao, P.; Stelzer, D.J.; Bergren, M.S.; Chao, R.S. 1999. Tablet dissolution affected by a moisture mediated solid-state interaction between drug and disintegrant. *Pharmaceutical Research*, **16**: 1850-1856.
7. Schmitt, E., Davis, C.W., and Long, S.T. 1996. Moisture-dependent crystallization of amorphous lamotrigine mesylate. *Journal of Pharmaceutical Sciences*, **85**: 1215-1219.
8. Listiohadi, Y.D., Hourigan, J.A., Sleigh, R.W., and Steele, R.J. 2005. Properties of lactose and its caking behaviour. *Australian Journal of Dairy Technology*, **60**: 33-52.
9. Nail, S.L. 2005. Physical and chemical stability considerations in the development and stress testing of freeze-dried pharmaceuticals. *Drugs and the Pharmaceutical Sciences*, **153**: 261-291.
10. Balbach, S. and Korn, C. 2004. Pharmaceutical evaluation of early development candidates "the 100 mg-approach". *International Journal of Pharmaceutics*, **275**: 1-12.
11. Gaviraghi, G., Barnaby, R.J., and Pellegatti, M. 2001. Pharmacokinetic challenges in lead optimization. *Pharmacokinetic Optimization in Drug Research: Biological, Physicochemical, and Computational Strategies, [LogP2000, Lipophilicity Symposium], 2nd, Lausanne, Switzerland, Mar. 5-9, 2000*, 3-14.
12. Newman, A.W., Reutzel-Edens, S.M., and Zografi, G. 2008. Characterization of the "hygroscopic" properties of active pharmaceutical ingredients. *Journal of Pharmaceutical Sciences*, **97**: 1047-1059.
13. Kontny, M.J. and Zografi, G. 1995. Sorption of water by solids. *Drugs and the Pharmaceutical Sciences*, **70**: 387-418.
14. Salameh, A.K. and Taylor, L.S. 2006. Role of deliquescence lowering in enhancing chemical reactivity in physical mixtures. *Journal of Physical Chemistry B*, **110**: 10190-10196.
15. Atassi, F. and Byrn, S.R. 2006. General trends in the desolvation behavior of calcium salts. *Pharmaceutical Research*, **23**: 2405-2412.

16. Griesser, U.J., *The importance of solvates*, in *Polymorphism in the Pharmaceutical Industry*, R. Hilfiker, Editor. 2006, Wiley-VCH: Weinheim, Germany. pp. 211-233.
17. Newman Ann, W., Reutzel-Edens Susan, M., and Zografi, G. 2008. Characterization of the "hygroscopic" properties of active pharmaceutical ingredients. *J Pharm Sci FIELD Full Journal Title:Journal of pharmaceutical sciences*, **97**: 1047-59.
18. Visalakshi, N., Mariappan, T., Bhutani, H., and Singh, S. 2005. Behavior of moisture gain and equilibrium moisture contents (EMC) of various drug substances and correlation with compendial information on hygroscopicity and loss on drying. *Pharmaceutical Development and Technology*, **10**: 489-497.
19. Callahan, J.C., Cleary, G.W., Elefant, M., Kaplan, G., Kensler, T., and Nash, R.A. 1982. Equilibrium moisture content of pharmaceutical excipients. *Drug Development and Industrial Pharmacy*, **8**: 355-69.
20. Kontny, M.J. and Zografi, G. 1995. Water-solid interactions in pharmaceutical systems. *Drugs and the Pharmaceutical Sciences*, **70**: 387-418.
21. Zografi, G. 1991. Report of the advisory panel on moisture specifications. *Pharmacopeial Forum*, **1**: 1459-1474.
22. Ahlneck, C. and Zografi, G. 1990. The molecular basis of moisture effects on the physical and chemical stability of drugs in the solid state. *International Journal of Pharmaceutics*, **62**: 87-95.
23. El-Sabaawi, M. and Pei, D.C.T. 1977. Moisture isotherms of hygroscopic porous solids. *Industrial & Engineering Chemistry Fundamentals*, **16**: 321-326.
24. Krzyzaniak, J.F., Williams, G.R., and Ni, N. 2007. Identification of phase boundaries in anhydrate/hydrate systems. *Journal of Pharmaceutical Sciences*, **96**: 1270-1281.
25. Salameh, A.K. and Taylor, L.S. 2005. Deliquescence in Binary Mixtures. *Pharmaceutical Research*, **22**: 318-324.
26. Petit, S. and Coquerel, G., *The amorphous state*, in *Polymorphism in the Pharmaceutical Industry*, R. Hilfiker, Editor. 2006, Wiley-VCH: Weinheim, Germany. pp. 259-285.
27. Hancock, B.C. and Zografi, a.G. 1996. Effects of solid-state processing on water vapor sorption by aspirin. *Journal of Pharmaceutical Sciences*, **85**: 246-8.
28. Carstensen, J.T., *Interactions of moisture with solids*, in *Drug Stability: Principles and Practices*. 2000, Marcel Dekker: New York, NY. pp. 191-208.
29. Labuza, T.P. 1977. The properties of water in relation to water binding in food. *Journal of Food Processing & Preservation*, **1**: 2-12.
30. Labuza, T.P. 1980. Enthalpy/entropy compensation in food reactions. *Food Technology (Chicago, IL, United States)*, **34**: 67-77.
31. Rouquerol, F., Rouquerol, J., and Sing, K., *Adsorption by Powders and Porous Solids: Principles, Methodology and Applications*. 1999 Academic Press, San Diego, CA.
32. Thiel, P.A. and Madey, T.F. 1987. The interaction of water with solid surfaces: fundamental aspects. *Surface Science Reports*, **7**: 211-385.

33. Rounsley, R.R. 1961. Multimolecular adsorption equation. *AIChE Journal*, 308-311.
34. Brunauer, S., *Adsorption of Gases and Vapors, I. Physical Adsorption*. 1943 Princeton Unversity Press, Princeton, NJ.
35. Einicke, W.-D., Schollner, R., Heuchel, M., Brauer, P., and Messow, U. 1995. Type III isotherms for the adsorption of ethanol-water mixtures on solid adsorbents. *Journal of the Chemical Society, Faraday Transactions*, **91**: 535-8.
36. Kluge, G. and Nagel, G. 1988. Modeling of nonisothermal multicomponent adsorption in adiabatic fixed beds - III. Some remarks on the type-III adsorption process. *Chemical Engineering Science*, **43**: 2885-9.
37. Gore, A.Y. and Banker, G.S. 1979. Surface chemistry of colloidal silica and a possible application to stabilize aspirin in solid matrixes. *Journal of Pharmaceutical Sciences*, **68**: 197-202.
38. Halasz, I., Kim, S., and Marcus, B. 2001. Uncommon adsorption isotherm of methanol on a hydrophobic Y-zeolite. *Journal of Physical Chemistry B*, **105**: 10788-10796.
39. Wendland, M., Salzmann, S., Heinbuch, U., and Fischer, J. 1989. Born-Green-Yvon results for adsorption of a simple fluid on plane walls. Structure, adsorption isotherms, and surface area determination. *Molecular Physics*, **67**: 161-72.
40. Rahaman, A., Grassian, V.H., and Margulis, C.J. 2008. Dynamics of water adsorption onto a calcite surface as a function of relative humidity. *Journal of Physical Chemistry C*, **112**: 2109-2115.
41. Ewing, G.E. 2006. Ambient thin film water on insulator surfaces. *Chemical Reviews*, **106**: 1511-1526.
42. Hancock, B.C. and Zografi, G. 1996. Effects of solid-state processing on water vapor sorption by aspirin. *J. Pharm. Sci.*, **85**: 246-248.
43. Newell, H.E., Buckton, G., Butler, D.A., Thielmann, F., and Williams, D.R. 2001. The use of inverse phase gas chromatography to measure the surface energy of crystalline, amorphous, and recently milled lactose. *Pharmaceutical Research*, **18**: 662-666.
44. Kontny, M.J., Grandolfi, G.P., and Zografi, G. 1987. Water vapor sorption of water-soluble substances: studies of crystalline solids below their critical relative humidities. *Pharmaceutical Research*, **4**: 104-112.
45. Hucher, M., Oberlin, A., and Hocart, R. 1967. Adsorption of water vapor on the cleavage surfaces of some alkali metal halides. *Bulletin de la Societe Francaise de Mineralogie et de Cristallographie*, **90**: 320-32.
46. Faqih, A.M.N., Mehrotra, A., Hammond, S.V., and Muzzio, F.J. 2007. Effect of moisture and magnesium stearate concentration on flow properties of cohesive granular materials. *International Journal of Pharmaceutics*, **336**: 338-345.
47. Binnig, G., Quate, C.F., and Gerber, C. 1986. Atomic force microscope. *Physical Review Letters*, **56**: 930-933.
48. Alexander, S., Hellemans, L., Marti, O., Schneir, J., Elings, V., Hansma, P.K., Longmiro, M., and Gurley, J. 1989. An atomic-resolution atomic-force microscope implemented using an optical lever. *Journal of Applied Physics*, **65**: 164-167.

49. Cappella, B. and Dietler, G. 1999. Force-distance curves by atomic force microscopy. *Surface Science Reports*, **34**: 1-104.
50. Lee, S. and Staehle, R.W. 1996. Adsorption of water on gold. *Corrosion (Houston)*, **52**: 843-852.
51. Verdaguer, A., Sacha, G.M., Luna, M., Ogletree, D.F., and Salmeron, M. 2005. Initial stages of water adsorption on NaCl (100) studied by scanning polarization force microscopy. *Journal of Chemical Physics*, **123**: 124703/1-124703/8.
52. Dai, Q., Hu, J., and Salmeron, M. 1997. Adsorption of Water on NaCl (100) Surfaces: Role of Atomic Steps. *Journal of Physical Chemistry B*, **101**: 1994-1998.
53. Xu, L., Bluhm, H., and Salmeron, M. 1998. An AFM study of the tribological properties of NaCl(100) surfaces under moist air. *Surface Science*, **407**: 251-255.
54. Foster, M.C. and Ewing, G.E. 2000. Adsorption of water on the NaCl(001) surface. II. An infrared study at ambient temperatures. *Journal of Chemical Physics*, **112**: 6817-6826.
55. Igarashi, N., Nakai, K., Hashimoto, K., and Tatsumi, T. 2001. Pore size analysis with H2O adsorption measurement of organically modified MCM-41 type materials. *Studies in Surface Science and Catalysis*, **135**: 2902-2911.
56. Hanzawa, Y. and Kaneko, K. 1997. Lack of a Predominant Adsorption of Water Vapor on Carbon Mesopores. *Langmuir*, **13**: 5802-5804.
57. Patrick, W.A. 1929. The adsorption of vapors. *Colloid Symposium Monograph*, **7**: 129-33.
58. Cantrell, W., McCrory, C., and Ewing, G.E. 2002. Nucleated deliquescence of salt. *Journal of Chemical Physics*, **116**: 2116-2120.
59. Zografi, G. 1988. States of water associated with solids. *Drug Development and Industrial Pharmacy*, **14**: 1905-1926.
60. Van Campen, L., Amidon, G.L., and Zografi, G. 1983. Moisture sorption kinetics for water-soluble substances. I: Theoretical considerations of heat transport control. *Journal of Pharmaceutical Sciences*, **72**: 1381-1388.
61. Ross, K.D. 1975. Estimation of water activity in intermediate moisture foods. *Food Technology*, **3**: 26-34.
62. Van Campen, L., Zografi, G., and Carstensen, J.T. 1980. An approach to the evaluation of hygroscopicity for pharmaceutical solids. *International Journal of Pharmaceutics*, **5**: 1-18.
63. Schuttlefield, J., Al-Hosney, H., Zachariah, A., and Grassian, V.H. 2007. Attenuated total reflection Fourier transform infrared spectroscopy to investigate water uptake and phase transitions in atmospherically relevant particles. *Applied Spectroscopy*, **61**: 283-292.
64. Li, X.-H., Wang, F., Lu, P.-D., Dong, J.-L., Wang, L.-Y., and Zhang, Y.-H. 2006. Confocal raman observation of the efflorescence/deliquescence processes of individual NaNO3 particles on quartz. *Journal of Physical Chemistry B*, **110**: 24993-24998.
65. Mirabel, P., Reiss, H., and Bowles, R.K. 2000. A theory for the deliquescence of small particles. *Journal of Chemical Physics*, **113**: 8200-8205.

66. Djikaev, Y.S., Bowles, R., Reiss, H., Haemeri, K., Laaksonen, A., and Vaekevae, M. 2001. Theory of Size Dependent Deliquescence of Nanoparticles: Relation to Heterogeneous Nucleation and Comparison with Experiments. *Journal of Physical Chemistry B*, **105**: 7708-7722.
67. Ewing, G.E. 2005. H2O on NaCl: from single molecule, to clusters, to monolayer, to thin films, to deliquescence. *Structure and Bonding (Berlin, Germany)*, **116**: 1-25.
68. Russell, L.M. and Ming, Y. 2002. Deliquescence of small particles. *Journal of Chemical Physics*, **116**: 311-321.
69. Biskos, G., Paulsen, D., Russell, L.M., Buseck, P.R., and Martin, S.T. 2007. Prompt deliquescence and efflorescence of aerosol nanoparticles. *Atmospheric Chemistry and Physics*, **6**: 4633-4642.
70. Biskos, G., Malinowski, A., Russell, L., Buseck, P., and Martin, S. 2006. Nanosize effect on the deliquescence and the efflorescence of sodium chloride particles. *Aerosol Science and Technology*, **40**: 97-106.
71. Martin, S.T. 2000. Phase transitions of aqueous atmospheric particles. *Chemical Reviews (Washington, D. C.)*, **100**: 3403-3453.
72. Parsons, M.T., Mak, J., Lipetz, S.R., and Bertram, A.K. 2004. Deliquescence of malonic, succinic, glutaric, and adipic acid particles. *Journal of Geophysical Research, [Atmospheres]*, **109**: D06212/1-D06212/8.
73. Chen, L.R., *Solid state behavior of pharmaceutical hydrates*. Ph.D dissertation. 1999.
74. Vippagunta, S.R., Brittain, H.G., and Grant, D.J.W. 2001. Crystalline solids. *Advanced Drug Delivery Reviews*, **48**: 3-26.
75. Burley, J.C., van de Streek, J., and Stephens, P.W. 2006. Ampicillin trihydrate from synchrotron powder diffraction data. *Acta Crystallographica, Section E: Structure Reports Online*, **E62**: o797-o799.
76. Zhu, H., Young, V.G., Jr., and Grant, D.J.W. 2002. Crystal structures and thermal analysis of nedocromil bivalent metal salt hydrates. *Journal of Chemical Crystallography*, **31**: 421-434.
77. Haleblian, J.K. 1975. Characterization of habits and crystalline modification of solids and their pharmaceutical applications. *Journal of Pharmaceutical Sciences*, **64**: 1269-1288.
78. Kim, Y.-s. and Rousseau, R.W. 2004. Characterization and Solid-State Transformations of the Pseudopolymorphic Forms of Sodium Naproxen. *Crystal Growth & Design*, **4**: 1211-1216.
79. Zhu, H. and Grant, D.J.W. 2001. Dehydration behavior of nedocromil magnesium pentahydrate. *International Journal of Pharmaceutics*, **215**: 251-262.
80. Zhu, H., Halfen, J.A., Young, V.G., Jr., Padden, B.E., Munson, E.J., Menon, V., and Grant, D.J.W. 1997. Physicochemical Characterization of Nedocromil Bivalent Metal Salt Hydrates: 3. Nedocromil Calcium. *Journal of Pharmaceutical Sciences*, **86**: 1439-1447.
81. Zhu, H., Khankari, R.K., Padden, B.E., Munson, E.J., Gleason, W.B., and Grant, D.J.W. 1996. Physicochemical Characterization of Nedocromil Bivalent Metal

Salt Hydrates. 1. Nedocromil Magnesium. *Journal of Pharmaceutical Sciences*, **85**: 1026-1034.
82. Reutzel, S.M. and Russell, V.A. 1998. Origins of the Unusual Hygroscopicity Observed in LY297802 Tartrate. *Journal of Pharmaceutical Sciences*, **87**: 1568-1571.
83. Chen, L.R., Young, V.G., Jr., Lechuga-Ballesteros, D., and Grant, D.J. 1999. Solid-state behavior of cromolyn sodium hydrates. *Journal of Pharmaceutical Sciences*, **88**: 1191-200.
84. Cox, J.S.G., Woodard, G.D., and McCrone, W.C. 1971. Solid-state chemistry of cromolyn sodium (disodium cromoglycate). *Journal of Pharmaceutical Sciences*, **60**: 1458-1465.
85. Apperley, D.C., Basford, P.A., Dallman, C.I., Harris, R.K., Kinns, M., Marshall, P.V., and Swanson, A.G. 2005. Nuclear magnetic resonance investigation of the interaction of water vapor with sildenafil citrate in the solid state. *Journal of Pharmaceutical Sciences*, **94**: 516-523.
86. Te, R.L., Griesser, U.J., Morris, K.R., Byrn, S.R., and Stowell, J.G. 2003. X-ray Diffraction and Solid-State NMR Investigation of the Single-Crystal to Single-Crystal Dehydration of Thiamine Hydrochloride Monohydrate. *Crystal Growth & Design*, **3**: 997-1004.
87. Watanabe, A., Tasaki, S., Wada, Y., and Nakamachi, H. 1979. Polymorphism of thiamine hydrochloride. II. Crystal structure of thiamine hydrochloride hemihydrate and its stability. *Chemical & Pharmaceutical Bulletin*, **27**: 2751-9.
88. Bandyopadhyay, R., Erixon, K., Young, V.G., and Grant, D.J.W. *Effects of water activity on recrystallized L-lysine monohydrochloride*. in *World Congress on Particle Technology 3, Brighton, UK, July 6-9*. 1998.
89. Stephenson, G.A., Stowell, J.G., Toma, P.H., Pfeiffer, R.R., and Byrn, S.R. 1997. Solid-State Investigations of Erythromycin A Dihydrate: Structure, NMR Spectroscopy, and Hygroscopicity. *Journal of Pharmaceutical Sciences*, **86**: 1239-1244.
90. Stephenson, G.A., Groleau, E.G., Kleemann, R.L., Xu, W., and Rigsbee, D.R. 1998. Formation of isomorphic desolvates: creating a molecular vacuum. *Journal of Pharmaceutical Sciences*, **87**: 536-542.
91. Han, J., Gupte, S., and Suryanarayanan, R. 1998. Applications of pressure differential scanning calorimetry in the study of pharmaceutical hydrates. II. Ampicillin trihydrate. *International Journal of Pharmaceutics*, **170**: 63-72.
92. Chen, L.R., *Solid state behavior of pharmaceutical hydrates*. Ph.D dissertation. 1999 University of Minnesota, Minneapolis.
93. Griesser, U.J. and Burger, A. 1995. The effect of water vapor pressure on desolvation kinetics of caffeine 4/5-hydrate. *International Journal of Pharmaceutics*, **120**: 83-93.
94. Phadnis, N.V. and Suryanarayanan, R. 1997. Polymorphism in anhydrous theophylline--implications on the dissolution rate of theophylline tablets. *Journal of Pharmaceutical Sciences*, **86**: 1256-63.

95. Lin, C.T., Perrier, P., Clay, G.G., Sutton, P.A., and Byrn, S.R. 1982. Solid-state photooxidation of 21-cortisol tert-butylacetate to 21-cortisone tert-butylacetate. *Journal of Organic Chemistry*, **47**: 2978-81.
96. Katdare, A.V. and Bavitz, J.F. 1984. Hydrate related dissolution characteristics of norfloxacin. *Drug Development and Industrial Pharmacy*, **10**: 789-807.
97. Kahela, P., Aaltonen, R., Lewing, E., Anttila, M., and Kristoffersson, E. 1983. Pharmacokinetics and dissolution of two crystalline forms of carbamazepine. *International Journal of Pharmaceutics*, **14**: 103-12.
98. Khankari, R.K. and Grant, D.J.W. 1995. Pharmaceutical hydrates. *Thermochimica Acta*, **248**: 61-79.
99. Ticehurst, M.D., Storey, R.A., and Watt, C. 2002. Application of slurry bridging experiments at controlled water activities to predict the solid-state conversion between anhydrous and hydrated forms using theophylline as a model drug. *International Journal of Pharmaceutics*, **247**: 1-10.
100. Zhu, H., Yuen, C., and Grant, D.J.W. 1996. Influence of water activity in organic solvent + water mixtures on the nature of the crystallizing drug phase. 1. Theophylline. *International Journal of Pharmaceutics*, **135**: 151-160.
101. Murphy, D., Rodriguez-Cintron, F., Langevin, B., Kelly, R.C., and Rodriguez-Hornedo, N. 2002. Solution-mediated phase transformation of anhydrous to dihydrate carbamazepine and the effect of lattice disorder. *International Journal of Pharmaceutics*, **246**: 121-134.
102. O'Brien, L.E., Timmins, P., Williams, A.C., and York, P. 2004. Use of in situ FT-Raman spectroscopy to study the kinetics of the transformation of carbamazepine polymorphs. *Journal of Pharmaceutical and Biomedical Analysis*, **36**: 335-340.
103. Otsuka, M., Ishii, M., and Matsuda, Y. 2003. Effect of surface modification on hydration kinetics of carbamazepine anhydrate using isothermal microcalorimetry. *AAPS PharmSciTech*, **4**: E5.
104. Kelly, R.C. and Rodriguez-Hornedo, N. 2003. Directed nucleation and solution-mediated phase transformation of carbamazepine in aqueous and organic solutions. *Abstracts of Papers, 225th ACS National Meeting, New Orleans, LA, United States, March 23-27, 2003*, IEC-055.
105. Rodriguez-Hornedo, N. and Murphy, D. 2004. Surfactant-facilitated crystallization of dihydrate carbamazepine during dissolution of anhydrous polymorph. *Journal of Pharmaceutical Sciences*, **93**: 449-460.
106. Tanninen, V.P., Luhtala, S., and Yliruusi, J. 1992. X-ray powder diffraction line profile analysis in the study on the effect of surface active agent on the crystal properties of carbamazepine. *Acta Pharmaceutica Nordica*, **4**: 277-282.
107. Katzhendler, I., Azoury, R., and Friedman, M. 1998. Crystalline properties of carbamazepine in sustained release hydrophilic matrix tablets based on hydroxypropyl methylcellulose. *Journal of controlled release*, **54**: 69-85.
108. Jorgensen, A.C., Airaksinen, S., Karjalainen, M., Luukkonen, P., Rantanen, J., and Yliruusi, J. 2004. Role of excipients in hydrate formation kinetics of theophylline in wet masses studied by near-infrared spectroscopy. *European Journal of Pharmaceutical Sciences*, **23**: 99-104.

109. Yu, L. 2001. Amorphous pharmaceutical solids: preparation, characterization and stabilization. *Advanced Drug Delivery Reviews*, **48**: 27-42.
110. Gordon, M. and Taylor, J.S. 1952. Ideal copolymers and the second-order transitions of synthetic rubbers. I. Noncrystalline copolymers. *Journal of Applied Chemistry*, **2**: 493-500.
111. Andronis, V. and Zografi, G. 1998. The molecular mobility of supercooled amorphous indomethacin as a function of temperature and relative humidity. *Pharmaceutical Research*, **15**: 835-842.
112. Fitzpatrick, S., McCabe, J.F., Petts, C.R., and Booth, S.W. 2002. Effect of moisture on polyvinylpyrrolidone in accelerated stability testing. *International Journal of Pharmaceutics*, **246**: 143-151.
113. Schmitt, E.A., Law, D., and Zhang, G.G. 1999. Nucleation and crystallization kinetics of hydrated amorphous lactose above the glass transition temperature. *Journal of Pharmaceutical Sciences*, **88**: 291-6.
114. Carstensen, J.T. and Van Scoik, K. 1990. Amorphous-to-crystalline transformation of sucrose. *Pharmaceutical Research*, **7**: 1278-1281.
115. Zografi, G., Kontny, M.J., Yang, A.Y.S., and Brenner, G.S. 1984. Surface area and water vapor sorption of microcrystalline cellulose. *International Journal of Pharmaceutics*, **18**: 99-116.
116. Brunauer, S., Emmett, P.H., and Teller, E. 1938. Adsorption of gases in multimolecular layers. *Journal of the American Chemical Society*, **60**: 309-319.
117. Zografi, G. and kontony, M.J. 1986. The interactions of water with cellulose- and starch-derived pharmaceutical excipients. *Pharmaceutical research*, 187-194.
118. Stubberud, L., Arwidsson, H.G., Larsson, A., Graffner, C. 1996. Water solid interactions II. Effect of moisture sorption and glass transition temperature on compactibility of microcrystalline cellulose alone or in binary mixtures with polyvinyl pyrrolidone. *International Journal of Pharmaceutics*, **134**: 79-88.
119. Sun, C.C. 2008. Mechanism of moisture induced variations in true density and compaction properties of microcrystalline cellulose. *International Journal of Pharmaceutics*, **346**: 93-101.
120. Li, S., Wei, B., Fleres, S., Comfort, A., and Royce, A. 2004. Correlation and prediction of moisture-mediated dissolution stability for benazepril hydrochloride tablets. *Pharmaceutical Research*, **21**: 617-624.
121. Flory, P.J. 1942. Thermodynamics of high-polymer solutions. *Journal of Chemical Physics*, **10**: 51-61.
122. MacKenzie, A.P. and Rasmussen, D.H., *Interactions in the water-polyvinylpyrrolidinone system at low temperatures*, in *Water Struct. Water-Polym. Interface, Proc. Symp.* 1972. p. 146-172.
123. Hancock, B.C. and Zografi, G. 1993. The use of solution theories for predicting water vapor absorption by amorphous pharmaceutical solids: A test of the Flory-Huggins and Vrentas models. *Pharmaceutical Research*, **10**: 1262-1267.
124. Gupta, P. and Bansal, A.K. 2005. Molecular interactions in celecoxib-PVP-meglumine amorphous system. *Journal of Pharmacy and Pharmacology*, **57**: 303-310.

125. Andronis, V., Yoshioka, M., and Zografi, G. 1997. Effects of sorbed water on the crystallization of indomethacin from the amorphous state. *J Pharm Sci FIELD Full Journal Title:Journal of pharmaceutical sciences*, **86**: 346-51.
126. Fujita, H. 1961. Free diffusion in a two-component system in which there is a volume change on mixing. *Journal of the American Chemical Society*, **83**: 2862-2865.
127. Hageman, M.J. 1992. Water sorption and solid-state stability of proteins. *Pharmaceutical Biotechnology*, **2**: 273-309.
128. Kocherbitov, V., Arnebrant, T., and Soederman, O. 2004. Lysozyme-water interactions studied by sorption calorimetry. *Journal of Physical Chemistry B*, **108**: 19036-19042.
129. Kaneniwa, N., Yamaguchi, T., Watari, N., and Otsuka, M. 1984. Hygroscopicity of carbamazepine crystalline powders. *Yakugaku Zasshi*, **104**: 184-90.
130. Danesh, A., Connell, S.D., Davies, M.C., Roberts, C.J., Tendler, S.J., Williams, P.M., and Wilkins, M.J. 2001. An in situ dissolution study of aspirin crystal planes (100) and (001) by atomic force microscopy. *Pharmaceutical research*, **18**: 299-303.
131. Zhang, J., Ebbens, S., Chen, X., Jin, Z., Luk, S., Madden, C., Patel, N., and Roberts, C.J. 2006. Determination of the surface free energy of crystalline and amorphous lactose by atomic force microscopy adhesion measurement. *Pharmaceutical Research*, **23**: 401-407.
132. Ecke, S., Raiteri, R., Bonaccurso, E., Reiner, C., Deiseroth, H.-J., and Butt, H.-J. 2001. Measuring normal and friction forces acting on individual fine particles. *Review of Scientific Instruments*, **72**: 4164-4170.
133. Hu, J., Xiao, X.d., Ogletree, D.F., and Salmeron, M. 1995. Atomic scale friction and wear of mica. *Surface Science*, **327**: 358-70.
134. Cappella, B., Kaliappan, S.K., and Sturm, H. 2005. Using AFM force-distance curves to study the glass-to-rubber transition of amorphous polymers and their elastic-plastic properties as a function of temperature. *Macromolecules*, **38**: 1874-1881.
135. Schaer-Zammaretti, P. and Ubbink, J. 2003. Imaging of lactic acid bacteria with AFM - elasticity and adhesion maps and their relationship to biological and structural data. *Ultramicroscopy*, **97**: 199-208.
136. Carpick, R.W., Ogletree, D.F., and Salmeron, M. 1997. Lateral stiffness: a new nanomechanical measurement for the determination of shear strengths with friction force microscopy. *Applied Physics Letters*, **70**: 1548-1550.
137. Hansma, H.G., Kasuya, K., and Oroudjev, E. 2004. Atomic force microscopy imaging and pulling of nucleic acids. *Current Opinion in Structural Biology*, **14**: 380-385.
138. Hussain, M.A., Agnihotri, A., and Siedlecki, C.A. 2005. AFM Imaging of Ligand Binding to Platelet Integrin aIIbb3 Receptors Reconstituted into Planar Lipid Bilayers. *Langmuir*, **21**: 6979-6986.
139. Kendall, T.A. and Martin, S.T. 2007. Water-induced reconstruction that affects mobile ions on the surface of calcite. *Journal of Physical Chemistry A*, **111**: 505-514.

140. Cleaver, J.A.S. and Wong, P. 2004. Humidity-induced surface modification of boric acid. *Surface and Interface Analysis*, **36**: 1592-1599.
141. Sedin, D.L. and Rowlen, K.L. 2000. Adhesion forces measured by atomic force microscopy in humid air. *Analytical Chemistry*, **72**: 2183-2189.
142. Binggeli, M. and Mate, C.M. 1994. Influence of capillary condensation of water on nanotribology studied by force microscopy. *Applied Physics Letters*, **65**: 415-17.
143. Ducker, W.A., Senden, T.J., and Pashley, R.M. 1991. Direct measurement of colloidal forces using an atomic force microscope. *Nature (London, United Kingdom)*, **353**: 239-41.
144. Young, P.M., Price, R., Tobyn, M.J., Buttrum, M., and Dey, F. 2004. The influence of relative humidity on the cohesion properties of micronized drugs used in inhalation therapy. *Journal of Pharmaceutical Sciences*, **93**: 753-761.
145. Frisbie, C.D., Rozsnyai, L.F., Noy, A., Wrighton, M.S., and Lieber, C.M. 1994. Functional group imaging by chemical force microscopy. *Science*, **265**: 2071-2074.
146. Begat, P., Morton, D.A.V., Staniforth, J.N., and Price, R. 2004. The Cohesive-Adhesive Balances in Dry Powder Inhaler Formulations II: Influence on Fine Particle Delivery Characteristics. *Pharmaceutical Research*, **21**: 1826-1833.
147. van der Werf, K.O., Putman, C.A.J., de Grooth, B.G., and Greve, J. 1994. Adhesion force imaging in air and liquid by adhesion mode atomic force microscopy. *Applied Physics Letters*, **65**: 1195-7.
148. Allen, S., Connell, S.D.A., Chen, X., Davies, J., Davies, M.C., Dawkes, A.C., Roberts, C.J., Tendler, S.J.B., and Williams, P.M. 2001. Mapping the surface characteristics of polystyrene microtiter wells by a multimode scanning force microscopy approach. *Journal of Colloid and Interface Science*, **242**: 470-476.
149. Reich, G. 2005. Near-infrared spectroscopy and imaging: Basic principles and pharmaceutical applications. *Advanced Drug Delivery Reviews*, **57**: 1109-1143.
150. Giangiacomo, R. 2006. Study of water-sugar interactions at increasing sugar concentration by NIR spectroscopy. *Food Chemistry*, **96**: 371-379.
151. Duong, N.-H., Arratia, P., Muzzio, F., Lange, A., Timmermans, J., and Reynolds, S. 2003. A homogeneity study using NIR spectroscopy: Tracking magnesium stearate in bohle bin-blender. *Drug Development and Industrial Pharmacy*, **29**: 679-687.
152. Grant, A., Davies, A.M.C., and Bilverstone, T. 1989. Simultaneous determination of sodium hydroxide, sodium carbonate and sodium chloride concentrations in aqueous solutions by near-infrared spectrometry. *Analyst (Cambridge, United Kingdom)*, **114**: 819-22.
153. Jones, J.A., Last, I.R., MacDonald, B.F., and Prebble, K.A. 1993. Development and transferability of near-infrared methods for determination of moisture in a freeze-dried injection product. *Journal of Pharmaceutical and Biomedical Analysis*, **11**: 1227-31.
154. Reich, G. 2002. Potential of attenuated total reflection infrared and near-infrared spectroscopic imaging for quality assurance/quality control of solid pharmaceutical dosage forms. *Pharmazeutische Industrie*, **64**: 870-874.

155. Kramer, K. and Ebel, S. 2000. Application of NIR reflectance spectroscopy for the identification of pharmaceutical excipients. *Analytica Chimica Acta*, **420**: 155-161.
156. Ulmschneider, M., Barth, G., and Trenka, E. 2000. Building transferable cluster calibrations for the identification of different solid excipients with near-infrared spectroscopy. *Pharmazeutische Industrie*, **62**: 374-376.
157. Buning-Pfaue, H. 2003. Analysis of water in food by near infrared spectroscopy. *Food Chemistry*, **82**: 107-115.
158. Gergely, S. and Salgo, A. 2007. Changes in protein content during wheat maturation-what is measured by near infrared spectroscopy? *Journal of Near Infrared Spectroscopy*, **15**: 49-58.
159. Soller, B.R., Favreau, J., and Idwasi, P.O. 2003. Investigation of electrolyte measurement in diluted whole blood using spectroscopic and chemometric methods. *Applied Spectroscopy*, **57**: 146-151.
160. Zhou, X., Hines, P., and Borer, M.W. 1998. Moisture determination in hygroscopic drug substances by near infrared spectroscopy. *Journal of Pharmaceutical and Biomedical Analysis*, **17**: 219-225.
161. Zhou, G.X., Ge, Z., Dorwart, J., Izzo, B., Kukura, J., Bicker, G., and Wyvratt, J. 2003. Determination and differentiation of surface and bound water in drug substances by near infrared spectroscopy. *Journal of Pharmaceutical Sciences*, **92**: 1058-1065.
162. Cao, W., Mao, C., Chen, W., Lin, H., Krishnan, S., and Cauchon, N. 2006. Differentiation and quantitative determination of surface and hydrate water in lyophilized mannitol using NIR spectroscopy. *Journal of Pharmaceutical Sciences*, **95**: 2077-2086.
163. Al-Abadleh, H.A. and Grassian, V.H. 2003. Phase transitions in magnesium nitrate thin films: a transmission FT-IR study of the deliquescence and efflorescence of nitric acid reacted magnesium oxide interfaces. *Journal of Physical Chemistry B*, **107**: 10829-10839.
164. Ide, M., Yoshikawa, D., Maeda, Y., and Kitano, H. 1999. State of water inside and at the surface of poly(ethylene glycol) films examined by FT-IR. *Langmuir*, **15**: 926-929.
165. Kalutskaya, E.P. 1988. IR-spectroscopic study of the interaction of sorbed water and xylan. *Vysokomolekulyarnye Soedineniya, Seriya A*, **30**: 867-73.
166. Shen, Y. and Wu, P. 2003. Two-dimensional ATR-FTIR spectroscopic investigation on water diffusion in polypropylene film: water bending vibration. *Journal of Physical Chemistry B*, **107**: 4224-4226.
167. Kitano, H., Ichikawa, K., Ide, M., Fukuda, M., and Mizuno, W. 2001. Fourier transform infrared study on the state of water sorbed to poly(ethylene glycol) films. *Langmuir*, **17**: 1889-1895.
168. Gemmei-Ide, M., Motonaga, T., and Kitano, H. 2006. State of irremovable water in solid polymer films examined by Fourier transform infrared spectroscopy I: Poly(ethylene glycol) dimethyl ether. *Langmuir*, **22**: 2422-2425.

169. Shen, Y., Wang, H.-t., Zhong, W., and Wu, P.-y. 2006. Two-dimensional ATR-FTIR spectroscopic study on the water diffusion behavior in polyimide/silica nanocomposite. *Chinese Journal of Chemical Physics*, **19**: 481-484.
170. Chan, K.L.A. and Kazarian, S.G. 2004. Visualization of the heterogeneous water sorption in a pharmaceutical formulation under controlled humidity via FT-IR imaging. *Vibrational Spectroscopy*, **35**: 45-49.
171. Lemus, R. 2004. Vibrational excitations in H2O in the framework of a local model. *Journal of Molecular Spectroscopy*, **225**: 73-92.
172. Al-Abadleh, H.A. and Grassian, V.H. 2003. FT-IR study of water adsorption on aluminum oxide surfaces. *Langmuir*, **19**: 341-347.
173. Bouteiller, Y. and Perchard, J.P. 2004. The vibrational spectrum of (H2O)2: comparison between anharmonic ab initio calculations and neon matrix infrared data between 9000 and 90 cm-1. *Chemical Physics*, **305**: 1-12.
174. Ohno, K., Okimura, M., Akai, N., and Katsumoto, Y. 2005. The effect of cooperative hydrogen bonding on the OH stretching-band shift for water clusters studied by matrix-isolation infrared spectroscopy and density functional theory. *Physical Chemistry Chemical Physics*, **7**: 3005-3014.
175. Fornes, V. and Chaussidon, J. 1978. An interpretation of the evolution with temperature of the v2 + v3 combination band in water. *Journal of Chemical Physics*, **68**: 4667-71.
176. Wagner, R., Benz, S., Moehler, O., Saathoff, H., Schnaiter, M., and Schurath, U. 2005. Mid-infrared extinction spectra and optical constants of supercooled water droplets. *Journal of Physical Chemistry A*, **109**: 7099-7112.
177. Praprotnik, M., Janezic, D., and Mavri, J. 2004. Temperature dependence of water vibrational spectrum: A molecular dynamics simulation study. *Journal of Physical Chemistry A*, **108**: 11056-11062.
178. Schaefer, J. and Stejskal, E.O. 1976. Carbon-13 nuclear magnetic resonance of polymers spinning at the magic angle. *Journal of the American Chemical Society*, **98**: 1031-2.
179. Tishmack, P.A., Bugay, D.E., and Byrn, S.R. 2003. Solid-state nuclear magnetic resonance spectroscopy-pharmaceutical applications. *Journal of Pharmaceutical Sciences*, **92**: 441-474.
180. Harris, R.K. 2006. NMR studies of organic polymorphs & solvates. *Analyst (Cambridge, United Kingdom)*, **131**: 351-373.
181. Offerdahl, T.J. and Munson, E.J. 2004. Solid state NMR spectroscopy of pharmaceutical materials. *American Pharmaceutical Review*, **7**: 109-112.
182. Harris, R.K. 2004. NMR crystallography: the use of chemical shifts. *Solid State Science*, **6**: 1025-1037.
183. Reutzel-Edens, S.M. and Bush, J.K. 2002. Solid-state NMR spectroscopy of small molecules: from NMR crystallography to the characterization of solid oral dosage forms. *American Pharmaceutical Review*, **5**: 112-115.
184. Majolino, D., Corsaro, C., Crupi, V., Venuti, V., and Wanderlingh, U. 2008. Water diffusion in nanoporous glass: an NMR study at different hydration levels. *The Journal of Physical Chemistry. B*, **112**: 3927-30.

185. Soria, J., Sanz, J., Sobrados, I., Coronado, J.M., Maira, A.J., Hernandez-Alonso, M.D., and Fresno, F. 2007. FTIR and NMR study of the adsorbed water on nanocrystalline anatase. *Journal of Physical Chemistry C*, **111**: 10590-10596.
186. Benesi, A.J., Grutzeck, M.W., O'Hare, B., and Phair, J.W. 2004. Room temperature solid surface water with tetrahedral jumps of 2H nuclei detected in 2H2O-hydrated porous silicates. *Journal of Physical Chemistry B*, **108**: 17783-17790.
187. Yoshioka, S., Aso, Y., Osako, T., and Kawanishi, T. 2008. Wide-ranging molecular mobilities of water in active pharmaceutical ingredient (API) hydrates as determined by NMR relaxation times. *Journal of Pharmaceutical Sciences*, **4258-4268**.
188. Yoshioka, S., Aso, Y., Osako, T., and Kawanishi, T. 2008. Wide-ranging molecular mobilities of water in active pharmaceutical ingredient (API) hydrates as determined by NMR relaxation times. *Journal of Pharmaceutical Sciences*, **97**: 4258-4268.
189. Vogt, F.G., Dell'Orco, P.C., Diederich, A.M., Su, Q., Wood, J.L., Zuber, G.E., Katrincic, L.M., Mueller, R.L., Busby, D.J., and DeBrosse, C.W. 2006. A study of variable hydration states in topotecan hydrochloride. *Journal of Pharmaceutical and Biomedical Analysis*, **40**: 1080-1088.
190. Vogt, F.G., Brum, J., Katrincic, L.M., Flach, A., Socha, J.M., Goodman, R.M., and Haltiwanger, R.C. 2006. Physical, crystallographic, and spectroscopic characterization of a crystalline pharmaceutical hydrate: understanding the role of water. *Crystal Growth & Design*, **6**: 2333-2354.
191. Labuza, T.P. and Busk, G.C. 1979. An analysis of the water binding in gels. *Journal of Food Science*, **44**: 1379-1385.
192. Yoshioka, S. and Aso, Y. 2005. A quantitative assessment of the significance of molecular mobility as a determinant for the stability of lyophilized insulin formulations. *Pharmaceutical Research*, **22**: 1358-1364.
193. Masuda, K., Tabata, S., Sakata, Y., Hayase, T., Yonemochi, E., and Terada, K. 2005. Comparison of molecular mobility in the glassy state between amorphous indomethacin and salicin based on spin-lattice relaxation times. *Pharmaceutical Research*, **22**: 797-805.
194. Aso, Y., Yoshioka, S., and Terao, T. 1994. Effect of the binding of water to excipients as measured by 2H-NMR relaxation time on cephalothin decomposition rate. *Chemical & Pharmaceutical Bulletin*, **42**: 398-401.
195. Aso, Y., Yoshioka, s., and Kojima, S. 1996. Relationship between water mobility, measured as nuclear magnetic relaxation time, and the crystallization rate of amorphous nifedipine in the presence of some pharmaceutical excipients. *Chemical & Pharmaceutical Bulletin*, **44**: 1065-1067.
196. Yoshioka, S., Aso, Y., and Miyazaki, T. 2006. Negligible contribution of molecular mobility to the degradation rate of insulin lyophilized with poly(vinylpyrrolidone). *Journal of Pharmaceutical Sciences*, **95**: 939-943.
197. Xiang, T.-X. and Anderson, B.D. 2005. Distribution and effect of water content on molecular mobility in poly(vinylpyrrolidone) glasses: a molecular dynamics simulation. *Pharmaceutical Research*, **22**: 1205-1214.

198. Aso, Y., Yoshioka, S., Zhang, J., and Zografi, G. 2002. Effect of water on the molecular mobility of sucrose and poly(vinylpyrrolidone) in a colyophilized formulation as measured by 13C-NMR relaxation time. *Chemical & Pharmaceutical Bulletin*, **50**: 822-826.
199. Glasstone, S., *Textbook cf. Physical Chemistry. 2nd ed*. 1946 Van Nostrand, New York.
200. Carpick, R.W. and Salmeron, M. 1997. Scratching the surface: fundamental investigations of tribology with atomic force microscopy. *Chemical Reviews (Washington, D. C.)*, **97**: 1163-1194.
201. Finot, E., Lesniewska, E., Mutin, J.C., Hosain, S.I., and Goudonnet, J.P. 1996. Contact force dependence on relative humidity: investigations using atomic force microscopy. *Scanning Microscopy*, **10**: 697-708.
202. Berard, V., Lesniewska, E., Andres, C., Pertuy, D., Laroche, C., and Pourcelot, Y. 2002. Affinity scale between a carrier and a drug in DPI studied by atomic force microscopy. *International Journal of Pharmaceutics*, **247**: 127-137.

Chapter 2

A Survey of Hygroscopicity of Pharmaceutical Crystals

2.1 Abstract

The aim of the present study is (i) to investigate the water sorption behavior of pharmaceutical crystals and (ii) to assess the potential risk involved in predicting long-term water uptake from short-term water sorption studies. Forty pharmaceutical compounds were randomly chosen from the United States Pharmacopoeia, and their hygroscopicity was determined by automated sorption microbalance (ASM) and RH (relative humidity) chamber storage methods. The different water sorption behaviors of these compounds could be categorized into four groups: surface sorption, hydrate formation, liquid crystal formation, and deliquescence. ASM and RH chamber storage methods showed consistent water uptake results in 37 of the 40 compounds. Discrepancy between these two techniques was observed in homochlorcyclizine·2HCl, trifluoperazine·2HCl and theophylline, which underwent polymorphic transition, liquid crystal formation, and hydrate formation, respectively. The RH_0, which is the RH over their saturated solutions, of 19 water soluble compounds correlated well with their solubilities when the solute mole fraction in their saturated solutions was < 0.1. The initial water sorption rate of urea during deliquescence showed a linear correlation with the difference between environmental RH and RH_0. Carbamazepine form **II** showed higher tendency of hydrate formation in the solid state than form **III**, which was attributed to the existence of vacancy channels in the crystal lattice of form **II**. The water uptake of 20 pharmaceutical excipients was also investigated by RH storage and ASM.

2.2 Introduction

Pharmaceutical solids may be exposed to water vapor during formulation manufacture or subsequent storage.[1, 2] Water can be adsorbed to the surface[3, 4] or absorbed into the bulk.[5-7] The sorbed (adsorbed/absorbed) water molecules can interact with the surrounding drug molecules through hydrogen bonding, van der Waals forces, and, if the solid is ionic, ion-dipole interactions.[8] The physical and chemical properties of pharmaceutical materials are critically dependent on the sorbed water.[9] Flow,[10] compaction,[11] caking,[12, 13] disintegration,[14] dissolution,[15] hardness,[16] and chemical stability[17] are some of the properties influenced by the presence of water in the solid. Below the deliquescence RH, the equilibrium water content of the solid has a finite value that can be determined at a given temperature and RH.

The rate and extent of water sorption depends on the nature of water-solid interactions.[18] Five types of interactions of water with pharmaceutical solids have been reported: surface adsorption, capillary condensation, hydrate formation, deliquescence, and absorption into disordered regions.[8, 9, 17, 19] The amount of surface adsorption is theoretically very small (< 0.5%, wlw) and determined by the surface area of the solid.[8] Capillary condensation might occur in porous samples.[20] Water can be incorporated into the lattice to form a hydrate.[21] Drug could dissolve in the surface adsorbed water and deliquesce at RH > RH_0, which is defined as the RH above its saturated solution.[22] Amorphous compounds, when compared to their crystalline counterparts, sorb much more water because of their high free volume.[23] Pharmaceutical processes, such as milling and compaction, can generate lattice disorder, which may lead to significant changes in the water sorption behavior of a compound.[24] It should be noted that more than one type of interaction may be involved in the water sorption process observed in a pharmaceutical solid.

Hygroscopicity has become an important criterion in selecting drug candidates during development.[25] A 5% water uptake without hydrate formation will probably pose challenges both in compound handling and in formulation processing.[25, 26] Automated sorption microbalance (ASM) is routinely used in industry to investigate the hygroscopicity of drug candidates, in which a small amount of sample (~ 5 mg) is exposed to humid nitrogen purge for a period of time and the weight changes are recorded automatically. Due to compressed time lines and limited resources, the hygroscopicity of a compound is usually determined over a short period of time. The question to be thus answered is how confident can we be in predicting the long-term (6 months - 2 years) water sorption behavior from the ASM studies (several hours at each RH step).

There are two possible scenarios when we compare the short term water uptake determined by ASM with the results of long term RH chamber storage. If there is a good agreement between the two techniques, the ASM could be effectively used to predict long-term water uptake. When the water sorption storage results from ASM and RH chambers storage are not in agreement, the possibility of water sorption induced phase transformation (hydrate formation, liquid crystal formation, deliquescence) needs to be taken into consideration. This lack of agreement may result from long lag time for nucleation controlled solid-state reactions. The purpose of this study is to determine the percentage of drugs that fall into the first category and the factors contributing to the lack of agreement.

In the present study, 40 compounds were randomly chosen from USP XXVIII (2005). The water uptake of these compounds was quantified by ASM and RH chamber storage techniques. The result enabled us to evaluate the possibility of predicting long-term water uptake from short-term sorption studies. The correlation between deliquescence RH and solubility was studied. The initial rate of water uptake of urea during deliquescence was determined at different RH

values. The effect of crystal structure on the water sorption behavior was investigated using carbamazepine and indomethacin as model compounds.

2.3 Materials and Methods

2.3.1 Materials

List of pharmaceutical active ingredients used in this study

Name	Purity	Batch number	Company
Atropine	99%	Lot No. 094K0833	Sigma
Benzocaine	99%	Lot No. 044K0697	Sigma
Carbamazepine	98%	Lot No. 54H0869	Sigma
Chloramphenicol	99%	Lot No. 123K0588	Sigma
Chloramphenicol	99%	Lot No. 03627EC	Sigma
Chloroquine diphosphate salt	99%	Lot No. 044K0782	Sigma
Chlortetracycline	99%	Lot No. 073K1208	Sigma
CrO3	99%	Lot No. 004701	Fisher
Dichlofenac sodium salt	99%	Lot No. 024K1437	Sigma
Diphehydramine hydrochloride	98%	Lot No. 033K0106	Sigma
Droperidol	99%	Lot No. 093K13336	Sigma
Ephedrine	99%	Lot No. 91H0890	Sigma
Fluphenazine dihydrochloride	99%	Lot No. 079F0400	Sigma
Haloperidol	99%	Lot No. 044K0798	Sigma
Histamine dihydrochloride	99%	Lot No. 014K1037	Sigma
Homochlorcyclizine dihydrochloride	99%	Lot No. 053F0024	Sigma
Hydralazine hydrochloride	99%	Lot No. 103K0132	Sigma
Hydroflumethizaide	98%	Lot No. 122F0832	Sigma
Hydroxyzine dihydrochloride	99%	Lot No. 0540846	Sigma
Indomethacin	99%	Lot No. 450544/1	Fluka
Isoniazid	99%	Lot No. 034K0623	Sigma
Isoxsuprine hydrochloride	99%	Lot No. 126H0421	Sigma
Methacholine chloride	98%	Batch No. 123k0641	Sigma
Methocarbamol	99%	Lot No. 086H0468	Sigma
Nalidixic acid	99%	Lot No. 102K1118	Sigma
Neostigmine bromide	99%	Lot No. 044K1636	Sigma
Nortriptyline hydrochloride	99%	Lot No. 044K1243	Sigma
Papaverine hydrochloride	99%	Lot No. 093K1359	Sigma
Phenazopyridine hydrochloride	99%	Lot No. 018F0184	Sigma
Phenytoin sodium	99%	Batch No. 072k0778	Sigma
Primidone	99%	Lot No. 048F0043	Sigma
Procaine hydrochloride	99%	Batch No. 424019/1	Fluka

Pyrazine	99%	Lot No. 044K0198	Sigma
Pyrimethamine	99%	Lot No. 010K0270	Sigma
Sodium valproate	99%	Batch No. 112k0593	Sigma
Succinyl-sulfathiazole	99%	Lot No. 56H0974	Sigma
Sulfacetamide	99%	Lot No. 103K2515	Sigma
Sulfadiazine	99%	Lot No. 96H1175	Sigma
Sulfamethoxazole	99%	Lot No. 064K1257	Sigma
Sulfisoxazole	99%	Lot No. 011K1522	Sigma
Tetraethylthiuram disulfide	98%	Lot No. 1067428 13404256	Fluka
Theophylline	99%	Lot No. 54H0640	Sigma
Trifluoperazine dihydrochloride	99%	Lot No. 120K1538	Sigma
Triflupromazine hydrochloride	99%	Lot No. 103K1059	Sigma
Urea	99.0%-100.5%	Batch No. 033k0113	Sigma
Griseofulvin	97%	Lot No. G8629A	Alfa Aesar
Phenytoin	99%	Lot No. 100K1608	Sigma)
Prednisone	99%	Lot No. 113K0753	Sigma

List of pharmaceutical excipients used in this study (obtained from Pfizer)

ID	Material	Lot. ID	Date dispersed	Material review date
RM0198	Microcrystalline cellulose (avicel PH101)	GR00138	6/29/2005	4/11/2005
RM0300	Sodium carboxymethylcellulose 7LF PH	GR00192	6/30/2005	10/6/2005
RM0370	Magnesium stearate	R15758	7/5/2005	8/31/2005
RM0528	Polysorbate 80	GR00158	7/3/2005	3/8/2005
RM0772	Ferrous sulfate 7-hydrate crystal	R17843	7/3/2005	3/31/2005
RM0945	Edetate disodium dihydrate	GR00028	6/3/2005	9/9/2005
RM1160	Dextrose anhydrous powder	R18677	7/5/2005	9/27/2006
RM1209	Lactose, anhydrous. Direct tableting	GR00198	7/5/2005	9/21/2005
RM1222	Mannitol powder	R15775	7/5/2005	11/31/2005
RM1275	Sorbitol	R17738	7/3/2005	5/10/2005
RM1303	Sucrose, extra fine granular	R16543	7/5/2005	1/31/2005
RM2097	Croscarmellose sodium, acdi-sol	GR00130	6/29/2005	4/19/2005
RM2293	Cellulose acetate: type 39810	GR00131	7/5/2005	11/5/2005
RM2610	Citric acid: anhyd fine granular	GR00154	7/3/2005	5/21/2005
RM2705	Sodium benzoate	R18568	7/5/2005	4/30/2005
RM3902	Calcium stearate	R18551	6/30/2005	3/20/2005
RM3929	HPMC acetate succinate AS/HF	R18616	7/5/2005	3/17/2005
RM4368	Calcium phosphate dibasic anhydous (unmilled, A-tab)	GR00060	7/3/2005	1/5/2005
RM4451	Calcium carbonate	GR00139	7/5/2005	2/11/2005
RM5270	Hypromellose (methocel E3 premium LV)	GR00339	7/5/2005	10/3/2005

2.3.2 Long-term Water Sorption Studies

The water sorption experiments of 40 compounds were conducted at 75 and at 93% RH (RT). For the RH chamber storage, saturated NaCl or KNO_3 solutions (in contact with excess solid) were placed in the well of desiccators to maintain the RH at 75.3% or 93.5%, respectively. All the drugs were used as received and the initial water content was < 0.1% w/w. The powder sample (200-400 mg) was placed in a 20 ml scintillation vial. The depth of the powder bed was < 2 mm. Vials were then stored in the humidity chambers and their weights were recorded monthly using an electronic balance (± 0.0001 g) up to one year. The experiments were conducted in triplicate. The water uptake was represented as a percent weight change with respect to the initial weight.

2.3.3 Automated Sorption Microbalance (ASM)

Sample powder (~5 mg), as received, was placed in the sample quartz boat of an automated vapor sorption microbalance (DVS-1000, Surface Measurement Systems, London, UK). The microbalance was calibrated using a 100 mg standard weight. The relative humidity sensor was calibrated at 5.0, 11.3, 32.8, 52.8, 75.3, and 84.3% RH (25°C), using saturated salt solutions. Unless stated otherwise, all the experiments were performed at 25°C under a nitrogen purge at 200 ml/min. The samples were initially dried at 0% RH (25°C) for 3 hours and then exposed to the desired RH. The rate and extent of water uptake was determined over a range of RH conditions. The exposure time at each step varied from 1 to 3 h depending on the time required for equilibration. The attainment of equilibrium was assumed when the weight change was < 0.02% w/w in one hour. The microbalance weight drift was confirmed to be < 1 µg/hour. The experiments were conducted in duplicate. The water uptake was represented as a percent weight change with respect to the initial weight.

2.3.4 Powder X-ray Diffractometry (PXRD)

The degree of crystallinity of samples was measured by ambient temperature powder X-ray diffractometry (PXRD). About 200 mg of sample were poured into an aluminum holder by the side-drift method and exposed to Cu Kα radiation (45 kV, 40 mA) in a wide-angle X-ray diffractometer (Model D5005, Siemens, Madison, WI, USA). The instrument was operated in the step-scan mode in increments of 0.05° 2θ and counts were accumulated for 1 second at each step. A 5 - 50° 2θ angular range was employed. The data collection and analyses were performed using commercially available software (JADE, version 5.1, Materials Data Inc., Livermore, CA, USA).

2.3.5 Water Activity Measurements

The water activities of saturated solutions were determined using an RH sensor (Rotronic, Huntington, NY). Saturated solutions were typically prepared by mixing ~ 1 g of solid with ~ 500 µl deionized water. In every case, there was excess solid in contact with the solution. To enable the attainment of saturation, the water activity was obtained after equilibration for 24 h in the closed chamber.

2.3.6 Preparation of Carbamazepine Polymorphs

Anhydrous carbamazepine form **III** was obtained from Sigma Inc. (98%, Sigma) and used as received. Carbamazepine form **II** was prepared by adding ether (antisolvent) into chloroform solution of form **III**. The chloroform solution of form **III** was prepared by dispersing 10 mg of form **III** powder in 10 ml of chloroform,

followed by filtering through a 0.45 µm membrane. The form **II** precipitate was filtered by suction and dried for 30 minutes at 25ºC.

2.3.7 Preparation of Indomethacin Polymorphs

The γ- form of Indomethacin was obtained from Sigma and used as received. The α-form was precipitated from a saturated ethanol solution of γ- form by addition of DI water. The saturated ethanol solution of γ-form was prepared by dispersing 10 mg of the γ- polymorph in 10 ml of ethanol, followed by filtration through a 0.45 µm membrane filter. Ten ml of DI water was added dropwise to the saturated ethanol solution of γ-form with constant stirring. The α-form precipitate was collected by filtering through a 0.45 µm membrane filter.

2.3.8 Molecular Modeling

Using water molecules as a probe, the lattice free volumes of carbamazepine and indomethacin polymorphs were calculated by Cerius2^{TM} (version 4.6 Accelrys, San Diego, CA, USA). The crystal structures, downloaded from the Cambridge Crystallographic Data Center (http://www.ccdc.cam.ac.uk), were visualized in the crystal builder module of Cerius2^{TM}. The radius of probe was set at 1.42 Å, which is the van der Waals radius of water molecules.[27] The total free volume, occupiable, and accessible volumes were calculated assuming atoms in the lattice to be hard balls.[28]

2.4 Results and Discussion

2.4.1 Water sorption in the RH chambers

Table 2.1 lists the compounds with < 0.5% w/w water sorption after storage at 75 and 93% RH for one year in RH chamber. The solubility, melting point, the molecular weight of each compound, and the water uptake after storage in ASM for several hours are also shown. Of the 27 compounds that sorbed < 0.5% w/w water, 12, 8, and 7 compounds are basic, acidic, and neutral, respectively.

The amount of adsorbed water is proportional to the surface area of the sample. Surface adsorbed water usually does not exceed three layers of water molecules.[27] Very few active pharmaceutical ingredients have BET specific surface areas exceeding 10 m^2/g or particle size less than 1 μm.[18] Therefore, capillary condensation is not likely to occur for most pharmaceuticals. It has been shown that 0.1% water content in a powder sample with particle size of 10 μm was equivalent to 11 layers of water molecules on the surface.[8] However, the thickness of 11 layers of water amount to about 30 Å on the surface, which could not exist below the deliquescence RH.[8] Assuming no hydrate formation, a large fraction of sorbed water below RH_0 could be attributed to sorption into disordered regions (amorphous) in the surface.[8, 17, 19] Thus the amount of sorbed water would be much more than that of adsorbed water.

Table 2.2 lists the compounds which exhibited anhydrate → hydrate transformation following storage at 75 and 93% RH for one year. Theophylline anhydrate completely transformed to monohydrate after storage at 93% RH for 2 weeks. Interestingly, there was no hydrate formation nor water sorption after storage at 75% RH for one year. Theophylline monohydrate has been reported to be the thermodynamically stable form at $a_w \geq 0.5$ at 4°C and $a_w \geq 0.64$ at 30°C.[29] The apparent stability of theophylline anhydrate at 75% RH, observed in our

study, could be attributed to the high energy barrier for hydrate nucleation in the solid state.

Storage at 75 and 94% RH resulted in 27% water sorption by diclofenac sodium. The amount of water sorbed corresponded to the water content in a pentahydrate.[30] Chloroquine diphosphate (CQ) sorbed 1.8 and 2.5% (w/w) water respectively after storage at 75% and 93% RH for one year. CQ forms a non-stoichiometric hydrate with the mole ratio of water and drug ranging from 0 to 2.[31, 32] Water sorption by CQ at both RH values was very slow and the final water content in the solid did not reach the stoichiometric value for the dihydrate even after storage at 93% RH for one year. The water uptake kinetics could be attributed to the slow diffusion rate of water in the CQ crystal lattice. Hydralazine·HCl forms a monohydrate when suspended in water with a stoichiometric water content of 9%.[33] However, the water content in the sample after storage at 75 and 93% RH (25°C) for one year were 0.6 and 0.8% (w/w), respectively. The low water uptake could be attributed to slow hydrate formation kinetics in the solid state. Table 2.3 lists the solids that are thermodynamically capable of forming hydrates but sorbed < 1% w/w water after storage at 93% RH (25°C) for one year. The slow kinetics could be attributed to high transition water activity for hydrate formation (thermodynamic reason) or high energy barrier for hydrate nucleation in the solid state (kinetic reason).

Table 2.4 lists 7 compounds that deliquesced following storage at 93% RH (25°C). These compounds were found to be salts with high aqueous solubility (> 700 mg/ml, 25°C). There are also salts that sorbed < 0.5% w/w water after storage at 93% RH (25°C) for one year (Table 2.5). These compounds have much lower solubilities (< 250 mg/ml) than those in Table 2.4.

Table 2.6 lists the salts that formed liquid crystals following storage at 93% RH (25°C). Trifluoperazine·2HCl (TFP) sorbed 8 and 33.5% water after storage at 75

and 93% RH, respectively. TFP sorbed 1.4 and 8% water after storage at 75% RH (25°C) for two weeks and four months, respectively. Fluphenazine·2HCl sorbed 0.3 and 32.8% water after storage at 75 and 93% RH for one year, respectively. The formation of liquid crystalline phase was confirmed by X-ray diffractometry and is discussed in detail in Chapter 5.

2.4.2 Correlation of Short-term and Long-term Water Uptakes

The water content in the 40 compounds determined by RH chamber storage and ASM were compared at 75% (Fig. 2.1) and 93% RH (**Error! Reference source not found.**). The line with a slope of 1 represents the "ideal situation" of a prefect agreement in the amount of water uptake by the two methods. In Fig. 2.1, it could be observed that most data points showed water content < 0.5% (w/w). Water sorption < 0.5% w/w could be caused by surface disordered regions, which may not significantly affect the physicochemical properties of a compound.[7] Extra attention was paid to compounds exhibiting water uptake > 0.5% w/w by either of the two methods.

When the water sorption studies were conducted at 75% RH (25°C), in 3 compounds, the results of RH chamber storage showed poor agreement with the ASM results (Fig. 2.1). It was found that the water sorption of histamine·2HCl at 75% RH (25°C) did not reach a plateau even after storage for one year, therefore, histamine·2HCl was not further studied. HCC sorbed 1% w/w water after storage at 75% RH for one year, while a much higher uptake of 3.5% was observed in the ASM (75% RH, 25°C). From Fig. 2.2, it is evident that the water content in HCC reached a maximum of 3.5% after 3 days of storage, followed by a pronounced decrease at ~ 1%. This decrease is attributed the crystallization of a stable polymorph with a much higher deliquescence RH (details in Chapter 3). The water content of TFP reached ~ 1.5% after about 2 weeks of storage and was approximately constant thereafter for about 3 months. The water content

sharply increased to ~8% (Fig. 2.3). The second increase was attributed to a partial transformation to a liquid crystalline phase (details in Chapter 5).

Similarly, when the water sorption studies were conduced at 93% RH (25°C), in chloroquine diphosphate and theophylline, the results of RH chamber storage showed poor agreement with the ASM results (Fig. 2.4). Chloroquine diphosphate (CQ) can exist as a nonstoichiometric hydrate with varying water content depending on the environmental conditions, with mole ratio of water to drug ranging from 0 to 2.[34] In both ASM and RH chambers, the sample weight had not reached a plateau at the end of the experiments. Therefore, CQ was not further studied. Theophylline sorbed 10% w/w water and formed a monohydrate after storage at 93% RH (25°C) for 10 days. There was an induction time of 2 days before the anhydrate → hydrate transformation was detectable (Fig. 2.5). The mechanism of this transformation to hydrate was further studied in Chapter 4. When the induction time is long, the use of ASM can lead to erroneous conclusions.

ASM is widely used in industry to evaluate the water sorption potential of drug candidates. The small sample size, coupled with rapid nitrogen purge should facilitate rapid attainment of equilibrium, by increasing the rate of water vapor diffusion and heat transfer across the gas-solid interface.[35, 36] When the rate of water sorption is limited by other factors such as the rate of water diffusion in the solid or the crystallization rate of a new phase, the equilibration time can be so long as to make ASM an unsuitable technique.

2.4.3 Kinetics of Water Uptake above the Critical Relative Humidity

The kinetics of water uptake during deliquescence is influenced by the environmental conditions including water activity and temperature, as well as by the properties of the solid such as the surface area and crystallinity. Eq. 2.2 expresses the kinetics of initial water uptake:[37]

$$(dW/dt)_{initial} = k \cdot A_s \cdot p_W^0 \cdot (a_w - a_{W.C}) \qquad \text{Eqn. 2.2}$$

where k is the water uptake rate constant, A_s is the initial surface area of the solid, p_w^o is the saturated vapor pressure of water at the given temperature, a_w is the atmospheric water activity, and $a_{w,c}$ is the water activity (RH) in equilibrium with the saturated solution of the substance. If $(dW/dt)_{initial}$ is plotted against a_w, the intercept on the x-axis should be equal to $a_{w,c}$. Thus, Eqn. 2.2 links the kinetics $(dW/dt)_{initial}$ with the thermodynamic driving force (a_w - $a_{w,c}$). During pharmaceutical processing, once the compound deliquesces, even a small amount of water would cause the physical and chemical stability to deteriorate. The initial rate of water uptake during deliquescence could help us estimate the approximate water content after exposing to RH > RH0 for a short period of time.

The kinetics of water absorption above RH_0 was studied using urea as the model compound (Fig. 2.6). From this water sorption data, the initial rate of weight increase was determined based on the water uptake in the first 20 minutes. The vapor pressure of pure water is 24.9 Torr at 25˚C.[38] The specific surface area of urea was determined to be 1.0 m^2/g by the BET method. The rate of water sorption as a function of the water activity of the environment increased linearly (Fig. 2.7). RH_0, the intercept on the X axis, was determined to be 74.1% RH (25°C). The RH_0 was also determined as the RH above the saturated urea solution and was found to be 74.2 ± 0.2 % (n = 3).

2.4.4 Crystal Structure and Hygroscopicity

Polymorphs have different crystal structures, which could lead to differences in their water sorption behaviors.[39] In this section, the effect of lattice packing on rate of hydrate formation was investigated using carbamazepine and indomethacin as the model compounds.

Carbamazepine can exist in four anhydrous forms and as two dihydrate forms.[40] The water vapor sorption isotherms of forms **II** and **III** are shown in Fig. 2.8. Form **III** sorbed no more than 0.1% water at 90% RH, with little hysteresis between the sorption and desorption curves. Form **II** sorbed 2% water at 90% RH, and dehydration occurred only below 30% RH. The water sorption by Form **II** was attributed to dihydrate formation, which was confirmed by X-ray diffractometry. The tendency of form **II** to sorb water can be explained by its crystal structure. The accessible volumes for form **II** was calculated to be 521 $Å^3$/unit cell, while there was no occupiable volume for form **III** (Table 2.7). The occupiable volume in the crystal lattice is defined as the vacant space that can accommodate defined probe molecules without causing expansion of the host lattice.[41] These calculation was performed using Cerius2^{TM} software and a probe radius of 1.45 Å, (van der Waals radius of water molecule).[27] Although carbamazepine has been reported to form a hydrate above 66% RH (25°C), the mechanism of hydrate formation in the solid state has not been investigated.[42, 43] Based on the theoretical calculation, it could be proposed that water may diffuse into the crystal lattice of form **II** through the vacancy channels, followed by crystallization of a hydrate phase. In solution, anhydrous carbamazepine form **III** readily transformed to hydrate.[44, 45] However, in our studies, form **III** sorbed little water and did not undergo hydrate transformation after storage at 94% RH (25°C) for 2 weeks. This could be attributed to the high energy barrier for hydrate nucleation in the solid state.

Anhydrous indomethacin forms α- and γ- sorbed $\leq$ 0.2% water after storage at 90% RH for 3 h in ASM despite the significant difference in their lattice accessible volumes for water molecules, which are 2.36 and 27.46 $Å^3$/unit cell, respectively. It appeared that vacancy in lattice does not necessarily lead to significant water uptake unless there is a possibility to convert to a hydrate phase.

2.4.5 Water Uptake of Excipients in RH Chamber and ASM

The 20 pharmaceutical excipients can be categorized into four groups: (1) cellulose derivatives (6 excipients), (2) salts (6 excipients), (3) sugars (5 excipients), and (4) others (3 excipients). The water uptake of these excipients, following storage in RH chamber for 5 months or in ASM for several hours is tabulated (Table 2.8). In a number of compounds, storage in ASM for 3 hours resulted in approximately the same water uptake as that following storage in RH chambers for 5 months. This was however not the case in the cellulose derivatives, ferrous sulfate, dextrose, and citric acid.

The cellulose derivatives are microcrystalline cellulose (MCC), sodium carboxymethylcellulose, crosscarmellose sodium, cellulose acetate, HPMC acetate succinate, and hypromellose. The cellulose derivatives sorbed more water in the ASM than in the desiccators. This difference could be attributed to the effect of nitrogen purge in ASM, likely leading to rapid diffusion of water vapor into the powder.

The observed difference in the water uptake of ferrous sulfate heptahydrate could be attributed to the initial drying step which was done in ASM, but not in the RH chamber. When stored at 0% RH (25°C), ferrous sulfate heptahydrate partially dehydrated to form a tetrahydrate.[46] The tetrahydrate was stable between 0 and 60% RH and transformed to the heptahydrate at 70% RH.

Dextrose is capable of forming a monohydrate.[47] It sorbed 9.7% at 75% RH and deliquesced at 93% RH. In the ASM, dextrose sorbed 0.1% water at 75% RH and deliquesced at 94% RH. Storage in the RH chamber at 75% RH for 45 days, caused complete anhydrous → monohydrate transformation. However, this transformation was not observed during the short experimental time in the ASM. This is not surprising, in light of the long induction time for hydrate nucleation. The deliquescence of dextrose was very slow in the RH chamber, but occurred very rapidly in the ASM. . The behavior of citric acid can be explained along the same lines.[48]

2.5 Conclusions

The water sorption behavior of the 40 anhydrous compounds at 90% RH (25°C) was categorized into four groups: Twenty seven compounds sorbed < 0.5% w/w), 4 compounds formed hydrates, 2 compounds converted to liquid crystals, and 7 compounds deliquesced. The compounds that deliquesced and transformed to liquid crystals had high aqueous solubility (> 700 mg/ml). In most cases (37 out of 40), the water uptake in the ASM showed good agreement with the results from long-term RH chamber storage. There were three exceptions: homochlorcyclizine·2HCl, trifluoperazine·2HCl and anhydrous theophylline. It is concluded that short-term studies can serve as good predictors when water uptake is limited by the rate of water diffusion across the solid-vapor interface. The initial water sorption rate of urea during deliquescence showed a linear correlation with the difference between environmental RH and RH_0. The form **II** of anhydrous carbamazepine showed higher tendency of hydrate formation in the solid state than form **III**, which was attributed to the existence of channels in the crystal lattice of form **II**.

Table 2.1 Compounds that sorbed < 0.5% w/w water following storage at 75% and 93% RH (RT) for one year in RH chambers and 3 hours in ASM. All of these compounds were obtained and used in the anhydrous state.

				Weight change at 75% RH (%)			Weight change at 93% RH (%)			
				RH chamber		ASM[f]	RH Chamber		ASM	
Compound	M.W.[a]	m.p.[b]	Solubility[c]	Mean[d]	SD[e]		Mean	SD		Reference
Atropine	289.4	115	2.17	0.0	0.0	0.1	0.0	0.0	0.2	[49]
Benzocaine	165.2	92	0.4	0.0	0.0	0.1	0.0	0.0	0.3	[50]
Caffeine	194.2	238	21.7	0.0	0.1	0.1	0.0	0.0	0.3	[51]
Chloramphenicol	323.1	150	2.5	0.1	0.0	0.2	0.1	0.1	0.4	[52]
Chlorpheniramine maleate	390.9	129-134	160	0.0	0.0	0.1	0.0	0.1	0.4	[53]
Diphenylhydrazine	184.2	123	N/A	-0.5	0.1	-0.2	0.3	-0.9	0.1	[54]
Droperidol	379.4	145	0.001	0.4	0.4	0.0	0.1	0.4	0.1	[55]
Ephedrine HCl	201.7	208	250	0.2	0.0	0.1	0.0	0.1	0.4	[56]
Hydroflumethiazide	331.3	273	0.3	0.0	0.0	0.1	0.0	0.0	0.2	[57]
Isoniazid	137.1	172	140	0.0	0.0	0.0	0.0	0.0	0.1	[58]
Isoxsuprine HCl	301.4	203	2	0.0	0.0	0.1	0.0	0.0	0.2	[54]
Mebendazole	295.3	288	0.001	0.1	0.0	0.2	0.0	0.1	0.3	[59]
Methocarbamol	241.2	92	25	0.2	0.0	0.1	0.1	0.1	0.2	[59]
Nalidixic acid	232.2	227	0.1	0.1	0.0	0.1	0.0	0.2	0.2	[60]
Nortriptyline HCl	299.8	211	11	0.1	0.0	0.0	0.1	0.2	0.1	[61]
Papaverine HCl	339.3	147	25	0.1	0.1	0.1	0.2	0.0	0.3	[62]
Phenazopyridine HCl	213.2	235	3.2	0.2	0.0	0.2	0.3	0.0	0.4	[63]
Primidone	218.2	284	0.5			0.1	0.0	0.1	0.2	[64]
Pyrazinecarboxamide	123.1	189	20	0.2	0.1	0.1	0.1	0.1	0.2	[65]
Pyrimethamine	248.7	233-234	0.001	0.0	0.0	0.1	0.0	0.0	0.1	[66]
Succynyl-sulfathiazole	355.3	185	0.21	0.2	0.1	0.3	0.1	0.4	0.3	[67]
Sulfadiazine	250.3	254	0.08	0.1	0.0	0.1	0.0	0.2	0.2	[68]
Sulfamethoxazol	253.2	169	0.5	0.0	0.0	0.0	0.0	0.0	0.1	[69]
Sulfanilamide	172.2	164.5	7.5	0.0	0.0	0.1	0.0	0.0	0.2	[54]
Sulfisoxazole	267.3	195	0.2	0.0	0.0	0.1	0.0	0.0		[70]
Tetraethylthiuram disulfide	296.5	70	0.2	0.0	0.0	0.1	0.0	0.0	0.2	[54]
Theobromine	180.2	357	1	0.0	0.0	0.0	0.0	0.0	0.0	[54]

a. Molecular weight (molar mass, g/mol)
b. Melting point (°C)
c. Aqueous solubility at 25°C (mg of drug in 1 ml of solution)
d. Mean weight change of solid after storage for one year in RH chambers.
e. Standard deviation (n = 3).
f. Weight change of sample after storage for 3 hours in ASM

Table 2.2 Compounds that exhibit propensity for anhydrate → hydrate transformation after storage at 75% and 93% RH (25°C) for one year in RH chambers and 3 hours in ASM.

				Weight change at 75% RH (%)			Weight change at 93% RH (%)			
				RH Chamber		ASM[f]	RH Chamber		ASM	
Compound	M.W.[a]	m.p.[b]	Solubility[c]	Mean[d]	SD[e]		Mean[d]	SD[e]		Reference
Chloroquine diphosphate	dihydrate	515.86	freely soluble	1.8	0.0	0.6	2.5	0.0	1.1	[31, 71]
Diclofenac sodium	pentahydrate	318.13	9	27.1	0.0	27.6	27.3	0.0	28.0	[30, 72]
Hydralazine HCl	monohydrate	160.18	39	0.6	0.0	0.4	0.8	0.0	0.8	[73]
Theophylline	monohydrate	180.17	8.3	-0.2	0.0	0.1	9.9	0.0	0.1	[51]

a. Molecular weight (molar mass, g/mol)
b. Melting point (°C)
c. Aqueous solubility at 25°C (mg of drug in 1 ml of solution)
d. Mean weight change of solid after storage for one year in RH chambers. The increase in weight was attributed to water uptake.
e. Standard deviation (n = 3).
f. Weight change of sample after storage for 3 hours in ASM

Table 2.3 Compounds that sorbed < 0.5% w/w water after storage at 75% and 93% RH (25°C) for one year in RH chambers and 3 hours in ASM. These compounds can exist as hydrates, though hydrate formation was not observed in our experiments.

				Weight change at 75% RH (%)			Weight change at 93% RH (%)			
				RH Chamber		ASM[f]	RH Chamber		ASM[f]	
Compound	M.W.[a]	m.p.[b]	Solubility[c]	Mean[d]	SD[e]		Mean	SD		Reference
Caffeine	0.8 hydrate	194.2	21.7	0.0	0.1	0.1	0.0	0.0	0.3	[51]
Droperidol	dihydrate	379.4	0.001	0.4	0.4	0.0	0.4	0.1	0.1	[74]
Succynyl-sulfathiazol-e	Monohydrate	355.4	0.21	0.2	0.1	0.3	0.4	0.1	0.3	[75]
Sulfanilami-de	Monohydate	172.2	7.5	0.0	0.0	0.1	0.0	0.1	0.2	[76]

a. Molecular weight (molar mass, g/mol)
b. Melting point (°C)
c. Aqueous solubility at 25°C (mg of drug in 1 ml of solution)
d. Mean weight change of solid after storage for one year in RH chambers. The increase in weight was attributed to water uptake.
e. Standard deviation (n = 3).
f. Weight change of sample after storage for 3 hours in ASM

Table 2.4 Compounds that deliquesced following storage at 75 and 93% RH (25°C) for one year in RH chamber and 3 hours in ASM.

				Weight change at 75% RH (%)			Weight change at 93% RH (%)			
				RH Chamber		ASM[f]	RH Chamber		ASM[f]	
Compound	M.W.[a]	m.p.[b]	Solubility[c]	Mean[d]	SD[e]		Mean	SD		Reference
Diphendydramin--e HCl	291.8	167-172	858	0.1	0.0	0.0	41.1	0.8	40.2	[77]
Histamine 2HCl	111.1	250-256	freely soluble	15.0	4.2	85.8	32.5	5.9	168.0	[54]
Homochlorcyclizi-ne 2HCl	387.7	227	~ 2000	1.1	0.2	4.0	34.4	1.8	44.8	[78]
Hydroxyzine 2HCl	447.8	192-193	700.0	3.3	0.1	4.2	29.7	1.9	36.8	[79]
Neostigmine Br	303.2	167	freely soluble	0.1	0.1	0.1	17.0	1.2	40.8	[80]
Sodium valproic	166.2		2500	72.9	0.2	72.6	112.7	1.7	131.0	[81]
Triflupromazine HCl	388.8	173	1000	0.3	0.1	0.3	22.4	3.7	49.6	[82]

a. Molecular weight (molar mass, g/mol)
b. Melting point (°C)
c. Aqueous solubility at 25°C (mg of drug in 1 ml of solution)
d. Mean weight change of solid after storage for one year in RH chambers. The increase in weight was attributed to water uptake.
e. Standard deviation (n = 3).
f. Weight change of sample after storage for 3 hours in ASM

Table 2.5 Compounds that are salts but sorbed < 0.5% w/w after storage at 93% RH (25°C) for one year in RH chambers and 3 hours in ASM.

				Weight change at 75% RH (%)			Weight change at 93% RH (%)			
				RH Chamber		ASM[f]	RH Chamber		ASM[f]	Reference
Compounds	M.W.[a]	m.p.[b]	Solubility[c]	Mean[d]	SD[e]		Mean	SD		
Chlorphenirami-ne maleate	390.87	129-134	0.8	0.0	0.0	0.1	0.1	0.0	0.3	[69]
Isoxsuprine HCl	301.38	203	2	0.0	0.0	0.1	0.0	0.0	0.2	[63]
Nortriptyline HCl	299.84	211	11	0.1	0.0	0.1	0.2	0.1	0.1	[55]
Papaverine HCl	339.39	147	25	0.1	0.1	0.1	0.2	0.0	0.3	[50]
Phenazopyridi-ne HCl	213.24	235	3.2	0.2	0.0	0.2	0.3	0.0	0.4	[65]

a. Molecular weight (molar mass, g/mol)
b. Melting point (°C)
c. Aqueous solubility at 25°C (mg of drug in 1 ml of solution)
d. Mean weight change of solid after storage for one year in RH chambers. The increase in weight was attributed to water uptake.
e. Standard deviation (n = 3).
f. Weight change of sample after storage for 3 hours in ASM

Table 2.6 Compounds that formed liquid crystals after storage at 75% and 93% RH (25°C) for one year in RH chambers and 3 hours in ASM.

				Weight change at 75% RH (%)			Weight change at 93% RH (%)			
				RH Chamber		ASM[f]	RH Chamber		ASM[f]	
Compound	M.W.[a]	m.p.[b]	Solubility[c]	Mean[d]	SD[e]		Mean	SD		Reference
Fluphenazine 2HCl	510.5	235-237	70% (w/v)	0.3	0.2	0.2	32.8	0.1	38.0	83
Trifluoperazine 2HCl	480.4	243-244	660	9.8	2.3	1.7	33.5	0.0	37.8	84

a. Molecular weight (molar mass, g/mol)
b. Melting point (°C)
c. Aqueous solubility at 25°C (mg of drug in 1 ml of solution)
d. Mean weight change of solid after storage for one year in RH chambers. The increase in weight was attributed to water uptake.
e. Standard deviation (n = 3).
f. Weight change of sample after storage for 3 hours in ASM

Table 2.7 Van der Waals volume of the water molecule, total volume of the unit cell, available, occupiable, and accessible volume in the unit cell of carbamazepine and indomethacin polymorphs determined using Cerius2^{TM}

		Probe Volume[a] (Å^3)	Total Volume[b] (Å^3/unit cell)	Available Volume[c] (Å^3/unit cell)	Occupiable Volume[d] (Å^3/ unit cell)	Accessible Volume[e] (Å^3/unit cell)
Carbamazepine	Form **III**	12.77	1168.30	298.92	0.00	0.00
	Form **II**	12.77	5718.52	2250.10	521.21	521.21
Indomethacin	Form α	12.77	2501.88	663.70	27.46	27.46
	Form γ	12.77	865.77	254.18	2.36	2.36

a. Volume occupied by a water molecule as the probe[85]
b. Total volume of the unit cell in the crystal lattice of drug
c. Volume of the unit cell that is not occupied by drug molecules in the crystal lattice
d. Volume of the unit cell that can be occupied by water molecules
e. Volume of the unit cell in the crystal lattice that is accessible to water molecules from outside

Table 2.8 Water uptake of excipients following storage at 75 and 93% RH (RT) for 5 months in RH chambers and 3 hours in ASM.

	Weight change at 75% RH (%)			Weight change at 93% RH (%)		
	RH chamber		ASM[c]	RH Chamber		ASM
Compound	Mean[a]	SD[b]		Mean	SD	
Calcium phosphate dibasic anhydous (unmilled, A-tab)	0.3	0.0	1.0	3.7	0.1	6.6
Calcium stearate	0.2	0.1	0.1	0.4	0.0	0.2
Cellose acetate: type 39810	5.1	0.1	7.6	8.0	0.2	12.9
Citric acid: anhydrous fine granular	9.4	0.0	3.7	140.5	0.7	111.1
Croscarmellose sodium, acdi-sol	22.1	0.2	23.5	58.3	0.2	65.7
Dextrose anhydrous powder	10.0	0.0	0.1	133.8	1.2	19.2
Edetate disodium dihydrate	0.0	0.1	0.0	0.0	0.1	0.1
Ferrous sulfate 7-hydrate crystal	0.2	0.1	24.0	3.5	0.3	25.9
HPMC acetate succinate AS/HF	3.0	0.3	5.5	6.8	0.2	10.7
Lactose, anhydrous. Direct tableting	2.0	0.0	0.2	4.8	0.1	1.7
Magnesium stearate	0.1	0.2	1.0	1.3	0.6	3.3
Mannitol powder	0.0	0.1	0.3	0.4	0.2	1.7
Microcrystalline cellulose (avicel PH101)	3.7	0.2	8.4	8.0	0.6	16.1
Polysorbate 80	16.2	0.2	19.0	50.6	0.4	31.0
Sodium benzoate	1.9	0.0	1.3	237.7	9.6	36.6
Sodium carboxymethylcellulose 7LF PH	23.3	0.2	34.3	75.8	0.4	95.5
Sorbitol	40.0	0.2	28.2	127.5	2.6	119.0
Sucrose, extra fine granular	0.0	0.1	0.1	83.3	1.6	46.6

a. Mean weight change of solid after storage for 5 months in RH chambers. The increase in weight was attributed to water uptake.
b. Standard deviation (n = 3).
c. Weight change of sample after storage for 3 hours in ASM

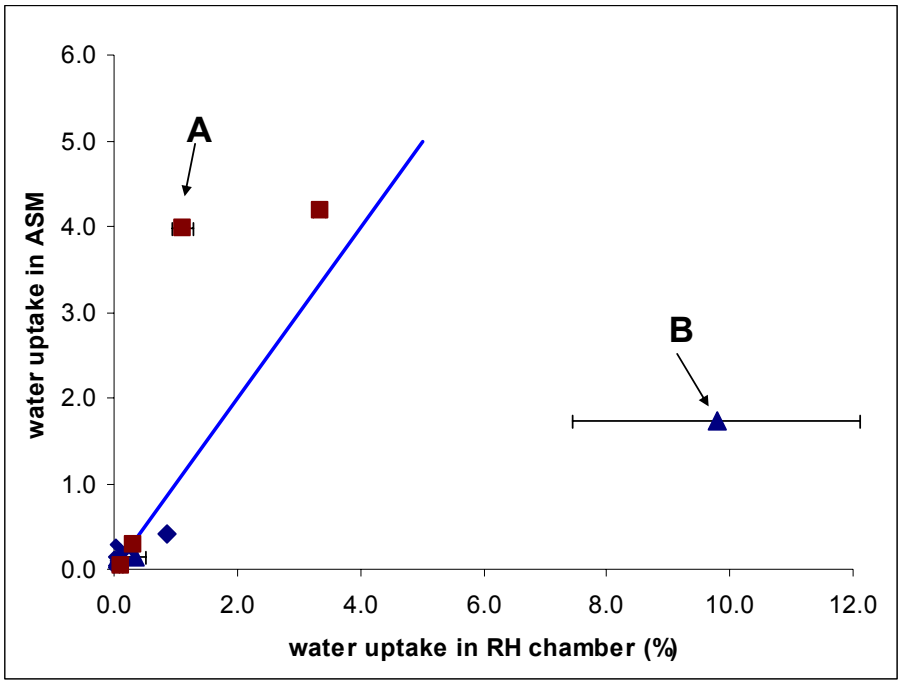

Fig. 2.1 Comparison of water uptake values in ASM for 3 hours and in RH chamber for 6 months at 75% RH (25°C). The line represents the "ideal situation" of a prefect agreement in the amount of water uptake by the two methods. A and B represent homochlorcyclizine.2HCl and trifluoperazine.2HCl, respectively. Error bars represent SD in the weight change (n = 3).

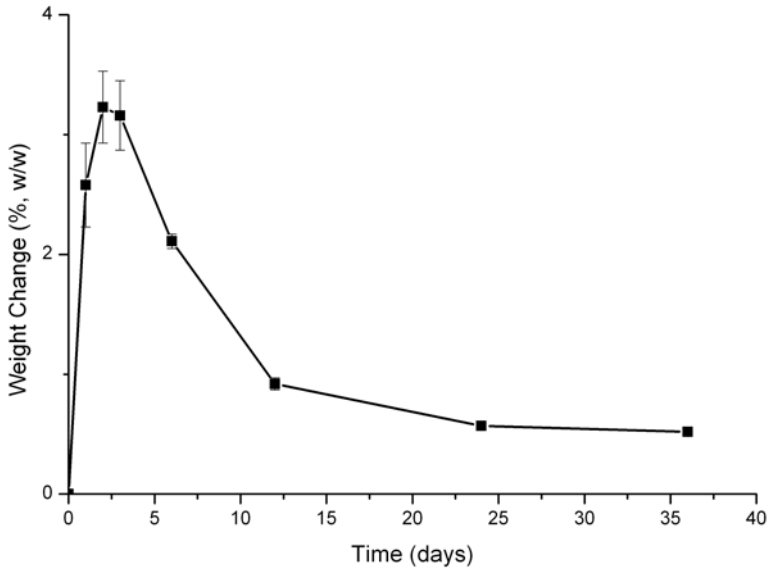

Fig. 2.2 Water uptake kinetics of homochlorcyclizine·2HCl at 75% RH (RT) in RH chamber. Error bars represent SD in the weight change (n = 3).

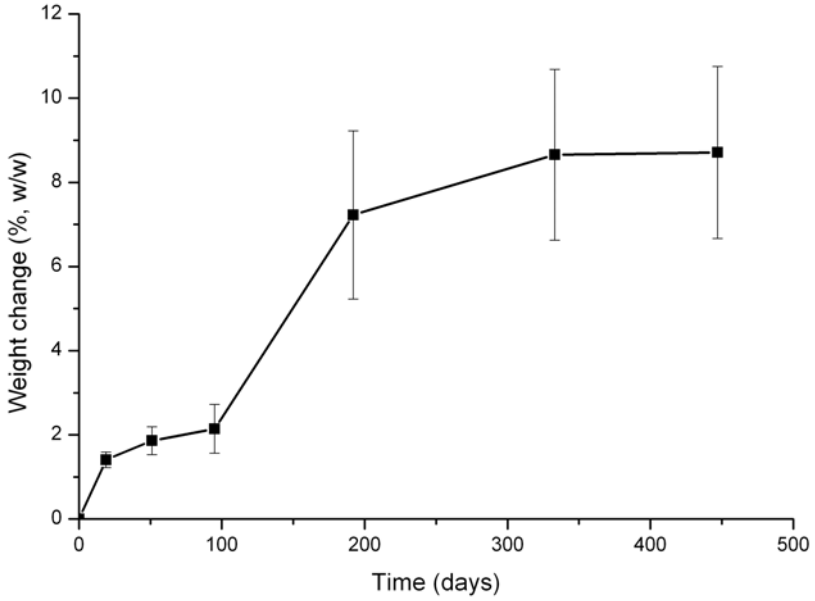

Fig. 2.3 Water sorption kinetics of trifluoperazine·2HCl in RH chamber at 75% RH (RT). Error bars represent SD in the weight change (n = 3).

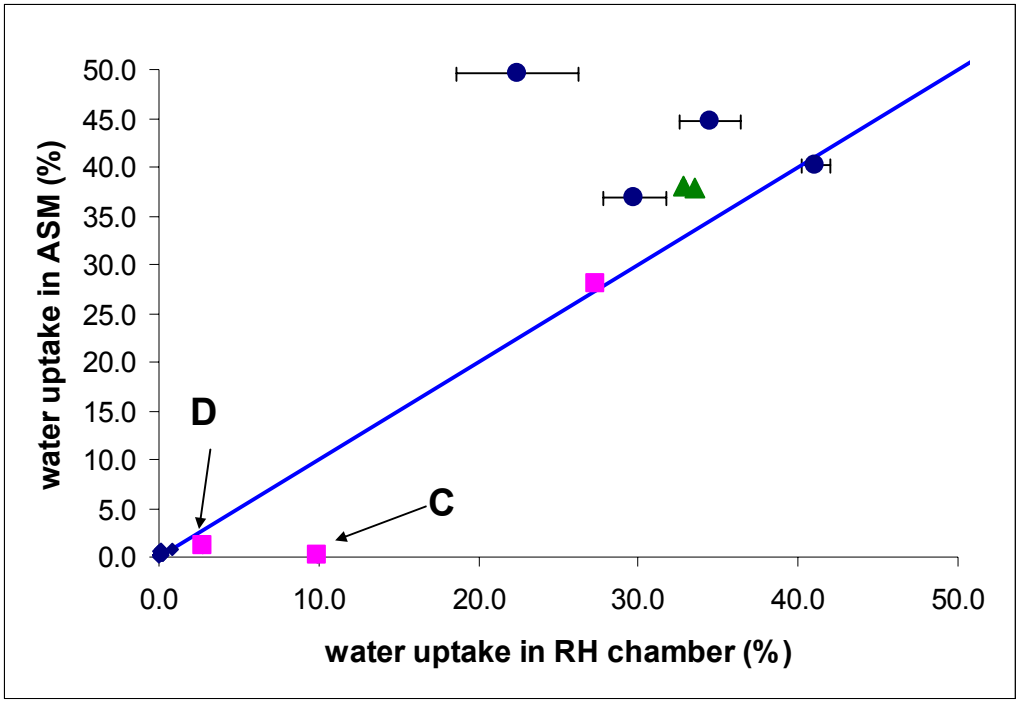

Fig. 2.4 Comparison of water uptake values in ASM for 3 hours and in RH chamber for 6 months at 93% RH (RT). The line represents the "ideal situation" of a prefect agreement in the amount of water uptake by the two methods. C and D represent theophylline and chloroquine diphosphate, respectively. Error bars represent SD in the weight change (n = 3).

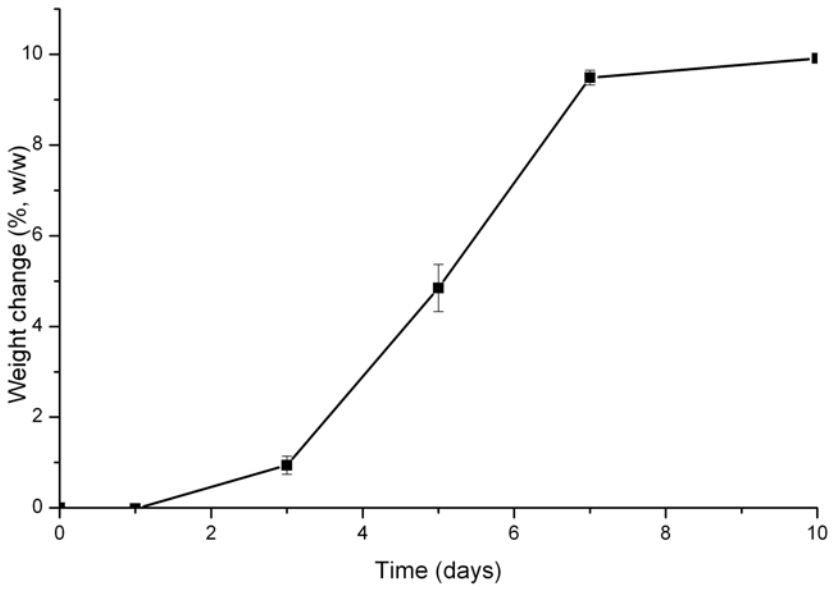

Fig. 2.5 Water uptake kinetics of theophylline at 90% RH (RT). Error bars represent SD in the weight change (n = 3).

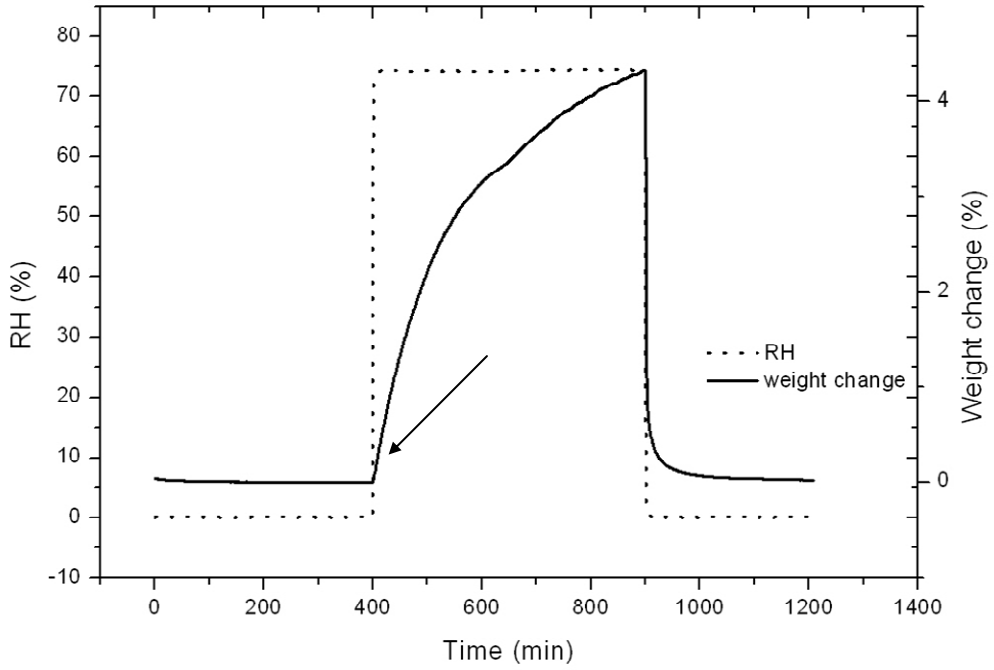

Fig. 2.6 The weight change of urea as function of time, following exposure to 75% RH (25°C), in an automated water sorption apparatus. The rate of water uptake during the first 20 min (arrow) is plotted in Fig. 2.8.

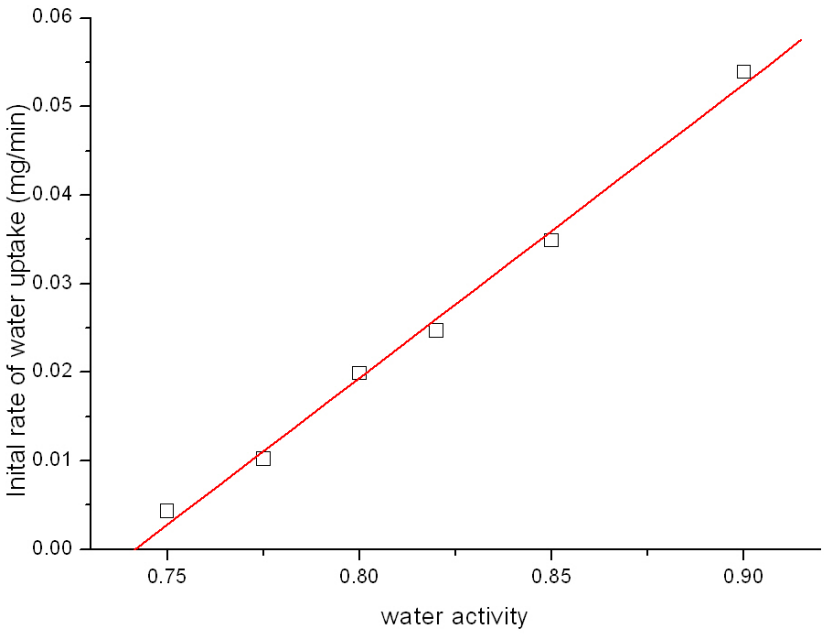

Fig. 2.7 The rate of water uptake by urea during the first 20 min after exposure to the desired water activity (at 25°C). The experiments were conducted in the ASM.

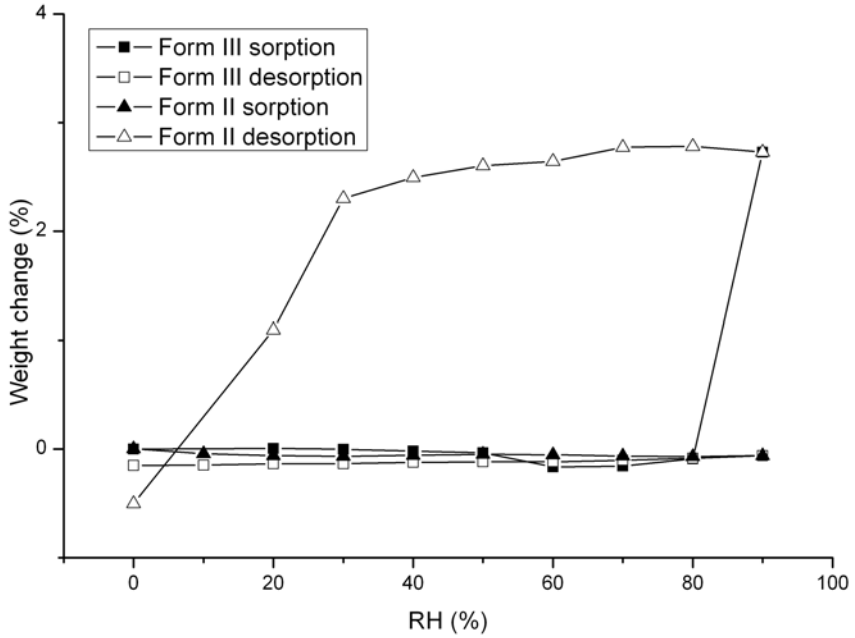

Fig. 2.8 Comparison of water sorption isotherms of carbamazepine forms **II** and **III** at 25°C. The experimental conditions are provided in the text.

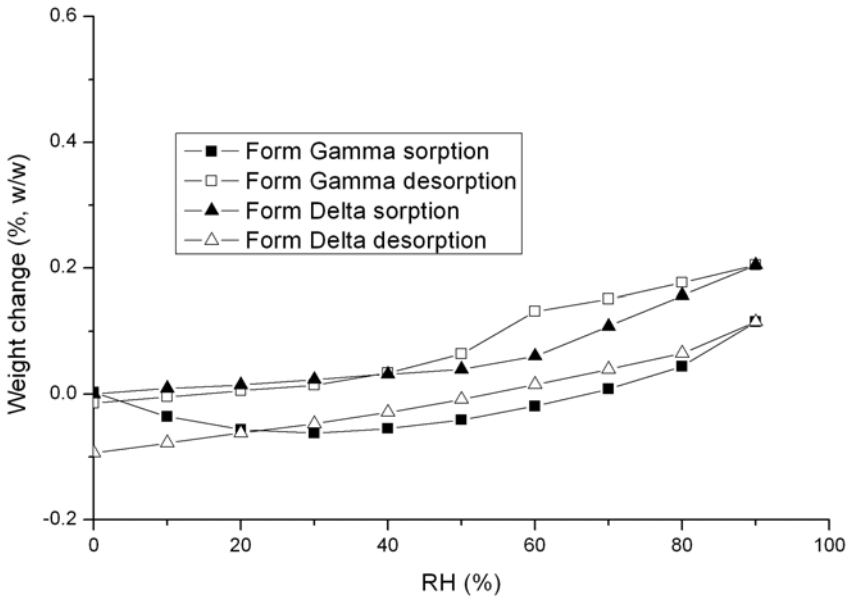

Fig. 2.9 Comparison of water vapor sorption isotherms of indomethacin γ- and α-forms at 25°C. The experimental conditions are provided in the text.

2.6 References

1. Reutzel-Edens, S.M. and Newman, A.W., *Physical characterization of hygroscopicity in pharmaceutical solids*, in *Polymorphism in the Pharmaceutical Industry*, R. Hilfiker, Editor. 2006, Wiley-VCH: Weinheim, Germany. pp. 235-258.
2. Govindarajan, R. and Suryanarayanan, R., *Processing-induced phase transformations and their implications on pharmaceutical products quality*, in *Polymorphism in the Pharmaceutical Industry*, R. Hilfiker, Editor. 2006, Wiley-VCH: Weinheim, Germany. pp. 333-364.
3. Ewing, G.E. 2006. Ambient thin film water on insulator surfaces. *Chemical Reviews*, **106**: 1511-1526.
4. Verdaguer, A., Sacha, G.M., Luna, M., Ogletree, D.F., and Salmeron, M. 2005. Initial stages of water adsorption on NaCl (100) studied by scanning polarization force microscopy. *Journal of Chemical Physics*, **123**: 124703-124703.
5. Amado Ana, M., Nolasco Mariela, M., and Ribeiro-Claro Paulo, J.A. 2007. Probing pseudopolymorphic transitions in pharmaceutical solids using Raman spectroscopy: Hydration and dehydration of theophylline. *Journal of Pharmaceutical Sciences*, **96**: 1366-79.
6. Burnett, D.J., Thielmann, F., Sokoloski, T., and Brum, J. 2006. Investigating the moisture-induced crystallization kinetics of spray-dried lactose. *International Journal of Pharmaceutics*, **313**: 23-28.
7. Newman, A.W., Reutzel-Edens, S.M., and Zografi, G. 2008. Characterization of the "hygroscopic" properties of active pharmaceutical ingredients. *Journal of Pharmaceutical Sciences*, **97**: 1047-1059.
8. Ahlneck, C. and Zografi, G. 1990. The molecular basis of moisture effects on the physical and chemical stability of drugs in the solid state. *International Journal of Pharmaceutics*, **62**: 87-95.
9. Kontny, M.J. and Zografi, G. 1995. Water-solid interactions in pharmaceutical systems. *Drugs and the Pharmaceutical Sciences*, **70**: 387-418.
10. Faqih, A.M.N., Mehrotra, A., Hammond, S.V., and Muzzio, F.J. 2007. Effect of moisture and magnesium stearate concentration on flow properties of cohesive granular materials. *International Journal of Pharmaceutics*, **336**: 338-345.
11. Sun, C.C. 2008. Mechanism of moisture induced variations in true density and compaction properties of microcrystalline cellulose. *International Journal of Pharmaceutics*, **346**: 93-101.
12. Padmadisastra, Y., Kennedy, R.A., and Stewart, P.J. 1994. Solid bridge formation in sulfonamide-Emdex interactive systems. *International Journal of Pharmaceutics*, **112**: 55-63.
13. Cleaver, J.A.S., Karatzas, G., Louis, S., and Hayati, I. 2004. Moisture-induced caking of boric acid powder. *Powder Technology*, **146**: 93-101.
14. Rohrs, B.R., Thamann, T.J., Gao, P., Stelzer, D.J., Bergren, M.S., and Chao, R.S. 1999. Tablet dissolution affected by a moisture mediated solid-state interaction between drug and disintegrant. *Pharmaceutical Research*, **16**: 1850-1856.

15. Fassihi, A.R. and Persicaner, P.H.R. 1987. Solid state interaction of bromazepam with poly(vinylpyrrolidone) in the presence of moisture. *International Journal of Pharmaceutics*, **37**: 167-170.
16. Koizumi, N.A., T.; Kouji, M.; Itai, S. 1997. Effect of water content and temperature on the stability of lornoxicam tablets. *Drug Stability*, **1**: 202-208.
17. Zografi, G. 1991. Report of the advisory panel on moisture specifications. *Pharmacopeial Forum*, **1**: 1459-1474.
18. Zografi, G. 1988. States of water associated with solids. *Drug Development and Industrial Pharmacy*, **14**: 1905-1926.
19. Kontny, M.J. and Zografi, G. 1995. Sorption of water by solids. *Drugs and the Pharmaceutical Sciences*, **70**: 387-418.
20. El-Sabaawi, M. and Pei, D.C.T. 1977. Moisture isotherms of hygroscopic porous solids. *Industrial & Engineering Chemistry Fundamentals*, **16**: 321-326.
21. Krzyzaniak, J.F., Williams, G.R., and Ni, N. 2007. Identification of phase boundaries in anhydrate/hydrate systems. *Journal of Pharmaceutical Sciences*, **96**: 1270-1281.
22. Salameh, A.K. and Taylor, L.S. 2005. Deliquescence in Binary Mixtures. *Pharmaceutical Research*, **22**: 318-324.
23. Petit, S. and Coquerel, G., *The amorphous state*, in *Polymorphism in the Pharmaceutical Industry*, R. Hilfiker, Editor. 2006, Wiley-VCH: Weinheim, Germany. pp. 259-285.
24. Hancock, B.C. and Zografi, a.G. 1996. Effects of solid-state processing on water vapor sorption by aspirin. *Journal of Pharmaceutical Sciences*, **85**: 246-8.
25. Balbach, S. and Korn, C. 2004. Pharmaceutical evaluation of early development candidates "the 100 mg-approach". *International Journal of Pharmaceutics*, **275**: 1-12.
26. Callahan, J.C., Cleary, G.W., Elefant, M., Kaplan, G., Kensler, T., and Nash, R.A. 1982. Equilibrium moisture content of pharmaceutical excipients. *Drug Development and Industrial Pharmacy*, **8**: 355-69.
27. Thiel, P.A. and Madey, T.F. 1987. The interaction of water with solid surfaces: fundamental aspects. *Surface Science Reports*, **7**: 211-385.
28. Sheth, A.R., Brennessel, W.W., Young, V.G., Jr., Muller, F.X., and Grant, D.J.W. 2004. Solid-state properties of warfarin sodium 2-propanol solvate. *Journal of Pharmaceutical Sciences*, **93**: 2669-2680.
29. Ticehurst, M.D., Storey, R.A., and Watt, C. 2002. Application of slurry bridging experiments at controlled water activities to predict the solid-state conversion between anhydrous and hydrated forms using theophylline as a model drug. *International Journal of Pharmaceutics*, **247**: 1-10.
30. Muangsin, N., Prajaubsook, M., Chaichit, N., Siritaedmukul, K., and Hannongbua, S. 2002. Crystal structure of a unique sodium distorted linkage in diclofenac sodium pentahydrate. *Analytical Sciences*, **18**: 967-968.
31. Furuseth, S., Karlsen, J., Mostad, A., Roemming, C., Salmen, R., and Toennesen, H.H. 1990. N4-(7-Chloro-4-quinolinyl)-N1,N1-diethyl-1,4-pentanediamine. An X-ray diffraction study of chloroquine diphosphate hydrate. *Acta Chemica Scandinavica*, **44**: 741-745.

32. Preston, H.S. and Stewart, J.M. 1970. Crystal structure of the antimalarial chloroquine diphosphate monohydrate. *Journal of the Chemical Society [Section] D: Chemical Communications*, 1142-3.
33. Okabe, N., Fukuda, H., and Nakamura, T. 1993. Structure of hydralazine hydrochloride. *Acta Crystallographica, Section C: Crystal Structure Communications*, **C49**: 1844-5.
34. Griesser, U.J., *The importance of solvates*, in *Polymorphism in the Pharmaceutical Industry*, R. Hilfiker, Editor. 2006, Wiley-VCH: Weinheim, Germany. pp. 211-233.
35. Van Campen, L., Amidon, G.L., and Zografi, G. 1983. Moisture sorption kinetics for water-soluble substances. II: Experimental verification of heat transport control. *Journal of Pharmaceutical Sciences*, **72**: 1388-1393.
36. Van Campen, L., Amidon, G.L., and Zografi, G. 1983. Moisture sorption kinetics for water-soluble substances. I: Theoretical considerations of heat transport control. *Journal of Pharmaceutical Sciences*, **72**: 1381-1388.
37. Carstensen, J.T., *Physical characteristics of solids.*, in *Drug Stability: Principles and Practices*, J.T.R. Carstensen, C.T., Editor. 2000, Marcel Dekker: New York, NY. pp. 209-236.
38. Weast, R.C. and Selby, S.M., *Handbook of Chemistry and Physics*. 47th ed. 1966 The Chemical Rubber, Cleveland, OH.
39. Carvajal, M.T. and Staniforth, J.N. 2006. Interactions of water with the surfaces of crystal polymorphs. *International Journal of Pharmaceutics*, **307**: 216-224.
40. Grzesiak, A.L., Lang, M., Kim, K., and Matzger, A.J. 2003. Comparison of the four anhydrous polymorphs of carbamazepine and the crystal structure of form I. *Journal of Pharmaceutical Sciences*, **92**: 2260-2271.
41. Connolly, M.L. 1985. Computation of molecular volume. *Journal of the American Chemical Society*, **107**: 1118-24.
42. McMahon, L.E.T., P.; Williams, A.; York, P. 1996. Characterization of dihydrates prepared from carbamazepine polymorphs. *Journal of Pharmaceutical Sciences*, 1064-1069.
43. Krahn, F.U. and Mielck, J.B. 1987. Relations between several polymorphic forms and the dihydrate of carbamazepine. *Pharmaceutica Acta Helvetiae*, **62**: 247-254.
44. Murphy, D., Rodriguez-Cintron, F., Langevin, B., Kelly, R.C., and Rodriguez-Hornedo, N. 2002. Solution-mediated phase transformation of anhydrous to dihydrate carbamazepine and the effect of lattice disorder. *International Journal of Pharmaceutics*, **246**: 121-134.
45. Rodriguez-Hornedo, N. and Murphy, D. 2004. Surfactant-facilitated crystallization of dihydrate carbamazepine during dissolution of anhydrous polymorph. *Journal of Pharmaceutical Sciences*, **93**: 449-460.
46. Mitchell, A.G. 1984. The preparation and characterization of ferrous sulfate hydrates. *Journal of Pharmacy and Pharmacology*, **36**: 506-10.
47. Hough, E., Neidle, S., Rogers, D., and Troughton, P.G.H. 1973. Crystal structure of a-D-glucose monohydrate. *Acta Crystallographica, Section B: Structural Crystallography and Crystal Chemistry*, **29**: 365-7.

48. Roelofsen, G. and Kanters, J.A. 1972. Citric acid monohydrate, C6H8O7.H2O. *Crystal Structure Communications*, **1**: 23-6.
49. Al-Badr, A.A. and Muhtadi, F.J., *Atropine*, in *Analytical Profiles of Drug Substances*, K. Florey, Editor. 1985, Academic Press: New York, NY. pp. 325-390.
50. Ali, S.L., *Benzocaine*, in *Analytical Profiles of Drug Substances*, K. Florey, Editor. 1983, Academic Press: New York, NY. pp. 73-104.
51. Edwards, H.G.M., Lawson, E., de Matas, M., Shields, L., and York, P. 1997. Metamorphosis of caffeine hydrate and anhydrous caffeine. *Journal of the Chemical Society, Perkin Transactions 2*, **2**: 1985-1990.
52. Szulczewski, D. and Eng, F., *Chloramphenicol*, in *Analytical Profiles of Drug Substances*, K. Florey, Editor. 1975, Academic Press: New York, NY. pp. 47-90.
53. Eckhart, C.G. and McCorkle, T., *Chlorpheniramine maleate*, in *Analytical Profiles of Drug Substances*, K. Florey, Editor. 1978, Academic Press: New York, NY. pp. 43-80.
54. *The United States Pharmacopeia*. 2005, United States Pharmacopieal Convention: Rockville, MD.
55. Janicki, C.A. and Gilpin, R.K., *Droperidol*, in *Analytical Profiles of Drug Substances*, K. Florey, Editor. 1978, Academic Press: New York, NY. pp. 171-192.
56. Ali, S.L., *Ephedrine hydrochloride*, in *Analytical Profiles of Drug Substances*, K. Florey, Editor. 1986, Academic Press: New York, NY. pp. 233-282.
57. Orzech, C.E., Nash, N.G., and Daley, R.D., *Hydroflumethiazide*, in *Analytical Profiles of Drug Substances*, K. Florey, Editor. 1978, Academic Press: New York, NY. pp. 297-318.
58. Brewer, G.A., *Isoniazid*, in *Analytical Profiles of Drug Substances*, K. Florey, Editor. 1977, Academic Press: New York, NY. pp. 183-258.
59. Al-Badr, A.A. and Tariq, M., *Mebendazole*, in *Analytical Profiles of Drug Substances*, K. Florey, Editor. 1987, Academic Press: Orlando, FL. pp. 291-326.
60. Grubb, P.E., *Nalidixic Acid*, in *Analytical Profiles of Drug Substances*, K. Florey, Editor. 1979, Academic Press: New York, NY. pp. 371-398.
61. Hale, J.L., *Nortriptyline hydrochloride*, in *Analytical Profiles of Drug Substances*, K. Florey, Editor. 1972, Academic Press: New York, NY. pp. 233-248.
62. Hifnawy, M.S. and Muhtadi, F.J., *Analytical profile of papaverine hydrochloride*, in *Analytical Profiles of Drug Substances*, K. Florey, Editor. 1988, Academic Press: New York, NY. pp. 367-448.
63. Blessel, K.W., Rudy, B.C., and Senkowski, B.Z., *Phenazopyridine hydrochloride*, in *Analytical Profiles of Drug Substances*, K. Florey, Editor. 1974, Academic Press: New York, NY. pp. 465-482.
64. Daley, R.D., *Primidone*, in *Analytical Profiles of Drug Substances*, K. Florey, Editor. 1973, Academic Press: New York, NY. pp. 409-438.
65. Felder, E. and Pitre, D., *Pyrazinamide*, in *Analytical Profiles of Drug Substances*, K. Florey, Editor. 1983, Academic Press: New York, NY. pp. 433-462.

66. Loutfy, M.A. and Aboul-Enein, H.Y., *Pyrimethamine*, in *Analytical Profiles of Drug Substances*, K. Florey, Editor. 1983, Academic Press: New York, NY. pp. 463-482.
67. Gu, C.-H. and Grant, D.J.W. 2001. Estimating the relative stability of polymorphs and hydrates from heats of solution and solubility data. *Journal of Pharmaceutical Sciences*, **90**: 1277-1287.
68. Stober, H. and DeWitte, W., *Sulfadiazine*, in *Analytical Profiles of Drug Substances*, K. Florey, Editor. 1982, Academic Press: New York, NY. pp. 523-554.
69. Rudy, B.C. and Senkowski, B.Z., *Sulfamethoxazole*, in *Analytical Profiles of Drug Substances*, K. Florey, Editor. 1973, Academic Press: New York, NY. pp. 467-486.
70. Rudy, B.C. and Senkowski, B.Z., *Sulfisoxazole*, in *Analytical Profiles of Drug Substances*, K. Florey, Editor. 1973, Academic Press: New York, NY. pp. 487-506.
71. Hong, D.D., *Chloroquine phosphate*, in *Analytical Profiles of Drug Substances*, K. Florey, Editor. 1976, Academic Press: New York, NY. pp. 61-86.
72. Adeyeye, C.M. and Li, P.-K., *Diclofenac sodium*, in *Analytical Profiles of Drug Substances*, K. Florey, Editor. 1990, Academic Press: San Diego, CA. pp. 123-144.
73. Orzech, C.E., Nash, N.G., and Daley, R.D., *Hydralazine hydrochloride*, in *Analytical Profiles of Drug Substances*, K. Florey, Editor. 1979, Academic Press: New York, NY. pp. 283-314.
74. Blaton, N.M., Peeters, O.M., and De Ranter, C.J. 1980. 1-{1-[4-(4-Fluorophenyl)-4-oxobutyl]-1,2,3,6-tetrahydro-4-pyridyl}-1,3-dihydro-2H-benzimidazol-2-one dihydrate (dehydrobenzperidol). *Acta Crystallographica, Section B: Structural Crystallography and Crystal Chemistry*, **B36**: 2828-30.
75. Rodier, N., Chauvet, A., and Masse, J. 1978. Crystal structure of succinylsulfathiazole monohydrate. *Acta Crystallographica, Section B: Structural Crystallography and Crystal Chemistry*, **B34**: 218-21.
76. Alleaume, M. and Decap, J. 1968. Three-dimensional refinement of sulfanilamide monohydrate structure. *Acta Crystallographica, Section B: Structural Crystallography and Crystal Chemistry*, **24**: 214-22.
77. Holcombe, I.J. and Fusari, S.A., *Diphenhydramine hydrochloride*, in *Analytical Profiles of Drug Substances*, K. Florey, Editor. 1974, Academic Press: New York, NY. pp. 173-232.
78. Nakano, K. 1968. Kinetic studies on the decomposition of homochlorocyclizine in aqueous solution. *Yakugaku Zasshi*, **88**: 259-65.
79. Tsau, J. and DeAngelis, N., *Hydroxyzine dihydrochloride*, in *Analytical Profiles of Drug Substances*, K. Florey, Editor. 1978, Academic Press: New York, NY. pp. 319-342.
80. Al-Badr, A.A. and Tariq, M., *Neostigmine*, in *Analytical Profiles of Drug Substances*, K. Florey, Editor. 1987, Academic Press: Orlando, FL. pp. 403-444.

81. Chang, Z.L., *Sodium valproate and valproic acid*, in *Analytical Profiles of Drug Substances*, K. Florey, Editor. 1979, Academic Press: New York, NY. pp. 529-553.
82. Florey, K., *Trifluprομazine hydrochloride*, in *Analytical Profiles of Drug Substances*, K. Florey, Editor. 1973, Academic Press: New York, NY. pp. 523-550.
83. Florey, K., *Fluphenazine hydrochloride*, in *Analytical Profiles of Drug Substances*, K. Florey, Editor. 1973, Academic Press: New York, NY. pp. 263-295.
84. Post, A., Warren, R.J., and Zarembo, J.E., *Trifluoperazine hydrochloride*, in *Analytical Profiles of Drug Substances*, K. Florey, Editor. 1980, Academic Press: New York, NY. pp. 543-582.
85. Henderson, M.A. 2002. The interaction of water with solid surfaces: fundamental aspects revisited. *Surface Science Reports*, **46**: 1-308.

Chapter 3

Polymorphic Transition of Homochlorcyclizine Dihydrochloride Induced by Water Vapor Sorption

.

3.1 Abstract

Our goal is to understand the role of the water in the solid state polymorphic transformation in anhydrous homochlorcyclizine·2HCl (HCC). HCC can exist in two anhydrous forms, **I** and **II**. The RH_0 of forms **I** and **II** was determined to be 75 and 85%, respectively, indicating that form **I** was metastable at 25°C. When form **I** was stored at 75% RH (25°C), the water content increased to 3.5% and then decreased to 1% and X-ray diffractometry (XRD) revealed that during storage form **I** had transformed to form **II**. The unit cell parameters, calculated from the synchrotron diffraction patterns, showed that form **II** is denser than form **I**. The crystal structure of the acetonitrile solvate of HCC was determined by X-ray crystallography. Based on XRD, the desolvated form was found to be structurally similar to form **I**. The polymorphic transformation was continuously monitored by infrared spectroscopy and XRD. Water sorption led to lattice rearrangement, followed by the crystallization of **II**. The polymorphic transformation (**I** → **II**), occurred only at RH values close to RH_0 of form **I**. It is proposed that water acted as "structure loosener" during the polymorphic transformation.

3.2 Introduction

Most pharmaceutical compounds can exist in different crystalline forms, in which the same molecule is packed in different 3-dimensional structures[1] and/or exhibit different conformations.[2] Different polymorphs exhibit different physical and chemical properties such as melting point, solubility, dissolution kinetics, and stability.[1] Formulations containing the metastable forms may undergo polymorphic transformations during manufacture or storage, which could cause decrease in dissolution rate or bioavailability.[3-5] In the summer of 1998, ritonavir capsule formulation was recalled because of the emergence of a new stable polymorph during manufacture. Polymorphs are also patentable in US, which may have considerable economic benefit.[6]

When a saturated solution of the metastable polymorph is prepared, the solution would be supersaturated with respect to the stable form because the stable form has a lower free energy and thus lower solubility than the metastable form. The solubility difference between the metastable and stable form would be the driving force for the crystallization of the stable form. Once the stable form nucleates, the solution-mediated metastable → stable transformation will proceed through dissolution and crystal growth.[7, 8] Ultimately, only the stable form will remain in contact with the saturated solution. The kinetics of transformation will be influenced by many factors including the type and concentration of impurities[6] and the solvent used.[7]

Many pharmaceuticals, including phenylbutoazone,[9] succinylsulfathiazole,[10] and sulfameter,[11, 12] are known to undergo polymorphic transformations in the solid state. A detailed four-step mechanism of solid-state polymorphic transformation has also been proposed by Paul and Curtin: 1) lattice “loosening” in the initial stage; 2) formation of intermediate solid solution; 3) nucleation of the new solid phase; and 4) growth of the new phase.[13] Solid state polymorphic transformation

can be brought about by heat[14], vapor pressure[15, 16] or mechanical stress[17-19]. In an enantiotropic system, the low temperature stable form, when heated, may undergo transformation to the high temperature stable form (endothermic process).[20] In a monotropic system, the metastable form can spontaneously transform to the stable form (exothermic process).[21] Pressure induced polymorphic transformation are often kinetically controlled process, which could result in metastable forms.[22] The physical form of the final product can depend on many operational parameters including the compression rate, and the dwell time.[23] Mechanical processes, by providing the activation energy for the nucleation of the stable form, could induce metastable $\rightarrow$ stable polymorphic transformations.[24] Mechanical processing could also cause stable $\rightarrow$ metastable transformations. This could occur through an amorphous intermediate state wherein the metastable form may have a higher nucleation rate leading to its domination in the final product.[24]

In addition to deliquescence,[25] water sorption can also induce amorphous → crystalline[26, 27] and anhydrate → hydrate phase transformations.[28, 29] There are only a few examples of polymorphic transformations induced by water sorption. The δ- form of anhydrous mannitol sorbed water and transformed to the β-form.[30] However, close examination revealed crystallization of the stable β- form only when a slurry of a partially deliquesced δ-form was dried. Water sorption accelerated the metastable → stable transition of anhydrous theophylline in the solid state.[31, 32] Matsue and Matsuoka speculated that an "intermediate local hydrate" formed during this polymorphic transformation.[29] Interestingly, water sorption did not affect the polymorphic transition of anhydrous caffeine, a compound structurally similar to theophylline.[31]

The model compound in this study is homochlorcyclizine·2HCl (HCC). HCC is commercially available as a white or pale brown crystalline powder and is known to be hygroscopic.[33] As discussed in Chapter 2, HCC showed an interesting

water sorption behavior, wherein initial water uptake was followed by a gradual desorption (75% RH; 25°C). We propose that water sorption by the metastable form leads to structural rearrangement followed by crystallization of the stable anhydrous form. Our objective was to investigate the mechanism of water sorption induced HCC polymorphic transformation (**I** → **II**). For this purpose, in addition to crystal structure (using laboratory and synchrotron sources) studies, spectroscopic and diffraction techniques were used.

3.3 Material and Method

Homochlorcyclizine dihydrochloride (HCC) form **I** (Sigma, St. Louis, MO) was used as received. HCC form **II** was prepared by storing form **I** at 75% RH (25°C) for 30 days.

3.3.1 Water Sorption Study in RH Chamber

HCC powder sample (~200 mg) was stored in a chamber containing saturated NaCl solution (75.3% RH; 25°C) until a constant weight was attained. The experiments were conducted in triplicate. The water uptake was represented as a percent weight change with respect to the initial weight.

3.3.2 Automated Sorption Microbalance (ASM)

HCC (3 - 7 mg), as received, was placed in the sample quartz boat of an automated vapor sorption microbalance (DVS-1000, Surface Measurements Systems, London, UK). The microbalance was calibrated using a 100 mg standard weight. The relative humidity sensor was calibrated at 5.0, 11.3, 32.8, 52.8, 75.3, and 84.3% RH (25°C), using saturated salt solutions. Unless stated

otherwise, all experiments were performed at 25°C under a nitrogen purge at 200 ml/min. The sample was initially dried at 0% RH (25°C) for 3 hours then exposed to the desired RH. The rate and extent of water uptake was determined over a range of RH values from 0 to 90%. The exposure time at each step varied from 1 to 6 h depending on the time required for equilibration. The attainment of equilibrium was assumed when the weight change was < 0.02% in one hour.

3.3.3 Ambient temperature powder X-ray Diffractometry

About 200 mg of sample were packed into an aluminum holder by the side-drift method and exposed to Cu Kα radiation (45 kV, 40 mA) in a wide-angle X-ray diffractometer (Model D5005, Siemens, Madison, WI, USA). The instrument was operated in the step-scan mode over the angular range of 2 to 50° 2θ. The step size was 0.05° 2θ and counts were accumulated for 1 s at each step. The data collection and analyses were performed with commercially available software (JADE, version 5.1 Materials Data Inc., Livermore, CA, USA).

3.3.4 Variable Temperature X-ray Diffractometry (VTXRD)

An X-ray powder diffractometer (Model XDS 2000, Scintag, Cupertino, CA, USA) equipped with a variable temperature stage (Model 828D, Micristar, R. G. Hansen and Associates, Santa Barbara, CA) was used to control the sample temperature. About 50 mg of sample was filled into a copper holder and heated at 5°C/min to the temperatures of interest, held isothermally for at least 5 min, and the XRD patterns were obtained. A constant temperature was maintained during XRD scans. The angular range was from 2 to 50° 2θ in increments of 0.05° 2θ, and counts were accumulated for 1 s.

3.3.5 Differential Scanning Calorimetry (DSC)

A differential scanning calorimeter (Model 2920, TA Instruments, New Castle, DE) with a refrigerated cooling accessory was used. The instrument was calibrated with pure samples of tin and indium. About 5 mg sample was packed in aluminum pans, crimped with lids having several pinholes, and heated under dry nitrogen purge (70 ml/min) from 10 to 320°C.

3.3.6 Thermogravimetric analysis (TGA)

The sample was heated in an open aluminum pan from room temperature to 300°C, under nitrogen purge (70 ml/ min), at 10°C/min in a thermogravimetric analyzer (Q50, TA Instruments, New Castle, DE).

3.3.7 Surface Area

Specific surface area was determined by the multipoint (10 points) Brunauer-Emmett-Teller (BET) method using a surface area analyzer (Gemini 2360, Micromeritics, Norcross, GA) with nitrogen as the adsorbate and helium as a carrier gas. Accurately weighed samples were degassed under vacuum at room temperature for at least 12 h. No weight loss was detected in the samples after the surface area determination.

3.3.8 Raman Spectroscopy

The spectra, collected in a Raman spectrometer (Ram **II**, Bruker optics, Madison, WI, USA), were obtained by averaging 32 scans over 4000 to 0 cm^{-1} range at a 4-cm^{-1} resolution.

3.3.9 Near Infrared (NIR) Spectroscopy

The spectra were obtained in the reflectance mode (Vertex 70, Bruker optics, Madison, WI, USA), with a NIR fiber-coupling module. Each spectrum was the average of 32 scans over the range of 15000 to 3800 cm^{-1} with a 2 cm^{-1} resolution. The spectrum of a white ceramic plate served as the reference. The data analysis was performed with a commercially available software (OPUS, Ver. 5.05, Madison, WI, USA).

3.3.10 Water Activity Measurements

The water activities of saturated solutions were determined by an RH sensor (Rotronic, Huntington, NY). Saturated solution was prepared by mixing ~ 1 g solid with ~ 100 µl deionized water. To ensure the attainment of saturation, the water activity was obtained after equilibration for 24 h in the closed chamber.

3.3.11 Scanning Electron Microscopy

The samples were mounted on scanning electron microscopy (SEM) stubs with double-sided carbon tape, coated with platinum (50 Å) and observed under a scanning electron microscope (JEOL 6500, Tokyo, Japan).

3.3.12 Synchrotron Powder Diffraction

Synchrotron powder diffraction data were collected using the 1-BM beam line at the Advanced Photon Source (Argonne National Lab). The experimental setup used the Debye-Scherrer geometry with an image plate detector (Mar345) and a wavelength of 0.619355 Å. The calibration was performed using a silicon standard (SRM 640c; NIST) with a Si (111) crystal analyzer and a scintillation counter point detector. The sample to detector distance was set at 490.8 mm. HCC form **I** and **II** samples were filled into a capillary (1.0 mm diameter) and spun at 2 Hz. Ten diffraction frames (each was a 20 s exposure) were collected and summed. Diffraction frames were also collected at room temperature (~ 21°C) with an empty capillary and subtracted from the data frames. The powder pattern was analyzed using the FIT2D software (developed by Andy Hammersley).[34]

3.3.13 Lattice Parameter Simulation using Material Studio™

The simulations were performed using modeling and simulation product suite (Material Studio, Accelrys, San Diego, CA). The synchrotron powder diffraction data were indexed. The cell parameters, background, zero-point shift, profile parameters, and peak intensities were refined by the Pawley method, implemented using Reflex Plus. The Pseudo-Voigt profile function was used for simulating the peak shape. The background was determined by linear interpolation using 20 coefficients. The Finger-Cox-Jephcoat method of asymmetry correction was used due to axial divergence.

3.3.14 X-ray Crystallography

A single crystal of HCC acetonitrile solvate was exposed to Mo Kα radiation (λ = 0.71073 Å) at 173 K in a diffractometer (Bruker AXS, Wisconsin) with a CCD detector. The data were integrated using a commercial program (SAINT, Version 6.2, Bruker, Madison, WI, USA). The structure of the acetonitrile solvate was solved by SHELEXS-97 (SHELXTL-PLUS, version 6.1, Bruker, Madison, WI, USA). The structure was refined by full-matrix least square against F^2 using SHELXL-97. All non-hydrogen atoms were refined with anisotropic displacement parameters.

3.4 Results and discussion

3.3.1 Baseline Physical Characterization

The XRD patterns of HCC forms **I** and **II**, obtained using a synchrotron source, showed pronounced differences (Fig. 3.1). In both solids, the water content was < 0.5%. The elemental composition of forms **I** and **II** were virtually identical. The DSC curves exhibited an endotherm at ~ 240°C, attributed to melting accompanied by decomposition (Figs. 3.2 and 3.3). However, the TGA curves revealed a discernible weight loss, starting at ~ 180°C. In light of the thermal instability of HCC, DSC may not be a suitable tool to characterize the solid forms of HCC.

SEM revealed that both forms **I** and **II** were rod-shaped particles, with form **II** particles being considerably larger than form **I** (Fig. 3.4). The specific surface areas of form **I** and **II** were determined to be 8.5 and 5.4 m^2/g, respectively.

The RH_0 of forms **I** and **II** were determined to be 76.6 ± 0.4 and 84.9 ± 1.1% (n=3), respectively. The higher RH_0 value of form **II** indicates that it has a lower solubility and is more stable than form **I**.

3.4.2 Water Vapor Sorption

Fig. 3.5 shows the water sorption/desorption isotherms of form **I** at 25°C. There was negligible water uptake up to 70% RH. It sorbed 3.4% and 20% water at 75% and 80% RH, respectively. At each RH value, since the sample was exposed for only 4 hours, the system had not attained equilibrium. When exposed to 80% RH, it deliquesced and formed a viscous solution. When the RH was then progressively lowered, crystallization was not evident, probably due to the high viscosity of the system. The water uptake of 3.5% by the ASM method was considerably higher than that following storage in the RH chamber (0.5% w/w) for one year. This discrepancy can be understood by monitoring the kinetics of water sorption at 75% RH (Fig. 3.6). The water content increased to 3% and then decreased to 0.5% after storage for 3 and 36 days, respectively. At the end of the sorption experiment, the solid was identified to be form **II** by XRD.

3.4.3 HCC Acetonitrile Solvate

The molecular packing in HCC acetonitrile solvate is shown in Fig. 3.8. The unit cell parameters (monoclinic crystal system; R value of 9.2%; space group:$P2^1_c$) are: a = 16.6 Å, b = 9.7 Å, c = 13.3 Å, β = 93.7°). In the crystal structure, the two aromatic rings are at an angle of 112.5°, with disorder in the position of acetonitrile molecules. There are four HCC and four acetonitrile molecules in each unit cell with the latter along the b axis forming a channel. Since the acetonitrile did not hydrogen bond with neighboring molecules, it might have a predominantly space filling role in the lattice.

When the solvate was heated, changes in XRD pattern were readily perceptible. In particular, the intensity of the peak at 10.4° 2θ decreased with a concomitant increase in the 9.5° 2θ peak intensity (Fig. 3.9). This change could be attributed to structural adjustment after the removal of ACN from the crystal lattice. When the XRD patterns of HCC acetone desolvate (obtained by heating the acetone solvate to 90C), forms **I** and **II** were compared, the structural similarity between the desolvate and form **I** became readily apparent (Fig. 3.10). The desolvation process, as has been observed in many other pharmaceutical solvates, caused a decrease in crystallinity.[35]

The fingerprint regions in the Raman spectra of these three forms were very similar and could be explained by the lack of hydrogen bonding between HCC molecules in the crystal lattice.[36] The absence of peaks in the 2200-2000 cm^{-1} region, the region of stretching vibration of nitriles,[37] confirmed the complete removal of ACN in the desolvate. The peaks at 2455 and 2429 cm^{-1} in the desolvate, can be assigned to the stretching vibration of C-H in the piperazine ring.[38] The differences in the spectra of forms **I** and **II**, between 3000 and 3100 cm^{-1}, could be explained as being due to differences in lattice structure (Fig. 3.11).

Based on XRD and Raman spectroscopy, we propose that the lattice structures of form **I** and the acetonitrile desolvate are similar. Both forms **I** and **II** transformed to the ACN solvate when recrystallized from ACN. When exposed to dry air, the solvate could transform to form **I**, which in turn converted to form **II** at RH values ≥ 75%.

3.4.4 Thermodynamic Relation between HCC Forms I and II

The thermodynamic relationship of the two polymorphs was investigated by comparing the enthalpies and melting points. The heat-of-fusion rule states that the polymorph with higher melting point will have lower heat of fusion in an enantiotropic system. The polymorph with higher melting point will have higher heat of fusion in a monotropic system.[39] The melting of both forms of HCC was accompanied by decomposition (Fig. 3.2 and Fig. 3.3). Therefore, the heat-of-fusion rule cannot be used to evaluate the thermodynamic relationship of the two forms.

Kitaigorodskii proposed that the most stable crystal structure should be expected to have the most efficient packing, resulting in highest density.[40] This rule is expected to hold when van der Waals interactions are dominant. However, strong hydrogen bonding could lead to large voids in the crystal structure with lower density, as in ice.[16] Since there is no hydrogen bonding in HCC, the stable form should have lower cell volume. To calcuate the true density of the two forms, the cell dimensions were simulated from synchrotron diffraction patterns.[41]

The best fit for HCC form **I** was a monoclinic model, with a = 34.8 Å, b = 9.5 Å, c = 13.3 Å, α = 90.0°, β = 102.3°, γ = 90.0 (R = 9.5%) (Fig. 3.12). The best fit for HCC form **II** is an orthorhombic model, with a = 31.4 Å, b = 9.9 Å, c = 13.3 Å, α = 90.0°, β = 90.0°, and γ = 90.0° (R = 5.1%). The lattice cell volumes of HCC form **I** and **II** were calculated to be 4340 and 4170 Å^3, respectively. The simulated lattice parameters of form **I** was similar to that of HCC ACN solvate (Fig. 3.8).

The solubility ratio of polymorphs reflects the difference in free energy of different polymorphs through equation:

$$\Delta G = -RT \ln(\frac{S_1}{S_2}) . \qquad \text{Eqn. 3.1}$$

where s_1 and s_2 are the solubility of form **I** and **II**, respectively.

The free energy difference (ΔG) between two polymorphs is an intrinsic property, related to the lattice energy (enthalpy) and arrangement (entropy). Therefore, the solubility ratio should be solvent independent. HCC is very soluble in water, forming a viscous solution at high concentrations. Due to sampling difficulties, it is practically impossible to directly determine the solubility in water. From the RH_0, the approximate aqueous solubility could be estimated using the following equation:

$$s(g/ml) = \frac{1 - RH_0}{RH_0} * 387.8/18 \qquad \text{Eqn. 3.2}$$

where s is the solubility of the form, RH_0 is the RH above its saturated solution. This equation assumes that the activity coefficient of water in the saturated solution to be unity. In light of the high aqueous solubility of HCC in water, it is recognized that this assumption is unlikely to hold. However, based on the elevated RH_0 of form **II**, it could be postulated that form **II** has a lower aqueous solubility compared to form **I**. We next attempted to determine the solubility in acetone and chloroform. In both cases, form **I** transformed to form **II**, making the solubility value of form **I** unreliable. Based on the spontaneous transformation pf form **I** to form **II**, it can be concluded that form **II** is the stable form at 25°C.

3.4.5 Near Infrared Spectroscopy (NIR)

Liquid water usually shows strong NIR peaks at 6900 and 5150 cm^{-1}, which are overtones and combinations of fundamental stretching vibrations of O-H bonds.[42] The frequencies of water NIR peaks reflect the structure of hydrogen bonds between drug and water molecules.[43] The positions of water NIR peaks have been used to study the molecular mobility and chemical environment of water in pharmaceutical systems.[44-46] It was shown that sugar molecules can disrupt the

hydrogen bonding between water molecules, leading to shifting of water peaks to a longer wavelength of 5181 cm^{-1}.[47] Hydrogen bonding between water and mannitol in mannitol hemihydrate led to a shift of water peaks from 7000 to 6825 cm^{-1}.[48] Water peaks are also very sensitive to the ions presented in the solution. Even low level of salts could cause a significant shift in the water peak.[49, 50]

HCC form **I** showed a continuous increase in the intensity of the peaks at 5126 and 6872 cm^{-1} when stored at 93% RH, which could be attributed to O-H vibrations of water (Fig. 3.13). This shift of the water peak from 6900 cm^{-1} in liquid water to 6872 cm^{-1} in HCC-water system could be explained by strong ion-dipole interaction between water and HCC molecules. It was interesting to observe that HCC form **I** showed the water peaks at the same position at 75% as that at 93% RH (Fig. 3.14). It could be proposed that water strongly interacts with the ions during the polymorphic transformation at 75% RH (25°C). At 75% RH, **I** transforms to **II**, while at 94% RH, **I** undergoes deliquescence. It could be postulated that, at 75% RH, "deliquescence-like" process is initiated, followed by crystallization of form **II**.

3.4.6 Mechanism of polymorphic transformation

Form **I** was subjected to a controlled temperature program, both in the DSC and XRD. When heated up to 150°C, no thermal events were observed in the DSC. Variable temperature XRD revealed no changes in the powder pattern up to 150°C, confirming the DSC results. As discussed earlier, there was significant sample decomposition, starting at ~ 170°C (Figs. 3.2 and 3.3).

XRD patterns were also obtained as a function of time, following storage at 75% RH (25°C). Water sorption caused a decrease in the intensity of the peak at 5.2° 2θ (characteristic peak of form **I**), and a concomitant increase in the intensity of the peak at 5.4° 2θ (characteristic peak of form **II**). Interestingly, another

characteristic peak of form **II** at 10.5° 2θ was not observed during the water sorption stage. During water desorption stage, the peak at 10.5° 2θ appeared and its intensity gradually increased.

The appearance of the peak at 5.4° 2θ, and the gradual increase in its intensity, at the expense of the 5.2° 2θ peak, could be explained by the entry of water into the lattice and inducing lattice rearrangement. The crystal structure of the HCC ACN solvate was also helpful in this regard (Fig. 3.8). The chloride ions in the HCC ACN solvate were not in the immediate vicinity of the solvent channels. When water entered the lattice, rearrangement of the lattice will be required to accommodate the water molecules. A similar rearrangement of form **I** lattice might lower the activation energy barrier for the nucleation of the stable polymorph (form **II**). As the crystallization of form **II** proceeded, water was continuously expelled from the lattice (Figs. 3.6 and 3.17).

Fig. 3.15 contains the XRD patterns of HCC form **I** after storage at 68 and 54% RH (25°C) for 3 months. While no phase transformation was observed following storage at 54% RH, a small fraction of HCC form **I** transformed into form **II** after storage at 68% RH. This partial transformation may be attributed to a low concentration of lattice disorder in 'as is' form **I**. These results suggest that in crystalline **I**, the polymorphic transformation could only be induced by water sorption, and occurs at RH values close to RH_0.

Automated sorption microbalances (ASM) are widely used to evaluate the water sorption and desorption behavior of active pharmaceutical ingredients as well as excipients. As described in Chapter 2, in a large fraction of pharmaceuticals, the results obtained using the microbalance are in agreement with the results from long-term constant humidity chamber storage. However, if water sorption induces a phase transformation, the process may occur in a timescale (days or weeks) much longer than the automated sorption microbalance experimental timescale

(typically a few hours). In such instances, the automated moisture sorption balance is unsuitable to detect the phase changes.

3.5 Conclusion

In this chapter, we have investigated the mechanism of water sorption induced polymorphic transformation of anhydrous homochlorcyclizine·2HCl (HCC). HCC form **I**, when stored at 75% RH (25°C) transformed to form **II**. The RH_0 (at 25°C) of forms **I** and **II** were determined to be 76 and 85%, respectively. The unit cell parameters of form **I** and the acetonitrile solvate were substantially similar suggesting that form **I** could be a desolvated solvate. The polymorphic transformation is induced by water sorption, and occurred at RH values close to RH_0.

Acknowledgement

The synchrotron XRD experiments were performed by the stuff in the Argonne national lab. We thank Dr. Yuegang Zhang for help in molecular modeling.

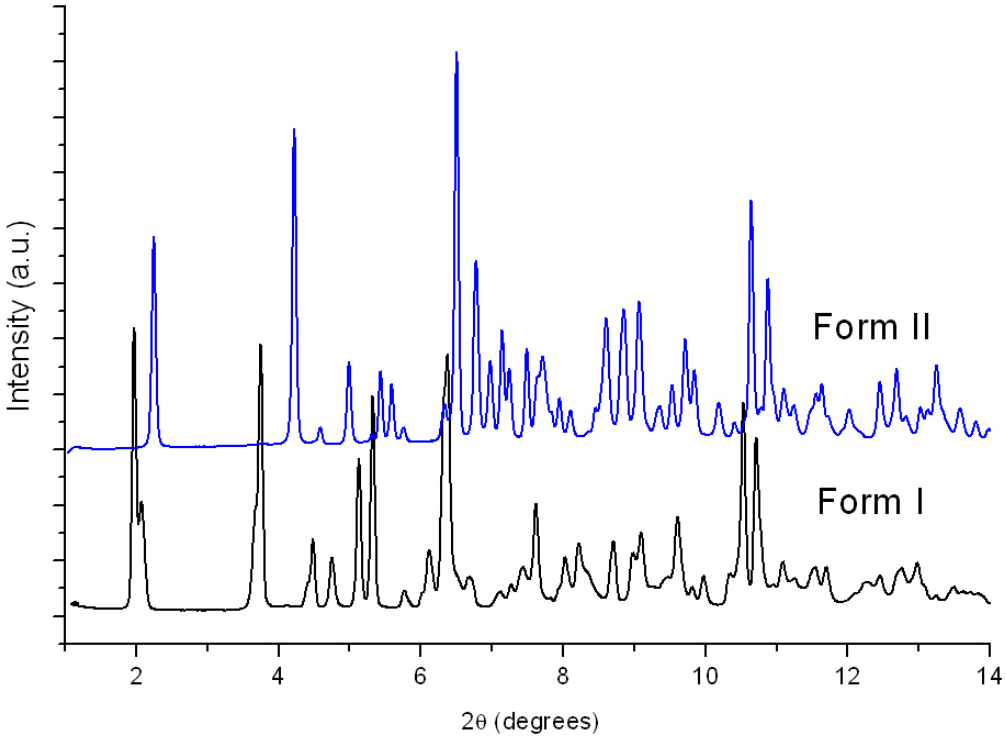

Fig. 3.1 The X-ray diffraction patterns of HCC forms **I** and **II** at RT. These were obtained using a synchrotron source (λ = 0.6193 Å).

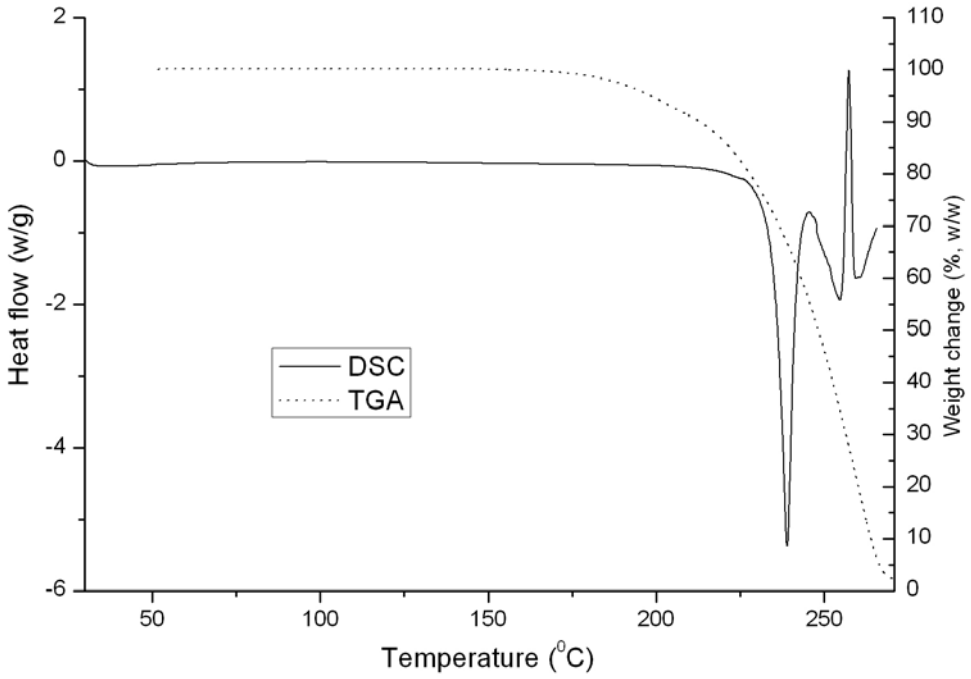

Fig. 3.2 Thermogravimetric analysis (TGA) and differential scanning calorimetry (DSC) curves of HCC form **I**.

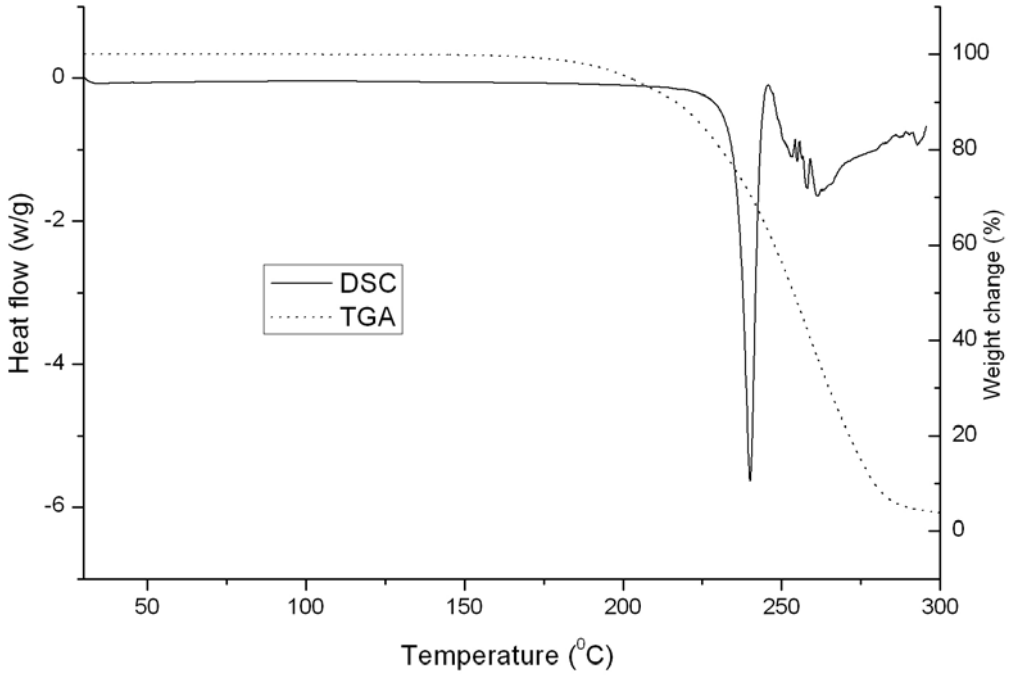

Fig. 3.3 Thermogravimetric analysis (TGA) and differential scanning calorimetry (DSC) curves of HCC form **II**.

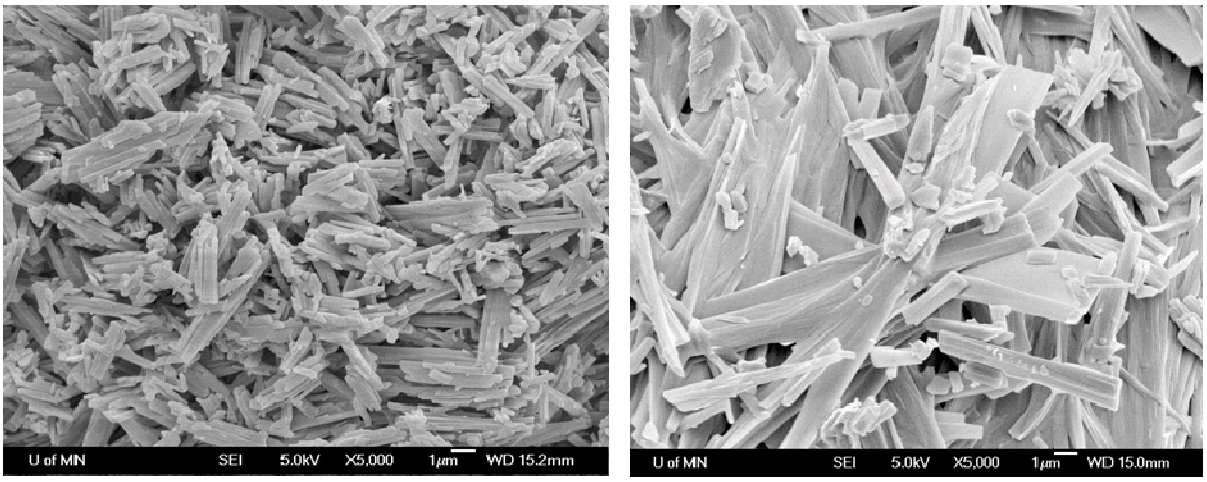

Fig. 3.4 Scanning electron microscopy images of HCC forms **I** (left) and **II** (right).

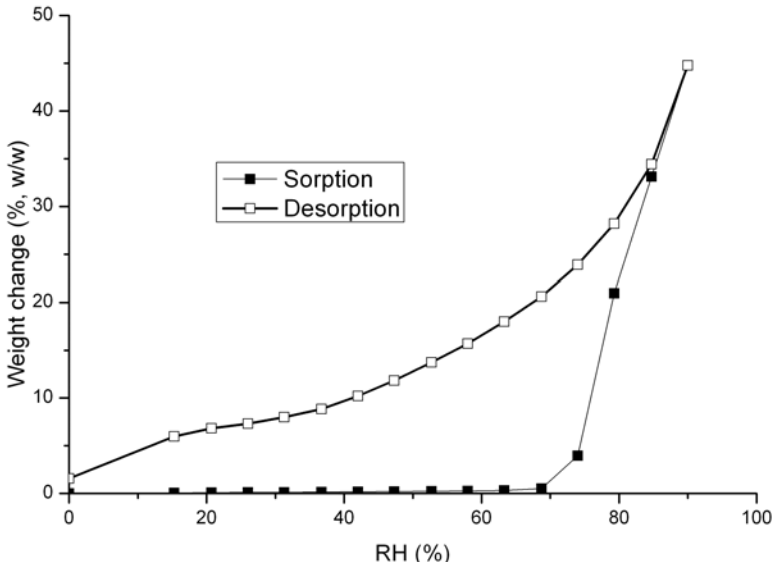

Fig. 3.5 Water sorption/desorption isotherm of HCC form **I** at 25°C.

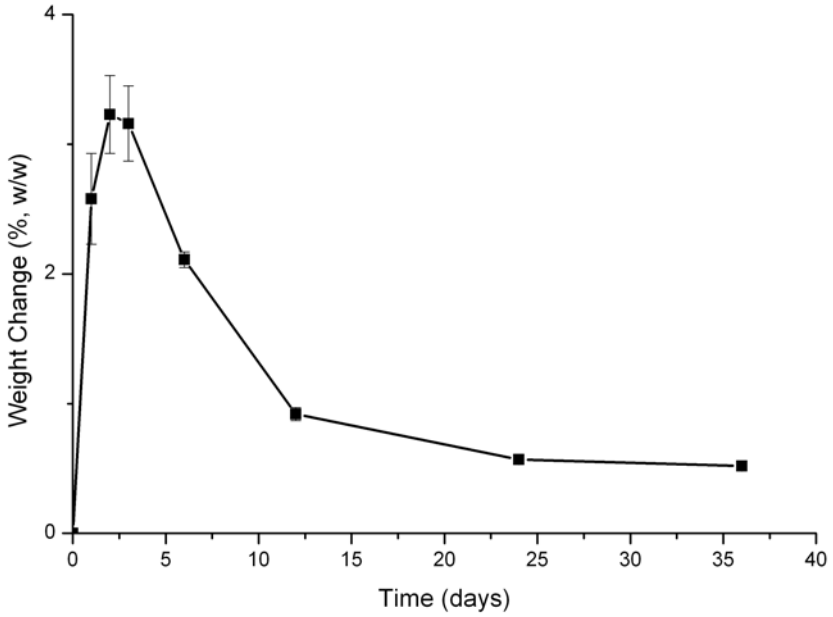

Fig. 3.6 Water uptake kinetics of HCC form **I** at 75% RH (RT). Error bars represent SD in the weight change (n = 3). In some cases, they were smaller than the size of the symbol.

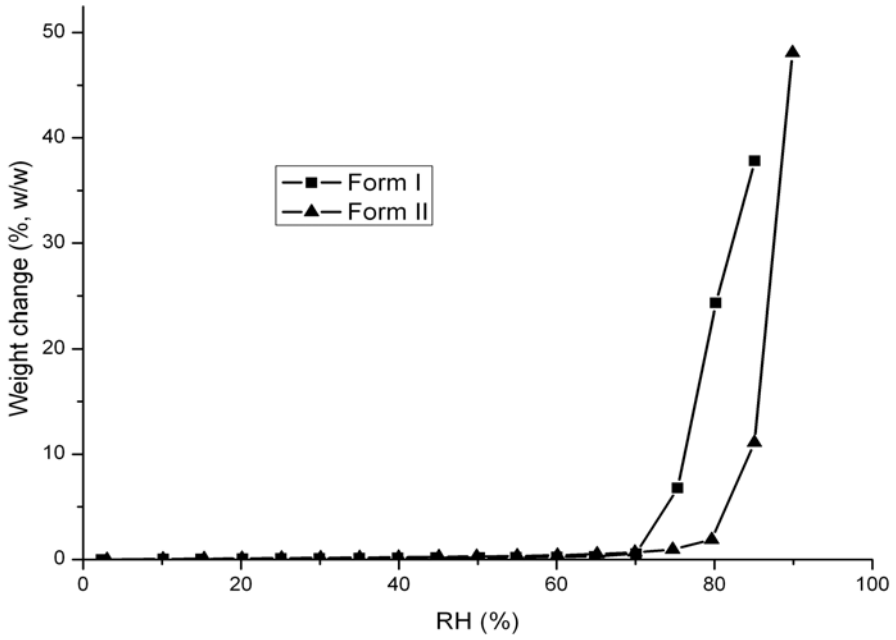

Fig. 3.7 Water sorption Isotherms of HCC forms **I** and **II** at 25°C.

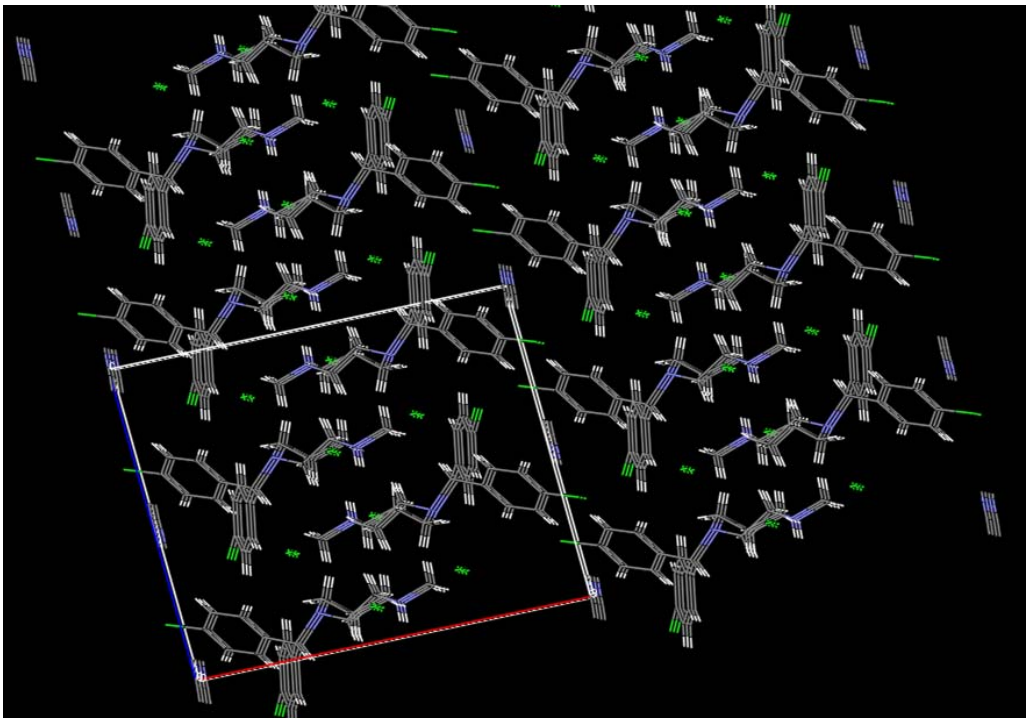

Fig. 3.8 Crystal packing of HCC acetonitrile solvate seen along *axis b*. Crystal was determined to be monoclinic (a = 16.6 Å, b = 9.7 Å, c = 13.3 Å, β = 93.7°), with a space group of $P2^1_c$.

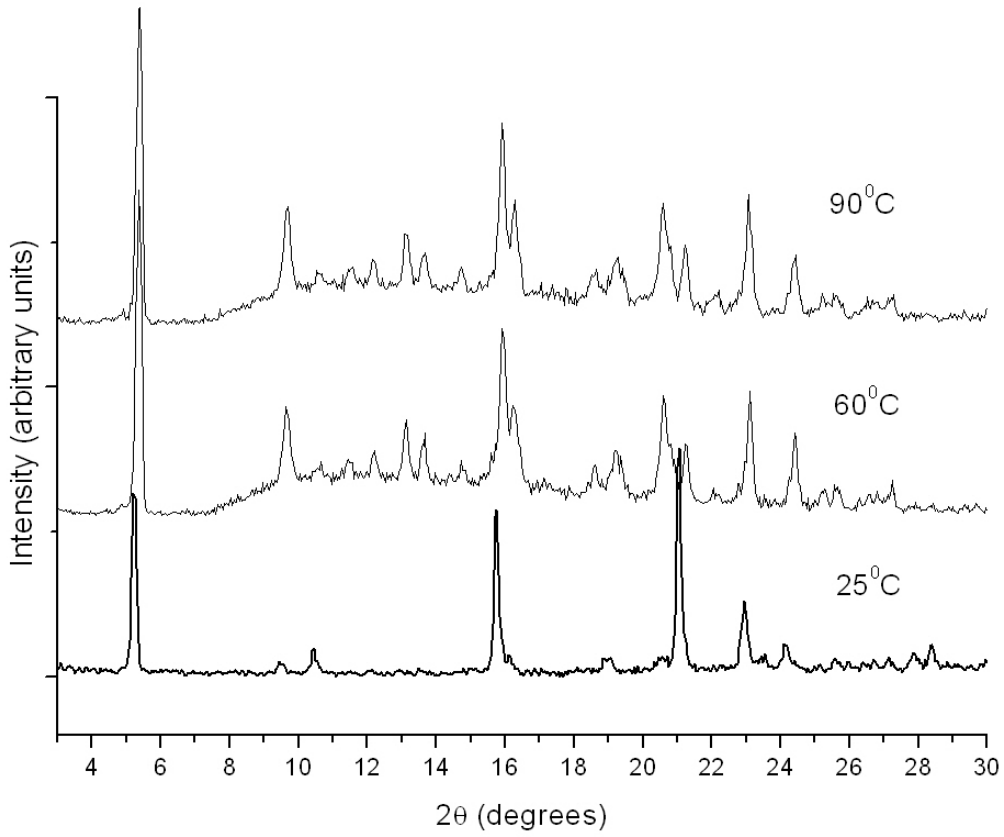

Fig. 3.9 Variable temperature XRD patterns of HCC ACN solvate. XRD patterns were obtained at the temperature indicated in the figure.

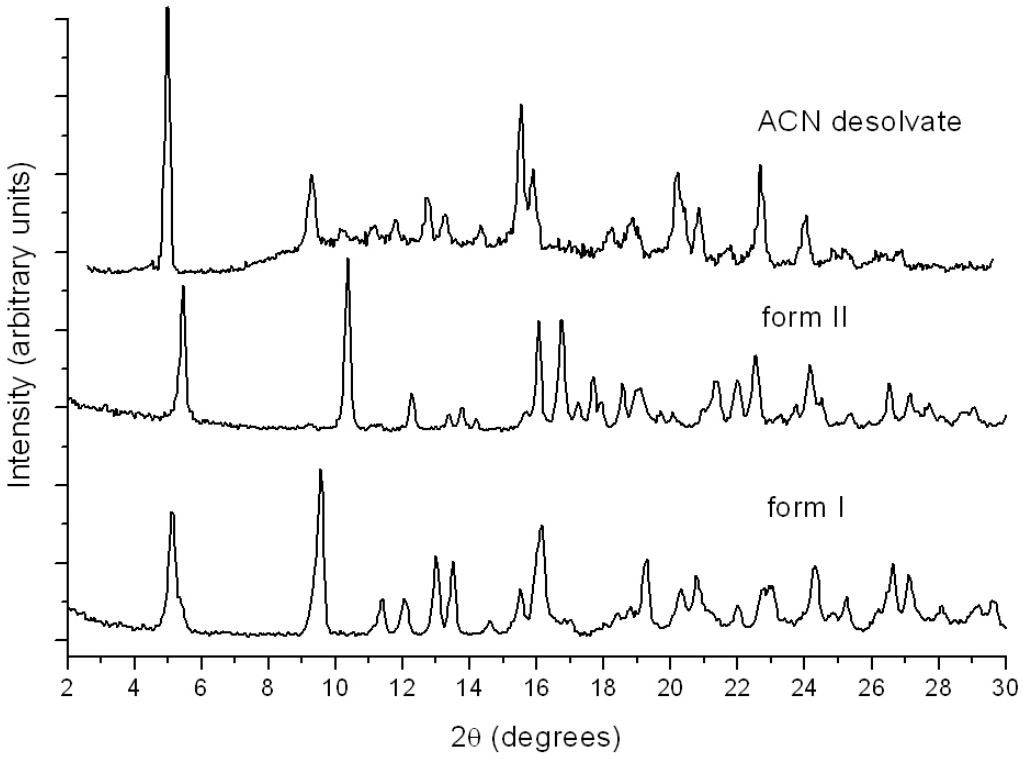

Fig. 3.10 Overlay of the ambient temperature XRD patterns of HCC acetonitrile desolvate, form **I**, and form **II**.

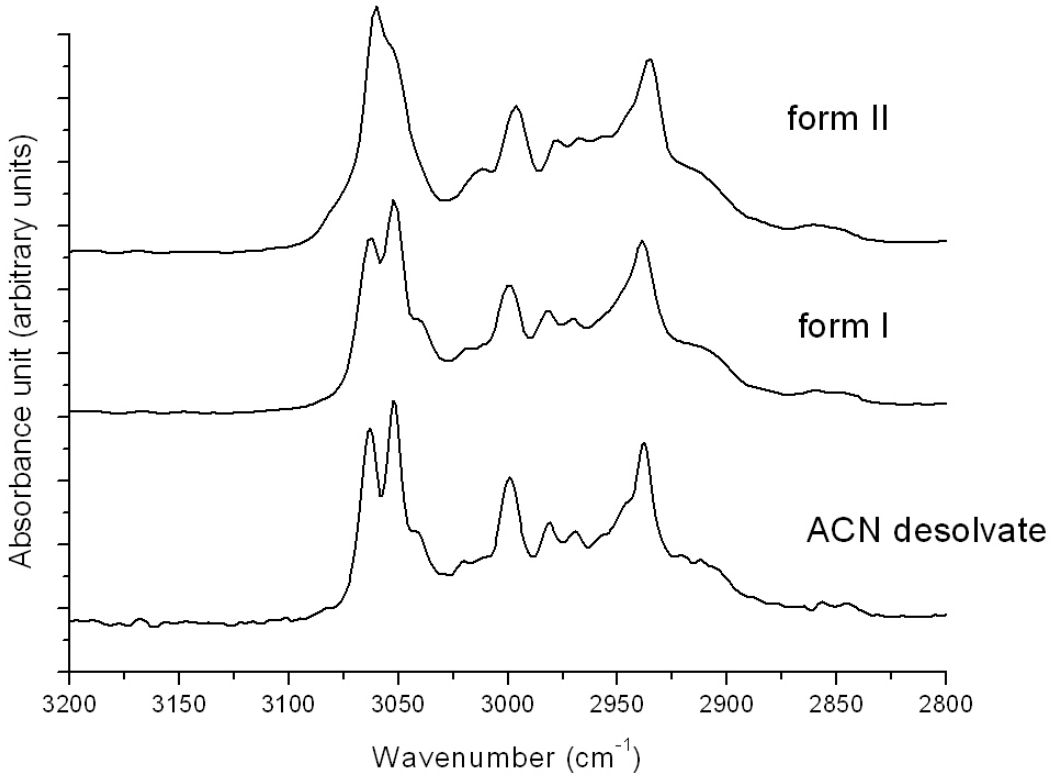

Fig. 3.11 Raman spectra of HCC ACN desolvate, form **I**, and form **II**.

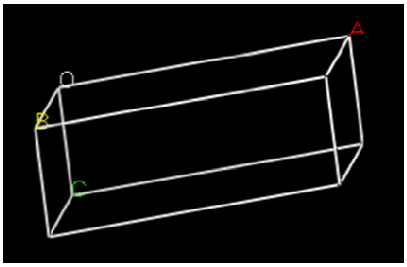

Form I Monoclinic
Volume = 4340 Å^3
a = 34.8 Å
b = 9.5 Å
c = 13.3 Å
α = 90.0°
β = 102.3°
γ = 90.0°

Form II Orthorhombic
Volume = 4170 Å^3
a = 31.4 Å
b = 9.9 Å
c = 13.3 Å
α = 90.0°
β = 90.0°
γ = 90.0°

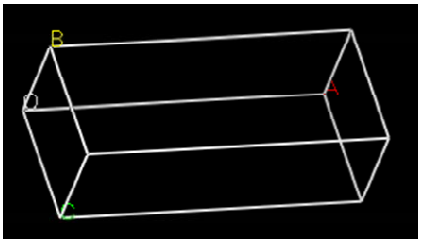

Fig. 3.12 Simulated crystal lattice structure of HCC form **I** and **II** from powder synchrotron diffraction pattern using Accelrys Material Studio™.

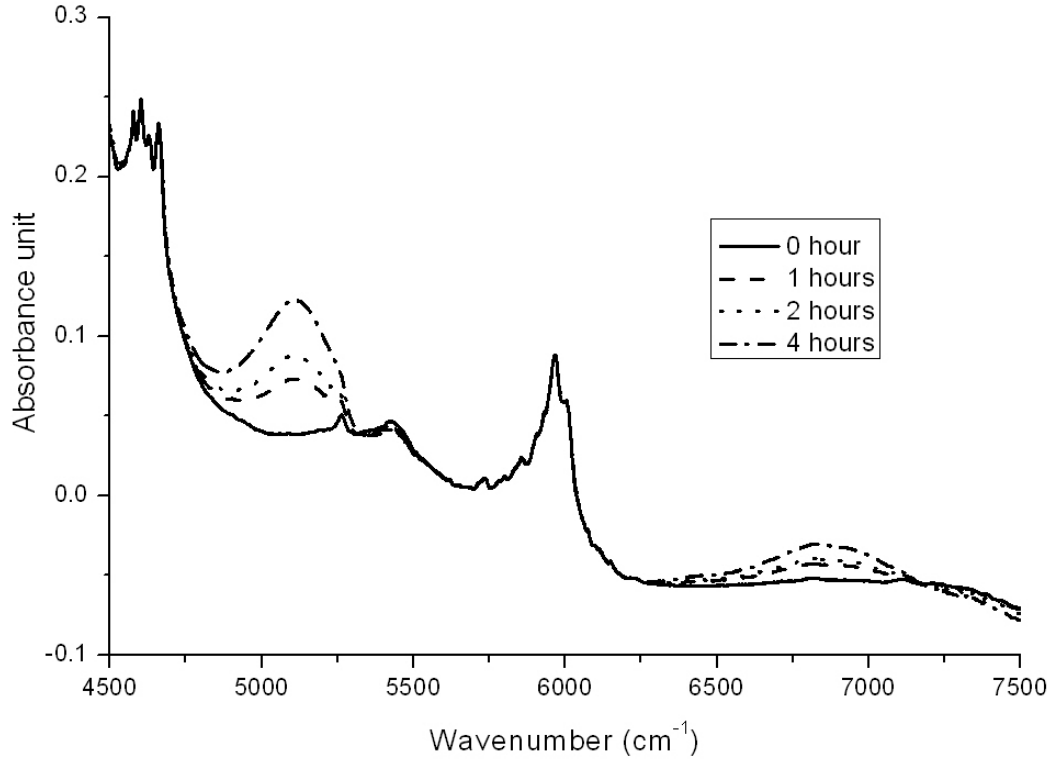

Fig. 3.13 Near infrared spectra of HCC form **I** at 75% RH (RT). Peak at 5118 cm^{-1} and 6870 cm^{-1}, which are O-H vibrations in water, increased in intensity with time.

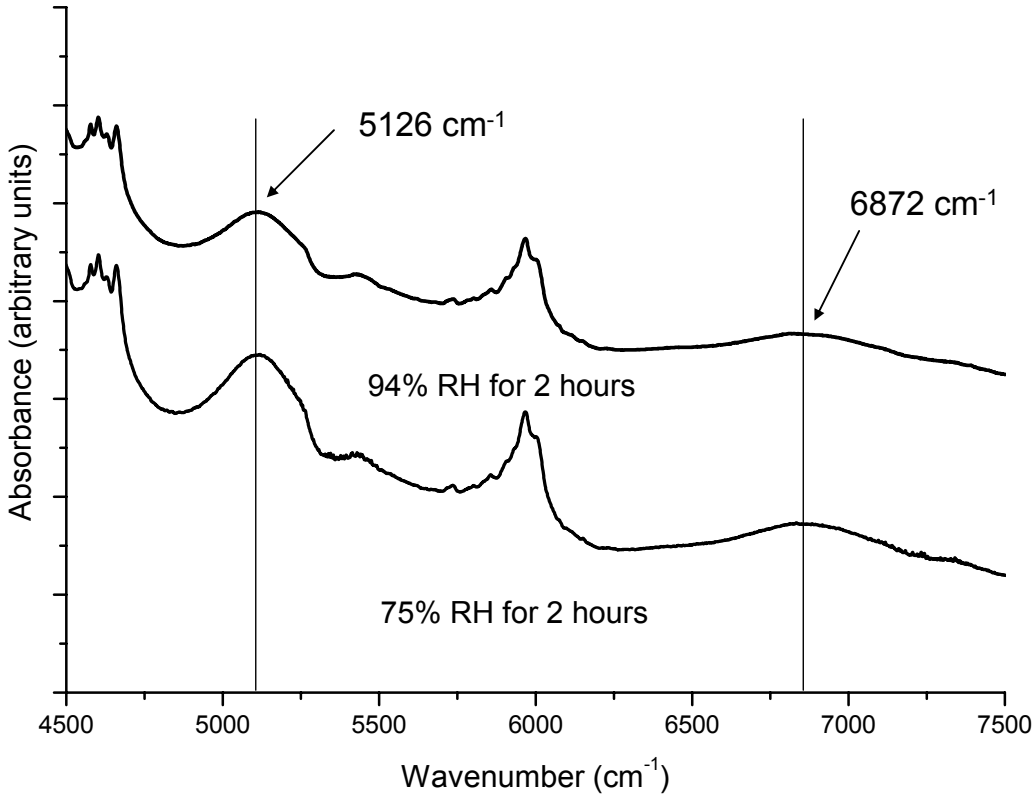

Fig. 3.14 Near infrared spectra of HCC form **I** at 75 and 93% RH (RT). Water peak positions are shown.

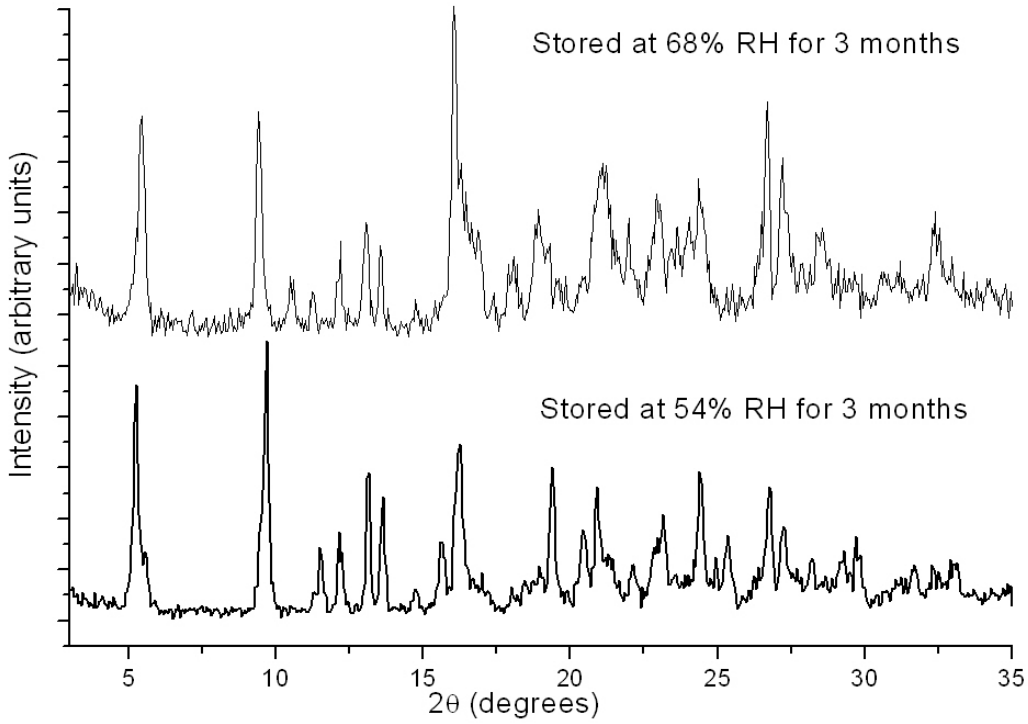

Fig. 3.15 Powder X-ray diffraction patterns of HCC form **I** after storage at 68 and 54% RH (RT) for 3 months.

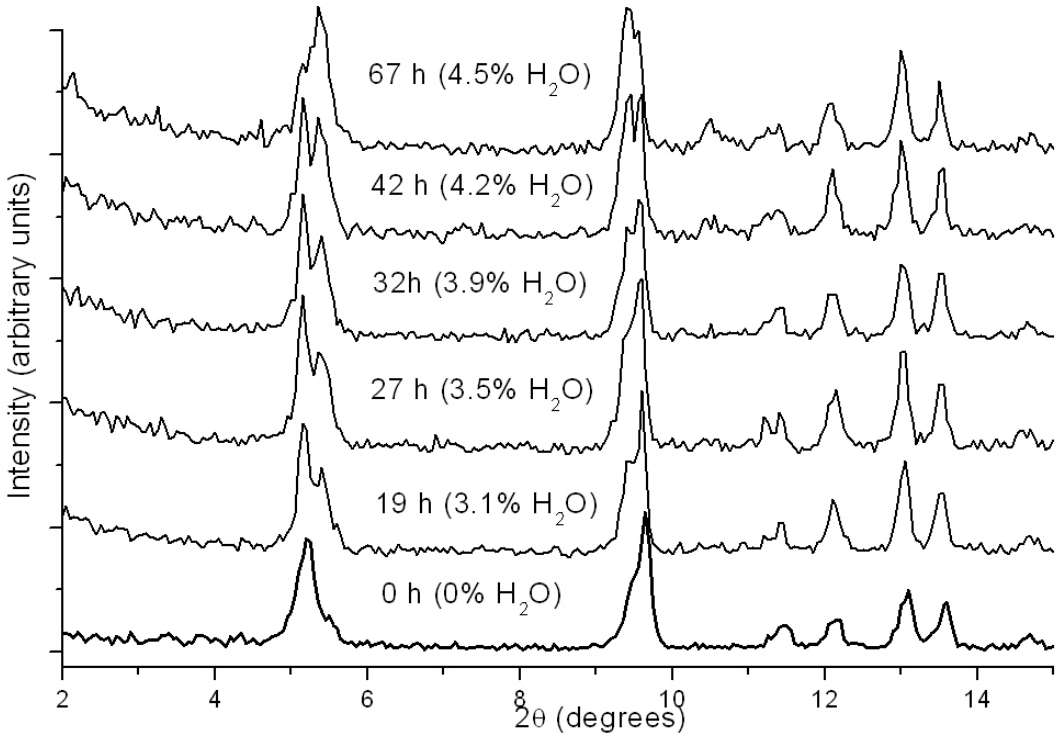

Fig. 3.16 Powder X-ray diffraction of HCC form **I** stored at 75% RH (25°C). The storage time and the water content (in parenthesis) are provided over each pattern.

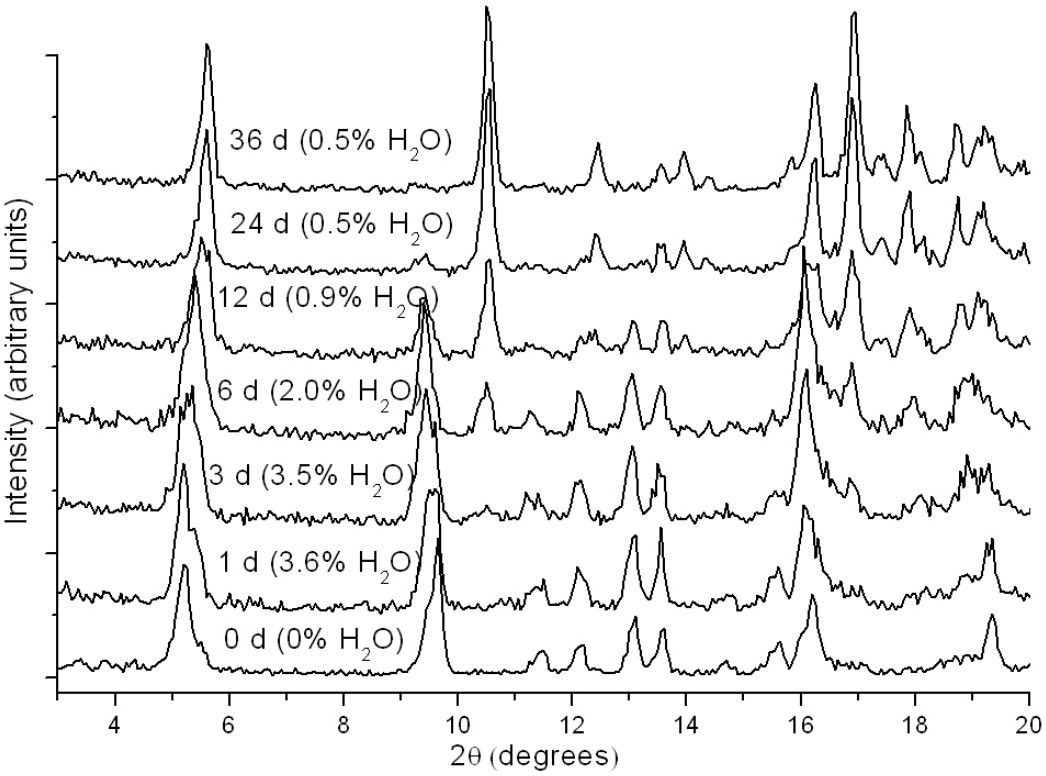

Fig. 3.17 Powder X-ray diffraction patterns of form **I** stored at 75% RH (25°C). The storage time and the water content (in parenthesis) are provided over each pattern.

3.6 References

1. Lohani, S. and Grant, D.J.W., *Thermodynamics of polymorphs*, in *Polymorphism in the Pharmaceutical Industry*, R. Hilfiker, Editor. 2006, Wiley-VCH: Weinheim, Germany. pp. 21-42.
2. Griesser, U.J., Jetti, R.K.R., Haddow, M.F., Brehmer, T., Apperley, D.C., King, A., and Harris, R.K. 2008. Conformational polymorphism in oxybuprocaine hydrochloride. *Crystal Growth & Design*, **8**: 44-56.
3. Phadnis, N.V. and Suryanarayanan, R. 1997. Polymorphism in anhydrous theophylline--implications on the dissolution rate of theophylline tablets. *Journal of Pharmaceutical Sciences*, **86**: 1256-63.
4. Zhang, G.G.Z., Gu, C., Zell, M.T., Burkhardt, R.T., Munson, E.J., and Grant, D.J.W. 2002. Crystallization and transitions of sulfamerazine polymorphs. *Journal of Pharmaceutical Sciences*, **91**: 1089-1100.
5. Boldyreva, E.V., Drebushchak, V.A., Drebushchak, T.N., Paukov, I.E., Kovalevskaya, Y.A., and Shutova, E.S. 2003. Polymorphism of glycine. Thermodynamic aspects. Part I. Relative stability of the polymorphs. *Journal of Thermal Analysis and Calorimetry*, **73**: 409-418.
6. Bauer, J., Spanton, S., Henry, R., Quick, J., Dziki, W., Porter, W., and Morris, J. 2001. Ritonavir: an extraordinary example of conformational polymorphism. *Pharmaceutical Research*, **18**: 859-66.
7. Gu, C.H., Young, V., Jr., and Grant, D.J. 2001. Polymorph screening: influence of solvents on the rate of solvent-mediated polymorphic transformation. *Journal of Pharmaceutical Sciences*, **90**: 1878-90.
8. Yang, X., Lu, J., Wang, X.-J., and Ching, C.-B. 2008. Effect of sodium chloride on the nucleation and polymorphic transformation of glycine. *Journal of Crystal Growth*, **310**: 604-611.
9. Matsumoto, T., Ichikawa, J., Kaneniwa, N., and Otsuka, M. 1988. Effect of environmental temperature on the polymorphic transformation of phenylbutazone during grinding. *Chemical & Pharmaceutical Bulletin*, **36**: 1074-85.
10. Rankell, A.S., *Influence of compressional force on solid-state crystal conversion of succinylsulfathiazole*. Ph.D dissertation. 1969 University of Wisconsin, WI.
11. Ebian, A.R., Moustafa, M.A., Khalil, S.A., and Motawi, M.M. 1973. Effect of additives on the kinetics of interconversion of sulphamethoxydiazine crystal forms. *Journal of Pharmacy and Pharmacology*, **25**: 13-20.
12. Moustafa, M.A., Khalil, S.A., Ebian, A.R., and Motawi, M.M. 1972. Kinetics of interconversion of sulphamethoxydiazine crystal forms. *The Journal of Pharmacy and Pharmacology*, **24**: 921-6.
13. Paul, I.C. and Curtin, D.Y. 1973. Thermally induced organic reactions in the solid state. *Accounts of Chemical Research*, **6**: 217-25.
14. Beckham, G.T., Peters, B., Starbuck, C., Variankaval, N., and Trout, B.L. 2007. Surface-mediated nucleation in the solid-State polymorph transformation of terephthalic acid. *Journal of the American Chemical Society*, **129**: 4714-4723.
15. McMillan, P.F., Shebanova, O., Daisenberger, D., Cabrera, R.Q., Bailey, E., Hector, A., Lees, V., Machon, D., Sella, A., and Wilson, M. 2007. Metastable

phase transitions and structural transformations in solid-state materials at high pressure. *Phase Transitions*, **80**: 1003-1032.
16. Klotz, S., Straessle, T., Nelmes, R.J., Loveday, J.S., Hamel, G., Rousse, G., Canny, B., Chervin, J.C., and Saitta, A.M. 2005. Nature of the polymorphic transition in ice under pressure. *Physical Review Letters*, **94**: 1-4.
17. Linol, J. and Coquerel, G. 2007. Influence of high energy milling on the kinetics of the polymorphic transition from the monoclinic form to the orthorhombic form of (+-)5-methyl-5-(4'-methylphenyl)hydantoin. *Journal of Thermal Analysis and Calorimetry*, **90**: 367-370.
18. Boldyrev, V.V. 2006. Mechanochemistry and mechanical activation of solids. *Russian Chemical Reviews*, **75**: 177-189.
19. Kuznetsov, P.N., Kuznetsova, L.I., Zhyzhaev, A.M., Kovalchuk, V.I., Sannikov, A.L., and Boldyrev, V.V. 2006. Investigation of mechanically stimulated solid phase polymorphic transition of zirconia. *Applied Catalysis, A: General*, **298**: 254-260.
20. Kawakami, K. 2007. Reversibility of enantiotropically related polymorphic transformations from a practical viewpoint: thermal analysis of kinetically reversible/irreversible polymorphic transformations. *Journal of Pharmaceutical Sciences*, **96**: 982-989.
21. Byrn, S.R., Pfeffer, R.R., and Stowell, J.G., *Solid-State Chemistry of Drugs*, ed. 2nd. 1999 SSCI, West Lafayette, Indiana.
22. Okumura, T., Ishida, M., Takayama, K., and Otsuka, M. 2006. Polymorphic transformation of indomethacin under high pressures. *Journal of Pharmaceutical Sciences*, **95**: 689-700.
23. Boldyreva, E. 2007. High-pressure polymorphs of molecularsolids: when are they formed, and when are they not? Some examples of the role of kinetic control. *Crystal Growth & Design*, **7**: 1662-1668.
24. Senna, M. 1985. Problems on the mechanically induced polymorphic transformation. *Crystal Research and Technology*, **20**: 209-17.
25. Salameh, A.K. and Taylor, L.S. 2006. Role of deliquescence lowering in enhancing chemical reactivity in physical mixtures. *Journal of Physical Chemistry B*, **110**: 10190-10196.
26. Schmitt, E.A., Law, D., and Zhang, G.G. 1999. Nucleation and crystallization kinetics of hydrated amorphous lactose above the glass transition temperature. *Journal of Pharmaceutical Sciences*, **88**: 291-6.
27. Saltmarch, M. and Labuza, T.P. 1980. Influence of relative humidity on the physicochemical state of lactose in spray-dried sweet whey powders. *Journal of Food Science*, **45**: 1231-1236.
28. Chen, L., *Solid State Behavior of Pharmaceutical Hydrates*. Ph.D dissertation. 1999 University of Minnesota, Minneapolis.
29. Matsuo, K. and Matsuoka, M. 2007. Solid-State Polymorphic Transition of Theophylline Anhydrate and Humidity Effect. *Crystal Growth & Design*, **7**: 411-415.

30. Yoshinari, T., Forbes, R.T., York, P., and Kawashima, Y. 2002. Moisture induced polymorphic transition of mannitol and its morphological transformation. *International Journal of Pharmaceutics*, **247**: 69-77.
31. Matsuo, K. and Matsuoka, M. 2007. Kinetics of solid state polymorphic transition of caffeine. *Journal of Chemical Engineering of Japan*, **40**: 468-472.
32. Morris, K.R., Griesser, U.J., Eckhardt, C.J., and Stowell, J.G. 2001. Theoretical approaches to physical transformations of active pharmaceutical ingredients during manufacturing processes. *Advanced Drug Delivery Reviews*, **48**: 91-114.
33. *Patient Package Insert: Homoclomin Tablets (10mg)*. 2007, Eisai Co., Ltd.: Tokyo, Japan.
34. Hammersley, A.P., Svensson, S.O., Hanfland, M., Fitch, A.N., and Häusermann, D. 1996. Two-dimensional detector software: from real detector to idealised image or two-theta scan. *High Pressure Research*, 235-248.
35. Griesser, U.J., *The importance of solvates*, in *Polymorphism in the Pharmaceutical Industry*, R. Hilfiker, Editor. 2006, Wiley-VCH: Weinheim, Germany. pp. 211-233.
36. Tang, X.C., Pikal, M.J., and Taylor, L.S. 2002. A spectroscopic investigation of hydrogen bond patterns in crystalline and amorphous phases in dihydropyridine calcium channel blockers. *Pharmaceutical Research*, **19**: 477-483.
37. Volkmann, H., *Handbook of Infrared Spectroscopy*. 1972 Verlag Chemie, Weinheim, Germany.
38. Post, A., Warren, R.J., and Zarembo, J.E., *Trifluoperazine hydrochloride*, in *Analytical Profiles of Drug Substances*, K. Florey, Editor. 1980, Academic Press: New York, NY. pp. 543-582.
39. Burger, A. and Ramberger, R. 1979. On the polymorphism of pharmaceuticals and other molecular crystals. II. Applicability of thermodynamic rules. *Mikrochimica Acta*, **2**: 273-316.
40. Kitaigorodskii, A.I., *Organic Chemical Crystallography*. 1961 Consultants Bureau, New York, NY.
41. Stephenson, G.A. and Liang, C. 2006. Structural determination of the stable and meta-stable forms of atomoxetine HCl using single crystal and powder X-ray diffraction methods. *Journal of Pharmaceutical Sciences*, **95**: 1677-1683.
42. Jerry Workman, J. and Weyer, L., *Practical Guide to Interpretive Near-Infrared Spectroscopy*. Angewandte Chemie, International Edition. 2008 CRC Press, Boca Raton, FL.
43. Fornes, V. and Chaussidon, J. 1978. An interpretation of the evolution with temperature of the v2 + v3 combination band in water. *Journal of Chemical Physics*, **68**: 4667-71.
44. Nieuwmeyer, F.J.S., Damen, M., Gerich, A., Rusmini, F., Voort Maarschalk, K., and Vromans, H. 2007. Granule characterization during fluid bed drying by development of a near infrared method to determine water content and median granule size. *Pharmaceutical Research*, **24**: 1854-1861.
45. Zhou, G.X., Ge, Z., Dorwart, J., Izzo, B., Kukura, J., Bicker, G., and Wyvratt, J. 2003. Determination and differentiation of surface and bound water in drug

substances by near infrared spectroscopy. *Journal of Pharmaceutical Sciences*, **92**: 1058-1065.
46. Derbyshire, H.M., Feldman, Y., Bland, C.R., Broadhead, J., and Smith, G. 2002. A study of the molecular properties of water in hydrated mannitol. *Journal of Pharmaceutical Sciences*, **91**: 1080-1088.
47. Giangiacomo, R. 2006. Study of water-sugar interactions at increasing sugar concentration by NIR spectroscopy. *Food Chemistry*, **96**: 371-379.
48. Cao, W., Mao, C., Chen, W., Lin, H., Krishnan, S., and Cauchon, N. 2006. Differentiation and quantitative determination of surface and hydrate water in lyophilized mannitol using NIR spectroscopy. *Journal of Pharmaceutical Sciences*, **95**: 2077-2086.
49. Grant, A., Davies, A.M.C., and Bilverstone, T. 1989. Simultaneous determination of sodium hydroxide, sodium carbonate and sodium chloride concentrations in aqueous solutions by near-infrared spectrometry. *Analyst (Cambridge, United Kingdom)*, **114**: 819-22.
50. Hirschfeld, T. 1985. Salinity determination using NIRA. *Applied Spectroscopy*, **39**: 740-1.

Chapter 4

Water-sorption induced Transformations in Crystalline Solid Surfaces – Characterization by Atomic Force Microscopy

4.1 Abstract

We studied the effect of water sorption on the mobility of molecules on the surface of a crystalline anhydrous solid with the goal of understanding the mechanism of its transformation to the corresponding hydrate. Theophylline was chosen as the model compound. The transition water activity for anhydrate → hydrate transformation in theophylline, the model compound, was determined. Atomic force microscopy (AFM) was used to study the surface changes of theophylline above and below the transition water activity. Contact-mode AFM showed that the jump-to-contact distance increased significantly above the transition water activity, suggesting formation of surface solution on the anhydrate crystal. At these water activities, using alternating current (AC) mode AFM, the movement of surface steps was visualized. When the anhydrate crystal surface was seeded with the hydrate, the propagation of new hydrate phase was observed by polarized light microscopy. It is concluded that water adsorption below the deliquescence water activity facilitated crystallization of theophylline hydrate by increasing the mobility of surface molecules.

4.2 Introduction

Under ambient conditions, water sorption can result in film formation on the solid surfaces of NaCl,[1, 2] calcite,[3, 4] mica,[5] α-Al_2O_3,[6] and ice.[7, 8] The adsorption of water onto the sample surface below the deliquescence point is usually reversible and can be described by the BET equation. In a variety of compounds, the adsorbed layer has been reported to be ~ 1 nm thick,[9] which can account for approximately three layers of adsorbed water. Since the heat of adsorption is comparable to the heat of condensation of water, multiple layers of water can often form before the surface is completely covered.[10] The surface heterogeneity in pharmaceutical solids can also lead to uneven distribution of adsorbed water. Surface water has high molecular mobility in directions parallel to the surface, and act as the medium for chemical reactions and facilitate degradation.[11,12] Infrared spectroscopy and molecular simulation studies have found that the hydrogen bonding network between the adsorbed water molecules are similar to that in liquid water.[13, 14]

Interestingly, water sorption resulted in an increase in the surface mobility of ionic crystals.[2, 3, 15] For example, when the RH of storage of NaCl crystals was increased from 40 to 75% RH (25°C), there was an abrupt change in surface mobility,[16] conductivity,[15] and morphology.[17] Between 40 and 75% RH, the adsorbed water solvated the ions on the crystal surface, leading to a pronounced increase in their mobility. Even in poorly water soluble solids, for example calcite, water adsorption increased the lateral growth rate of individual islands on the surface.[3]

A large fraction of pharmaceuticals can exist both in the anhydrous state and as hydrates, wherein water is incorporated in the crystal lattice. When exposed to water vapor, either during product manufacture or storage, anhydrous materials can transform into their corresponding hydrates. The anhydrate → hydrate

transformation, in addition to causing variation of water content in the final product, can also lower the aqueous solubility,[18] cause a decrease in dissolution rate,[19] and also have *in vivo* implications.[20, 21] It is important to understand the mechanism of hydrate formation in the solid state so as to control such transformations during product manufacture and use.

Two pathways have been proposed for the transformation of anhydrous theophylline to theophylline monohydrate. 1) Solid-solid transformation, a process in which water diffuses into the anhydrate lattice, followed by nucleation of new hydrate phase. [22, 23] 2) Solution-mediated transformation, where the anhydrous form goes into solution, forms a supersaturated solution, with respect to the hydrate, resulting in hydrate crystallization. It has been shown that anhydrate crystals served as the template for hydrate crystallization from solution.[24] Surfactants, which adsorbed on the anhydrate crystal surface, inhibited hydrate nucleation and decelerated hydrate formation.[25]

Anhydrate → hydrate transformation can occur in the solid state and can also be solution-mediated. There might be similarities in the mechanism of these two pathways. The solid state hydrate formation may also be mediated through the formation of a "surface solution". From a thermodynamic perspective, dissolution of the solid in the adsorbed water should occur only at and above RH_0, the RH over a saturated solution of the solute. Thus the formation of a solution on the crystalline surface, at $RH < RH_0$, is not expected.

Hydrate formation has been proposed to occur through the diffusion of water into the crystal lattice through channels.[26, 27] However, based on the structure of anhydrous theophylline, and the van der Waal's radius of water molecule (1.4 Å), it was evident that water could not be accommodated without the lattice undergoing expansion.[28, 29] This calculation is supported by the following experiment. A single crystal of anhydrous theophylline, recrystallized from

chloroform, did not sorb water or transform into hydrate even after storage at 94% RH for two weeks. This is well above the reported transition RH (~ 60%; 25C) for the anhydrate → hydrate transition in theophylline powder. The high surface area, coupled with the surface disordered regions in polycrystalline samples is likely responsible for the observed difference in the hydration behavior. We hypothesize that the hydrate formation in the solid state is a "surface solution" mediated process. Above the transition RH, water adsorption could significantly increase the mobility of surface molecules and facilitate hydrate formation in the solid state.

Using anhydrous theophylline as the model compound, we investigated the effect of water sorption on the surface mobility with the goal of understanding the mechanism of solid state hydrate formation. In addition to imaging surface topography, AFM can determine the adhesion and repulsion forces between a sharp tip and sample surface molecules.[30] Unlike other techniques, such as XRD and SS-NMR, AFM is a surface specific technique; the interior molecules (100 Å deep into the surface) have little impact on the interaction between the AFM tip and a rigid substrate.[31] AFM has been proven to be a powerful tool to probe various surface properties of solid samples, such as surface free energies[32, 33] and surface frictional properties.[34] AFM also can determine the surface topography along with high spatial resolution.[6] Therefore, AFM can be a suitable tool to investigate the existence of surface solution and test our hypothesis in this chapter. The surface solution was investigated by contact mode (quasistatic) AFM in force- Z measurements.

The mobility of the surface molecules was visualized by AC mode AFM. Finally, polarized light microscopy was used to observe hydrate crystallization on the surface of anhydrous theophylline crystals.

4.3 Material and methods

4.3.1 Materials

Theophylline anhydrate powder was purchased from Sigma chemicals (St. Louis, MO, USA). Theophylline anhydrate powder was sieved through a series of stainless steel meshes, and the fraction passing through 120 mesh (<125 μm) and retained on 140 mesh (> 106 μm) used. Theophylline monohydrate was prepared by storing anhydrous theophylline powder at 93% RH (25˚C) for 2 weeks.

Single crystals of anhydrous theophylline and theophylline monohydrate were crystallized from water and chloroform respectively by the solvent evaporation method. Carbamazepine anhydrate was recrystallized from ethanol by the solvent evaporation method.

4.3.2 Automated Sorption Microbalance (ASM)

Sample powder (~ 5 mg) was placed in the sample quartz boat of an automated vapor sorption microbalance (DVS-1000, Surface Measurements Systems, London, UK). The microbalance was calibrated using a 100 mg standard weight. The relative humidity sensor was calibrated at 5.0, 11.3, 32.8, 52.8, 75.3, and 84.3% RH (25°C), using saturated salt solutions. Unless stated otherwise, all the experiments were performed at 25°C. The samples were initially dried at 0% RH for 3 hours then exposed to the desired RH. The rate and extent of water uptake was determined over a range of RH conditions from 0 to 90%. The exposure time at each step varied from 1 to 6 h depending on the time required for equilibration. The experiment was conducted in duplicate.

4.3.3 Face Indexing of Theophylline Anhydrate Single Crystal

A single crystal of anhydrous theophylline (0.3 mm × 0.2 mm × 0.2 mm) was selected and mounted on a glass capillary in a diffractometer (Siemens, SMART Platform CCD) for data collection at 173 K (Mo Kα radiation; λ = 0.71073 Å). A preliminary set of cell parameters was calculated from reflections harvested from three sets of 20 diffraction frames. The face indexing was performed using commercial software (SMART, Bruker, Madison, WI, USA).

4.3.4 Water Uptake by Theophylline Anhydrous – Dihydrate Mixtures

A 1:1 w/w mixture of anhydrous and hydrate forms of theophylline were stored at 21, 33, 54, 68, and 80% RH at room temperature (~ 21°C). The mixtures were weighed after storage for 24 hours. The mixture stored at 54% RH was also weighed after storage for one month.

4.3.5 Solution Mediated Theophylline Hydrate Formation

The anhydrous – hydrate (1:1 w/w) mixture (about 200 mg) was dispersed in methanol-water mixtures of different compositions at room temperature. The water activity of these mixtures ranged from 0.5 to 0.7.[35] In order to facilitate the attainment of equilibrium, the vials were shaken. The hydration state of theophylline in contact with the solution was characterized by Raman spectroscopy. The excess solid was also filtered and characterized by XRD. The final water content of the remaining solution was determined by Karl Fischer titrimetry.

4.3.6 Karl Fischer Titrimetry (KFT)

The water content of the solvent mixture (mixture of methanol and water of different compositions) was determined using a coulometric moisture meter (CA05, Mitsubishi Chemical Industries Ltd., Tokyo, Japan). One µl of the solvent mixture was injected into the analyte chamber. The density of the methanol-water mixture was determined by weighing 2.00 ml of the solvent mixture. The water content is reported as µg of water / mg of solvent mixture.

4.3.7 Raman Spectroscopy

The spectra, collected in a Raman spectrometer (Ram **II**, Bruker optics, Madison, WI, USA), were obtained by averaging 32 scans over 4000 to 0 cm^{-1} range at a 4-cm^{-1} resolution.

4.3.8 Powder X-ray Diffractometry

About 200 mg of sample were packed into an aluminum holder by the side-drift method and exposed to Cu Kα radiation (45 kV, 40 mA) in a wide-angle X-ray diffractometer (Model D5005, Siemens, Madison, WI, USA). The instrument was operated in the step-scan mode over the angular range of 2 to 50° 2θ. The step size was 0.05° 2θ and counts were accumulated for 1 s at each step. The data collection and analyses were performed with commercially available software (JADE, version 5.1 Materials Data Inc., Livermore, CA, USA).

4.3.9 Polarized Light Microscopy

An anhydrous theophylline crystal was glued on a glass slide, stored at 93% RH (RT), and periodically observed in a microscope with a dual polarizer (Nikon Instruments Inc, Melville, NY, USA). The image was processed using commercial software (Metamorph, Molecular Devices Corporation, Downingtown, PA, USA). The experiments were also conducted after seeding the sample with theophylline monohydrate.

4.3.10 Environmental Atomic Force Microscopy (AFM)

A scanning probe microscope (Molecular Imaging PicoPlus since renamed Agilent 5500 AFM/SPM system) was used in contact and AC mode (sometimes called “tapping” or dynamic AFM). The PicoPlus system physically isolates the sample stage and its immediate environment from the system electronics, piezo-elements and optics by utilizing an O-ring sealed glass environmental chamber. This chamber includes multiple ports for *in situ* measurements as well as plastic tube attachments for gas/liquid exchange. A hygrometer was mounted in the chamber near the sample plate (the latter uses clips, not tape, to secure a slide- or wafer-affixed sample). The hygrometer was monitored with an external humidity controller unit (model HMM30D), which toggles power on and off to either an ultrasonic humidifier or a blower circulating air through a desiccator column, to maintain a user-specified set point humidity (controllable from 1-95% RH at RT). All the experiments were carried out at room temperature (~25°C). Before the experiment, the crystal sample was fixed onto a glass slide using epoxy glue to prevent movement during imaging. Integrated tip-cantilevers employed were oxide-sharpened silicon nitride tips on V-shaped cantilevers (NP-S, nominal spring constant 0.58 Nm^{-1}, Veeco, Woodbury, NY) for contact mode and etched-silicon tips on rectangular cantilevers (OTESP, nominal spring

constant 40 Nm-1, Veeco, Woodbury, NY) for AC mode. To increase the hydrophobicity, the tips used in contact mode were coated with a 50 Å layer of platinum.[36]

In digital pulsed force mode AFM (D-PFM) (Wissenschaftliche Instrumente und Technologie GmbH (WITec), Germany), local tip-sample adhesion and stiffness are simultaneously imaged with the sample topography. The D-PFM is attached to the AFM system as an external module. The D-PFM electronics introduces a sinusoidal modulation of the z-piezo of the AFM with an amplitude between 10 and 500 nm at a user-selectable frequency between 100 Hz and 2 kHz. A full cycle of force-versus-Z-displacement ("force-Z curve") is measured during each period of the oscillation. The set point for tracking topography is the maximum upward deflection of the cantilever (maximum pushing force F_{max}) during each cycle relative to the force baseline. In series with the Z modulation, the usual DC Z voltage is reactively and continuously varied in the attempt to keep F_{max} constant, thus providing the local height measurement. From the details of the force-Z curve, the adhesion (pull-off force, i.e., the most negative force during retraction) and semi-quantitative stiffness (differential cantilever deflection at two specified times during contact) can be directly imaged by setting the appropriate electronic triggers of the PFM module. The D-PFM control computer was occasionally configured to collect and save every force curve during imaging (GB-regime data file); this allows examination of full force versus distance behavior at any point of an image during post processing. For the D-PFM AFM measurements, Si probes (ThermoMicroscopes, San Francisco, CA) with a spring constant of 0.6 N/m were used.

In contact mode (quasistatic), the applied load was kept constant via the set point of cantilever deflection that is maintained by the AFM normal-force feedback system (and graphically determined within force-Z measurements,). Images of "height" (i.e., the feedback-driven Z scanner displacement to maintain constant

cantilever deflection) and lateral force (twisting of cantilever about principal axis due to torque on tip [37] were acquired simultaneously at 10%, 40% and 60% RH. A single AFM tip was used for these experiments. Quantitative friction force images were generated by subtracting the lateral force images collected during left-to-right and right-to-left tip excursions (offset to compensate for X-hysteresis), using in-house developed software (SPManalysis). This largely removes topographic effects[38] and a variable background (interferometry of laser light reflecting from cantilever and sample) from the lateral force signal while approximately doubling the physically meaningful, shear-derived friction force signal (energy dissipation, i.e. material contrast related to molecular degrees of freedom as well as intermolecular coupling).[31, 38] Force-Z curves also were acquired to characterize attractive tip-sample forces manifest in the jump-to-contact and jump-from-contact phenomena[39] in turn related to surface fluid behavior[40] as described in the Results.

In AC mode, the cantilever was oscillated vertically near its resonance frequency (~300 kHz). A drive frequency, approximately 0.2 kHz below resonance, and a drive amplitude yielding approximately 15 nm of free tip oscillation amplitude (as quantified in amplitude-Z approach-retract measurements), was employed in order to stabilize the repulsive regime, wherein the tip-sample interaction is dominated by solid-solid contact.[41] “Height” and phase images were collected, the latter indicating the interaction regime (i.e., net repulsive) as well as providing material contrast derived from energy dissipation during tip-sample interaction.[42]

4.4 Results and Discussion

4.4.1 Transition Water Activity for Theophylline Anhydrate → Hydrate Transformation

The transition of anhydrous theophylline to the monohydrate has been the subject of several investigations.[43-46] The wide range in the reported transition water activity (0.25 to 0.80; at 25°C) is attributed to the slow transformation kinetics.[44] We determined the transition water activity, in both solid and solution states. By using a ground hydrate-anhydrate mixture, the phase transformation was facilitated. After storage for 24 hours, the samples stored at 21 and 33% RH exhibited 3.5 and 2.8% weight decrease respectively. On the other hand, storage at 68 and 80% RH resulted in pronounced weight gain of 3.6 and 6.0% respectively. When stored at 54%, the weight loss was slow and was measurable only after a month (2.1%).

The stored samples were characterized by Raman spectroscopy and powder X-ray diffractometry. Theophylline anhydrate was characterized by Raman peaks at 1665 and 1708 cm^{-1}, while the hydrate had a unique peak at 1688 cm^{-1} (Fig. 4.2). The increase in the intensity of the 1688 cm^{-1} peak in the mixtures stored at 68 and 80% RH indicated an increase in hydrate content. On the other hand, storage at 21, 33 and 54% RH resulted in an increase in the peak intensities at 1665 and 1708 cm^{-1}, suggesting an increase in anhydrate content. Therefore, the solid state anhydrate → hydrate transition occurred between 54 and 68% RH at 25°C.

The precise determination of the transition water activity is hampered by the slow transition kinetics. Moreover, the use of different salt solutions results in discrete RH values, and the options are somewhat limited. Solution-mediated phase transformations occur at rates much faster than in the solid state and can enable

the accurate determination of the transition water activity (a_w). By varying the composition of organic solvent – water mixtures, the water activity can be systematically controlled. At any given water activity, only one phase (anhydrate or hydrate) will be stable and will be the phase in contact with the solution at equilibrium. The powder samples were slurried in methanol-water mixtures of different compositions to pinpoint the transition water activity.

An empirical equation was used to calculate the water activity of methanol-water mixtures.[35] The water content of these liquids were not measurably different, before and after equilibration with the powder for 2 days at 25°C. Theophylline monohydrate was the final phase in contact with the liquid at $a_w \geq 0.63$, while the anhydrate was the stable phase at $a_w \leq 0.61$ (Fig. 4.3). Therefore the transition a_w for the theophylline anhydrate-hydrate system is ~ 0.62 at 25°C. Earlier, we had bracketed the transition a_w in the solid state between 0.54 and 0.68 (at RT). Thus, there was a broad agreement of the values determined based on solution-mediated and the solid state transformation.

4.4.2 Water Sorption Studies of Theophylline Anhydrate

The anhydrate → hydrate transition in theophylline has been investigated in the solid state under very high RH conditions (95% or 100% RH, 25°C) or in the wet massing stage of the granulation process.[23, 46-49] We evaluated this transition at 90% RH (25°C) which is substantially below the deliquescence RH (~ 100%, 25°C). In anhydrous theophylline, there was an induction period of 2 days before transformation to the monohydrate was initiated (in Fig. 4.4). Gentle grinding in a mortar by a pestle for 2 min dramatically decreased the induction time to 400 minutes, while seeding with the hydrate, completely eliminated the induction time. The long induction time suggested that theophylline hydrate crystallization is a nucleation-controlled process. Grinding is known to create surface disorder,

leading to increased surface free energy and reactivity.[50, 51] This in turn could facilitate hydrate nucleation thereby shortening the induction time. When the anhydrate was seeded with hydrate, since the nucleation step is by-passed, the induction period was eliminated.

As mentioned in the Introduction section, based on molecular modeling studies, water molecules are unlikely to be able to penetrate the crystal lattice of anhydrous theophylline. Since the transformation is nucleation controlled, we propose that theophylline anhydrate → hydrate conversion occurs through a "surface solution". This solution formation, a consequence of water adsorption, increases the mobility of theophylline molecules on the surface and facilitates the crystallization of hydrate phase. There are reports in the literature of adsorbed water forming a "surface solution", at RH < RH_0. The IR absorption peak of the adsorbed water in NaCl (stored at 50% RH; 25°C) was similar to that of salt solution, suggesting the existence of "surface solution" below the deliquescence RH of 75% (25°C).[1] We therefore used atomic force microscopy (AFM) to investigate the surface properties of anhydrous theophylline crystals over an RH range of 10 - 75% (25°C).

4.4.3 Face Indexing of Theophylline Anhydrate and Hydrate Crystals

Large single crystals of theophylline were harvested from chloroform by slow solvent evaporation. The crystal structure was reported by Ebisuzaki.[52] The dominant faces of the plate-shaped single crystals were indexed to be 100 and -100 (Fig. 4.5). From the crystal structure, it was evident that there was no hydrogen bonding between (100) planes. It has been reported that (100) face of anhydrous theophylline crystal served as the template for hydrate crystallization in solution.[24] The surface properties of the (100) face of anhydrous theophylline crystal at different RH values could be relevant to the hydrate formation in the

solid state. Humidity controlled atomic force microscopy was used to probe the (100) surface in the following sections.

4.4.4 Effect of Water Adsorption on the Mobility of Surface Molecules

The general topographic and dissipative character of theophylline surfaces was compared semi-quantitatively in multiple imaging modes. There is no shear force between the tip and sample when imaging in AC mode AFM.,[42] As a result, the disturbance of imaging process on the surface topography in the AC mode was minimal compared to that in contact mode. Images of the surface of a single anhydrous theophylline crystal, in AC mode AFM, revealed two distinct domains: dome-shaped features and flat surrounding surfaces (Fig. 4.6, A). The domes were 5-10 nm in height, and 200-300 nm in diameter. They appeared as the dark regions in the phase images (Fig. 4.6, B). Phase shifts were numerically less than 90 degrees indicating that the imaging was performed in the repulsive regime. It could thus be concluded that the dome is more energy dissipative than the flat surface.[42] It has been shown that amorphous materials exhibit higher energy dissipation than their crystalline counterparts.[53]

To further investigate the nature of dome and flat regions on the surface, the tip-sample adhesion force on the crystalline and disordered regions of anhydrous theophylline under two RH conditions (40 and 75% RH; 25°C) were also determined using pulse force mode AFM (Fig. 4.6, D and F). The adhesion force on the dome appeared to be independent of RH, while the crystalline regions showed a pronounced decrease in adhesion force at 75% RH. The magnitude of the adhesion force for the crystalline and disordered regions was approximately the same at 40% RH, while the disordered regions showed a higher adhesion force at 75% RH.

Generally, the total adhesion force in air between AFM tip and substrate includes long-range attractive forces (van der Waals, electrostatic), capillary forces and solid-solid interactions that may include chemical bonding forces (hydrogen, ionic, and if reactive, covalent).[54] The higher adhesion force on the dome compared to crystalline surface at 75% RH could be attributed to the increase in adhesion hysteresis derived from the mobility of surfaces during bonding/debonding cycles.[55] The higher the molecular mobility at a surface, the greater the (stress-modified) thermal activation and rearrangement of surface molecules upon contact by another surface.[55] Greater force is required to separate the surfaces (hysteresis) because rearrangements take place energetically to yield a more stable interface. Disordered domains are less energetically stable and thus more mobile in the presence of sorbed water. At the lower water activity (40% RH), the tip-sample interfacial energy will dominate; at the higher water activity (70% RH), the increase in the interfacial water content increases the mobility of theophylline molecules and thus results in the dominance of adhesion hysteresis. In this picture, at low RH, the adhesion force exhibited by the dome-shaped disordered domains and the crystalline regions will be about the same. At the high RH condition, a decrease in tip-sample interfacial energy was apparently compensated by adhesion hysteresis in the disordered region, but not in the crystalline region.

The frictional images at 40% RH are shown in Fig. 4.6 (F and G). An inner portion (10 x 10 μm) had been repeatedly raster scanned at 40 and 75% RH , prior to collecting the shown (15x15 μm) image. The disordered regions exhibited higher frictional force than the flat regions at 40% RH and significant disruption due to scanning at 75% RH (25°C). When the RH was increased above the transition RH, the frictional force distribution showed only one wide peak. The frictional images showed that contact-mode scanning had induced significant plastic deformation to the disordered regions (Fig. 4.6).

To interpret these results, we firstly note that friction is dependent on chemical nature in that more polar (higher energy) surfaces will attract the (polar) AFM tip more strongly, thus requiring a greater shear force to maintain sliding.[56]-[57] Given that the adhesion force on the disordered surface was similar to that on the crystalline surface when operating below the transition RH, there seems to be little difference in surface energy. Secondly, elastic properties can affect frictional force,[58] because the softer component more greatly deforms, resulting in a larger tip-sample contact area, that in turn produces greater energy dissipation (being an extensive quantity). Force curves, however, did not reveal significant differences in contact stiffness, Thirdly, less crystalline molecular packing can result in higher susceptibility to plastic deformation, and thus more energy dissipation, translating into higher friction during sliding.[59] Given the observed scan-induced modifications under presumed plasticizing effects of absorbed water at high humidity, we attribute higher friction on the disordered domed regions to higher plasticity and poorer molecular packing.

Taken together, phase, adhesion, and friction images acquired in AC, pulsed force and contact modes, respectively, suggest that the domes and surrounding flat surfaces consist predominantly of disordered and crystalline theophylline, respectively. The mechanism of formation and the structure of the dome-shaped domains is likely related to kinetics in the final stages of sample preparation. The theophylline anhydrate crystal was harvested from the chloroform mother liquor, washed with chloroform, dried under reduced pressure over desiccants. During the final stages of evaporation of solvent from the theophylline surface, micro-droplets may locally solvate the crystal and upon evaporation yield droplet-shaped domains of primarily disordered theophylline atop the crystal surfaces.

Besides the surface disordered domes, numerous steps of approximately half unit cell height (12 Å), as revealed by horizontal cross section height profiles (Fig. 4.6, C), were observed. Surfaces with steps have been observed in bovine

insulin crystals,[60] which also have layered crystal structure. These steps are the result of surface nucleation and crystal growth. The crystallographic structure of theophylline anhydrate crystal showed a layer-by-layer structure along the (100) or (-100) plane. Between layers there is no hydrogen bonding, whereas an extensive hydrogen bond network connects molecules within each layer. The crystallization of anhydrous theophylline can thus be depicted as a 2-dimensional surface nucleation and growth process.[61] The apparently flat crystal surface is in fact made up of moving steps of monolayer height. Vacancies and growth units could be observed on the crystal surface. After exposure to 65% RH for 2 hours, the surface vacancies were gradually filled and the growth units retracted (Fig. 4.7). After water adsorption, the mobility of the surface molecules increased, leading to the filling of surface vacancies and retraction of growth units.

It has been shown that AFM tip-sample contact can promote local water condensation, which in turn can induce changes in surface properties, including topography.[62] To examine the effect of possible local condensation on the surface morphology, we zoomed out from areas repeatedly scanned in AC mode and compared the scanned central and fresh peripheral regions for any difference in topography. Fig. 4.8 exemplifies such a check. The left and right images show the 10 × 10 μm frame after the crystal was exposed to 65% RH for 0 and 117 min, respectively. The square boxes inside the images show the repeatedly scanned area. In the right image in Fig. 4.8, there is no noticeable difference between the morphologies inside and outside the box, with the small droplets merging to form larger droplets. The growth units to the upper left corner in the box also retracted after exposure to 65% RH. From the above observations, it is concluded that the changes in surface morphology were caused by water - surface interactions, rather than by surface - AFM tip interactions in AC mode. The same imaging process was conducted on the anhydrous theophylline crystal at 45% RH (RT). No change in surface morphology was observed after exposure to 45% RH for 2 hours.

Water can be adsorbed onto the crystal surfaces through different intermolecular interactions, such as hydrogen bonds, van der Waals forces, and ionic forces.[10] Below the transition water activity, anhydrous theophylline is the stable phase, wherein there is hydrogen bonding between theophylline molecules. Above the transition water activity for anhydrate → hydrate transformation, the interaction between water and theophylline could interrupt the hydrogen bonding between theophylline molecules. In other words, the hydrogen bonding between water and theophylline is preferred over that between theophylline molecules. This will lead to an increase in the mobility of surface molecules, thereby facilitating crystallization of theophylline monohydrate.

As discussed earlier, theophylline hydrate formation in the solid state is a nucleation controlled process.[63] The anhydrate → hydrate transformation was not detected after storing recrystallized anhydrous theophylline at 94% RH (25°C) for two weeks, suggesting a high energy barrier for nucleation in the solid state (we have pointed out later that the crystal growth occurs quite rapidly). The increase in mobility, while not facilitating nucleation, enabled the crystal growth.

4.4.5 Formation of Surface Solution by Water Adsorption

We have used AFM to demonstrate that the surface of anhydrous theophylline crystals, upon water adsorption, exhibit enhanced mobility above the hydrate transition RH. We also propose that water sorption above the hydrate transition RH leads to formation of water film or surface solution that could serve as the medium for crystallization of hydrate in the solid state. The surface solution was probed using contact mode AFM. AFM has been used to determine the thickness of thin films of a lubricant on flat surfaces.[40] This technique utilizes the sudden vertical displacement of the tip when the onset of attractive force pulls the tip into contact with the substrate. The jump-to-contact distance (JTC), the sum of the

distances moved by the tip (d_T) and the sample (d_S) from the point at which the tip first experiences a sudden attraction (point A, Fig. 4.9), to the point of solid contact (point B, Fig. 4.9), has been correlated with the thickness of the liquid films on the substrate surface. This jump-to-contact (JTC) phenomenon also results from an instability in the interaction between tip and substrate.[64] When a liquid film is present on a surface, a liquid bridge will form between the AFM tip and substrate because of capillary condensation. The capillary force will pull the tip into contact with the substrate surface. Thus the jump-to-contact (JTC) distance increases as a function of the thickness of the film for a given liquid, tip, and substrate. It was found that the thickness determined by AFM JTC measurements were consistently higher than that determined by ellipsometry.[65] To explain the origin of this difference, Forcada [66] showed that the water film could deform outward, under attraction towards the tip, to a distance of nanometers. This deformation leads to an overestimation of the thickness of the liquid film on the substrate surface.

In the present study, the JTC distance on anhydrous theophylline and carbamazepine crystals was measured as a function of relative humidity The anhydrous carbamazepine crystal served as the "reference standard" since the transition to carbamazepine dihydrate is known to occur at RH > 80% at RT.[67] The JTC distance on carbamazepine form III crystal (001) face exhibited a small increase when the RH was gradually increased from 10 to 70% (25°C), suggesting a minimal increase in the thickness of the water film, both on the AFM tip and carbamazepine crystal at progressively increasing RH values (Fig. 4.10). The JTC distance on theophylline crystals, by comparison, increased substantially when the RH was increased from 40 to 70% (25°C), and particularly from 60 to 70%. Importantly, the same full force-Z curves at 10 and 60% RH (25°C) showed no increase in pull-off force at 60% RH, suggesting that the increase in JTC distance could not be attributed to the higher water condensation at higher RH values. The increase in JTC distance, therefore, is attributed to the

formation of a thicker surface solution on the theophylline anhydrate crystal when the RH was increased from 40 to 60%. We should be cautious and avoid interpreting the increase in a quantitative manner, because the surface solution can deform in the force field exerted by the AFM tip.[66] The formation of surface solution could be attributed to the preferred hydrogen bonding between theophylline and water above transition water activity, which leads to detachment of surface theophylline molecules from the crystal lattice.

4.4.6 Mechanism of Hydrate Formation in the Solid State

Polarized light microscopy was used to visually ascertain the effect of seeding on the solid-state theophylline anhydrate → hydrate transformation. When a single crystal of anhydrous theophylline was stored at 93% RH (25°C) for two weeks, there were no perceptible changes. Though the solid-state anhydrate → hydrate transition RH is ~ 62% (25°C), we had earlier observed a long induction time for hydrate crystallization (Fig. 4.4). However, when an anhydrous crystal was seeded with a needle-shaped crystal of monohydrate, crystal grown from the contact point was evident after 10 hours of storage (Fig. 4.11). The growing phase was identified to be theophylline monohydrate by Raman spectroscopy. After storage for 20 hours, the continued propagation of the new hydrate phase was evident.

Therefore, we postulate the following steps in the anhydrous theophylline → theophylline monohydrate transformation. 1) Adsorption of water leading to the formation of "surface solution". This is believed to occur at RH values > transition RH, but at RH values << RH_0. 2) Nucleation of theophylline hydrate on the surface of the anhydrate. 3) Diffusion of theophylline molecules leading to crystal growth. The formation of "surface solution" was evident from AFM studies.

Interestingly, the long induction time for hydrate formation even at RH values >> transition RH could be explained by the activation energy barrier for hydrate nucleation. Pharmaceutical processing steps such as grinding or compaction, by introducing pronounced lattice disorder in the surface of anhydrate, could lower the activation energy barrier and facilitate hydrate nucleation.

4.5 Conclusion

Theophylline anhydrate→hydrate formation in the solid state is a "surface solution" mediated process. Above the transition RH, AC mode AFM studies revealed movement of surface steps and islands on the surface of anhydrous theophylline crystals, supporting the notion of a significant increase in the mobility of the surface molecules. Using contact mode AFM, a pronounced increase in the jump-to-contact distance on the crystalline surface was detected in the vicinity of the transition RH. This suggests that the thickness of surface solution on theophylline anhydrate increased significantly above the transition RH.

Acknowledgement

The help and support of Jingping Dong, Ph.D. and Victor Young, Ph.D. is gratefully acknowledged.

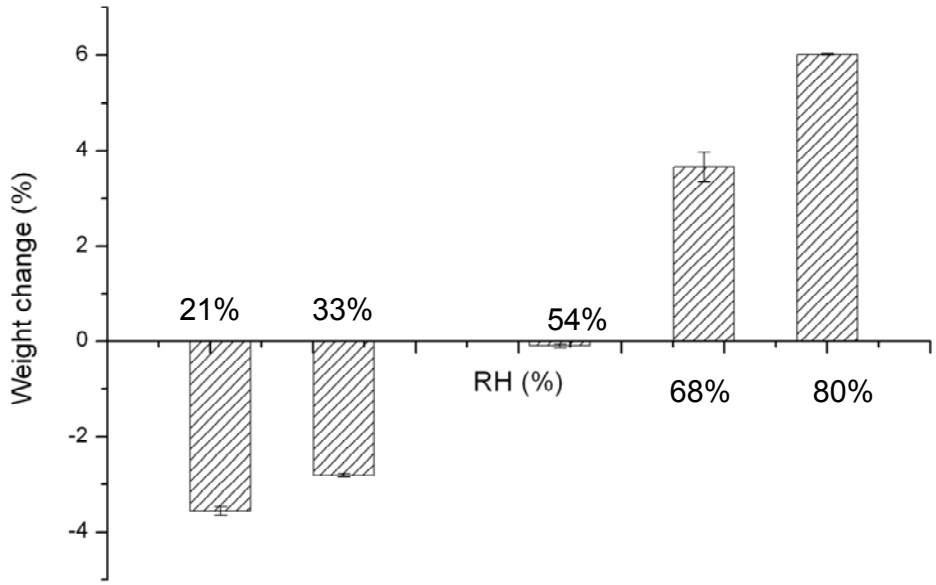

Fig. 4.1 The weight change of a physical mixture of anhydrous theophylline and theophylline monohydrate (1:1 w/w), following storage at different RH values (RT) for one day.

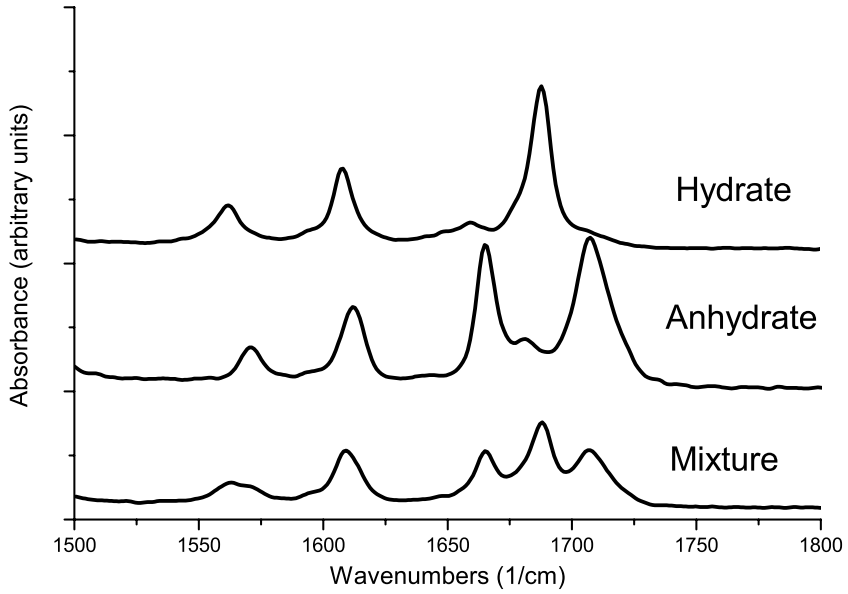

Fig. 4.2 Raman spectra of theophylline anhydrate, theophylline monohydrate, and a 1:1 (w/w) physical mixture of the anhydrate and monohydrate.

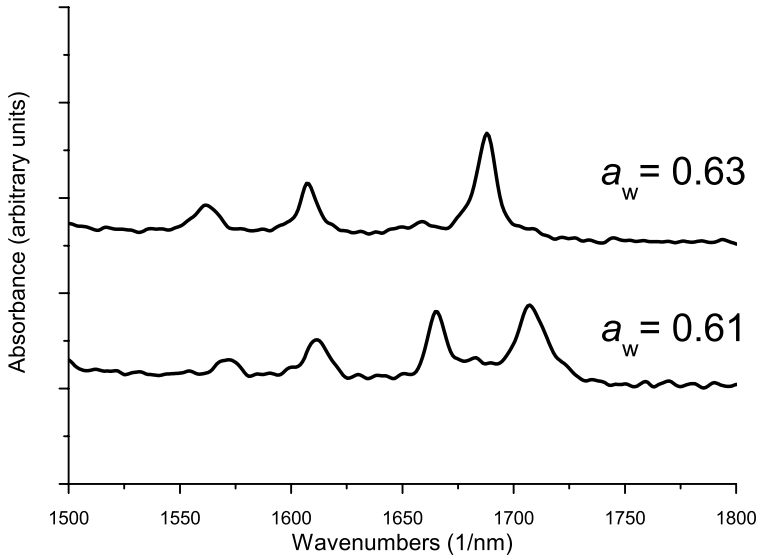

Fig. 4.3 Raman spectra of the solid in contact with water-methanol mixtures of water activities (a_w) 0.63 and 0.61. A 1:1 (w/w) physical mixture of the anhydrate and monohydrate were equilibrated with the solvent mixture for 48 hours at RT.

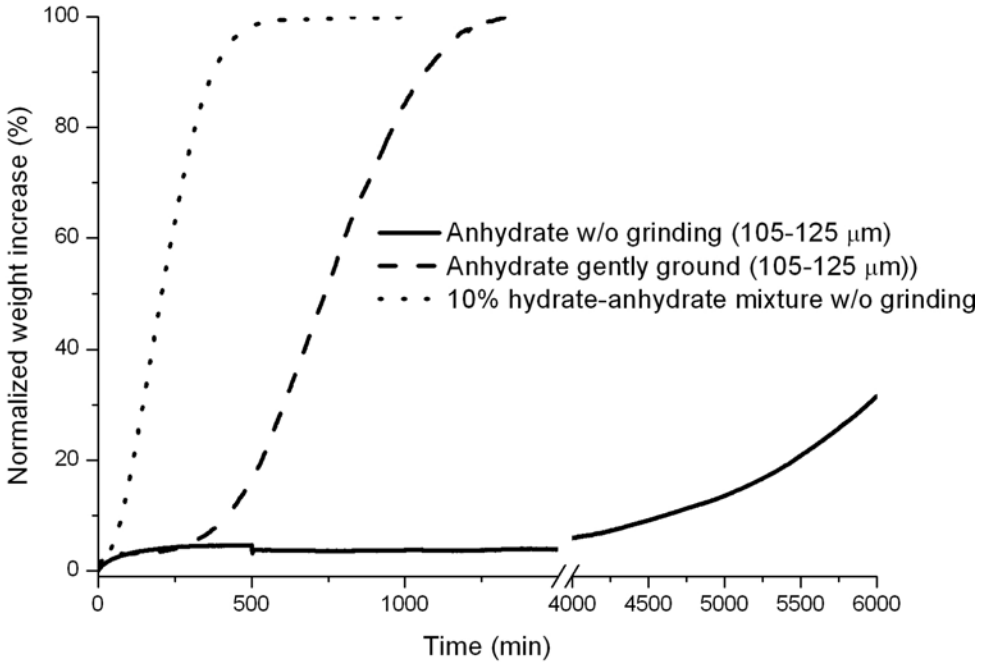

Fig. 4.4 Water uptake kinetics of (i) 'as is' anhydrous theophylline (__), (ii) gently ground anhydrous theophylline (---), and (iii) physical mixture of anhydrous theophylline and theophylline monohydrate (1:1, w/w) (….). The samples were stored at 90% RH (25°C).

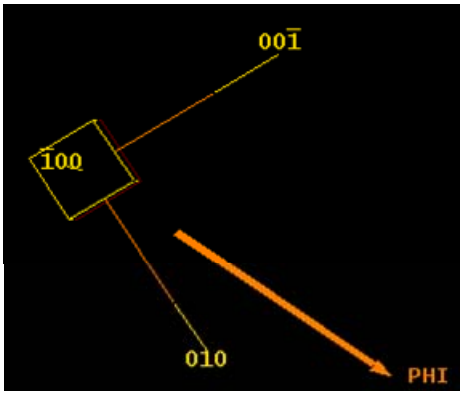

A	24.41(	1)
B	3.785(	2)
C	8.480(	6)
Alp	90.00(	7)
Bet	90.00(	6)
Gam	90.00(	8)
V	783.5(	7)

The dominant faces :

($\bar{1}$00) and (100) face

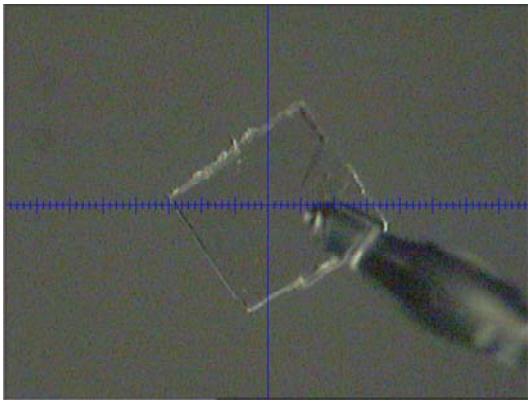

Fig. 4.5 Face indexing of anhydrous theophylline crystal.

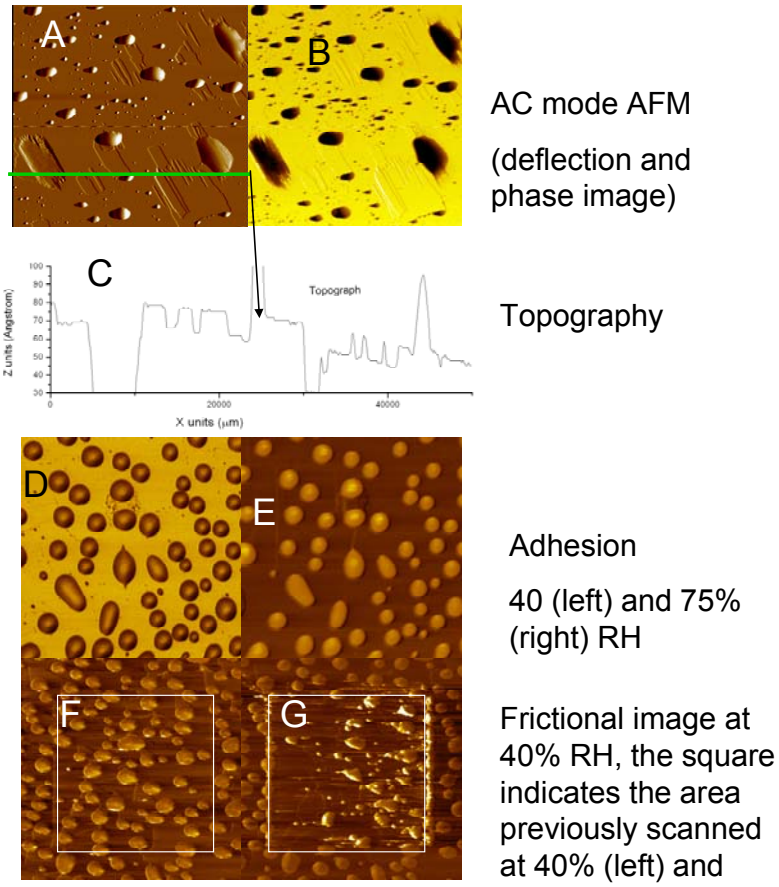

Fig. 4.6 Humidity and temperature controlled atomic force microscopy of anhydrous theophylline. Cantilever amplitude (A) and phase (B) images (5 x 5 µm) of anhydrous theophylline crystal at 30% RH. Cross sectional height plot (C) of the above, at y = 1170 nm. Adhesion (D and E, 10 x 10 µm) and friction (F and G) images (15 x 15 µm) of anhydrous theophylline crystal surface at 40% RH. All the experiments were conducted at 25°C.

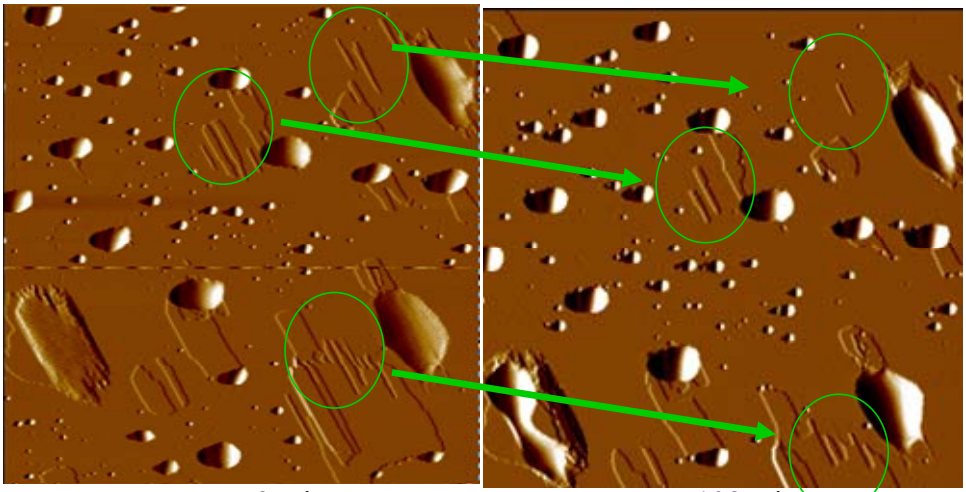

Fig. 4.7 AC mode AFM image (5 × 5 µm) of the surface of anhydrous theophylline crystal after storage at 65% RH for 9 min (left panel) and 108 min (RT). Notice that the prolonged storage at 65% RH caused the disappearance of surface scratches and retraction of surface islands.

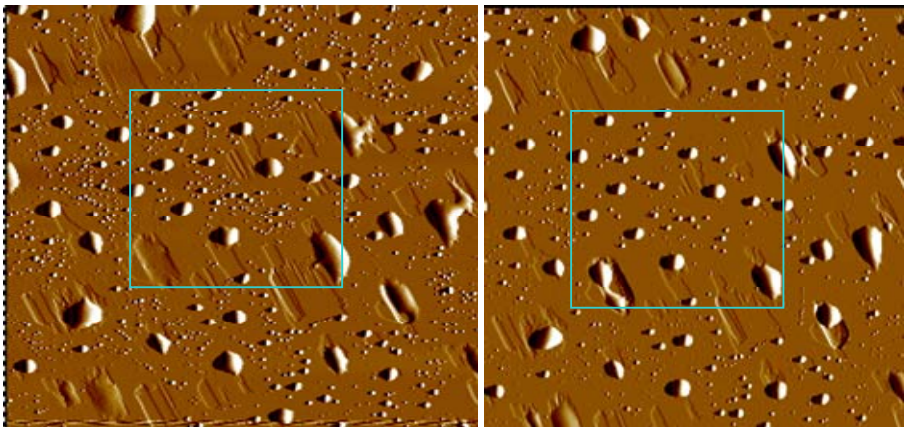

Fig. 4.8 AC mode AFM image (10 × 10 μm) of the surface of anhydrous theophylline crystal after storage at 65% RH for 0 min (left panel) and 117 min (RT).

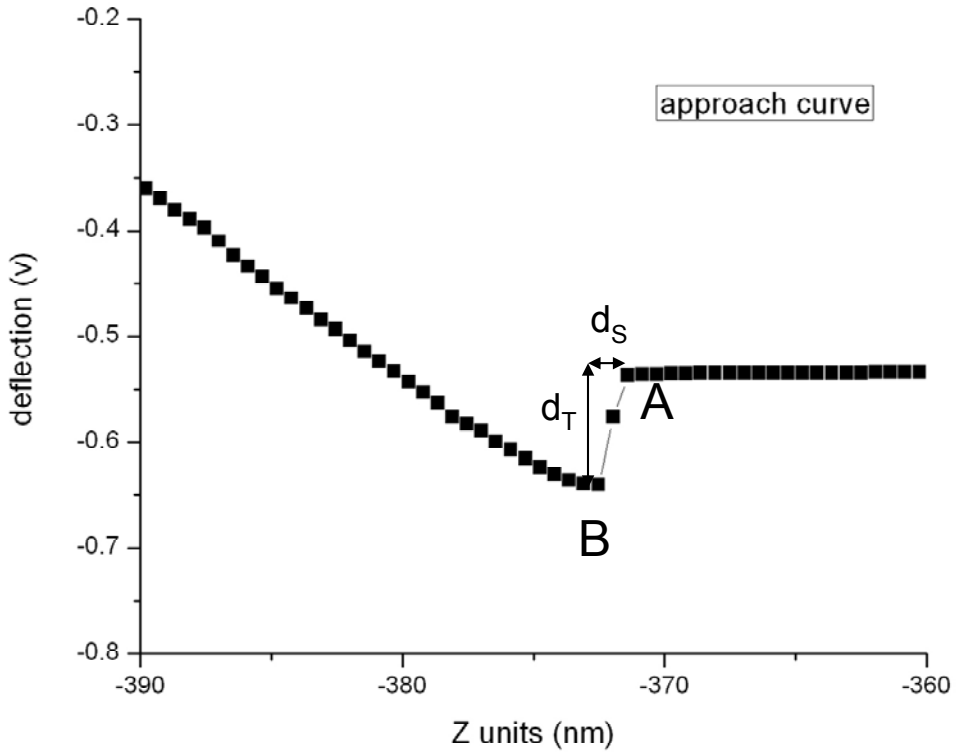

Fig. 4.9 The deflection of cantilever as the tip approached anhydrous theophylline crystal surface. A and B indicate the point where the tip experienced a sudden attraction and the point of solid contact, respectively. d_S and d_T respectively represent the distance moved by the sample and tip. The experiment was conducted in contact mode at 70% RH (RT).

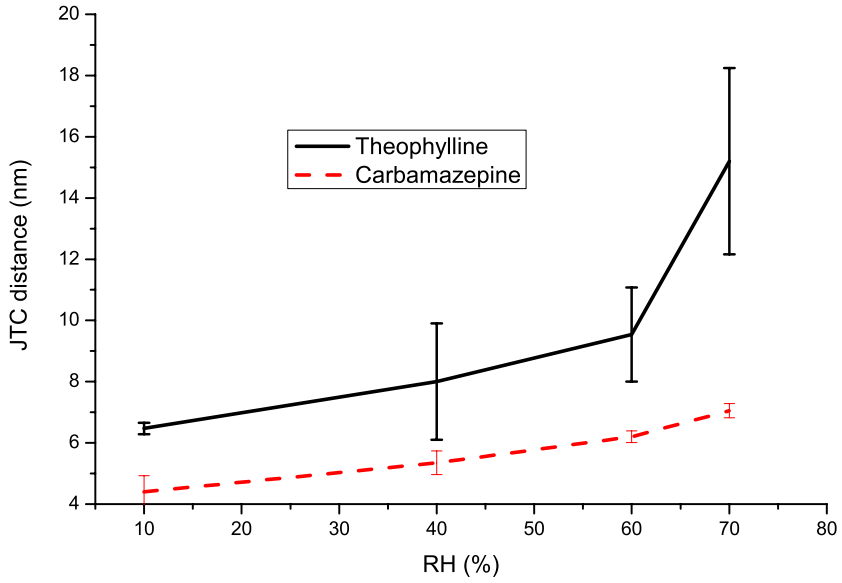

Fig. 4.10 Jump-to-contact distance determined by contact mode AFM on theophylline and carbamazepine crystals at different relative humidities (RT).

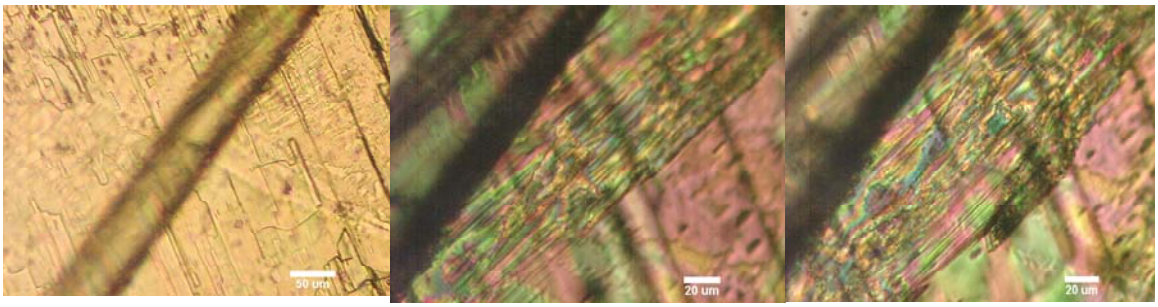

0 hour 10 hours 20 hours

Fig. 4.11 Polarized light micrographs following the seeding of a single crystal of anhydrous theophylline with a needle-shaped theophylline monohydrate crystal. The seeded single crystal was stored at 93% RH (RT) and photographed after 10 and 20 hours.

4.6 References:

1. Ewing, G.E. 2005. H_2O on NaCl: from single molecule, to clusters, to monolayer, to thin films, to deliquescence. *Structure and Bonding (Berlin, Germany)*, **116**: 1-25.
2. Ghosal, S., Verdaguer, A., Hemminger, J.C., and Salmeron, M. 2005. In situ study of water-induced segregation of bromide in bromide-doped sodium chloride by scanning polarization force microscopy. *Journal of Physical Chemistry A*, **109**: 4744-4749.
3. Kendall, T.A. and Martin, S.T. 2007. Water-induced reconstruction that affects mobile ions on the surface of calcite. *Journal of Physical Chemistry A*, **111**: 505-514.
4. Usher, C.R., Baltrusaitis, J., and Grassian, V.H. 2007. Spatially resolved product formation in the reaction of formic acid with calcium carbonate: the role of step density and adsorbed water-assisted ion mobility. *Langmuir*, **23**: 7039-7045.
5. Xu, L., Lio, A., Hu, J., Ogletree, D.F., and Salmeron, M. 1998. Wetting and capillary phenomena of water on mica. *Journal of Physical Chemistry B*, **102**: 540-548.
6. Verdaguer, A., Sacha, G.M., Bluhm, H., and Salmeron, M. 2006. Molecular structure of water at interfaces: Wetting at the nanometer scale. *Chemical Reviews*, **106**: 1478-1510.
7. Dash, J.G. 1999. History of the search for continuous melting. *Reviews of Modern Physics*, **71**: 1737-1743.
8. Dash, J.G., Rempel, A.W., and Wettlaufer, J.S. 2006. The physics of pre-melted ice and its geophysical consequences. *Reviews of Modern Physics*, **78**: 695-741.
9. Ewing, G.E. 2006. Ambient thin film water on insulator surfaces. *Chemical Reviews*, **106**: 1511-1526.
10. Thiel, P.A. and Madey, T.F. 1987. The interaction of water with solid surfaces: fundamental aspects. *Surface Science Reports*, **7**: 211-385.
11. Rahaman, A., Grassian, V.H., and Margulis, C.J. 2008. Dynamics of water adsorption onto a calcite surface as a function of relative humidity. *Journal of Physical Chemistry C*, **112**: 2109-2115.
12. Vogt, R. and Finlayson-Pitts, B.J. 1994. A diffuse reflectance infrared Fourier transform spectroscopic study of the surface reaction of NaCl with gaseous NO_2 and HNO_3. *Journal of Physical Chemistry*, **98**: 3747-55.
13. Foster, M., D'Agostino, M., and Passno, D. 2005. Water on MgO(100). An infrared study at ambient temperatures. *Surface Science*, **590**: 31-41.
14. Foster, M.C. and Ewing, G.E. 2000. Adsorption of water on the NaCl(001) surface. II. An infrared study at ambient temperatures. *Journal of Chemical Physics*, **112**: 6817-6826.
15. Hucher, M., Oberlin, A., and Hocart, R. 1967. Adsorption of water vapor on the cleavage surfaces of some alkali metal halides. *Bulletin de la Societe Francaise de Mineralogie et de Cristallographie*, **90**: 320-32.

16. Dai, Q., Hu, J., and Salmeron, M. 1997. Adsorption of water on NaCl (100) surfaces: role of atomic steps. *Journal of Physical Chemistry B*, **101**: 1994-1998.
17. Kontny, M.J., Grandolfi, G.P., and Zografi, G. 1987. Water vapor sorption of water-soluble substances: studies of crystalline solids below their critical relative humidities. *Pharmaceutical Research*, **4**: 104-112.
18. Khankari, R.K. and Grant, D.J.W. 1995. Pharmaceutical hydrates. *Thermochimica Acta*, **248**: 61-79.
19. Phadnis, N.V. and Suryanarayanan, R. 1997. Polymorphism in anhydrous theophylline--implications on the dissolution rate of theophylline tablets. *Journal of Pharmaceutical Sciences*, **86**: 1256-63.
20. Herman, J., Visavarungroj, N., and Remon, J.P. 1989. Instability of drug release from anhydrous theophylline-microcrystalline cellulose formulations. *International Journal of Pharmaceutics*, **55**: 143-6.
21. Kahela, P., Aaltonen, R., Lewing, E., Anttila, M., and Kristoffersson, E. 1983. Pharmacokinetics and dissolution of two crystalline forms of carbamazepine. *International Journal of Pharmaceutics*, **14**: 103-12.
22. Matsuo, K. and Matsuoka, M. 2007. Solid-state polymorphic transition of theophylline anhydrate and humidity effect. *Crystal Growth & Design*, **7**: 411-415.
23. Amado Ana, M., Nolasco Mariela, M., and Ribeiro-Claro Paulo, J.A. 2007. Probing pseudopolymorphic transitions in pharmaceutical solids using Raman spectroscopy: Hydration and dehydration of theophylline. *Journal of Pharmaceutical Sciences*, **96**: 1366-79.
24. Rodriguez-Hornedo, N., Lechuga-Ballesteros, D., and Wu, H.J. 1992. Phase transition and heterogeneous/epitaxial nucleation of hydrated and anhydrous theophylline crystals. *International Journal of Pharmaceutics*, **85**: 149-162.
25. Rodriguez-Hornedo, N. and Murphy, D. 2004. Surfactant-facilitated crystallization of dihydrate carbamazepine during dissolution of anhydrous polymorph. *Journal of Pharmaceutical Sciences*, **93**: 449-460.
26. Maji, T.K., Uemura, K., Chang, H.-C., Matsuda, R., and Kitagawa, S. 2004. Expanding and shrinking porous modulation based on Pillared-layer coordination polymers showing selective guest adsorption. *Angewandte Chemie, International Edition*, **43**: 3269-3272.
27. Thallapally, P.K., Lloyd, G.O., Atwood, J.L., and Barbour, L.J. 2005. Diffusion of water in a nonporous hydrophobic crystal. *Angewandte Chemie, International Edition*, **44**: 3848-3851.
28. Connolly, M.L. 1985. Computation of molecular volume. *Journal of the American Chemical Society*, **107**: 1118-24.
29. Connolly, M.L. 1983. Solvent-accessible surfaces of proteins and nucleic acids. *Science (Washington, DC, United States)*, **221**: 709-13.
30. Binnig, G., Quate, C.F., and Gerber, C. 1986. Atomic force microscope. *Physical Review Letters*, **56**: 930-933.
31. Israelachvili, J.N. 1992. Adhesion forces between surfaces in liquids and condensable vapors. *Surface Science Reports*, **14**: 109-59.
32. Zhang, J., Ebbens, S., Chen, X., Jin, Z., Luk, S., Madden, C., Patel, N., and Roberts, C.J. 2006. Determination of the surface free energy of crystalline and

amorphous lactose by atomic force microscopy adhesion measurement. *Pharmaceutical Research*, **23**: 401-407.
33. Davies, M., Brindley, A., Chen, X., Marlow, M., Doughty, S.W., Shrubb, I., and Roberts, C.J. 2005. Characterization of drug particle surface energetics and Young's modulus by atomic force microscopy and inverse gas chromatography. *Pharmaceutical Research*, **22**: 1158-1166.
34. Plassard, C., Lesniewska, E., Pochard, I., and Nonat, A. 2004. Investigation of the surface structure and elastic properties of calcium silicate hydrates at the nanoscale. *Ultramicroscopy*, **100**: 331-338.
35. Goles, F. 1961. The examination and calculation of thermodynamic data from experimental measurements. I. The numerical integration of the vapor-pressure curves of the system methanol-water. *Monatsh. Chem.*, **92**: 981-991.
36. Xu, L., Bluhm, H., and Salmeron, M. 1998. An AFM study of the tribological properties of NaCl(100) surfaces under moist air. *Surface Science*, **407**: 251-255.
37. Carpick, R.W. and Salmeron, M. 1997. Scratching the surface: fundamental investigations of tribology with atomic force microscopy. *Chemical Reviews (Washington, D. C.)*, **97**: 1163-1194.
38. Haugstad, G., Gladfelter, W.L., Weberg, E.B., Weberg, R.T., and Weatherill, T.D. 1994. Probing biopolymers with scanning force methods: adsorption, structure, properties, and transformation of gelatin on mica. *Langmuir*, **10**: 4295-306.
39. Butt, H.J. 1991. Measuring electrostatic, van der Waals, and hydration forces in electrolyte solutions with an atomic force microscope. *Biophysical Journal*, **60**: 1438-44.
40. Mate, C.M., Lorenz, M.R., and Novotny, V.J. 1989. Atomic force microscopy of polymeric liquid films. *Journal of Chemical Physics*, **90**: 7550-5.
41. Garcia, R. and Perez, R. 2002. Dynamic atomic force microscopy methods. *Surface Science Reports*, **47**: 197-301.
42. Cleveland, J.P., Anczykowski, B., Schmid, A.E., and Elings, V.B. 1998. Energy dissipation in tapping-mode atomic force microscopy. *Applied Physics Letters*, **72**: 2613-2615.
43. Zhu, H., Yuen, C., and Grant, D.J.W. 1996. Influence of water activity in organic solvent + water mixtures on the nature of the crystallizing drug phase. 1. Theophylline. *International Journal of Pharmaceutics*, **135**: 151-160.
44. Ticehurst, M.D., Storey, R.A., and Watt, C. 2002. Application of slurry bridging experiments at controlled water activities to predict the solid-state conversion between anhydrous and hydrated forms using theophylline as a model drug. *International Journal of Pharmaceutics*, **247**: 1-10.
45. Amado, A.M., Nolasco, M.M., and Ribeiro-Claro, P.J.A. 2007. Probing pseudopolymorphic transitions in pharmaceutical solids using Raman spectroscopy: hydration and dehydration of theophylline. *Journal of Pharmaceutical Sciences*, **96**: 1366-1379.
46. Otsuka, M., Kaneniwa, N., Kawakami, K., and Umezawa, O. 1990. Effect of surface characteristics of theophylline anhydrate powder on hygroscopic stability. *Journal of Pharmacy and Pharmacology*, **42**: 606-10.

47. Lehto, V.-P. and Laine, E. 2000. Simultaneous determination of the heat and the quantity of vapor sorption using a novel microcalorimetric method. *Pharmaceutical Research*, **17**: 701-706.
48. Vora, K.L., Buckton, G., and Clapham, D. 2004. The use of dynamic vapor sorption and near infra-red spectroscopy (DVS-NIR) to study the crystal transitions of theophylline and the report of a new solid-state transition. *European Journal of Pharmaceutical Sciences*, **22**: 97-105.
49. Otsuka, M., Kaneniwa, N., Otsuka, K., Kawakami, K., Umezawa, O., and Matsuda, Y. 1992. Effect of geometric factors on hydration kinetics of theophylline anhydrate tablets. *Journal of Pharmaceutical Sciences*, **81**: 1189-1193.
50. Heng, J.Y.Y., Thielmann, F., and Williams, D.R. 2006. The effects of milling on the surface properties of form I paracetamol crystals. *Pharmaceutical Research*, **23**: 1918-1927.
51. Ohta, M. and Buckton, G. 2004. Determination of the changes in surface energetics of cefditoren pivoxil as a consequence of processing induced disorder and equilibration to different relative humidities. *International Journal of Pharmaceutics*, **269**: 81-88.
52. Ebisuzaki, Y., Boyle, P.D., and Smith, J.A. 1997. Methylxanthines. I. Anhydrous theophylline. *Acta Crystallographica, Section C: Crystal Structure Communications*, **C53**: 777-779.
53. Allen, S., Connell, S.D.A., Chen, X., Davies, J., Davies, M.C., Dawkes, A.C., Roberts, C.J., Tendler, S.J.B., and Williams, P.M. 2001. Mapping the surface characteristics of polystyrene microtiter wells by a multimode scanning force microscopy approach. *Journal of Colloid and Interface Science*, **242**: 470-476.
54. Cappella, B. and Dietler, G. 1999. Force-distance curves by atomic force microscopy. *Surface Science Reports*, **34**: 1-104.
55. Israelachvili, J.N., *Intermolecular and Surface Forces*. 2 ed. 1991 Academic Press, San Diego, CA.
56. Frisbie, C.D., Rozsnyai, L.F., Noy, A., Wrighton, M.S., and Lieber, C.M. 1994. Functional group imaging by chemical force microscopy. *Science*, **265**: 2071-2074.
57. Green, J.-B.D., McDermott, M.T., Porter, M.D., and Siperko, L.M. 1995. Nanometer-scale mapping of chemically distinct domains at well-defined organic interfaces using frictional force microscopy. *Journal of Physical Chemistry*, **99**: 10965-10970.
58. Overney, R.M., Meyer, E., Frommer, J., Guentherodt, H.J., Fujihira, M., Takano, H., and Gotoh, Y. 1994. Force microscopy study of friction and elastic compliance of phase-separated organic thin films. *Langmuir*, **10**: 1281-1286.
59. Xiao, X., Hu, J., Charych, D.H., and Salmeron, M. 1996. Chain length dependence of the frictional properties of alkylsilane molecules self-assembled on mica studied by atomic force microscopy. *Langmuir*, **12**: 235-237.
60. Waizumi, K., Plomp, M., and van Enckevort, W. 2003. Atomic force microscopy studies on growing surfaces of bovine insulin crystals. *Colloids and Surfaces, B: Biointerfaces*, **30**: 73-86.

61. Kossel, W. 1934. The energy of surface processes. *Annalen der Physik (Berlin, Germany)*, **21**: 457-480.
62. Garcia, R., Martinez, R.V., and Martinez, J. 2006. Nanochemistry and scanning probe nanolithographies. *Chemical Society Reviews*, **35**: 29-38.
63. Amado, A.M., Nolasco Mariela, M., and Ribeiro-Claro Paulo, J.A. 2007. Probing pseudopolymorphic transitions in pharmaceutical solids using Raman spectroscopy: Hydration and dehydration of theophylline. *Journal of Pharmaceutical Sciences*, **96**: 1366-79.
64. Landman, U., Luedtke, W.D., Burnham, N.A., and Colton, R.J. 1990. Atomistic mechanisms and dynamics of adhesion, nanoindentation, and fracture. *Science (Washington, DC, United States)*, **248**: 454-461.
65. Dey, F.K., Cleaver, J.A.S., and Zhdan, P.A. 2000. Atomic force microscopy study of adsorbed moisture on lactose particles. *Advanced Powder Technology*, **11**: 401-413.
66. Forcada, M.L., Jakas, M.M., and Gras-Marti, A. 1991. On liquid-film thickness measurements with the atomic-force microscope. *Journal of Chemical Physics*, **95**: 706-708.
67. Kaneniwa, N., Yamaguchi, T., Watari, N., and Otsuka, M. 1984. Hygroscopicity of carbamazepine crystalline powders. *Yakugaku Zasshi*, **104**: 184-90.

Chapter 5

Water Sorption Induced Crystal → Liquid Crystal Transition of Trifluoperazine Dihydrochloride

5.1 Abstract

Water vapor sorption induced transformation of crystalline trifluoperazine dihydrochloride (**I**) to a liquid crystalline phase (**II**). **II** exhibited birefringence and was characterized to be a liquid crystalline phase by X-ray diffractometry (XRD). The transformation from **I** to **II** showed a long lag time of 3 months at 75% RH (RT), and the transition RH was determined to be between 68 and 75% (25°C). **II** was physically stable at 2% RH (25°C) for at least 6 months. When compared with its crystalline counterpart, **II** exhibited higher dissolution rate and decreased chemical stability, indicating its higher free energy state. The formation of liquid crystalline phase was studied by near-infrared spectroscopy, XRD, and isothermal calorimetry. TFP, consisting of a hydrophobic head group (phenothiazine ring) and a hydrophilic tail (piperazine side chain), is surface active and can form a lyotropic liquid crystalline phase by incorporating water into the hydrophilic layers through strong ion-dipole interactions. During the transformation, TFP molecules rearranged from a lamellar stacking in the crystalline phase to a hexagonal structure in the liquid crystalline phase. The hexagonal phase was constructed with the shell of stacked phenothiazine ring and the core of piperazine side chain and water. The transformation (crystal → liquid crystal) is proposed to be enthalpically driven. The findings from this study may help understand the water sorption induced liquid crystal formation in other surface active pharmaceutical compounds.

5.2 Introduction

Water sorption by pharmaceutical solids, which can occur during dosage form manufacture and subsequent storage, can cause phase transformation and affect product performance.[1-3] It is therefore prudent to investigate the interaction of water with the API early on in the development of solid dosage forms. In addition to adsorption, in crystalline materials, water sorption can lead to hydrate formation, capillary condensation, and deliquescence. Unless the surface area of the solid is very high, the adsorbed water in pharmaceutical solids tends to be < 0.1%.[4] About one-third of pharmaceuticals are known to form hydrates, and this subject has received extensive attention in the literature.[5-7] Capillary condensation occurs only in porous materials, and is therefore irrelevant for most pharmaceuticals.[8] Deliquescence, a phenomenon wherein drug dissolves in the sorbed water, is often observed in highly water soluble crystalline solids. In amorphous materials, water sorption, by lowering the glass transition temperature (T_g), can facilitate physical and chemical changes.

In addition to the water-solid interactions discussed above, water sorption by a crystalline solid can also lead to the formation of a mesophase, which is an intermediate state between the highly periodic crystalline state and the "disordered" amorphous state.[9, 10] Mesophases, because of their reduced stability compared to their crystalline counterparts, can pose challenges in solid dosage form development, manufacture and use. Therefore, this category of water-solid interaction warrants comprehensive investigation. In this paper, we have studied the crystal $\rightarrow$ liquid crystal (LC) transformation, and attempted to understand the mechanism of the water sorption induced transformation.

Mesophases are intermediate states of matter existing between the liquid and the crystalline states, characterized by a partial loss of three-dimensional order. As a subcategory of mesophases, liquid crystals possess orientational order without

positional order, and exhibit various degrees of birefringence.[11] In addition to applications in display and temperature probe devices,[12] liquid crystalline materials have been used in liposome and microemulsion formulations designed for sustained drug release.[13, 14]

Many compounds of pharmaceutical interest are known to form liquid crystals.[15, 16] Thermotropic liquid crystals, which are usually rod or disc shaped, undergo structural change before melting.[16] Calcium salts of ketoprofen, salicylic acid, fenoprofen, and mefenamic acid formed liquid crystals during dehydration.[9, 17-19] It was proposed that a two-dimensional lamellar structure was formed when carboxylic acid rearranged around the calcium ions after water removal.[19] Lyotropic liquid crystals consist of amphiphilic molecules and their formation is induced by the presence of a solvent. Surfactants[13], polymers[20], and macromolecules, including cyclosporine[21], and amylin[22] are known to form lyotropic liquid crystals. As the solvent concentration is changed, there can be phase transformation between liquid crystalline phases.[23] Dimethyldodecylamine-N-oxide - water system underwent a transition from lamellar to cubic and from cubic to hexagonal phase at approximately 81 and 85 mol % of water (25°C) respectively.[24] Pharmaceutical processing can also induce liquid crystal formation as was observed following the freeze-drying of nafcillin sodium.[25]

While liquid crystal formation in aqueous solution is well-known, there are only a few reports of liquid crystal formation in the “solid state” following water vapor sorption. A non-stoichiometric hydrate, cromolyn sodium, underwent hydrate → liquid crystal transformation at high RH values.[26] In this case, continuous water uptake, as a function of RH, occurred into the lattice resulting in a series of non-stoichiometric hydrates. At 97% RH (25°C), when the lattice could no longer hold the water, the hydrate transformed into a liquid crystalline phase. In another case, the crystallinity of L-660711, a leukotriene D_4 receptor antagonist, decreased following water sorption.[27] While the formation of a mesomorphic structure was

proposed, the structure and mechanism of the phase transformation remained unexplored.

In a previous investigation, the interaction between water and crystalline active pharmaceutical ingredients (API) was evaluated. In this comprehensive investigation, over 40 APIs were subjected to RH values ranging from 0 to 90% at 25^{o}C. Trifluoperazine dihydrochloride (TFP; form **I**), an antipsychotic and sedative, transformed to a liquid crystalline phase upon water sorption. However, we do not have a mechanistic understanding of the water sorption induced liquid crystal formation. This unusual and unique solid-vapor interaction forms the basis of the current investigation. Extensive investigation of the liquid crystal formation was carried out to understand the mechanism of water sorption induced liquid crystal formation. In addition, the interactions between water and solid as a function of water activity, and the thermodynamics of liquid crystal formation were studied.

5.3 Material and Methods

5.3.1 Material

Trifluoperazine·2HCl (**TFP**) crystalline powder were purchased from Sigma and used without further treatment. TFP liquid crystalline sample was prepared by storing crystalline powder at 94% RH for 3 days, followed by drying at 2% RH (anhydrous $CaSO_4$) for one day at 25°C.

5.3.2 Water Vapor Sorption

Sample powder (~ 5 mg) was placed in the sample quartz boat of an automated vapor sorption microbalance (DVS-1000, Surface Measurements Systems,

London, UK). The microbalance was calibrated using a 100 mg standard weight. The relative humidity sensor was calibrated at 5.0, 11.3, 32.8, 52.8, 75.3, and 84.3% RH (25°C), using saturated salt solutions. Unless stated otherwise, all the experiments were performed at 25°C. The samples were initially dried at 0% RH for 3 hours and then exposed to the desired RH. The rate and extent of water uptake was determined over a range of RH conditions. The exposure time at each step varied from 1 to 6 h depending on the time required for equilibration. The attainment of equilibrium was assumed when the weight change was < 0.02% in one hour. The water uptake was expressed as the percentage of weight increase with respect to the initial sample weight.

5.3.3 Powder X-ray Diffractometry (XRD)

About 200 mg of sample were packed into an aluminum holder by the side-drift method and exposed to Cu Kα radiation (45 kV, 40 mA) in a wide-angle X-ray diffractometer (Model D5005, Siemens, Madison, WI, USA). The instrument was operated in the step-scan mode over the angular range of 2 to 50° 2θ. The step size was 0.05° 2θ and counts were accumulated for 1 s at each step. The data collection and analyses were performed with commercially available software (JADE, version 5.1 Materials Data Inc., Livermore, CA, USA).

5.3.4 Polarized Light Microscopy (PLM)

Powder was sprinkled on a glass slide. The images were taken in transmittance mode in a microscope equipped with crossed polarizers (Nikon, Japan). The images were processed using commercial software (Metamorph® Imaging System, Molecular Devices, Downingtown, PA).

5.3.5 Scanning Electron Calorimetry (SEM)

The samples were mounted on scanning electron microscopy (SEM) stubs with double-sided carbon tape, coated with platinum (50 Å), and observed under a scanning electron microscope (JEOL 6500, Tokyo, Japan).

5.3.6 Isothermal Calorimetry

The heat flow (*P* in mW), following exposure of TFP to different RH values (at 25°C), was monitored in an isothermal calorimeter, TAM (Thermal Activity Monitor, Model 2277 Thermometric AB, Sweden). About 70 mg of sample was placed in a stainless steel ampul and connected to a gas pressure controller (TA instruments, Delaware, US), which accurately controls the RH within the ampul (0 – 90 ± 0.1 % RH) by mixing dry and wet nitrogen in different ratios. An empty closed ampul was used as the reference cell. Dry nitrogen was used as carrier gas at a constant flow rate of 50 ml/min.

5.3.7 Near Infrared Spectroscopy (NIR)

The spectra were obtained in the reflectance mode (Vertex 70, Bruker optics, Madison, WI, USA), with a NIR fiber-coupling module. Each spectrum was the average of 32 scans over the range of 15000 to 3800 cm^{-1} with a 2 cm^{-1} resolution. The spectrum of a white ceramic plate served as the reference. The data analysis was performed with a commercially available software (OPUS, Ver. 5.05, Madison, WI, USA).

5.3.8 Water Activity Measurement

The water activities of saturated solutions were determined by an RH sensor (Rotronic, Huntington, NY). Saturated solution was prepared by mixing ~ 1 g solid with ~ 100 µl deionized water. To ensure the attainment of saturation, the water activity was obtained after equilibration for 24 h in the closed chamber.

5.3.9 High Pressure Liquid Chromatography

The HPLC system included a pump (Model LC-10AT VP, Shimatsu, Columbia, MD), a HPLC column (Angilent Zorbox SB-C18, 5µm, 4.6 × 150 mm, Santa Clara, CA), and a UV detector (Shimatsu, SPD-10AV VP, Shimatsu, Columbia, MD). The mobile phase contained 50% v/v acetonenitrile, 25% v/v methanol, and 25% v/v phosphate buffer (pH 4.2). The mobile phase was filtered through a 0.45 µm membrane (Millipore, Milford, MA) and degassed prior to use. The flow rate was 1 ml/min. The absorbance was determined at 240 nm.

5.3.10 Dissolution of TFP Phases at 25°C

The dissolution rates of form **I** and liquid crystal in ethyl acetate and acetone were determined at 25°C. Excess solid (~30 mg) was suspended in 10 ml solvent and the suspension was equilibrated in a water bath with magnetic stirrer. Aliquots were drawn at time intervals of 3 hours, 1, 2, 3, and 7 days, and dried under a nitrogen purge for 5 min. The solid residues were then reconstituted with 5 ml of 0.1 M aqueous hydrochloric acid solution. The absorbance of the solution at 257 nm was determined by a UV spectrophotometer (Beckman Coulter Du 530, Fullerton, CA, USA).

5.4 Results and Discussion

5.4.1 Water Vapor Sorption

In Fig. 5.1, the water sorption/desorption isotherms of form **I** (**I**) are provided. The water content in **I** was constant at 1.5% (w/w) from 20% to 75% RH, followed by a rapid increase to 7% and 32% at 80% and 94% RH, respectively. The hockey-stick shaped sorption isotherms have been commonly observed for many hygroscopic crystalline pharmaceutical materials which deliquesce at high RH.[28] However, after storage at 94% RH (25°C) for 3 days, the sample contained 32% (w/w) water and exhibited birefringence. The XRD pattern revealed a broad halo, over the angular range of 15 to 30° 2θ and an intense XRD peak at 3.2° 2θ. This suggested the formation of a liquid crystalline phase. During the desorption cycle, there was a linear decrease in water content. The sample exhibited a pronounced hysteresis. This issue is discussed in detail later. During the second cycle, the sample showed a linear water sorption – desorption profile with no hysteresis.

The water sorption microbalance is designed to study the water sorption behavior of materials in a short time period. As a result, equilibrium may not be attained. Since there was a need to determine the long-term water uptake, three samples of **I** were stored at 75% RH (25°C) for a prolonged time period with monthly sampling. During the first three months of storage, there was a small (< 2% w/w) weight increase, with no appreciable changes in the XRD and DSC. However, after 4 months, the water content increased to 8% (Fig. 5.2). While a low intensity peak appeared at 3.5° 2θ, the characteristic peaks of form **I** did not show any appreciable change in position or intensity (Fig. 5.3). The peak at 3.5° 2θ is assigned to a liquid crystalline phase (details follow). The coexistence of crystalline and liquid crystalline phases at 75% RH, suggested that the form **I** → liquid crystal transition occurred at RH close to 75% (25°C).

5.4.2 Structural Characterization of Liquid Crystalline Phase

Our preliminary studies indicate that the sample obtained following storage of form **I** (**I)** at 93% RH was a liquid crystalline phase. It was subjected to detailed characterization. Fig. 5.4 presents the XRD patterns of **I** (<1% w/w water) and liquid crystal (**II**) (2% w/w water) at 25°C. **I,** as reported in the literature**,** exhibited peaks at 9.9°, 15.1°, 20.2°, 21.8°, and 24.6° 2θ.[29] **II** showed one high intensity peak at 3.4° 2θ, three low intensity peaks (6.0°, 7.0°, and 9.5° 2θ), and a halo in the angular range of 15° to 35° 2θ. The four peaks (3.4, 6.0°, 7.0°, and 9.5° 2θ) below 10° 2θ had a position ratio of $1:\sqrt{3}:2:\sqrt{7}$ with respect to the peak at the lowest 2θ value. This is a characteristic of a hexagonal liquid crystalline structure.[11] Considering that the TFP molecule is T-shaped, one approach for efficient packing is to locate the bulky phenothiazine ring in the outer shell, and the long piperazine side-chain and water in the inner core of the hexagonal cylinder (Fig. 5.5).

The SEM images of **I** and **II** are shown in Fig. 5.6. **I** was rod-shaped and showed distinct edges, while **II** appeared to be particles fused together with fiber-shaped solid bridges. It could be proposed that at higher RH values, individual crystal particles sorbed water to form liquid crystals. As a result of the reduction in viscosity, the particles merged with solid bridges in between.

I and **II** exhibited birefringence when observed under a polarized light microscope (Fig. 5.7).

5.4.3 Phase Diagram of TFP at Different RH Values (25°C)

Only a very small fraction of **I** transformed to liquid crystals after storage at 75% RH (25°C) for 12 months (Figs. 5.2 and 5.3). This slow transition kinetics suggested that the form **I** → liquid crystal transition RH (RH_{LC}) was close to 75%

(25°C). The RH_0 of form **I** was determined to be 97% at 25°C. Based on the RH_{LC} and RH_0 values, a schematic phase diagram was drawn (Fig. 5.8). Below 75% RH, crystalline form **I** is stable. Between the RH_{LC} (75%) and RH_0 (97%), liquid crystal is the stable form and the water content increased as a function of RH. Above $RH_{0,}$ TFP exhibited deliquescence.

Phase transformations of TFP phases, at different RH values were also investigated to validate the proposed phase diagram. TFP liquid crystals slowly recrystallized after storage at 54% RH for 6 months, confirming instability at this RH value. Amorphous TFP, prepared by cryo-milling was stored at RH values ranging from 11 to 93%. It transformed into crystalline form **I** and liquid crystalline phase after storage at 68 and 75% RH for 2 weeks, respectively. Thus the RH_{LC} is likely to be between 68 and 75% at 25°C.

5.4.4 Thermodynamics of Liquid Crystal Formation

The sorption of water by form **I** (crystalline) leads to liquid crystal formation (Process 1). This could be divided into two hypothetical steps. The lattice rearrangement from crystalline form **I** to a hypothetical "dry" liquid crystalline state (process 2) and the sorption of water by the "dry" liquid crystals (process 3).

Crystal + Water vapor → Liquid crystal (wet) (1)
Crystal → Liquid crystal (dry) (2)
Liquid crystal (dry) + Water vapor → Liquid crystal (wet) (3)
(1) = (2) + (3)

For the water sorption induced crystalline to liquid crystalline transition to be spontaneous, the free energy change (ΔG) must be negative.

$$\Delta G = \Delta H - T\Delta S \qquad \text{Eqn. 5.1}$$

where ΔH and ΔS are the enthalpy and entropy change associated with form **I** → liquid crystal transformation.

During liquid crystal formation, water condensed from vapor to solid phase, a process resulting in a drastic decrease in the entropy of H_2O. On the other hand, when the crystalline TFP transforms to a liquid crystalline state, the entropy of TFP increases.

The change in the free energy could be negative when 1) ΔH is negative and its absolute value is higher than that of $T\Delta S$ or 2) $T\Delta S$ is positive and its absolute value is higher than that of ΔH. In the former case, the liquid crystal formation is enthalpically driven, and in the latter case, it is driven by entropy.

Isothermal microcalorimetry has been used to study transformations between different liquid crystalline phases and to determine the key thermodynamic factors driving the phase transformation.[30] To measure the heat involved during the water sorption induced liquid crystal formation, form **I** was exposed to 90% RH, to induce *in situ* transformation to liquid crystals (water content of 32% w/w) in the isothermal microcalorimetry. The RH was then abruptly decreased to 0%, to remove most of the water (residual water content < 2% w/w). However, the sample was retained in the liquid crystalline state. The RH was then progressively increased to 11, 54, 75 and 90%. It was held at each RH for 10 hours. Finally, the RH was again decreased to 0% (Fig. 5.9).

The water content at different RH values in the microcalorimeter was estimated using ASM at similar experimental conditions. The water content and heat flow at each RH step in the microcalorimeter have been tabulated (Table 5.3). The liquid crystal formation, following exposure to 90% RH, was an exothermic process (Fig.

5.9). When the RH was decreased to 0%, the endotherm is attributed to the removal of water from the liquid crystalline phase. In spite of the low water content (< 2% w/w), the liquid crystals were stable in the time scale of the experiment. When the RH was then increased incrementally, a pronounced heat flow was observed at each RH. This could be attributed to the enthalpy change associated with water sorption into the liquid crystalline phase. The two endotherms observed when decreasing RH from 90% to 0% were close (355.1 and 354.9 kJ/mol). The magnitude of the cumulative heat flow (the four exotherms, -354.5 kJ/mol) is approximately equal but opposite in sign to that associated with water removal (observed following storage at 0% RH, 355.1 kJ/mol). The small difference in the absolute values of the heats of sorption and desorption agreed with the observation that there was no hysteresis in the sorption/desorption isotherm in the ASM

The microcalorimetry enabled us to determine the enthalpy change associated with the transformation of form **I** to liquid crystal. In addition, we were able to correlate the enthalpy change with water content ranging from 2 to 32% w/w. A plot of the enthalpy change (in kJ/mol of TFP) as a function of the water content (weight of water / initial weight of TFP), revealed a linear relationship (Fig. 5.10). This suggests that the enthalpy change associated with lattice rearrangement (transformation of form **I** to the hypothetical “dry” liquid crystal) is constant and is independent of the water content. The value of the intercept on the y-axis, 27.5 kJ/mol of TFP, is therefore considered the enthalpy change for the lattice rearrangement.

From the slope value of the plot (-1170 kJ/mol of TFP), the enthalpy of water sorption into the liquid crystalline phase was calculated to be -43.8 kJ/mol of water. The enthalpy of solvation has been used to evaluate the strength of the host-solvent interaction in a solvate.[31, 32] The calculated enthalpy of -43.8 kJ/mol for water sorption into liquid crystals is very close to the heat of vaporization of

water at 25°C (44.0 kJ/mol).[33] This suggests a weak interaction between water and TFP molecules in the liquid crystals.[34]

We had earlier divided the overall liquid crystal formation into two hypothetical steps (Process 2 and 3). We were interested in quantifying the contribution of these steps to the overall liquid crystal formation process. The enthalpy and entropy changes associated with form **I** → liquid crystal formation were calculated at different RH values (25°C). This calculation was done assuming that the entropy change associated with the lattice rearrangement (form **I** → "dry" liquid crystal) is independent of the water content (Table 5.2). This assumption is likely to valid since the enthalpy change associated with this process is believed to be independent of the water content (Fig. 5.10).

We had earlier seen that the enthalpy of water sorption into liquid crystals (-43.8 kJ/mol) is very close to the heat of condensation of water at 25°C (-44.0 kJ/mol).[33] On this basis, we assume that the entropy change associated with water sorption into liquid crystals is equal to that of water condensation.

We had earlier observed that the form **I** and the liquid crystalline phase coexisted at 75% RH (25C) (Figs. 5.3 and 5.8). We therefore assume that the free energy change for form **I** → liquid crystal transformation is zero at 75% RH. The entropy change of lattice rearrangement was calculated using the following equation:

$$\Delta G_{75\%RH} = (\Delta H_{C\rightarrow LC} + \Delta H_{Sorption}) - T(\Delta S_{C\rightarrow LC} + \Delta S_{Sorption}) = 0 \quad \text{Eqn. 5.3}$$

where $\Delta H_{C\rightarrow LC}$ and $\Delta S_{C\rightarrow LC}$ are the enthalpy and entropy changes associated with lattice rearrangement, respectively, and $\Delta H_{Sorption}$ and $\Delta S_{Sorption}$ are respectively the enthalpy and entropy changes associated with water sorption,.

The entropy change of water condensation at different RH values can be calculated using the equation:[35]

$$\Delta S_{RHx} = \Delta S^{o} + R \ln (P_{RHx} / P_0) \quad \text{Eqn. 5.3}$$

where ΔS_{RHx} is the entropy change of water condensation at the RH value of x, ΔS^0 is the entropy change of water condensation at 100% RH (25°C). (P_{RHx} / is the water vapor pressure at RH value of x and P_0 is the saturated water vapor pressure at the same temperature.

From the calculations (Table 5.2), it is evident that the enthalpy change associated with water sorption is the major contributor to the overall enthalpy change associated with form **I** → liquid crystal transformation. Similarly the entropy change associated with water sorption into the liquid crystals is the major contributor to the overall entropy change associated with form **I** → liquid crystal transformation. At 93% RH, the enthalpy change associated with water sorption makes the predominant contribution to the free energy decrease (negative value of ΔG).

5.4.5 *In Situ* Near-Infrared Spectroscopy

Near infrared spectroscopy (NIR) has proven to be a powerful tool to investigate the state of water in solids.[36-38] Liquid water has strong absorption at 1420 and 1920 nm, which are attributed to the first overtone of O-H stretching and the combination of O-H stretching and bending,[39] respectively. The exact position and width of these bands vary slightly, depending on the chemical environment of water. Sugar and water can form strong hydrogen bond, leading to shifting of water peaks from 1420 and 1920 to 1430 and 1930 nm.[40] Ions have strong electron withdrawing effect, which can lead to a shift of the water peaks to even longer wavelengths.[41, 42] The water overtone peak shifts to 1440 nm in 5M NaCl solution.[42] To investigate the state of water during liquid crystal formation, form **I** was stored at 94% RH (25°C) and diffuse reflectance NIR spectra were obtained periodically (Fig. 5.11). Two NIR peaks at 1950 and 1450 nm were observed and attributed to water in the solid. The area under the water peaks (1950 and 1450 nm) increased as a function of water content during liquid crystal formation. The

pronounced shift of the water peaks to a longer wavelength (1450 nm) suggested strong ion-dipole interaction between water and TFP molecules in the liquid crystals. It is proposed that water is sorbed into the hydrophilic layers during liquid crystal formation, where the chloride and tertiary amine ions are located.

5.4.6 Phase Transformation during Liquid Crystal Formation

To investigate the lattice structural changes following water sorption, the XRD patterns of **I** were obtained (Fig. 5.12) following storage at 94% RH (25°C). Storage for 0, 9, 28, and 40 hours, resulted in water content of 1, 14, 22, and 32%, respectively. After storage for 9 hours, a peak appeared at 3.4° 2θ, and the intensity of the other peaks decreased. As the storage time was increased to 28 hours, while the intensity of the 3.4° 2θ peak increased, all the other peaks had virtually disappeared. At the same time, three low intensity peaks at 6.0°, 7.0°, and 9.2° 2θ were observed, which were attributed to the hexagonal liquid crystalline phase. After storage for 40 hours, no peaks over the angular range of 10° to 35° 2θ had, reflecting complete disappearance of form **I**. During liquid crystal formation, neither peak position nor peak shape of the crystalline peaks showed significant change.

Phenothiazine derivatives have shown strong tendency of self association through π-π interactions in aqueous solutions.[43-45] The hydrophilic layers sorbed water through ion-dipole interaction, which induced transformation from crystalline to liquid crystalline state. It is therefore postulated that liquid crystal formation may not significantly alter the stacking of phenothiazine rings in the crystal lattice during the form **I** → liquid crystal transformation.

5.4.7 Light-induced Oxidation

Phenothiazine derivatives are known to undergo light-induced oxidation.[46] TFP sulfoxide was detected by HPLC, following exposure of **I** and **II** to ambient light for 2 weeks. The peak area ratio of the sulfoxide to the parent compound (TFP) was used as a relative measure of the extent of oxidation. **I** and **II** were stored at 2% RH (25°C) for one month under exposure to ambient light. The ratio of sulfoxide to TFP in stored sample of **II** was 5 times that in **I**. The enhanced molecular mobility in the liquid crystal could be responsible for its decreased chemical stability.

5.4.8 Dissolution of TFP Crystal and Liquid Crystal

Mesophases, because of their higher free energy, exhibit higher solubility and dissolution rate when compared with their crystalline counterparts.[9] The dissolution rate of **II** (the liquid crystalline phase) was higher than that of form **I** in ethyl acetate. Powder samples of **I** and **II** were suspended in ethyl acetate at 25°C and stirred. After 3 hours, the TFP concentrations were determined to be 62 and 150 μg/ml in suspensions of **I** and **II** respectively. When the excess solid in contact with the solution was characterized by XRD, no phase transformation was evident.

Many compounds of pharmaceutical interest have been found to exist as mesophases,[9, 16, 19] This is different from the crystalline and amorphous states commonly encountered. In this paper, a crystalline phase was found to sorb water and transform into a liquid crystalline phase. This behavior could be explained by the amphiphilic nature of trifluoperazine·2HCl molecules, in which hydrophobic phenothiazine rings tended to stack over each other through π-π interactions, while the hydrophilic nature was brought about through the piperazine side chains. Liquid crystal formation significantly affected the

physicochemical properties of the solid, including hygroscopicity, physicochemical stability, and dissolution rate.

5.5 Conclusions

Crystalline TFP form **I** (**I**) sorbed water and transformed to a hexagonal liquid crystalline phase (**II**) in the solid state. The RH for the crystal $\leftrightarrow$ liquid crystal transformation (RH_{LC}) was between 68 and 75% (25°C). The form **I** $\rightarrow$ liquid crystal transformation was enthalpically driven. The liquid crystals, when compared with form **I**, exhibit increased tendency to sorb water, decreased chemical stability and increased dissolution rate.

Acknowledgement

We thank Mr. Michael Mathew in Boehringer Ingelheim for conducting the thermal activity experiments, and Prof. Timothy S. Wiedmann and Dr. Guifang Zhang for assisting in the HPLC work.

Table 5.1 The calculated diameters of the hexagonal cylinder (Å) and water content (%, w/w) of TFP LC stored at different RH values at RT.

RH, %	Water (%, w/w*)	Mole Ratio (water / TFP)	d-spacing (Å)
2	2	0.5	23
11	6	1.6	23
53	17	4.5	24
75	26	7.0	26
93	32	8.5	28

* with respect to dry weight

Table 5.2 Calculation of thermodynamic parameters of liquid crystal formation at different RH values at 25°C.

RH (%)	Water content[a]	Enthalpy change of water sorption[b]	Lattice enthalpy change[c]	Total enthalpy change[d]	Water entropy change[e]	Lattice entropy change[f]	Total entropy change[g]	TΔS	ΔG
		kJ/mol[h]	kJ/mol[h]	kJ/mol[h]	kJ/mol/K[i]	kJ/mol/K[i]	kJ/mol/K	kJ/mol[h]	kJ/mol[h]
11	0.06	-70.1	27.5	-42.6	-0.266	0.115	-0.15	-45.0	2.4
53	0.17	-198.7	27.5	-171.2	-0.695	0.115	-0.58	-172.8	1.6
75	0.26	-303.9	27.5	-276.4	-1.043	0.115	-0.93	-276.5	0.0
93	0.32	-374.1	27.5	-346.6	-1.268	0.115	-1.15	-343.6	-3.0

[a] weight of water / initial weight of TFP

[b], calculated from the best-fit line in Fig. 5.10. Enthalpy change of water sorption = slope x water content x molecular weight of TFP

[c] this was assumed to be constant and independent of water content.

[d] calculated as the sum of enthalpy change of solvation and lattice rearrangement.

[e] calculated using the equation: ΔS = water content * (480 /18) * (-0.148 + R (ln(RH))); entropy change of water condensation at 100% RH (25°C) = -0.148 kJ/mol/K

[f] assumed to be constant and independent of water content. It is calculated assuming the free energy change of liquid crystal formation at 75% RH (25°C) is zero.

[g] calculated as the sum of entropy change of solvation and lattice rearrangement.

[h] kJ/mol of TFP.

[i] kJ/mol/K of TFP

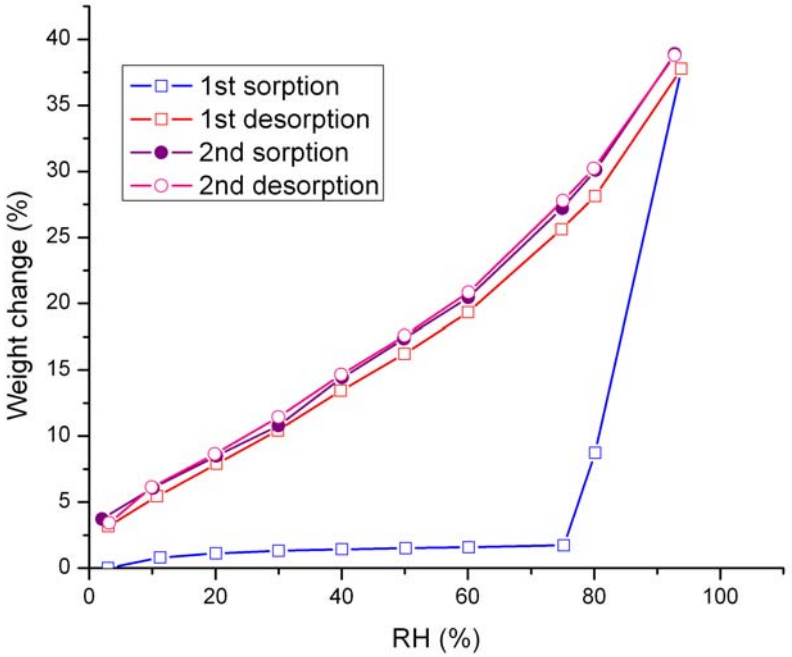

Fig. 5.1 Water sorption/desorption isotherms of form **I** at 25°C. Two sorption/desorption cycles are shown in this figure.

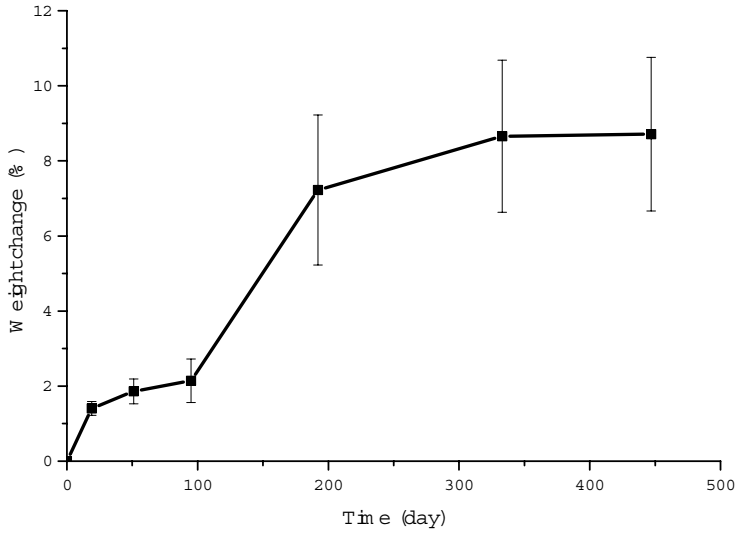

Fig. 5.2 Water uptake following storage of form **I** at 75% RH (RT). Error bars represent standard deviation (n=3).

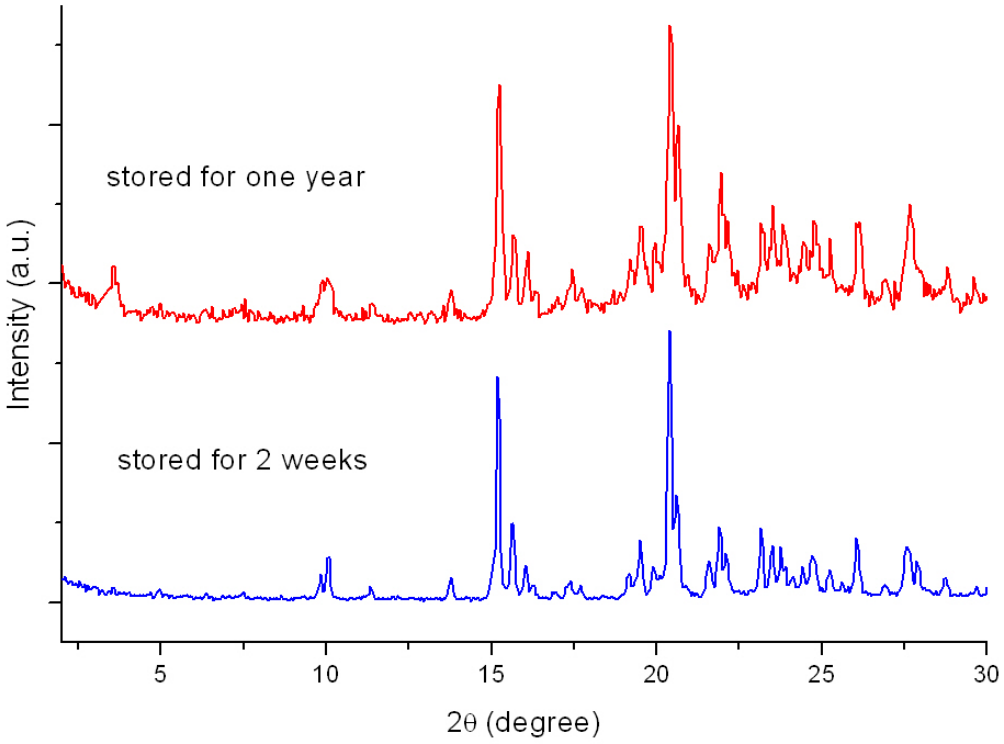

Fig. 5.3 The XRD patterns of TFP form **I** after storage at 75% RH (RT) for one year (with 8% H_2O) and two weeks (1.5% H_2O). The water content of TFP after 2 weeks of storage was 1.5% w/w and after 1 year of storage it increased to 8% w/w.

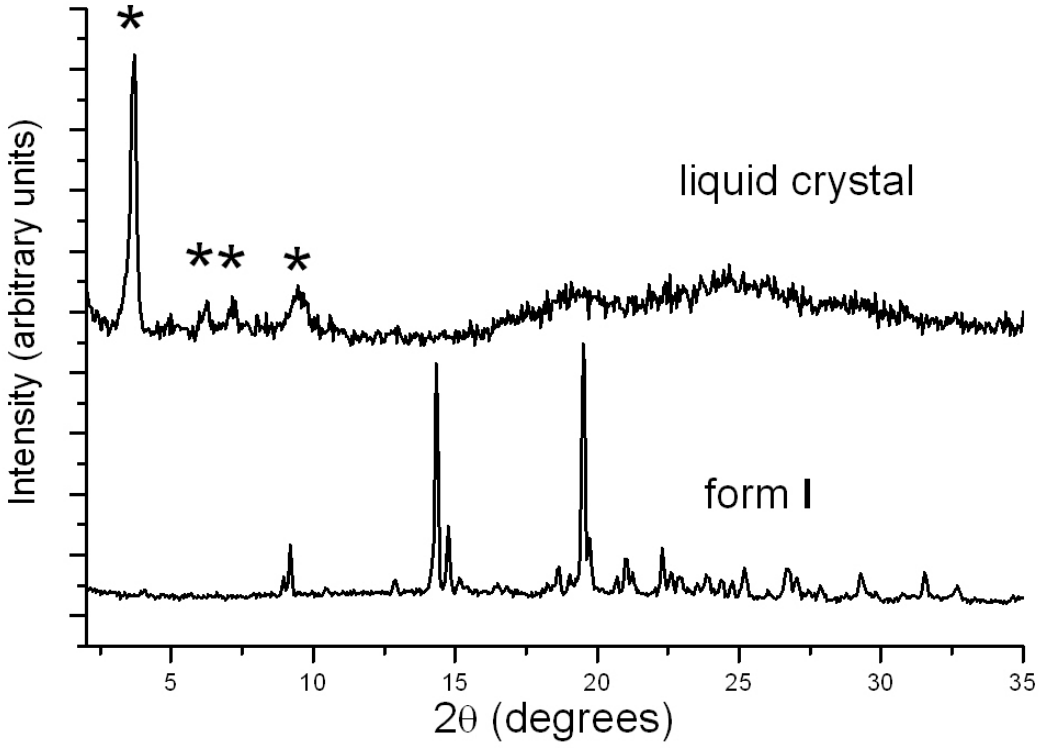

Fig. 5.4 XRD patterns of TFP form **I** and liquid crystal powders after storage at 2% RH (RT) for one week.

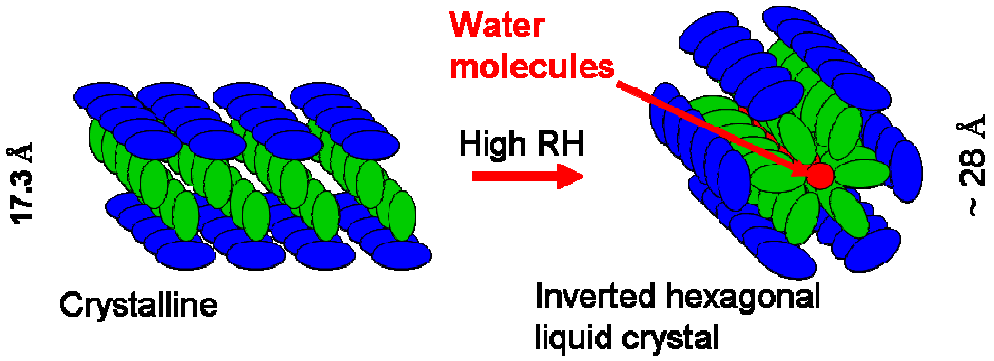

Fig. 5.5 A schematic representation of the mechanism of TFP crystal → liquid crystal transformation. Water sorption occurs in the hydrophilic regions (piperazine side chain indicated by the gray ellipsoids), resulting in rearrangement from lamellar into hexagonal structure. The phenothiazine rings (dark ellipsoids) and water (arrow) constitute the hydrophobic regions.

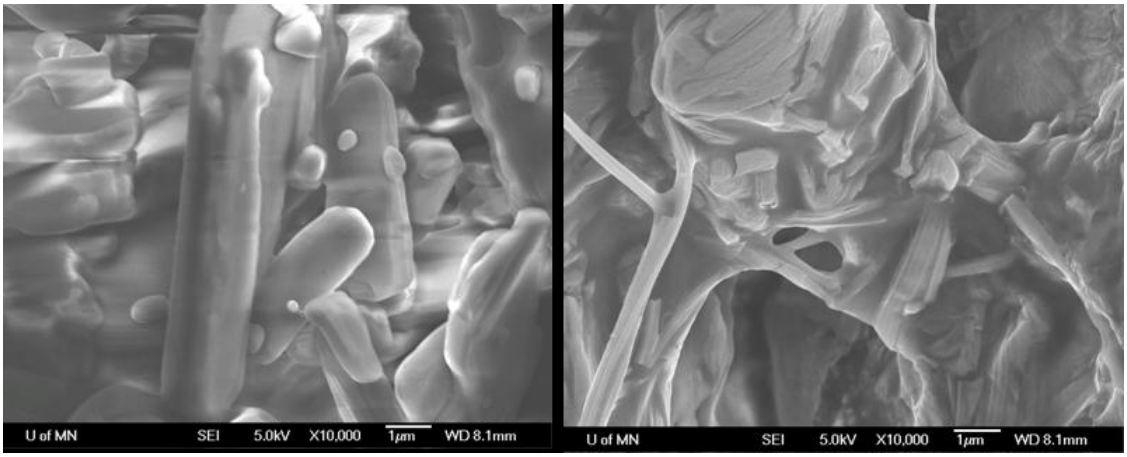

Fig. 5.6 Scanning electron microscopic images of TFP form **I** (left) and liquid crystal (right).

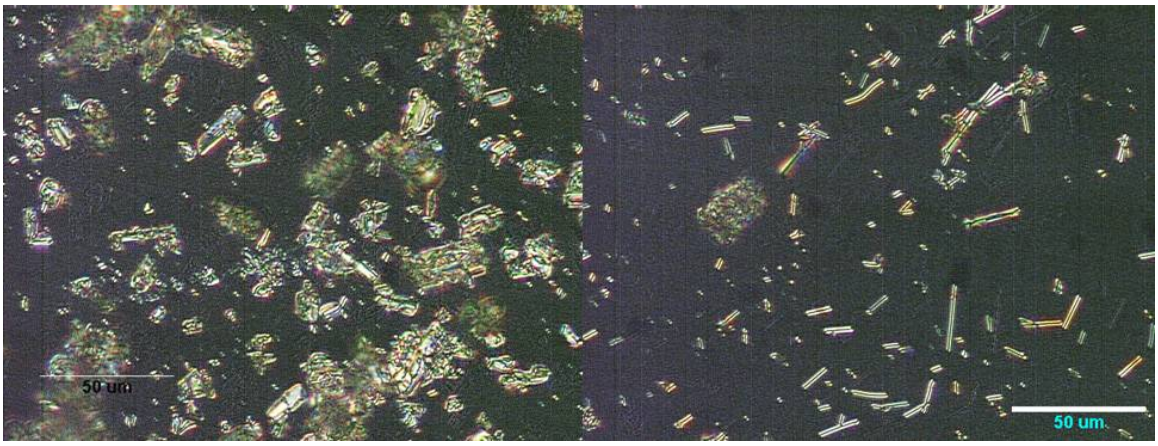

Fig. 5.7 Polarized light microscopic images of TFP form **I** (left) and liquid crystal (right).

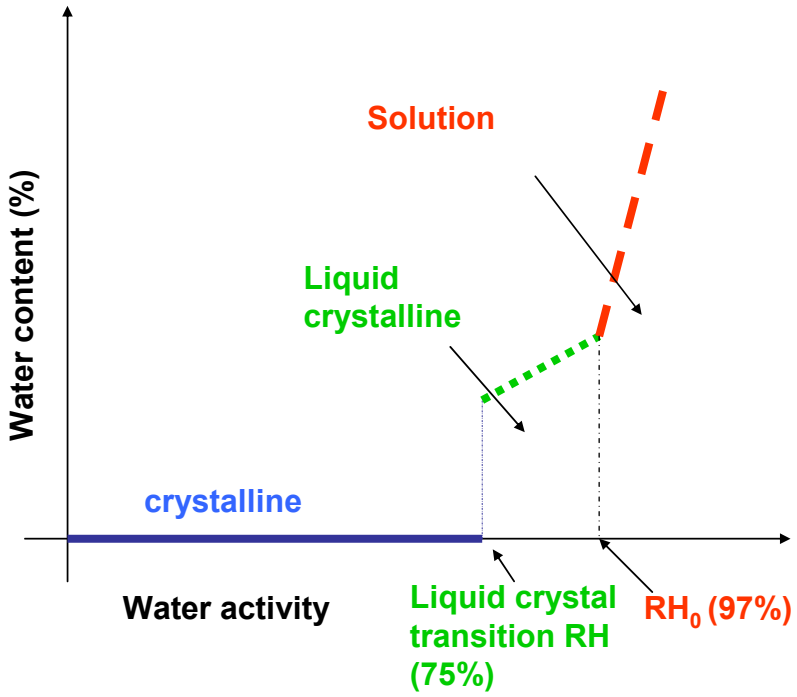

Fig. 5.8 A schematic phase diagram of TFP at 25°C. Below the liquid crystal transition RH, the crystalline TFP is the stable form with negligible water uptake. Between the liquid crystal transition RH and RH_0, TFP liquid crystal is the stable form with significant water uptake but still in the solid state. Above the RH_0, TFP sorbs water and forms solution.

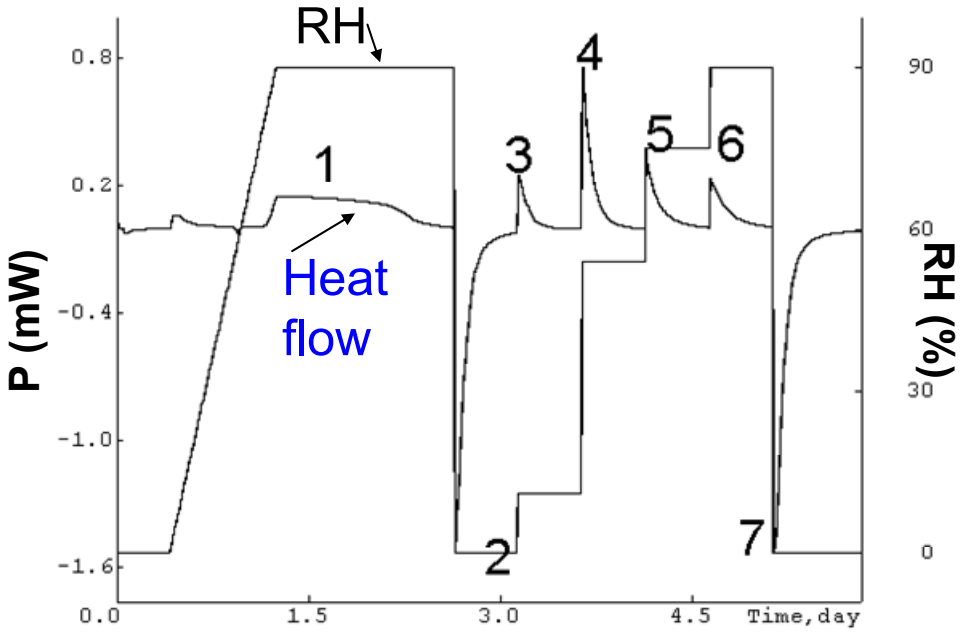

Fig. 5.9 Power-time curve of form **I** following exposing to different RH values (25°C).

Table 5.3 The water content and heat flow following exposing form **I** to different RH values (25°C) in isothermal microcalorimeter.

	RH (%)	H_2O (w/w of TFP)	Heat flow (kJ/mol of TFP)
1	90	0.32	-345.2
2	0	0.02	355.1
3	11	0.06	-52.0
4	54	0.17	-144.2
5	75	0.26	-83.0
6	90	0.32	-75.3
7	0	0.02	354.9

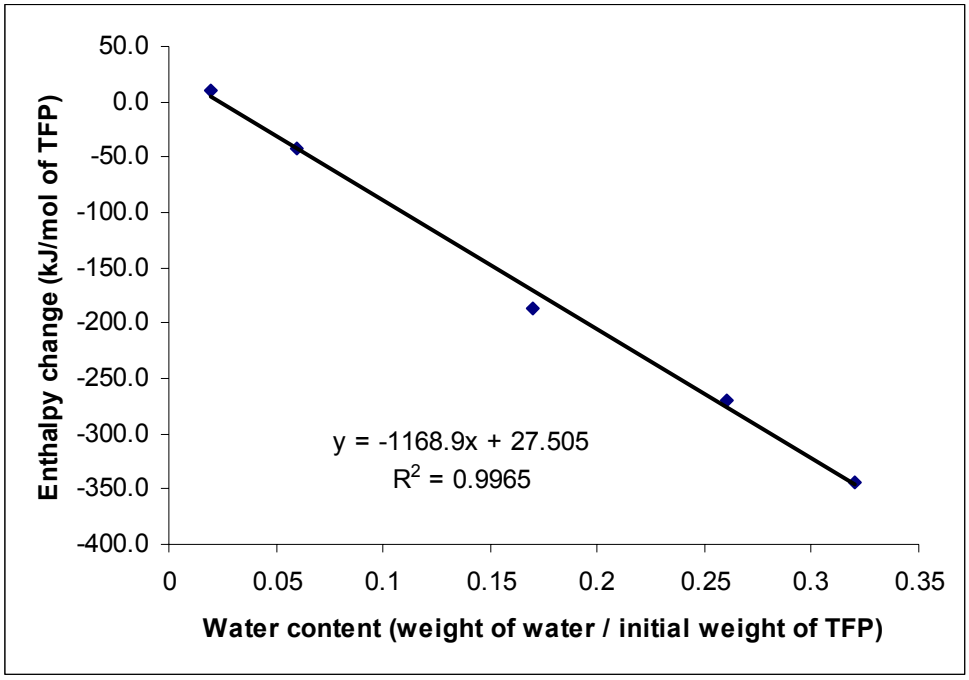

Fig. 5.10 Plot of enthalpy changes of the transformation from form **I** to liquid crystal containing different water contents.

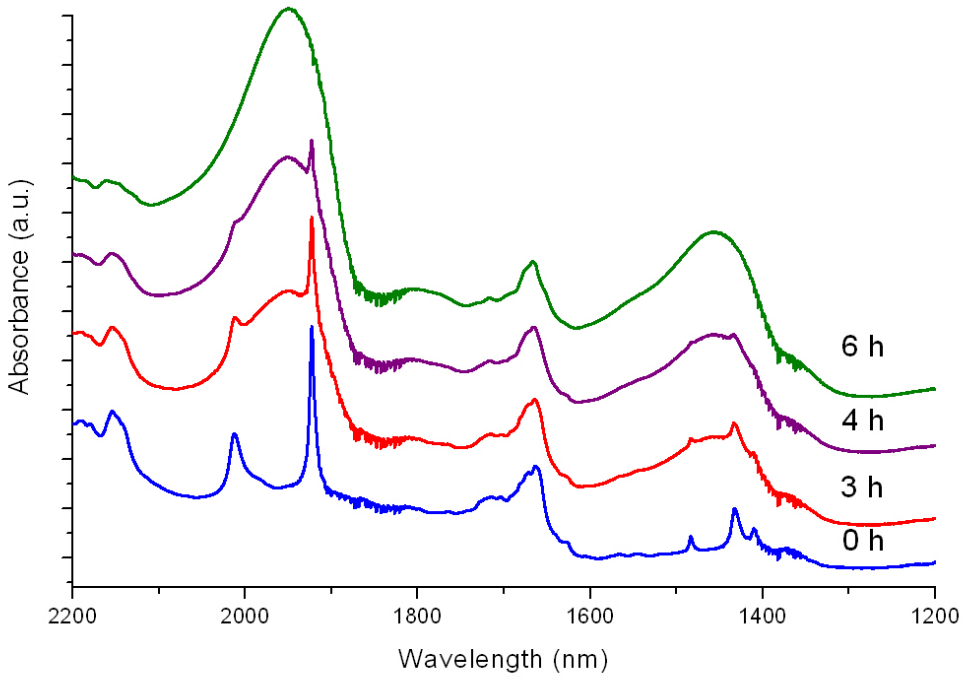

Fig. 5.11 Diffuse reflectance near infrared spectra of TFP form **I** powder following storage at 94% RH (RT) for different times.

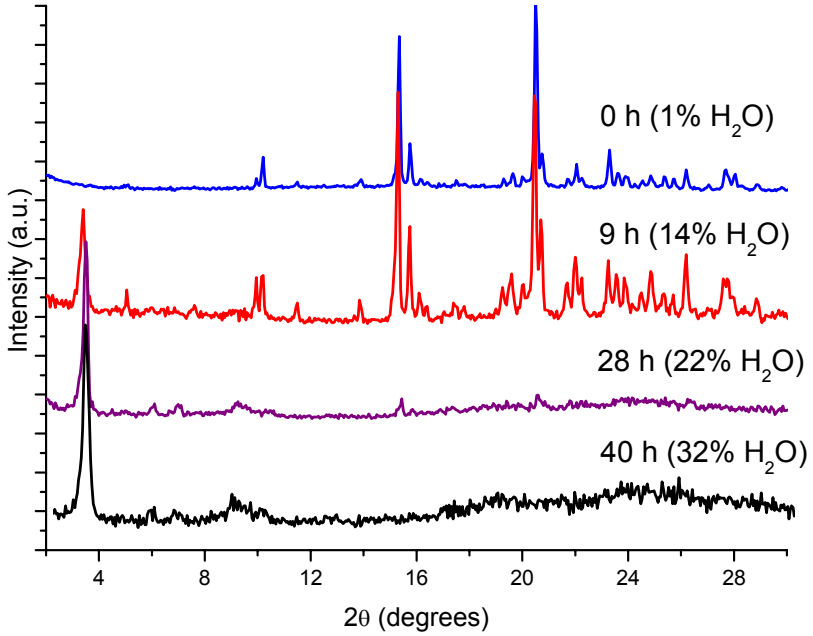

Fig. 5.12 XRD patterns of TFP form **I** powder following storage at 94% RH (RT) for different time periods.

5.6 References

1. Newman, A.W., Reutzel-Edens, S.M., and Zografi, G. 2008. Characterization of the "hygroscopic" properties of active pharmaceutical ingredients. *Journal of Pharmaceutical Sciences*, **97**: 1047-1059.
2. Reutzel-Edens, S.M. and Newman, A.W., *Physical characterization of hygroscopicity in pharmaceutical solids*, in *Polymorphism in the Pharmaceutical Industry*, R. Hilfiker, Editor. 2006, Wiley-VCH: Weinheim, Germany. pp. 235-258.
3. Govindarajan, R. and Suryanarayanan, R., *Processing-induced phase transformations and their implications on pharmaceutical products quality*, in *Polymorphism in the Pharmaceutical Industry*, R. Hilfiker, Editor. 2006, Wiley-VCH: Weinheim, Germany. pp. 333-364.
4. Kontny, M.J., Grandolfi, G.P., and Zografi, G. 1987. Water vapor sorption of water-soluble substances: studies of crystalline solids below their critical relative humidities. *Pharmaceutical Research*, **4**: 104-112.
5. Giron, D., Goldbronn, C., Mutz, M., Pfeffer, S., Piechon, P., and Schwab, P. 2002. Solid state characterizations of pharmaceutical hydrates. *Journal of Thermal Analysis and Calorimetry*, **68**: 453-465.
6. Vippagunta, S.R., Brittain, H.G., and Grant, D.J.W. 2001. Crystalline solids. *Advanced Drug Delivery Reviews*, **48**: 3-26.
7. Lohani, S. and Grant, D.J.W., *Thermodynamics of polymorphs*, in *Polymorphism in the Pharmaceutical Industry*, R. Hilfiker, Editor. 2006, Wiley-VCH: Weinheim, Germany. pp. 21-42.
8. El-Sabaawi, M. and Pei, D.C.T. 1977. Moisture isotherms of hygroscopic porous solids. *Industrial & Engineering Chemistry Fundamentals*, **16**: 321-326.
9. Terakita, A. and Byrn, S.R. 2006. Structure and physical stability of hydrates and thermotropic mesophase of calcium benzoate. *Journal of Pharmaceutical Sciences*, **95**: 1162-1172.
10. Wunderlich, B. 1999. A classification of molecules, phases, and transitions as recognized by thermal analysis. *Thermochimica Acta*, **340**: 37-52.
11. Figueiredo Neto, A.M. and Salinas, S.R.A., *The Physics of Lyotropic Liquid Crystals: Phase Transitions and Structural Properties*. 2005 University Press, Oxford.
12. Suzuki, Y., Fukunaga, K., Baba, M., Taki, M., and Watanabe, S. 2005. Three-dimensional temperature measurement with micro-capsulated thermo-chromic liquid crystal for assessment of dielectric and insulation materials. *Annual Report - Conference on Electrical Insulation and Dielectric Phenomena*, 609-612.
13. Boyd, B.J., Khoo, S.-M., Whittaker, D.V., Davey, G., and Porter, C.J.H. 2007. A lipid-based liquid crystalline matrix that provides sustained release and enhanced oral bioavailability for a model poorly water soluble drug in rats. *International Journal of Pharmaceutics*, **340**: 52-60.
14. Farkas, E., Kiss, D., and Zelko, R. 2007. Study on the release of chlorhexidine base and salts from different liquid crystalline structures. *International Journal of Pharmaceutics*, **340**: 71-75.

15. Stevenson, C.L., Bennett, D.B., and Lechuga-Ballesteros, D. 2005. Pharmaceutical liquid crystals: The relevance of partially ordered systems. *Journal of Pharmaceutical Sciences*, **94**: 1861-1880.
16. Bunjes, H. and Rades, T. 2005. Thermotropic liquid crystalline drugs. *Journal of Pharmacy and Pharmacology*, **57**: 807-816.
17. Rades, T. and Mueller-Goymann, C.C. 1992. Structural investigations on the liquid crystalline phases of fenoprofen. *Pharmaceutical and Pharmacological Letters*, **2**: 131-4.
18. Rades, T. and Mueller-Goymann Christel, C. 1994. Melting behavior and thermotropic mesomorphism of fenoprofen salts. *European Journal of Pharmaceutics and Biopharmaceutics*, **40**: 277-82.
19. Atassi, F. and Byrn, S.R. 2006. General trends in the desolvation behavior of calcium salts. *Pharmaceutical Research*, **23**: 2405-2412.
20. Zhou, M., Nemade, P.R., Lu, X., Zeng, X., Hatakeyama, E.S., Noble, R.D., and Gin, D.L. 2007. New type of membrane material for wate desalination based on a cross-linked bicontinuous cubic lyotropic liquid crystal assembly. *Journal of the American Chemical Society*, **129**: 9574-9575.
21. Lechuga-Ballesteros, D., Abdul-Fattah, A., Stevenson, C.L., and Bennett, D.B. 2003. Properties and stability of a liquid crystal form of cyclosporine-the first reported naturally occurring peptide that exists as a thermotropic liquid crystal. *Journal of Pharmaceutical Sciences*, **92**: 1821-1831.
22. Goldsbury, C., Kistler, J., Aebi, U., Arvinte, T., and Cooper, G.J.S. 1999. Watching amyloid fibrils grow by time-lapse atomic force microscopy. *Journal of Molecular Biology*, **285**: 33-39.
23. Zeng, X., Liu, Y., and Imperor-Clerc, M. 2007. Hexagonal close packing of nonionic surfactant micelles in water. *Journal of Physical Chemistry B*, **111**: 5174-5179.
24. Kocherbitov, V. and Soederman, O. 2006. Hydration of dimethyldodecylamine-N-oxide: enthalpy and entropydriven processes. *Journal of Physical Chemistry B*, **110**: 13649-13655.
25. Milton, N. and Nail, S.L. 1996. The physical state of nafcillin sodium in frozen aqueous solutions and freeze-dried powders. *Pharmaceutical Development and Technology*, **1**: 269-277.
26. Cox, J.S.G., Woodard, G.D., and McCrone, W.C. 1971. Solid-state chemistry of cromolyn sodium (disodium cromoglycate). *Journal of Pharmaceutical Sciences*, **60**: 1458-65.
27. Vadas, E.B., Toma, P., and Zografi, G. 1991. Solid-state phase transitions initiated by water vapor sorption of crystalline L-660711, a leukotriene D4 receptor antagonist. *Pharmaceutical Research*, **8**: 148-55.
28. Umprayn, K. and Mendes, R.W. 1987. Hygroscopicity and moisture adsorption kinetics of pharmaceutical solids: a review. *Drug Development and Industrial Pharmacy*, **13**: 653-693.
29. McDowell, J.J.H. 1980. Trifluoperazine hydrochloride, a phenothiazine derivative. *Acta Crystallographica, Section B: Structural Crystallography and Crystal Chemistry*, **B36**: 2178-81.

30. Kocherbitov, V. and Alfredsson, V. 2007. Hydration of MCM-41 studied by sorption calorimetry. *Journal of Physical Chemistry C*, **111**: 12906-12913.
31. Caira, M.R., Bettinetti, G., and Sorrenti, M. 2002. Structural relationships, thermal properties, and physicochemical characterization of anhydrous and solvated crystalline forms of tetroxoprim. *Journal of Pharmaceutical Sciences*, **91**: 467-481.
32. Ghosh, S., Ojala, W.H., Gleason, W.B., and Grant, D.J.W. 1995. Relationships between crystal structures, thermal properties, and solvate stability of dialkylhydroxypyridones and their formic acid solvates. *Journal of Pharmaceutical Sciences*, **84**: 1392-9.
33. Marsh, K.N., *Recommended reference materials for the relization of physicochemical properties*. 1987 Oxford, Blckwell.
34. Hosokawa, T., Datta, S., Sheth, A.R., and Grant, D.J.W. 2004. Relationships between crystal structures and thermodynamic properties of phenylbutazone solvates. *CrystEngComm*, **6**: 243-249.
35. Kocherbitov, V. 2005. Driving forces of phase transitions in surfactant and lipid systems. *Journal of Physical Chemistry B*, **109**: 6430-6435.
36. Nieuwmeyer, F.J.S., Damen, M., Gerich, A., Rusmini, F., Voort Maarschalk, K., and Vromans, H. 2007. Granule characterization during fluid bed drying by development of a near infrared method to determine water content and median granule size. *Pharmaceutical Research*, **24**: 1854-1861.
37. Ward, H.W. and Sistare, F.E. 2007. On-line determination and control of the water content in a continuous conversion reactor using NIR spectroscopy. *Analytica Chimica Acta*, **595**: 319-322.
38. Iwamoto, R. and Matsuda, T. 2007. Infrared and near-infrared spectral evidence for water clustering in highly hydrated poly(methyl methacrylate). *Analytical Chemistry*, **79**: 3455-3461.
39. Ellis, J.W. and Bath, J. 1938. Modifications in the near infrared absorption spectra of protein and of light and heavy water molecules when water is bound to gelatin. *Journal of Chemical Physics*, **6**: 723-729.
40. Giangiacomo, R. 2006. Study of water-sugar interactions at increasing sugar concentration by NIR spectroscopy. *Food Chemistry*, **96**: 371-379.
41. Doglia, S.M., Martini, M., Spinolo, G., and Villan, A.M. 1992. The NIR absorption spectrum of water in iron(**II**) chloride tetrahydrate single crystals. *Journal of Physics and Chemistry of Solids*, **53**: 1237-43.
42. Lin, J. and Brown, C.W. 1992. Near-IR spectroscopic determination of sodium chloride in aqueous solution. *Applied Spectroscopy*, **46**: 1809-15.
43. Cheema, M.A., Siddiq, M., Barbosa, S., Castro, E., Egea, J.A., Antelo, L.T., Taboada, P., and Mosquera, V. 2007. Compressibility, isothermal titration calorimetry and dynamic light scattering analysis of the aggregation of the amphiphilic phenothiazine drug thioridazine hydrochloride in water/ethanol mixed solvent. *Chemical Physics*, **336**: 157-164.
44. Hashmi, S.A.N., Hu, X., Immoos, C.E., Lee, S.J., and Grinstaff, M.W. 2002. Synthesis and characterization of p-stacked phenothiazine-labeled oligodeoxynucleotides. *Organic Letters*, **4**: 4571-4574.

45. Florence, A.T. and Parfitt, R.T. 1971. Micelle formation by some phenothiazine derivatives. **II**. Nuclear magnetic resonance studies in deuterium oxide. *Journal of Physical Chemistry*, **75**: 3554-60.
46. Roseboom, H. and Perrin, J.H. 1977. Mechanism for phenothiazine oxidation. *Journal of Pharmaceutical Sciences*, **66**: 1395-8.

Chapter 6

Effect of Preparation Method on the Physical Properties of Amorphous Trifluoperazine Dihydrochloride

6.1 Abstract

The goal of this study is to characterize amorphous trifluoperazine dihydrochloride (TFP) prepared by freeze-drying and cryo-milling, and to understand the effect of preparation method on the physicochemical properties of amorphous forms. Amorphous TFP samples were prepared by, (i) freeze-drying TFP solution (10% w/w), and (ii) cryo-milling of crystalline TFP (form I). Freeze-dried and cryo-milled TFP (FD and CM TFP) were characterized using small angle X-ray scattering, polarized light microscopy, and scanning electron microscopy. The physical stability of FD and CM TFP were studied following storage under different relative humidity (RH) conditions using X-ray diffractometry (XRD). The phase transformations during freeze-drying were monitored by *in situ* XRD. FD and CM TFP were both X-ray amorphous with identical glass transition temperature (T_g) of 104°C. However, CM and FD TFP recrystallized into different forms upon heating, and transformed respectively to crystalline and liquid crystalline TFP below 75% RH (25°C). The different phase transformation behavior of CM and FD TFP at increasing RH values was attributed to the difference in their local structures resulted from processing. Characterization of the intermediate phases during processing is very important in understanding the physical stability of amorphous solids.

6.2 Introduction

Amorphous solids are defined relative to their crystalline counterparts. Unlike crystalline solids, amorphous solids lack long-range order in molecular packing or well defined molecular conformations.[1] Partially or completely amorphous pharmaceutical materials are often created during pharmaceutical processes, such as milling, compaction, wet granulation, freeze-drying, and spray-drying.[2-4] Protein, peptides, some sugars, and polymers usually exist as amorphous solids.[2] Amorphous materials usually have higher solubility and dissolution rate than their corresponding crystalline phases, and therefore could potentially increase the bioavailability of drugs that have low solubility and high permeability.[5] However, amorphous materials have excess entropy, enthalpy and free energy compared to the stable crystalline forms, and hence often suffer from poor physical and chemical stabilities.[6-8] Presence of amorphous fractions in solids can lead to dramatic changes in many solid-state properties, such as water sorption,[9] flowability,[10, 11] and compactability.[12, 13] Therefore, a thorough understanding of physicochemical properties of amorphous materials is of great importance to the pharmaceutical industry.

Amorphous materials with different thermal histories or those prepared by different methods often show differences in physicochemical properties.[2] For example, amorphous trehalose, prepared by freeze-drying, spray-drying, dehydration, and melt quenching, showed similar T_g and fragility, but exhibited different enthalpic relaxation and crystallization behaviors.[14] Amorphous simvastatin prepared by cryo-milling and melt-quenching showed differences in physical stability and also in recrystallization enthalpy.[15] Cryo-milled samples showed less structural disorder, compared to that obtained from melt-quenching. Amorphous tri-O-methyl-β-cyclodextrin prepared by milling and melt-quenching were found to have different configurational entropies and different relaxation behaviors below T_g.[16]

The phenomenon of amorphous materials showing different physicochemical properties, such as differences in T_g and crystallization behavior, is sometimes referred to as pseudo-polyamorphism,[17] to differentiate from true polyamorphism, which is defined as two different thermodynamically stable amorphous states.[18] A well known example for true polyamorphism is triphenyl phosphite, which undergoes a liquid-liquid phase transition from a supercooled liquid to an amorphous 'glacial phase' at temperatures between 213 and 227 K, which lies between T_g (176 K) and Tm (295 K).[19-23] There usually is no true first-order transition between different amorphous states for pseudo-polyamorphism.[17] Pseudo-polyamorphism has been understood as existence of different relaxational states, or, in other words, occurrence of different extents of energetic departure from the equilibrium supercooled liquid, and does not represent distinct thermodynamic phases.[17] For example, amorphous moxalactam annealed for different times showed differences in molecular mobility and chemical reactivity.[24] Amorphous moxalactam prepared by foam-drying showed higher physical stability compared to freeze-dried samples, which was attributed to increased enthalpic relaxation at higher processing temperatures of the freeze-dried samples.[25]

Amorphous solids can be prepared via different routes, such as by melting followed by quench-cooling, from solution (spray-drying, freeze-drying, vacuum-drying, or fast precipitation), by dehydration of hydrates, or through mechanical activation (milling).[1] Solution method or melt-quench techniques usually completely destroy the existing molecular order, while some short-range order may be retained after mechanical activation or dehydration. However, it is challenging to analytically distinguish amorphous materials prepared by different methods. Another issue is heterogeneity in the amorphous samples.[26] For quench-cooled samples, heterogeneous nucleation could be facilitated in the cracks that developed on the surface during processing.[27] Different mechanical

stresses and surface properties in the amorphous solids, resulting from processing, could lead to differences in crystallization behavior.[28, 29]

Amorphous materials retain short-range order in the molecular arrangement.[3] For most organic solids, the short-range order or local structure is not expected to extend to more than 20-25 Å, which covers the nearest neighbor or next nearest neighbor molecules.[30] The characterization of short-range order or local structures in amorphous solids is usually beyond the capability of commonly used laboratory X-ray diffractometers.[31] Despite the difficulties in characterization, studies were conducted to understand the effect of short-range order on the physicochemical properties of amorphous solids. For example, amorphous indomethacin crystallized into anhydrous γ- and α-polymorph below and above its T_g, respectively.[32] It was proposed that the hydrogen-bonding pattern of amorphous indomethacin below T_g favored the formation of γ-form, while heating the glass above T_g hindered the formation of the strong hydrogen bonds and favored the formation of the less stable α-form.[33] FT-IR spectroscopy revealed significant difference in the hydrogen bonding patterns in cryo-milled γ- and α-indomethacin, which could explain the differences in crystallization behavior of amorphous indomethacin below and above its T_g. Amorphous carbonic acid samples, prepared from frozen methanolic and aqueous solutions, crystallized into α- and β- polymorphs.[34] Based on FT-IR, similar H-bonding networks were observed in corresponding amorphous and crystalline forms. The local structure in cryo-milled piroxicam was studied by pair wise distribution function transforms of the experimental PXRD pattern.[31] Different long-range orders were determined using PDF transform of amorphous piroxicam before and after cryo-grinding of form II, which explained the loss of polymorphic "memory" during recrystallization.[35]

In the present work, amorphous TFP was prepared by two different techniques: cryo-milling and freeze-drying. The aim of this work was to study the effect of

preparation method and local structure on the physicochemical properties of amorphous TFP. Our specific objectives were to study: (i) morphology, T_g and enthalpy of crystallization, and (ii) water sorption and subsequent crystallization behavior of the amorphous TFP prepared by different methods. It is proposed that the structural memories of the intermediate phases during processing leads to differences in water sorption and consequently, crystallization behavior of amorphous TFP.

6.3 Materials and Methods

6.3.1 Material

Trifluoperazine·2HCl was purchased from Sigma and used as is. TFP liquid crystalline powder was prepared by storing crystalline powder at 94% RH for 3 days, followed by storing at 2% RH (anhydrous $CaSO_4$) for 24 hrs at 25°C.

6.3.2 Small Angle X-ray Scattering (SAXS)

A small angle X-ray diffractometer (Saxess, Anton Paar, Germany) with a Cu Kα radiation source (40 kV x 50 mA) was used. About 3-5 mg powder was sealed between polyimide (Kapton®) films and the scattering trace was accumulated for 10 min at 25°C.

6.3.3 Differential Scanning Calorimetry (DSC)

A differential scanning calorimeter (MDSC, Model 2920,TA Instruments, New Castle, DE, USA) equipped with a refrigerated cooling accessory was used. The instrument was calibrated with pure samples of tin and indium. About 4–5 mg

sample was packed in aluminum pans with several pin holes in the lid, crimped, and heated under dry nitrogen purge at 10°C/min.

6.3.4 Attenuated Total Reflectance Fourier Transformed Infrared Spectroscopy (ATR-FTIR)

A small amount of solid powder was pressed onto the surface of an ATR crystal (ZnSe prism) (Pike technologies, Madison, WI, USA). A FTIR spectrometer (Vertex 70, Bruker optics, Madison, WI, USA) with a DTGS detector was used. Each spectrum was the average of 32 scans over the range of 4000 to 400 cm-1 with a resolution of 2 cm^{-1}.

6.3.5 Polarized Light Microscopy (PLM)

Powder was sprinkled on a glass slide. The images were taken in transmittance mode in a microscope equipped with crossed polarizers (Nikon, Japan). The images were processed using commercial software (Metamorph® Imaging System, Molecular Devices, Downingtown, PA).

6.3.6 Scanning Electron Microscopy (SEM)

The samples were mounted on scanning electron microscopy (SEM) stubs with double-sided carbon tape, coated with platinum (50 Å), and observed under a scanning electron microscope (JEOL 6500F, JEOL USA Inc., Peabody, MA, USA).

6.3.7 Cryogenic Milling

A cryogenic impact mill (model 6750, SPEX CertiPrep, Metuchen, NJ, USA) was used. consisting of a polycarbonate cylinder sample holder immersed in liquid nitrogen, within which the impact was produced by the vibrations of a stainless steel rod using a magnetic coil. Milling was carried out at an impact frequency of 10 cycles per second for 2 min periods separated by 2 min cool-down periods. The sample was milled for 20 min, immediately transferred into a 20 ml scintillation vial purged with nitrogen gas, and stored at –20°C over anhydrous $CaSO_4$ prior to use.

6.3.8 Water Vapor Sorption

Sample powder (~5 mg), as received, was placed in the sample quartz boat of an automated vapor sorption microbalance (DVS-1000, Surface Measurements Systems, London, UK). The microbalance was calibrated using a 100 mg standard weight. The relative humidity sensor was calibrated at 5.0, 11.3, 32.8, 52.8, 75.3, and 84.3% RH (25°C), using saturated salt solutions. Unless stated otherwise, all experiments were performed at 25°C. The samples were initially dried at 0% RH for 3 hours then exposed to the desired RH. The rate and extent of water uptake was determined over a range of RH conditions. The exposure time at each step varied from 1 to 6 h depending on the time required for equilibration. The attainment of equilibrium was assumed when the weight change was < 0.02% in one hour.

6.3.9 Thermogravimetric Analysis (TGA)

Approximately 2-4 mg of the samples were heated in an open pan, from 25 to 250°C, at 10°C/min, in a thermogravimetric analyzer (Model Q50, TA Instruments,

New Castle, DE) under dry nitrogen purge. The data analysis was performed using Universal Analysis 4.1D (TA Instruments, New Castle, DE).

6.3.10 Powder X-ray Diffractometry (XRD)

The degree of crystallinity of samples was measured by ambient powder X-ray diffractometry (PXRD). About 200 mg of sample were poured into an aluminum holder by the side-drift method and exposed to Cu Kα radiation (45 kV, 40 mA) in a wide-angle X-ray diffractometer (Model D5005, Siemens, Madison, WI, USA). The instrument was operated in step-scan mode in increments of 0.05° 2θ and counts were accumulated for 1 second at each step. A 5 - 50° 2θ angular range was employed. The data collection and analyses were performed using commercially available software (JADE, version 5.1 Materials Data Inc., Livermore, CA, USA).

6.3.11 Variable Temperature X-ray Diffractometry (VT-XRD)

PXRD patterns of the samples at various temperatures were obtained using a X-ray diffractometer (Scintag XDS 2000, Sunnyville, California, USA) equipped with a variable temperature stage (-50 to 300°C, model 828D, Micristar, R. G. Hansen & Associates). TFP liquid crystal powder (106-180 mg) was packed into a copper holder, heated at 5ºC/min and examined at following temperatures: 130ºC, 150ºC, 160ºC, 170ºC, and 180ºC. XRD patterns were recorded using Cu Kα radiation (40 mA x 45 kV) in the step scan mode, with a step size of 0.05° 2θ and a accumulation time of 1 s during cooling and warming. The angular range was 2 - 30° 2θ. The data collection and analyses were performed using DataScan and JADE 7.0 (Materials Data, Inc., Livermore, CA), respectively.

6.3.12 *In Situ* Freeze-drying

The prelyo solution (10%, w/w) was transferred to a copper holder (85 µL volume) and cooled to -50°C at 2°C/min where it was held for 30 minutes. Primary drying was performed for one hour at -30°C with a sample chamber pressure of 150 militorr. The sample was heated to 20°C at 2°C/min, and subjected to secondary drying for one hour.

6.3.13 Freeze-drying

Lyophilization of TFP aqueous solution (2 ml) was performed in 20 ml scintillation glass vials using a bench top freeze-dryer (VirTis Advantage, Gardiner, NY, USA). The solution was cooled to -40°C and held for 2 hours. Primary drying was carried out at a shelf temperature of -30°C and a chamber pressure of 100 militorr for 5 hours, followed by secondary drying at 20°C for 5 hours.

6.4 Results and Discussion

6.4.1 Characterization of Freeze-dried and Cryo-milled TFP

The small angle X-ray scattering (SAXS) traces of form I, liquid crystalline, freeze-dried (FD), cryo-milled (CM) TFP and the polyimide (Kapton®) film are overlaid in Fig. 6.1. TFP liquid crystal showed a peak at 2.75 nm^{-1}, from which the diameter of hexagonal cylinder in the liquid crystal phase was calculated to be ~ 26 Å. Form I showed peaks only in the wide angle range (> 4 nm^{-1} q, $q = 2\pi/d$). The SAXS traces of FD and CM TFP were identical without any crystalline peaks, suggesting that they were both X-ray amorphous (lacked long range periodicity) and were indistinguishable by SAXS. The broad halo in the SAXS traces may be due to the Kapton® film.

The DSC curves of FD and CM TFP are compared in Fig. 6.2. Both FD and CM TFP showed glass transition at 104°C and crystallization at 125°C. The enthalpies of crystallization of the two samples were not significantly different (~ 26 J/g).

The FT-IR spectra of FD, CM, and form I TFP are shown in Fig. 6.3. The IR spectra of FD and CM TFP were slightly different from that of form I. The crystalline form I showed two IR peaks at 1343 and 1315 cm^{-1}, while the X-ray amorphous samples showed only one IR peak at 1329 cm^{-1}. The two IR peaks around 1330 cm^{-1} of form I were assigned to C-F stretching.[36] It has been reported that form I lattice exhibits two packing arrangements. [37] Hence the two IR peaks could be explained by the two chemical environments experienced by the CF_3 groups. In the amorphous state, the CF_3 groups may not experience such distinct chemical environments. No significant differences were observed in the finger-print region of the IR spectra of form I and amorphous samples (FD and CM TFP).

The polarized light microscopic images of FD and CM TFP are compared in Fig. 6.4. In CM TFP, some bright spots were seen, indicating small crystallites in an amorphous matrix. FD TFP showed pronounced birefringence, suggesting existence of structural order. The SEM image of FD TFP (Fig. 6.5) revealed plate-like particles (< 1 μm in thickness and approximately 20 μm in length and width) while CM TFP occurred as an agglomerate.

6.4.2 Crystallization of Freeze-dried and Cryo-milled TFP during Heating

The phase behavior of CM and FD TFP upon heating was monitored using variable temperature XRD. At RT, both the samples were X-ray amorphous (not shown). In CM TFP, a low intensity peak appeared at 110°C, with significant crystallization at 140°C. On the other hand, in FD TFP, crystallization was

evident only when heated to 140°C, suggesting a reduced tendency to crystallize. The XRD patterns of FD and CM TFP, heated to 140°C, are compared in Fig. 6.6. In CM TFP, the peaks at 15.3, 20.5, and 22.0° 2θ, indicated crystallization of form I.[37] While FD TFP also crystallized on heating, the peak positions (for example at 14.1, 18.9 and 25.1° 2θ) revealed crystallization of a different physical form. Based on HPLC, there was no detectable degradation of the samples heated to 140°C. The crystallization of FD TFP into a new form suggests that the structural memory of form I is eradicated upon freeze-drying.

6.4.3 Water Sorption induced Phase Transformation of Freeze-dried and Cryo-milled TFP

The water sorption isotherms of FD, CM and form I TFP at 25°C are overlaid in Fig. 6.7. Form I sorbed a small amount of water (< 1.5%, w/w) below 75% RH, predominately attributed to adsorption. There was pronounced water uptake by fat RH > 75%, attributed to liquid crystal formation. The water content in CM TFP increased to 5% w/w at 30% RH, decreased to 1% w/w at RH values between 40 to 60%, and increased to 23% w/w at 80% RH. FD TFP showed a very different water sorption behavior - the water content increased linearly as a function of RH. Fig. 6.8 is a schematic phase diagram indicating that crystalline and liquid crystalline phases are the thermodynamically stable phases below and above 75% RH, respectively. Based on this diagram, the decrease in CM TFP water content between 40 and 60% RH (Fig. 6.7) could be attributed to crystallization. In contrast, the FD TFP sample retained a high water content and exhibited no tendency to crystallize.

The phase transformations in CM and FD TFP after water sorption were characterized by XRD. Fig. 6.9 shows the XRD patterns of CM TFP after storage at 54% RH for different times. The emergence of XRD peaks at 15.3, 20.5, and 22.0° 2θ indicated form I crystallization, which agreed with the phase diagram.

The crystallization could be explained by the plasticizing effect of water. Using the Gordon-Taylor equation and assuming the glass transition temperature of water to be 136K,[38] the T_g of the TFP-water system was calculated to be 63°C at 20% water content (w/w) and 82°C at 10% water content (w/w).. CM TFP crystallized at a temperature significantly below T_g. Fig. 6.10 shows the XRD patterns of FD TFP after storage at 54% RH (25°C) for different time periods. The intensity of a peak at 3.7° 2θ was found to increase progressively, as a function of storage time, suggesting liquid crystal formation. The DSC curves of the samples before and after water sorption showed a new endotherm at 120°C in FD TFP, which was attributed to melting of liquid crystalline phase (Fig. 6.11). Therefore, it could be concluded that CM TFP crystallized into form I, while FD TFP transformed into liquid crystals following storage at 54% RH (25°C).

The changes in the morphology of the samples after storage at 54% RH were investigated using SEM. The SEM images of CM and FD TFP before and after exposure to 54% RH are compared in Fig. 6.12. The increase in the roughness of CM TFP, following storage could be attributed to crystallization. A similar effect of water sorption was observed in lactose. [39]

It is relatively easy to understand the crystallization of CM TFP following storage at 54% RH since form I is the thermodynamically stable form below 75% RH. After grinding, small domains of form I could exist in the amorphous matrix, and act as seeds to facilitate crystallization. In case of FD TFP, transformation to crystalline state should be thermodynamically favored below 75% RH (25°C). However, FD TFP transformed to a liquid crystalline state at 54% RH. It is proposed that the formation of liquid crystal is kinetically favored, due to retention of structural memory of liquid crystalline phase.

6.4.4 Phase Transformation during Freeze-drying of TFP Solution

Amorphous materials may retain structural memory of intermediate or starting materials in their local structures.[31] The investigation of the phase transformation during freeze-drying may help us understand the local structure and consequent phase transformations of FD TFP.

The low temperature DSC curves of TFP solution (10% w/w) are shown in Fig. 6.14. An exotherm was observed at -20°C during cooling, which was attributed to crystallization of hexagonal ice.[40] An endotherm at 0°C, observed during warming, was due to ice melting. Although annealing has been reported to affect the mesophase formation of naficillin sodium in the frozen solution,[41] this is not the case for TFP. The DSC curves of TFP solution did not show any changes upon annealing the solution at -30°C for 30 min.

In situ low temperature XRD was performed to characterize TFP solution during freezing and thawing. The XRD patterns of TFP solution are overlaid in Fig. 6.15. As expected, no crystalline peaks were observed at 25 and 0°C. At -20°C, peaks at 23.1, 24.5, and 26.0° 2θ were observed, which were attributed to hexagonal ice. This was in good agreement with the exotherm at -20°C observed in the DSC curves.[42] XRD peaks were not observed between 2 and 5° 2θ, suggesting that liquid crystalline phases with d-spacing > 40 Å had not yet formed. At -40°C, the intensities of ice peaks increased, suggesting further crystallization of ice. Even with extensive ice crystallization and TFP concentration, peaks were not observed between 2 and 5° 2θ range. This suggests that liquid crystal formation in the freeze concentrate had not yet occurred. The critical micellar concentration (CMC) of TFP in water was determined to be 0.5 mmol/l at 25°C in Chapter 5. Therefore, TFP was expected to form micelles in the freeze concentrate, which was not detected by the XRD method.

To study the phase behaviors during freeze-drying, the X-ray diffractometer was attached to a vacuum pump, and the XRD patterns were collected *in situ* during freeze-drying. The XRD patterns of the frozen solution during the primary drying are overlaid in Fig. 6.16. Before primary drying, the frozen solution showed three strong peaks around 25° 2θ attributed to ice. No peak was observed between 2 and 5° 2θ. After drying for 30 min at -30°C (150 mm Hg), the intensity of ice peaks decreased significantly, indicating ice sublimation. A new peak at 3.7° 2θ was observed along with the sublimation of ice, suggesting the formation of liquid crystalline phase after water removal. After drying for 40 min at -30°C (150 mmHg), the ice peaks disappeared and only a peak at 3.7° 2θ was observed. It could be concluded that the liquid crystalline phase was formed as a result of water removal during the primary drying. The secondary drying was performed at 20°C (Fig. 6.17), during which water was further removed from the system. The intensity of the peak at 3.7° 2θ decreased after drying at 20°C for 20 min. The FD TFP appeared X-ray amorphous after drying for 40 min. The amorphization of liquid crystalline TFP during the secondary drying is very interesting. Since water played an important role in the structures of lyotropic liquid crystals,[43, 44] it is proposed that removal of water causes structural collapse and leads to amorphization of liquid crystalline TFP upon secondary drying.

The liquid crystalline → amorphous transition during the secondary drying might have a mechanism similar to that of the amorphization caused by dehydration. TFP molecules rearranged to form lamellar structures as the water was removed during primary drying. Water molecules in the lamellar liquid crystalline TFP would most likely play a space-filling role since TFP molecules cannot form hydrogen bonds with water. Water removal increases the free volume of TFP molecules and leads to structural collapse and formation of amorphous phase.[45] The resulting amorphous phase would have “memory” of the liquid crystal. In case of TFP, cryo-milled and freeze-dried TFP showed similar T_g and PXRD patterns. FD TFP showed birefringence while cryo-milled TFP did not, which

suggested some order of molecular arrangement in FD TFP. It could be proposed that during secondary drying, the liquid crystalline TFP lost its positional order, while some orientational order was preserved so that the birefringence was observed in FD TFP. FD TFP was observed to retain the lamellar shape of the liquid crystalline phase, while cryo-milled TFP was observed to be agglomerates of small particles.

6.4.5 Effect of Preparation Method on Physical Stability of Amorphous Solids

Cryogenic milling, a technique used to decrease particle size and thereby enhance dissolution rate, often causes lattice disorder.[2] During cryo-milling, mechanical activation transforms the crystalline drug into the amorphous state through a solid-state transition. The solid-state transition may lead to some "structural memory" of the starting crystalline material in the amorphous product,[35] which could facilitate crystallization during heating or water sorption.

In freeze-drying, the first step is the preparation of the prelyophilization solution. This step may effectively eradicate the structural memory of the starting materials. For surface active compounds, such as TFP, the drug molecules could self-associate in presence of water. The intermediate or final products may assume mesophase structures. When TFP solution was freeze-dried, a liquid crystalline phase formed during primary drying, which transformed to an amorphous phase during secondary drying. Structural memory of the liquid crystalline phase persisted in the final amorphous solid, which led to the formation of a metastable liquid crystalline phase upon water uptake by amorphous TFP. The liquid crystalline phase is a metastable form which crystallized after storage at 54% RH (25°C) for 6 months as discussed in Chapter 5.

6.5 Conclusion

The freeze-dried (FD) and cryo-milled (CM) TFP were X-ray amorphous with identical glass transition temperature. The morphologies of FD and CM TFP exhibited pronounced differences, and only FD TFP was birefringent. When subjected to water sorption, CM TFP readily crystallized at RH values between 30 and 75% RH, while FD TFP transformed to a liquid crystalline phase and showed a linear water sorption isotherm at 25°C. The different water sorption behaviors were explained by the difference in the local structures in the two samples as a result of different preparation methods. Residual crystalline domains in CM TFP facilitated crystallization to form I after water sorption.

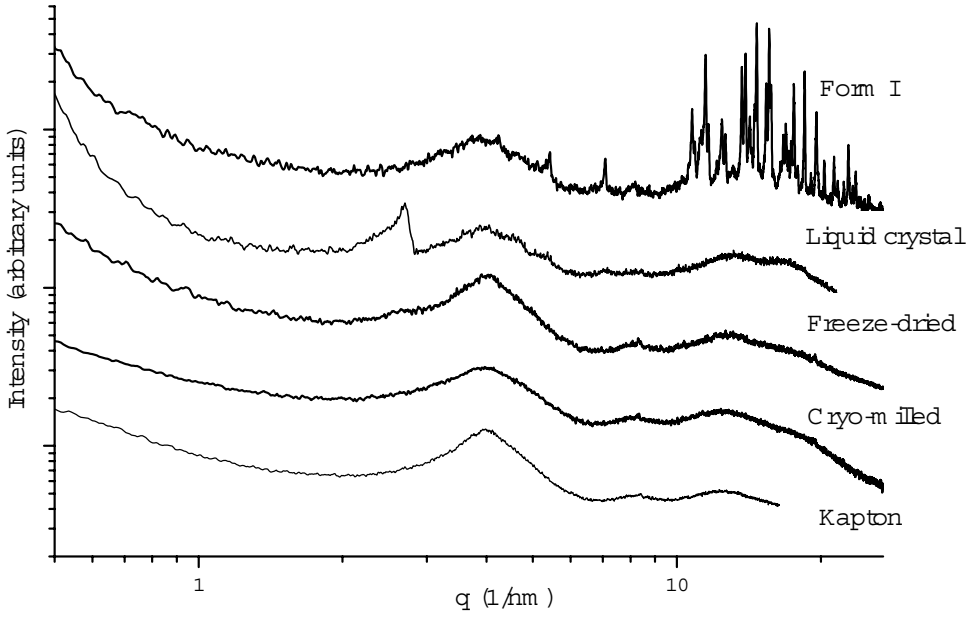

Fig. 6.1 Small angle X-ray scattering patterns of form I, liquid crystal, freeze-dried, and cryo-milled TFP and polyimide film at 25°C.

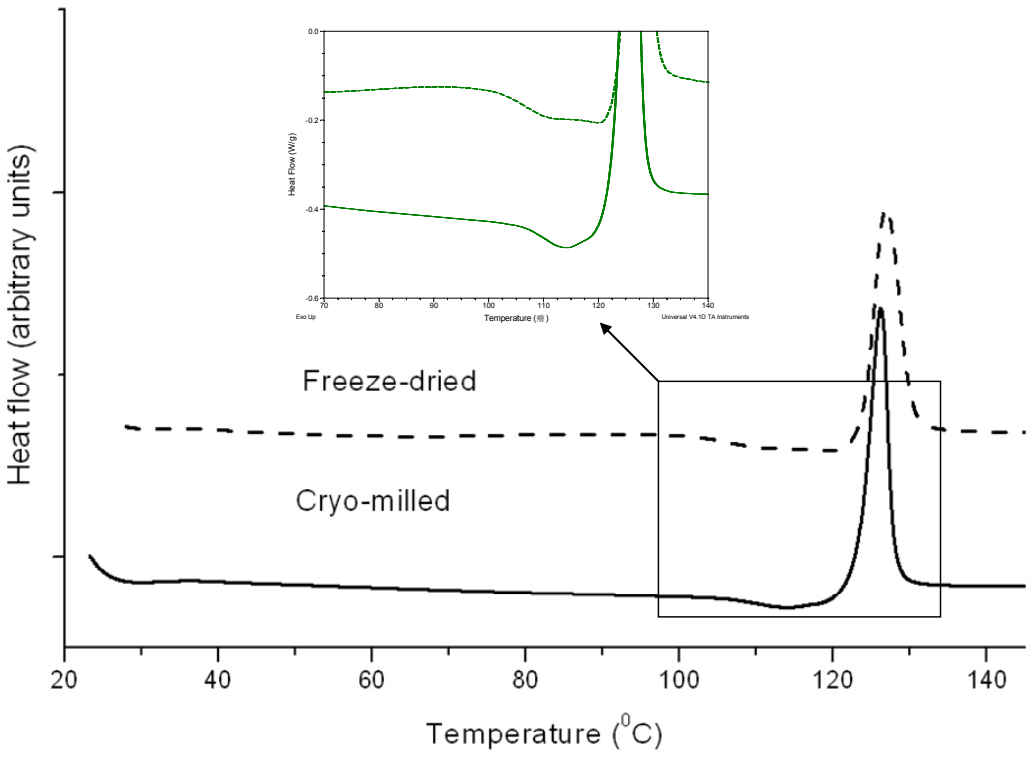

Fig. 6.2 Comparison of the DSC curves of freeze-dried and cryo-milled TFP.

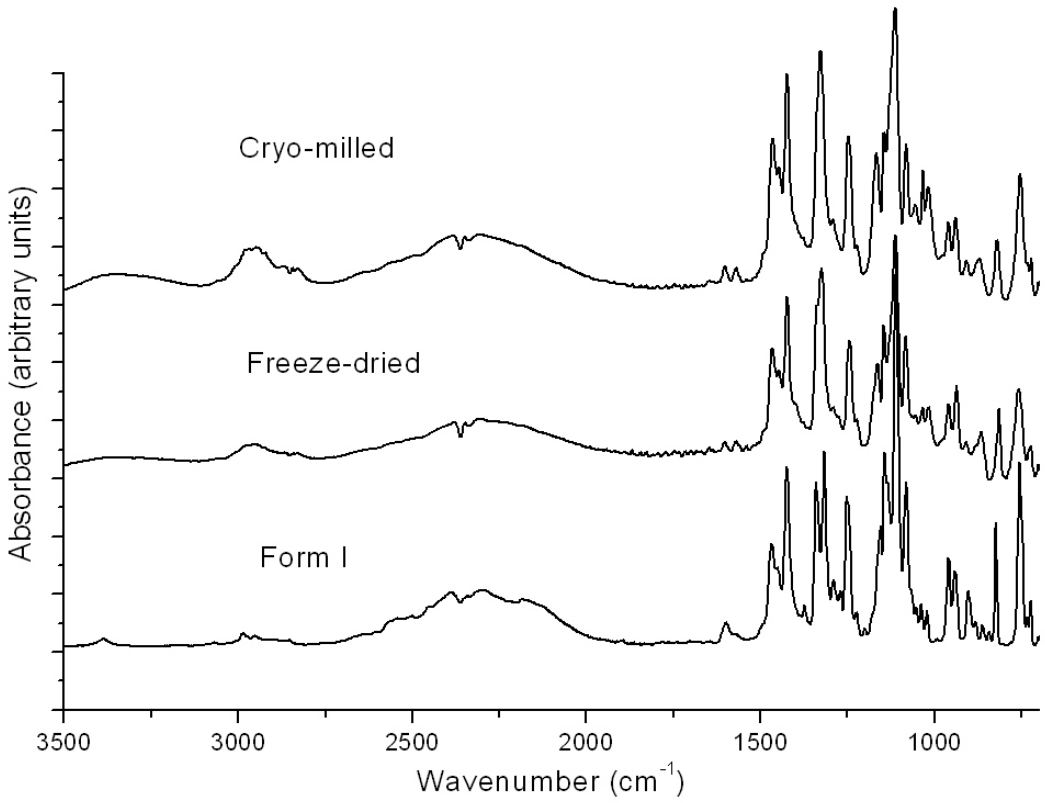

Fig. 6.3 FT-IR spectra of TFP form I, freeze-dried, and cryo-milled TFP (RT).

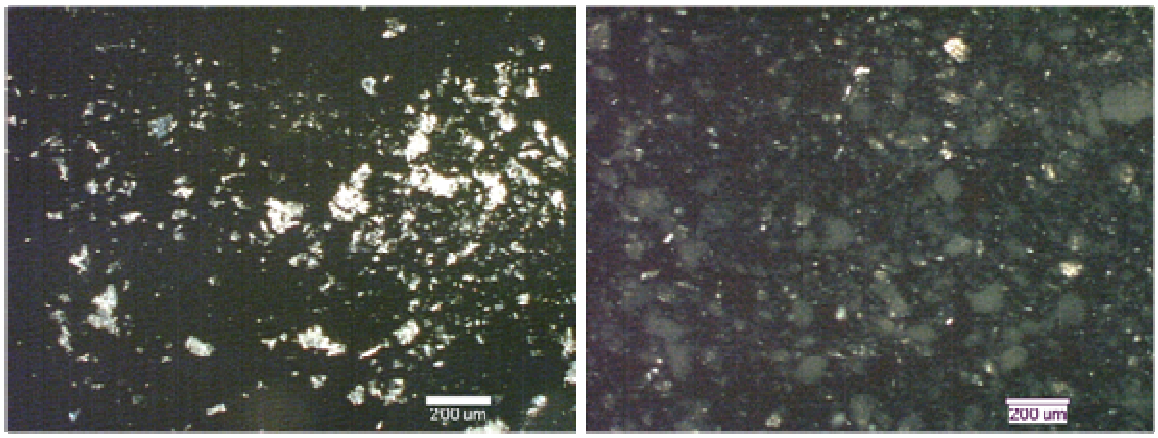

Fig. 6.4 Images of freeze-dried (left) and cryo-milled (right) TFP between crossed polarizors.

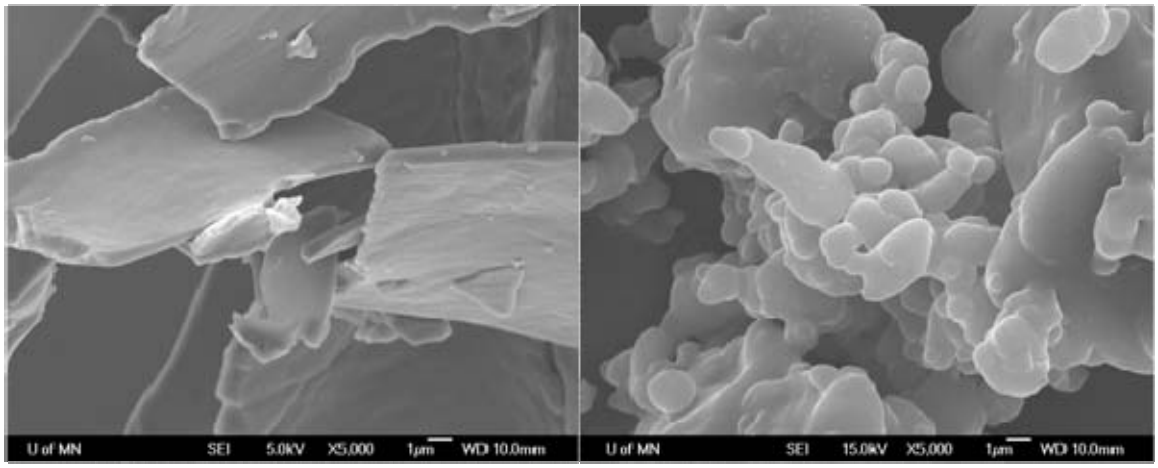

Fig. 6.5 SEM images of freeze-dried (left) and cryo-milled (right) TFP.

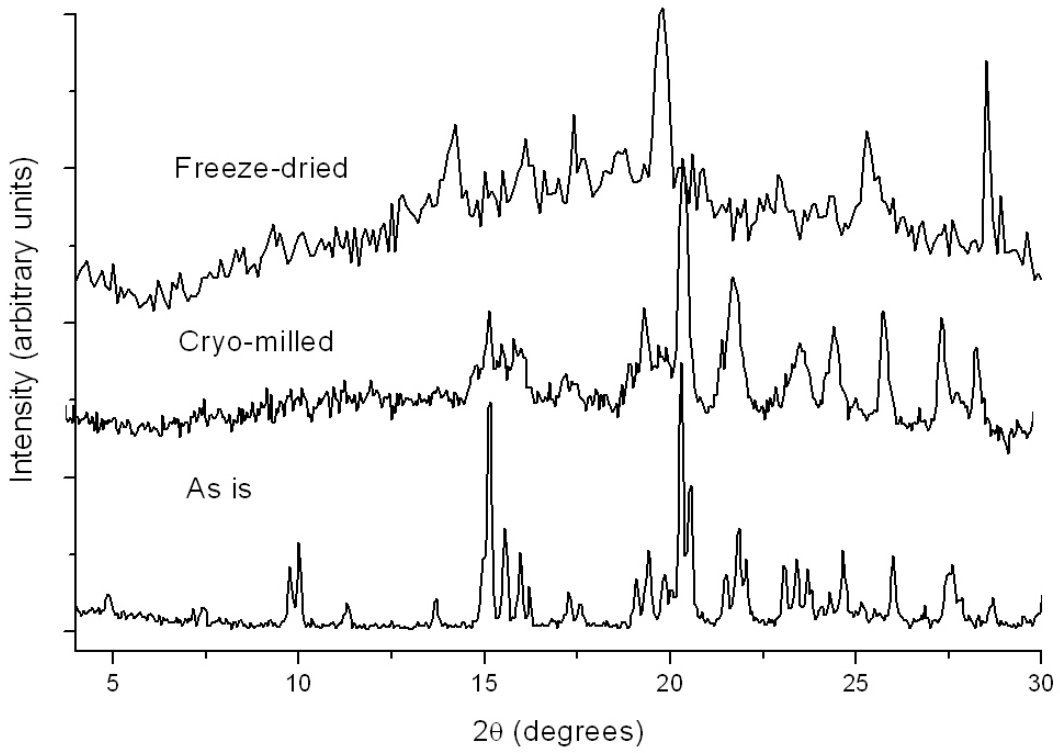

Fig. 6.6 XRD patterns of the freeze-dried and cryo-milled TFP after heating to 140°C using VT-XRD.

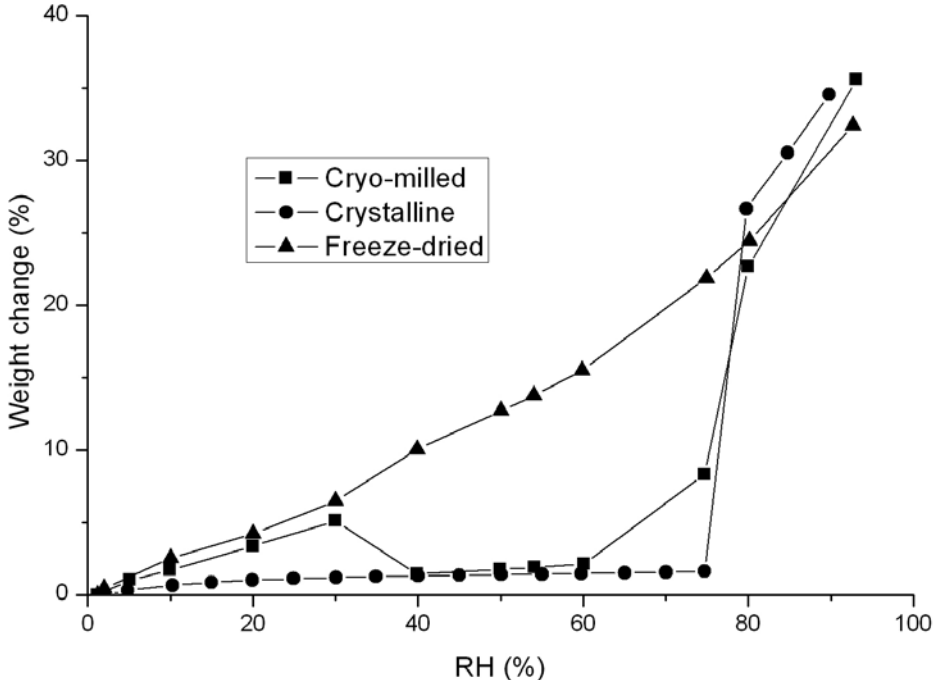

Fig. 6.7 Water sorption isotherms of form I, freeze-dried, and cryo-milled TFP at 25°C.

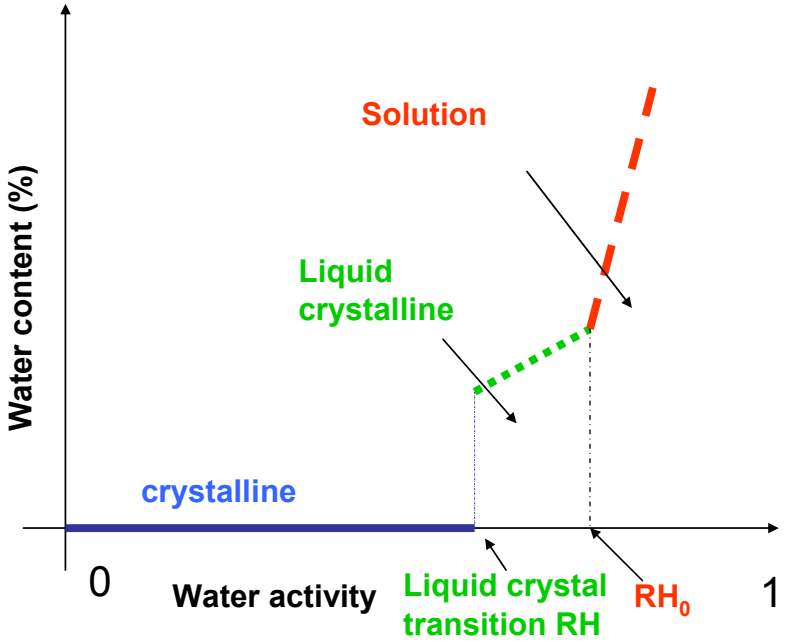

Fig. 6.8 The schematic phase diagram of TFP at different water activities at 25°C.

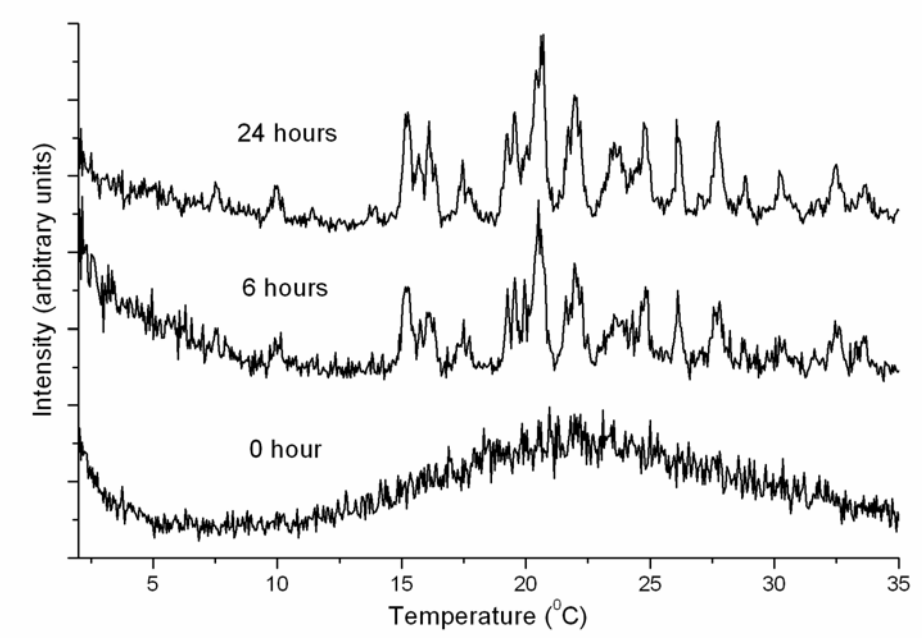

Fig. 6.9 PXRD patterns of cryo-milled TFP after stored at 54% RH (RT) for different times.

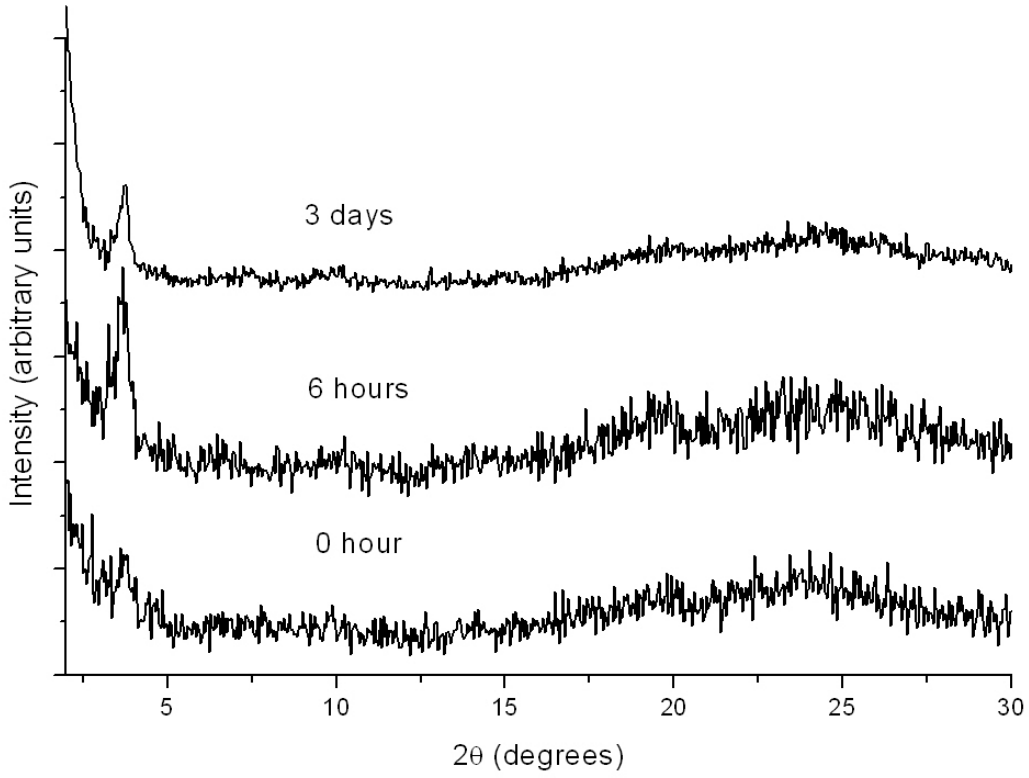

Fig. 6.10 PXRD patterns of freeze dried (10%) TFP after storage at 54% RH (RT) for different times.

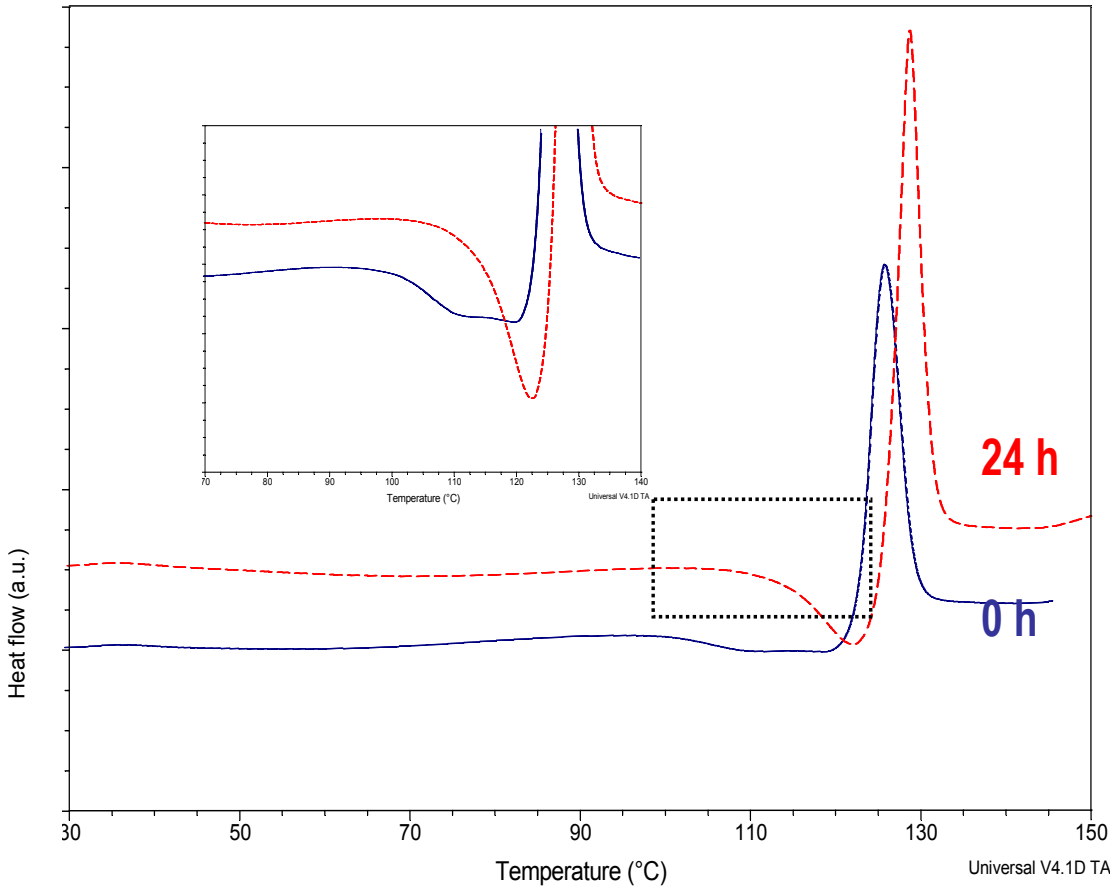

Fig. 6.11 DSC curve of freeze-dried TFP before and after exposure to 54% RH for 24 h (RT).

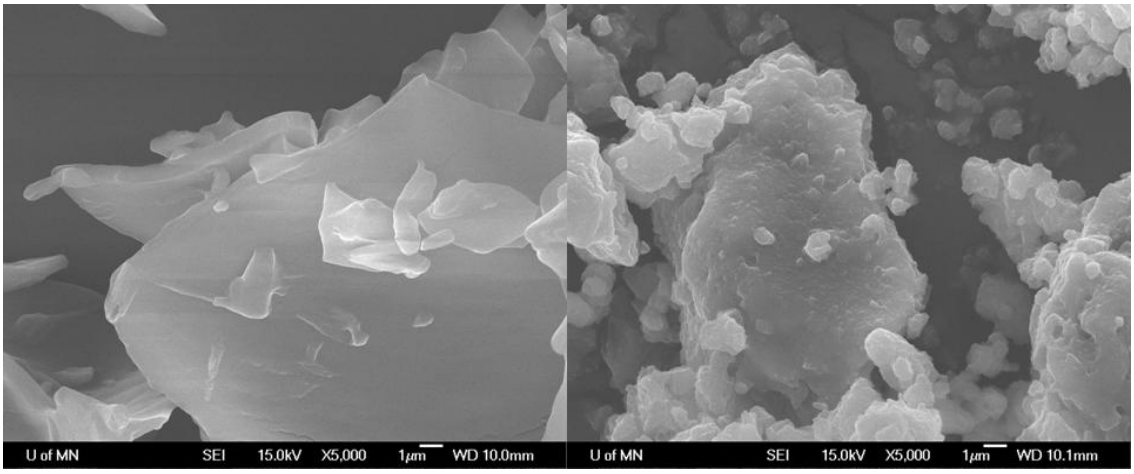

Fig. 6.12 SEM images of freeze-dried (left) and cryo-milled (right) TFP (10%) after storage at 54% RH (RT) for 3 days.

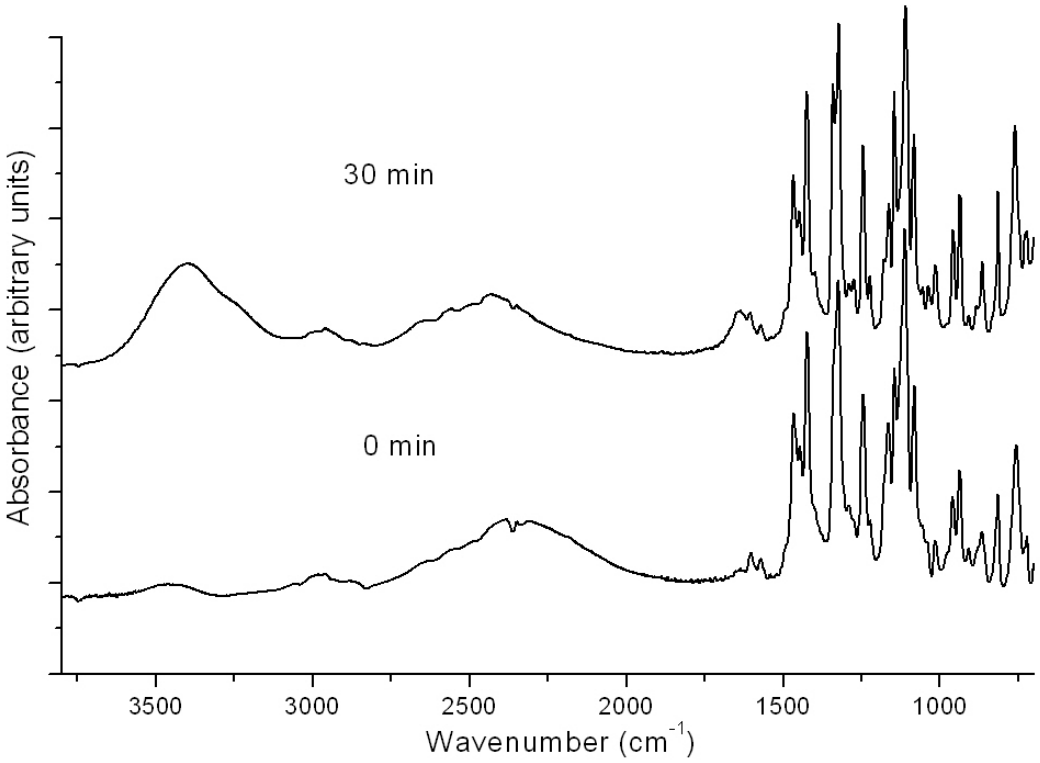

Fig. 6.13 FT-IR spectra of freeze-dried TFP before and after storage at 54% RH (RT) for 30 min.

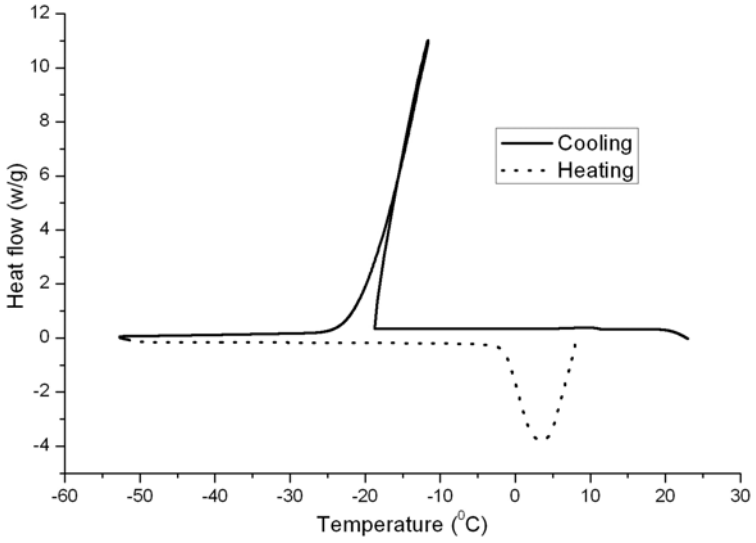

Fig. 6.14 DSC curves of TFP 10% aqueous solution during cooling and warming. The solution was first cooled to -50°C at 5°C/min, then heated to 10°C at 5°C/min

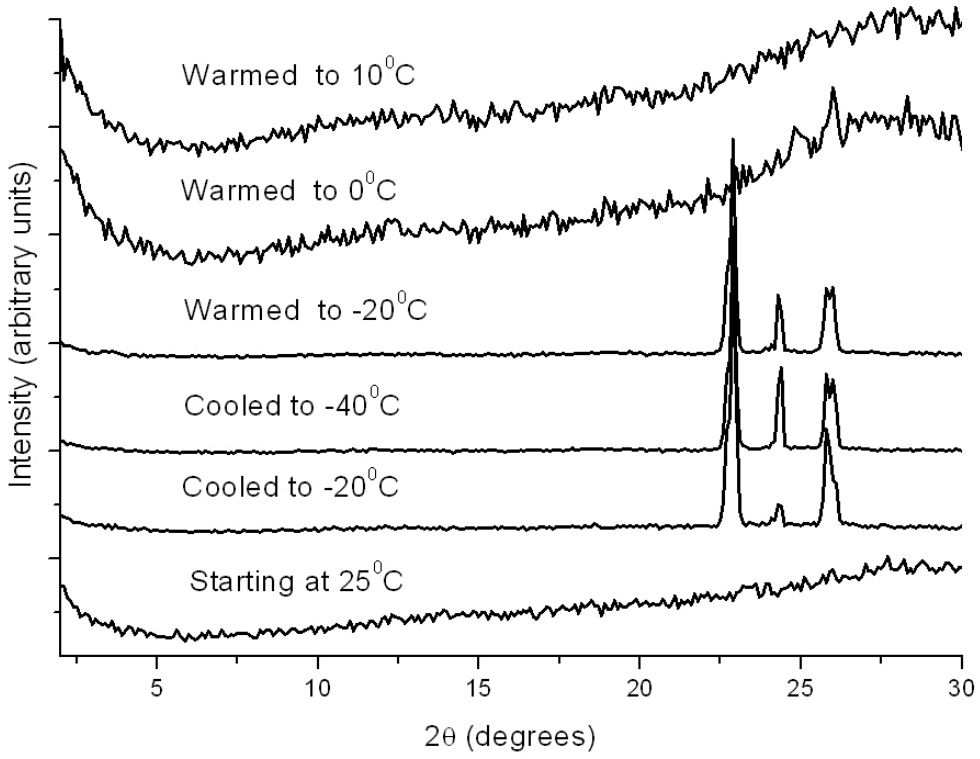

Fig. 6.15 XRD patterns of 10% TFP aqueous solution during cooling and warming. PXRD patterns were taken at 25, -20, -40, -20, 0, and 10°C. Both the heating and cooling rate were 2°C/min

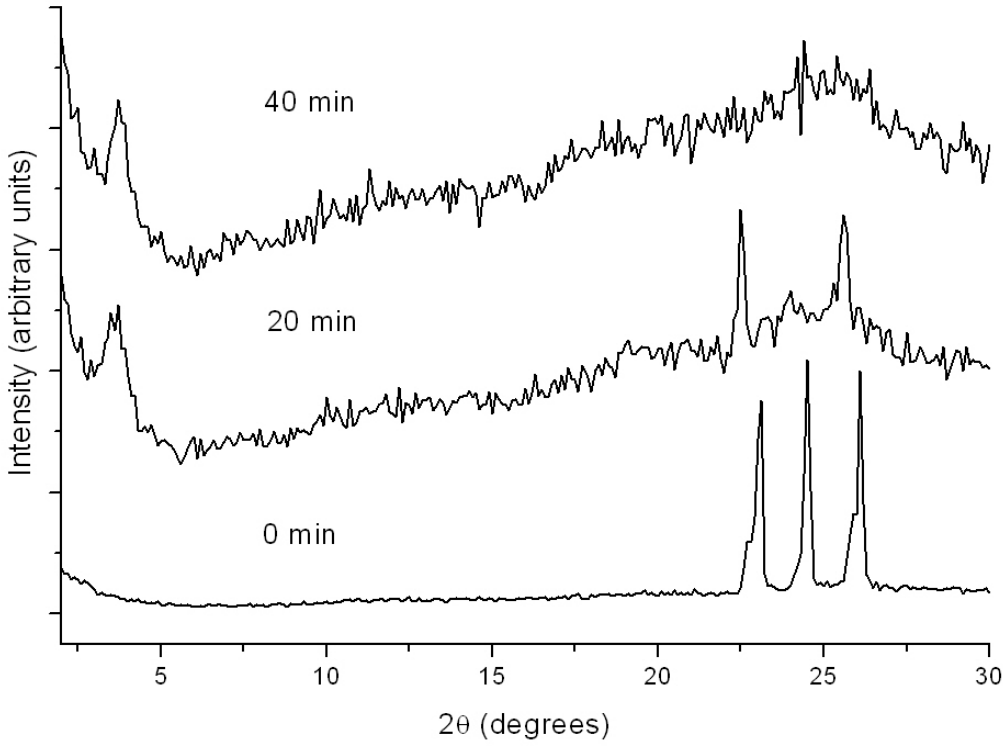

Fig. 6.16 XRD patterns of 10% TFP aqueous solution during primary drying at -30°C (100 mmHg). The XRD patterns were taken at time intervals of 0, 20, and 40 min.

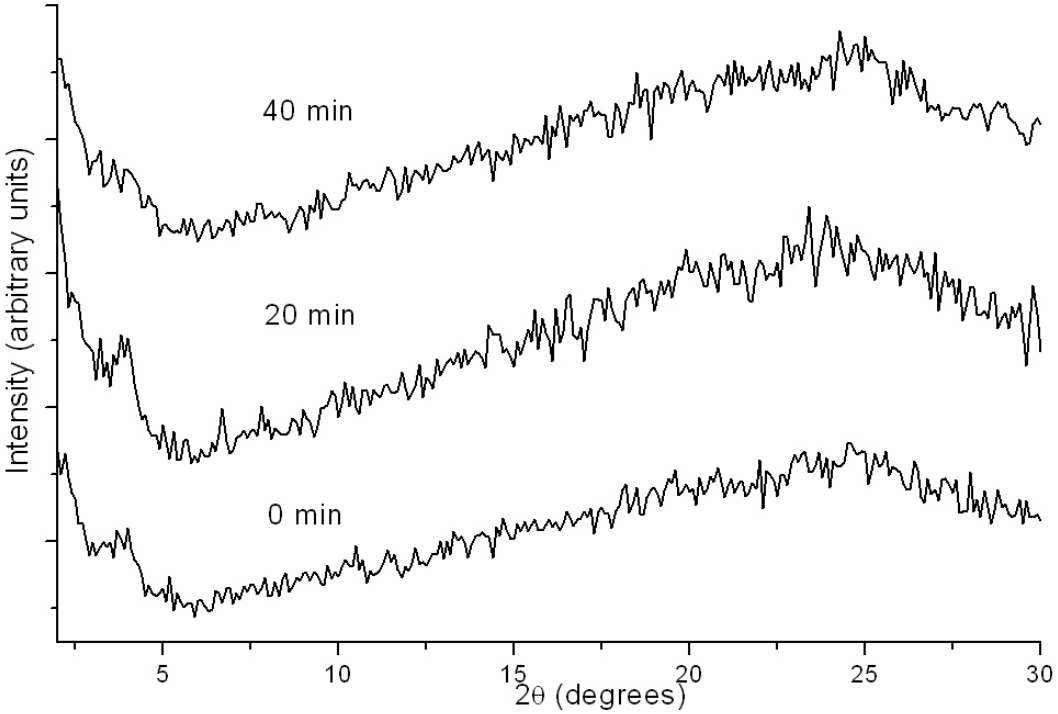

Fig. 6.17 XRD patterns of 10% TFP aqueous solution during secondary drying at 20°C (100 mmHg). The XRD patterns were taken at time intervals of 0, 20, and 40 min.

6.6 References:

1. Zhou, D., Zhang, G.G.Z., Law, D., Grant, D.J.W., and Schmitt, E.A. 2002. Physical stability of amorphous pharmaceuticals: importance of configurational thermodynamic quantities and molecular mobility. *Journal of Pharmaceutical Sciences*, **91**: 1863-1872.
2. Petit, S. and Coquerel, G., *The amorphous state*, in *Polymorphism in the Pharmaceutical Industry*, R. Hilfiker, Editor. 2006, Wiley-VCH: Weinheim, Germany. pp. 259-285.
3. Yu, L. 2001. Amorphous pharmaceutical solids: preparation, characterization and stabilization. *Advanced Drug Delivery Reviews*, **48**: 27-42.
4. Hilden, L.R. and Morris, K.R. 2004. Physics of amorphous solids. *Journal of Pharmaceutical Sciences*, **93**: 3-12.
5. Chono, S., Takeda, E., Seki, T., and Morimoto, K. 2008. Enhancement of the dissolution rate and gastrointestinal absorption of pranlukast as a model poorly water-soluble drug by grinding with gelatin. *International Journal of Pharmaceutics*, **347**: 71-78.
6. Shamblin, S.L., Hancock, B.C., and Pikal, M.J. 2006. Coupling between chemical reactivity and structural relaxation in pharmaceutical glasses. *Pharmaceutical Research*, **23**: 2254-2268.
7. Guo, Y., Byrn, S.R., and Zografi, G. 2000. Physical characteristics and chemical degradation of amorphous quinapril hydrochloride. *Journal of Pharmaceutical Sciences*, **89**: 128-143.
8. Aso, Y., Yoshioka, S., and Kojima, S. 2000. Relationship between the crystallization rates of amorphous nifedipine, phenobarbital, and flopropione, and their molecular mobility as measured by their enthalpy relaxation and ^{1}H NMR relaxation times. *Journal of Pharmaceutical Sciences*, **89**: 408-416.
9. Hancock, B.C. and Zografi, a.G. 1996. Effects of solid-state processing on water vapor sorption by aspirin. *Journal of Pharmaceutical Sciences*, **85**: 246-8.
10. Faqih, A.M.N., Mehrotra, A., Hammond, S.V., and Muzzio, F.J. 2007. Effect of moisture and magnesium stearate concentration on flow properties of cohesive granular materials. *International Journal of Pharmaceutics*, **336**: 338-345.
11. Burnett, D.J., Thielmann, F., Sokoloski, T., and Brum, J. 2006. Investigating the moisture-induced crystallization kinetics of spray-dried lactose. *International Journal of Pharmaceutics*, **313**: 23-28.
12. Sun, C.C. 2008. Mechanism of moisture induced variations in true density and compaction properties of microcrystalline cellulose. *International Journal of Pharmaceutics*, **346**: 93-101.
13. Stubberud, L., Arwidsson, H.G., Larsson, A., Graffner, C. 1996. Water solid interactions II. Effect of moisture sorption and glass transition temperature on compactibility of microcrystalline cellulose alone or in binary mixtures with polyvinyl pyrrolidone. *International Journal of Pharmaceutics*, **134**: 79-88.
14. Surana, R., Pyne, A., and Suryanarayanan, R. 2004. Effect of preparation method on physical properties of amorphous trehalose. *Pharmaceutical Research*, **21**: 1167-1176.

15. Graeser, K.A., Strachan, C.J., Patterson, J.E., Gordon, K.C., and Rades, T. 2008. Physicochemical properties and stability of two differently prepared amorphous forms of simvastatin. *Crystal Growth & Design*, **8**: 128-135.
16. Tsukushi, I., Yamamuro, O., and Suga, H. 1994. Heat capacities and glass transitions of ground amorphous solid and liquid-quenched glass of tri-O-methyl-b-cyclodextrin. *Journal of Non-Crystalline Solids*, **175**: 187-94.
17. Hancock, B.C., Shalaev, E.Y., and Shamblin, S.L. 2002. Polyamorphism: A pharmaceutical science perspective. *Journal of Pharmacy and Pharmacology*, **54**: 1151-1152.
18. Greaves, G.N., Meneau, F., Kargl, F., Ward, D., Holliman, P., and Albergamo, F. 2007. Zeolite collapse and polyamorphism. *Journal of Physics: Condensed Matter*, **19**: 415102/1-415102/17.
19. Demirjian, B.G., Dosseh, G., Chauty, A., Ferrer, M.-L., Morineau, D., Lawrence, C., Takeda, K., Kivelson, D., and Brown, S. 2001. Metastable solid phase at the crystalline-amorphous border: the glacial phase of triphenyl phosphite. *Journal of Physical Chemistry B*, **105**: 2107-2116.
20. Hedoux, A., Guinet, Y., Derollez, P., Hernandez, O., Lefort, R., and Descamps, M. 2004. Description and origin of the polyamorphism in triphenyl phosphite. *Recent Research Developments in Physics*, **5**: 887-902.
21. Hedoux, A., Guinet, Y., Derollez, P., Hernandez, O., Paccou, L., and Descamps, M. 2006. Micro-structural investigations in the glacial state of triphenyl phosphite. *Journal of Non-Crystalline Solids*, **352**: 4994-5000.
22. Kurita, R., Shinohara, Y., Amemiya, Y., and Tanaka, H. 2007. Microscopic structural evolution during the liquid-liquid transition in triphenyl phosphite. *Journal of Physics: Condensed Matter*, **19**: 152101/1-152101/8.
23. Kurita, R. and Tanaka, H. 2004. Critical-like phenomena associated with liquid-liquid transition in a molecular liquid. *Science*, **306**: 845-848.
24. Abdul-Fattah, A.M., Dellerman, K.M., Bogner, R.H., and Pikal, M.J. 2007. The effect of annealing on the stability of amorphous solids: chemical stability of freeze-dried moxalactam. *Journal of Pharmaceutical Sciences*, **96**: 1237-1250.
25. Abdul-Fattah, A.M., Truong-Le, V., Yee, L., Nguyen, L., Kalonia, D.S., Cicerone, M.T., and Pikal, M.J. 2007. Drying-induced variations in physico-chemical properties of amorphous pharmaceuticals and their impact on stability (I): stability of a monoclonal antibody. *Journal of Pharmaceutical Sciences*, **96**: 1983-2008.
26. Bhugra, C. and Pikal, M.J. 2008. Role of thermodynamic, molecular, and kinetic factors in crystallization from the amorphous state. *Journal of Pharmaceutical Sciences*, **97**: 1329-1349.
27. Moore, W.P., *Mechanical stress crystallization of thermoplastic polymers*. 2002, Agri-Nutrients Technology Group, Inc., USA: US.
28. Sahoo, K.L., Poddar, P., Das, G., and Kumar, B.R. 2007. Crystallization behaviour and mechanical properties of rapidly solidified amorphous alloy. *Journal of Materials Science*, **42**: 6665-6671.
29. Song, N.-K., Kim, M.-S., Han, S.-H., Kim, Y.-S., and Joo, S.-K. 2007. Effects of mechanical stress on the growth behaviors of metal-induced lateral crystallization. *Journal of the Electrochemical Society*, **154**: H370-H373.

30. Bates, S., Zografi, G., Engers, D., Morris, K., Crowley, K., and Newman, A. 2006. Analysis of amorphous and nanocrystalline solids from their X-ray diffraction patterns. *Pharmaceutical Research*, **23**: 2333-2349.
31. Sheth, A.R., Bates, S., Muller, F.X., and Grant, D.J.W. 2005. Local structure in amorphous phases of piroxicam from powder X-ray diffractometry. *Crystal Growth & Design*, **5**: 571-578.
32. Andronis, V. and Zografi, G. 2000. Crystal nucleation and growth of indomethacin polymorphs from the amorphous state. *Journal of Non-Crystalline Solids*, **271**: 236-248.
33. Shalaev, E. and Zografi, G. 2002. The concept of 'structure' in amorphous solids from the perspective of the pharmaceutical sciences. *Special Publication - Royal Society of Chemistry*, **281**: 11-30.
34. Winkel, K., Hage, W., Loerting, T., Price, S.L., and Mayer, E. 2007. Carbonic acid: from polyamorphism to polymorphism. *Journal of the American Chemical Society*, **129**: 13863-13871.
35. Sheth, A.R., Bates, S., Muller, F.X., and Grant, D.J.W. 2004. Polymorphism in Piroxicam. *Crystal Growth & Design*, **4**: 1091-1098.
36. Post, A., Warren, R.J., and Zarembo, J.E., *Trifluoperazine hydrochloride*, in *Analytical Profiles of Drug Substances*, K. Florey, Editor. 1980, Academic Press: New York, NY. pp. 543-582.
37. McDowell, J.J.H. 1980. Trifluoperazine hydrochloride, a phenothiazine derivative. *Acta Crystallographica, Section B: Structural Crystallography and Crystal Chemistry*, **B36**: 2178-81.
38. Ghormley, J.A. 1968. Enthalpy changes and heat-capacity changes in the transformations from high-surface-area amorphous ice to stable hexagonal ice. *Journal of Chemical Physics*, **48**: 503-8.
39. Mahlin, D., Berggren, J., Alderborn, G., and Engstroem, S. 2004. Moisture-induced surface crystallization of spray-dried amorphous lactose particles studied by atomic force microscopy. *Journal of Pharmaceutical Sciences*, **93**: 29-37.
40. Searles, J.A., Carpenter, J.F., and Randolph, T.W. 2001. The ice nucleation temperature determines the primary drying rate of lyophilization for samples frozen on a temperature-controlled shelf. *Journal of Pharmaceutical Sciences*, **90**: 860-871.
41. Milton, N. and Nail, S.L. 1996. The physical state of nafcillin sodium in frozen aqueous solutions and freeze-dried powders. *Pharmaceutical Development and Technology*, **1**: 269-277.
42. Nail, S.L., Jiang, S., Chongprasert, S., and Knopp, S.A. 2002. Fundamentals of freeze-drying. *Pharmaceutical Biotechnology*, **14**: 281-360.
43. Zeng, X., Liu, Y., and Imperor-Clerc, M. 2007. Hexagonal close packing of nonionic surfactant micelles in water. *Journal of Physical Chemistry B*, **111**: 5174-5179.
44. Fong, C., Wells, D., Krodkiewska, I., Weerawardeena, A., Booth, J., Hartley, P.G., and Drummond, C.J. 2007. Diversifying the solid state and lyotropic phase behavior of nonionic uea-based surfactants. *Journal of Physical Chemistry B*, **111**: 10713-10722.

45. Griesser, U.J., *The importance of solvates*, in *Polymorphism in the Pharmaceutical Industry*, R. Hilfiker, Editor. 2006, Wiley-VCH: Weinheim, Germany. pp. 211-233.

Chapter 7

Summary and Suggestions for Future Work

Summary of the Thesis

Many pharmaceutical crystalline solids sorb water vapor readily from the environment, and are considered to be hygroscopic. Compounds with low hygroscopicity are desired during drug discovery to minimize the downstream development risk of the drug candidates. An automated sorption microbalance (ASM) technique is being widely used in industry to evaluate the hygroscopicity of drug candidates. The short-term water sorption studies are used to predict the long-term water uptake during manufacture and storage. It is important to assess the risk in this prediction and understand the thermodynamic and kinetic factors that affect water uptake by pharmaceutical solids. In this thesis, we selected 40 APIs from US Pharmacopoeia, and compared the water uptake using static RH chamber and ASM techniques. .

In Chapter 2, the hygroscopicity of 40 APIs was investigated by long-term storage in RH chambers and short-term ASM studies. 27 compounds were found to sorb < 0.5% w/w water after storage at 94% RH (RT) for one year. In addition, 4 compounds formed hydrates, 2 compounds formed liquid crystals, and 7 compounds deliquesced after storage at 94% RH (RT) for one year. In 37 out of 40 compounds, the short-term water sorption studies showed good agreement with the long-term water uptake. Therefore, the hypothesis that long-term water uptake could be predicted using short-term sorption studies was proven to be valid (α = 0.1). In three compounds, water sorption induced phase transformation caused the ASM and RH chamber storage techniques to give different water uptake values which could not be explained by rate of water diffusion. These transformations were further investigated in the following chapters. The deliquescence RH values of pharmaceutical crystals were found to correlate well with the aqueous solubility when the solute mole fraction in their solutions was < 0.1.

In Chapter 3, the water content in homochlorcyclizine·2HCl (HCC) increased to 3.5% and then decreased to 0.5% after storage at 75% for 3 and 21 days, respectively. Polymorphic transformation from anhydrous form **I** to **II** was verified by XRD. FTIR and XRD revealed structural similarities between form **I** and the desolvate of HCC acetonitrile solvate. Water is believed to enter the cavities in the crystal lattice of form **I** and induce the polymorphic transformation to form **II**, which had a lower deliquescence RH (RH_0) and smaller unit cell compared to that of form **I**. XRD revealed the structural change during water sorption and form **II** crystallization during water desorption. The polymorphic transformation only occurred at RH values close to the RH_0 of form **I**.

Chapter 4 investigates the role of water adsorption in the anhydrous theophylline → hydrate transformation in the solid state. We used atomic force microscopy (AFM) to confirm the existence of water adsorption induced surface solution formation on the anhydrate crystal and visualized the surface mobility above the transitional water activity. Water sorption can significantly increase the surface mobility of anhydrate crystals and facilitate hydrate formation. The growth of hydrate phase on the surface of anhydrate crystal was observed using a polarized light microscope. This study showed that water adsorption played an important role in the anhydrate → hydrate transformation in the solid state.

The water content in trifluoperazine·2HCl (TFP) was 1.5 and 8% after storage at 75% RH (RT) for 3 and 6 months, respectively. XRD revealed that TFP partially converted to a liquid crystalline phase after storage at 75% RH (RT) for 6 months. An understanding of this rarely reported liquid crystal formation was the objective of Chapter 5. Based on the powder XRD pattern, the liquid crystalline phase was characterized to have a hexagonal structure. The transition RH was approximately 75% at 25°C. The enthalpy and entropy of liquid crystal formation at different RH values were calculated based on heat flow determinations using a

thermal activity monitor (TAM). This calculation suggested that liquid crystal formation in the solid state was an enthalpically driven process.

Chapter 6 investigated the effect of preparation method on the physicochemical properties of amorphous materials. Amorphous TFP prepared by freeze-drying (FD) and cryo-milling (CM) transformed to liquid crystalline and crystalline phases after storage at RH < 75% (25°C), respectively. FD TFP showed a much higher capacity of retaining water compared to CM TFP. An intermediate liquid crystalline phase was observed during freeze-drying of TFP solution. It is proposed that FD TFP has a structural memory of the intermediate liquid crystalline phase during preparation. FD TFP kinetically favored the formation of liquid crystals upon water sorption, which was thermodynamically unstable and would crystallize below 75% RH.

Suggestions for Future Work

Chapter 2

The 40 compounds included in this study were randomly selected from US pharmacopoeia and analytical profiles of drug substances. In other words, they are drugs already in market. Another pool of model compounds would be drug candidates that entered the drug preformulation and formulation stages during drug development, which will be more representative of the problems faced by pharmaceutical researchers during preformulation studies. However, the access to the drug candidate in the pharmaceutical industries would be very limited to academic researchers.

Chapter 3

The lattice parameters of the two homochlorcyclezine·2HCl (HCC) polymorphs have been simulated by modeling their synchrotron powder diffraction patterns. However, the accurate crystal packing patterns were not obtained by Material Studio^{TM} simulation possibly due to different molecular conformations of HCC in different crystal lattices. It would be interesting to solve the crystal structures of HCC Form **I** and **II** from the synchrotron powder diffraction patterns.

Further studies of the polymorphic transformation may also include the investigation of the thermodynamic relationship between the HCC polymorphs. It could be hypothesized that these two polymorphs are monotropically related, with form **I** being the metastable form. The solubility of the two polymorphs can be determined at different temperatures, and the difference in the free energies of the two polymorphs could be calculated from the solubilities. The free energy difference between HCC polymorphs could also be studied by solution

calorimetry. The polymorphs with higher free energy would have a lower enthalpy of solvation.

Chapter 4

Water vapor usually interacts with solid through the surface; therefore, the surface properties at different RH values would significantly affect the kinetics of phase transformations induced by water sorption. The existence of surface solution was only proven on anhydrous theophylline crystals. Another interesting model compound would be carbamazepine, which can form a dihydrate above 84% RH (25°C). It is likely that carbamazepine hydrate formation was also mediated by surface solution. Atomic force microscopy and vibrational spectroscopy could be used to study the surface properties of carbamazepine anhydrate crystals at different RH values and to determine the mechanism of hydrate formation in the solid state.

Chapter 5

The molecular structure of a compound determines its tendency to self-associate, both in solution and in solid state. Molecular dynamic modeling would provide more insight into the driving forces of liquid crystal formation in the solid state, such as the enthalpy changes due to stacking of phenothiazine rings and ionic interaction between piperazine side chains. The enthalpy changes calculated from molecular dynamics modeling could be validated by solution calorimetry studies, in which the enthalpies of solution of both crystalline and liquid crystalline forms could be determined separately.

Chapter 6

The amorphous trifluoperazine·2HCl prepared by freeze-drying and cryo-milling could not be differentiated by PXRD and DSC. The pair distribution function (PDF) transforms of the PXRD data are a powerful tool for study the local structures in the amorphous materials. The PDF transform of a XRD pattern can show the characteristic atom to atom distances within both amorphous and crystalline materials. By comparing PDF transforms of XRD patterns of the two amorphous TFP samples, it would be possible to identify the structural difference in the samples that resulted from the intermediate states during pharmaceutical processes.

References

Chapter 1

1. *Survey hygroscopicity*. Pharmeuropa. Vol. 4. 1992.
2. Reutzel-Edens, S.M. and Newman, A.W., *Physical characterization of hygroscopicity in pharmaceutical solids*, in *Polymorphism in the Pharmaceutical Industry*, R. Hilfiker, Editor. 2006, Wiley-VCH: Weinheim, Germany. pp. 235-258.
3. Labuza, T.P. and Altunakar, B., *Water activity prediction and moisture sorption isotherm*, in *Water Activity in Foods*, Gustavo V. Barbosa-Cánovas, et al., Editors. 2007, IFT Press: Ames, Iowa. pp. 109-154.
4. Labuza, T.P. 1980. The effect of water activity on reaction kinetics of food deterioration. *Food Technology (Chicago, IL, United States)*, **34**: 36-41.
5. Nelson, K.A. and Labuza, T.P. 1992. Relationship between water and lipid oxidation rates. Water activity and glass transition theory. *ACS Symposium Series*, **500**: 93-103.
6. Rohrs, B.R.T., T.J.; Gao, P.; Stelzer, D.J.; Bergren, M.S.; Chao, R.S. 1999. Tablet dissolution affected by a moisture mediated solid-state interaction between drug and disintegrant. *Pharmaceutical Research*, **16**: 1850-1856.
7. Schmitt, E., Davis, C.W., and Long, S.T. 1996. Moisture-dependent crystallization of amorphous lamotrigine mesylate. *Journal of Pharmaceutical Sciences*, **85**: 1215-1219.
8. Listiohadi, Y.D., Hourigan, J.A., Sleigh, R.W., and Steele, R.J. 2005. Properties of lactose and its caking behaviour. *Australian Journal of Dairy Technology*, **60**: 33-52.
9. Nail, S.L. 2005. Physical and chemical stability considerations in the development and stress testing of freeze-dried pharmaceuticals. *Drugs and the Pharmaceutical Sciences*, **153**: 261-291.
10. Balbach, S. and Korn, C. 2004. Pharmaceutical evaluation of early development candidates "the 100 mg-approach". *International Journal of Pharmaceutics*, **275**: 1-12.
11. Gaviraghi, G., Barnaby, R.J., and Pellegatti, M. 2001. Pharmacokinetic challenges in lead optimization. *Pharmacokinetic Optimization in Drug Research: Biological, Physicochemical, and Computational Strategies, [LogP2000, Lipophilicity Symposium], 2nd, Lausanne, Switzerland, Mar. 5-9, 2000*, 3-14.
12. Newman, A.W., Reutzel-Edens, S.M., and Zografi, G. 2008. Characterization of the "hygroscopic" properties of active pharmaceutical ingredients. *Journal of Pharmaceutical Sciences*, **97**: 1047-1059.
13. Kontny, M.J. and Zografi, G. 1995. Sorption of water by solids. *Drugs and the Pharmaceutical Sciences*, **70**: 387-418.
14. Salameh, A.K. and Taylor, L.S. 2006. Role of deliquescence lowering in enhancing chemical reactivity in physical mixtures. *Journal of Physical Chemistry B*, **110**: 10190-10196.

15. Atassi, F. and Byrn, S.R. 2006. General trends in the desolvation behavior of calcium salts. *Pharmaceutical Research*, **23**: 2405-2412.
16. Griesser, U.J., *The importance of solvates*, in *Polymorphism in the Pharmaceutical Industry*, R. Hilfiker, Editor. 2006, Wiley-VCH: Weinheim, Germany. pp. 211-233.
17. Newman Ann, W., Reutzel-Edens Susan, M., and Zografi, G. 2008. Characterization of the "hygroscopic" properties of active pharmaceutical ingredients. *J Pharm Sci FIELD Full Journal Title:Journal of pharmaceutical sciences*, **97**: 1047-59.
18. Visalakshi, N., Mariappan, T., Bhutani, H., and Singh, S. 2005. Behavior of moisture gain and equilibrium moisture contents (EMC) of various drug substances and correlation with compendial information on hygroscopicity and loss on drying. *Pharmaceutical Development and Technology*, **10**: 489-497.
19. Callahan, J.C., Cleary, G.W., Elefant, M., Kaplan, G., Kensler, T., and Nash, R.A. 1982. Equilibrium moisture content of pharmaceutical excipients. *Drug Development and Industrial Pharmacy*, **8**: 355-69.
20. Kontny, M.J. and Zografi, G. 1995. Water-solid interactions in pharmaceutical systems. *Drugs and the Pharmaceutical Sciences*, **70**: 387-418.
21. Zografi, G. 1991. Report of the advisory panel on moisture specifications. *Pharmacopeial Forum*, **1**: 1459-1474.
22. Ahlneck, C. and Zografi, G. 1990. The molecular basis of moisture effects on the physical and chemical stability of drugs in the solid state. *International Journal of Pharmaceutics*, **62**: 87-95.
23. El-Sabaawi, M. and Pei, D.C.T. 1977. Moisture isotherms of hygroscopic porous solids. *Industrial & Engineering Chemistry Fundamentals*, **16**: 321-326.
24. Krzyzaniak, J.F., Williams, G.R., and Ni, N. 2007. Identification of phase boundaries in anhydrate/hydrate systems. *Journal of Pharmaceutical Sciences*, **96**: 1270-1281.
25. Salameh, A.K. and Taylor, L.S. 2005. Deliquescence in Binary Mixtures. *Pharmaceutical Research*, **22**: 318-324.
26. Petit, S. and Coquerel, G., *The amorphous state*, in *Polymorphism in the Pharmaceutical Industry*, R. Hilfiker, Editor. 2006, Wiley-VCH: Weinheim, Germany. pp. 259-285.
27. Hancock, B.C. and Zografi, a.G. 1996. Effects of solid-state processing on water vapor sorption by aspirin. *Journal of Pharmaceutical Sciences*, **85**: 246-8.
28. Carstensen, J.T., *Interactions of moisture with solids*, in *Drug Stability: Principles and Practices*. 2000, Marcel Dekker: New York, NY. pp. 191-208.
29. Labuza, T.P. 1977. The properties of water in relation to water binding in food. *Journal of Food Processing & Preservation*, **1**: 2-12.
30. Labuza, T.P. 1980. Enthalpy/entropy compensation in food reactions. *Food Technology (Chicago, IL, United States)*, **34**: 67-77.
31. Rouquerol, F., Rouquerol, J., and Sing, K., *Adsorption by Powders and Porous Solids: Principles, Methodology and Applications*. 1999 Academic Press, San Diego, CA.

32. Thiel, P.A. and Madey, T.F. 1987. The interaction of water with solid surfaces: fundamental aspects. *Surface Science Reports*, **7**: 211-385.
33. Rounsley, R.R. 1961. Multimolecular adsorption equation. *AIChE Journal*, 308-311.
34. Brunauer, S., *Adsorption of Gases and Vapors, I. Physical Adsorption*. 1943 Princeton Unversity Press, Princeton, NJ.
35. Einicke, W.-D., Schollner, R., Heuchel, M., Brauer, P., and Messow, U. 1995. Type III isotherms for the adsorption of ethanol-water mixtures on solid adsorbents. *Journal of the Chemical Society, Faraday Transactions*, **91**: 535-8.
36. Kluge, G. and Nagel, G. 1988. Modeling of nonisothermal multicomponent adsorption in adiabatic fixed beds - III. Some remarks on the type-III adsorption process. *Chemical Engineering Science*, **43**: 2885-9.
37. Gore, A.Y. and Banker, G.S. 1979. Surface chemistry of colloidal silica and a possible application to stabilize aspirin in solid matrixes. *Journal of Pharmaceutical Sciences*, **68**: 197-202.
38. Halasz, I., Kim, S., and Marcus, B. 2001. Uncommon adsorption isotherm of methanol on a hydrophobic Y-zeolite. *Journal of Physical Chemistry B*, **105**: 10788-10796.
39. Wendland, M., Salzmann, S., Heinbuch, U., and Fischer, J. 1989. Born-Green-Yvon results for adsorption of a simple fluid on plane walls. Structure, adsorption isotherms, and surface area determination. *Molecular Physics*, **67**: 161-72.
40. Rahaman, A., Grassian, V.H., and Margulis, C.J. 2008. Dynamics of water adsorption onto a calcite surface as a function of relative humidity. *Journal of Physical Chemistry C*, **112**: 2109-2115.
41. Ewing, G.E. 2006. Ambient thin film water on insulator surfaces. *Chemical Reviews*, **106**: 1511-1526.
42. Hancock, B.C. and Zografi, G. 1996. Effects of solid-state processing on water vapor sorption by aspirin. *J. Pharm. Sci.*, **85**: 246-248.
43. Newell, H.E., Buckton, G., Butler, D.A., Thielmann, F., and Williams, D.R. 2001. The use of inverse phase gas chromatography to measure the surface energy of crystalline, amorphous, and recently milled lactose. *Pharmaceutical Research*, **18**: 662-666.
44. Kontny, M.J., Grandolfi, G.P., and Zografi, G. 1987. Water vapor sorption of water-soluble substances: studies of crystalline solids below their critical relative humidities. *Pharmaceutical Research*, **4**: 104-112.
45. Hucher, M., Oberlin, A., and Hocart, R. 1967. Adsorption of water vapor on the cleavage surfaces of some alkali metal halides. *Bulletin de la Societe Francaise de Mineralogie et de Cristallographie*, **90**: 320-32.
46. Faqih, A.M.N., Mehrotra, A., Hammond, S.V., and Muzzio, F.J. 2007. Effect of moisture and magnesium stearate concentration on flow properties of cohesive granular materials. *International Journal of Pharmaceutics*, **336**: 338-345.
47. Binnig, G., Quate, C.F., and Gerber, C. 1986. Atomic force microscope. *Physical Review Letters*, **56**: 930-933.
48. Alexander, S., Hellemans, L., Marti, O., Schneir, J., Elings, V., Hansma, P.K., Longmiro, M., and Gurley, J. 1989. An atomic-resolution atomic-force

microscope implemented using an optical lever. *Journal of Applied Physics*, **65**: 164-167.
49. Cappella, B. and Dietler, G. 1999. Force-distance curves by atomic force microscopy. *Surface Science Reports*, **34**: 1-104.
50. Lee, S. and Staehle, R.W. 1996. Adsorption of water on gold. *Corrosion (Houston)*, **52**: 843-852.
51. Verdaguer, A., Sacha, G.M., Luna, M., Ogletree, D.F., and Salmeron, M. 2005. Initial stages of water adsorption on NaCl (100) studied by scanning polarization force microscopy. *Journal of Chemical Physics*, **123**: 124703/1-124703/8.
52. Dai, Q., Hu, J., and Salmeron, M. 1997. Adsorption of Water on NaCl (100) Surfaces: Role of Atomic Steps. *Journal of Physical Chemistry B*, **101**: 1994-1998.
53. Xu, L., Bluhm, H., and Salmeron, M. 1998. An AFM study of the tribological properties of NaCl(100) surfaces under moist air. *Surface Science*, **407**: 251-255.
54. Foster, M.C. and Ewing, G.E. 2000. Adsorption of water on the NaCl(001) surface. II. An infrared study at ambient temperatures. *Journal of Chemical Physics*, **112**: 6817-6826.
55. Igarashi, N., Nakai, K., Hashimoto, K., and Tatsumi, T. 2001. Pore size analysis with H2O adsorption measurement of organically modified MCM-41 type materials. *Studies in Surface Science and Catalysis*, **135**: 2902-2911.
56. Hanzawa, Y. and Kaneko, K. 1997. Lack of a Predominant Adsorption of Water Vapor on Carbon Mesopores. *Langmuir*, **13**: 5802-5804.
57. Patrick, W.A. 1929. The adsorption of vapors. *Colloid Symposium Monograph*, **7**: 129-33.
58. Cantrell, W., McCrory, C., and Ewing, G.E. 2002. Nucleated deliquescence of salt. *Journal of Chemical Physics*, **116**: 2116-2120.
59. Zografi, G. 1988. States of water associated with solids. *Drug Development and Industrial Pharmacy*, **14**: 1905-1926.
60. Van Campen, L., Amidon, G.L., and Zografi, G. 1983. Moisture sorption kinetics for water-soluble substances. I: Theoretical considerations of heat transport control. *Journal of Pharmaceutical Sciences*, **72**: 1381-1388.
61. Ross, K.D. 1975. Estimation of water activity in intermediate moisture foods. *Food Technology*, **3**: 26-34.
62. Van Campen, L., Zografi, G., and Carstensen, J.T. 1980. An approach to the evaluation of hygroscopicity for pharmaceutical solids. *International Journal of Pharmaceutics*, **5**: 1-18.
63. Schuttlefield, J., Al-Hosney, H., Zachariah, A., and Grassian, V.H. 2007. Attenuated total reflection Fourier transform infrared spectroscopy to investigate water uptake and phase transitions in atmospherically relevant particles. *Applied Spectroscopy*, **61**: 283-292.
64. Li, X.-H., Wang, F., Lu, P.-D., Dong, J.-L., Wang, L.-Y., and Zhang, Y.-H. 2006. Confocal raman observation of the efflorescence/deliquescence processes of individual NaNO3 particles on quartz. *Journal of Physical Chemistry B*, **110**: 24993-24998.

65. Mirabel, P., Reiss, H., and Bowles, R.K. 2000. A theory for the deliquescence of small particles. *Journal of Chemical Physics*, **113**: 8200-8205.
66. Djikaev, Y.S., Bowles, R., Reiss, H., Haemeri, K., Laaksonen, A., and Vaekevae, M. 2001. Theory of Size Dependent Deliquescence of Nanoparticles: Relation to Heterogeneous Nucleation and Comparison with Experiments. *Journal of Physical Chemistry B*, **105**: 7708-7722.
67. Ewing, G.E. 2005. H2O on NaCl: from single molecule, to clusters, to monolayer, to thin films, to deliquescence. *Structure and Bonding (Berlin, Germany)*, **116**: 1-25.
68. Russell, L.M. and Ming, Y. 2002. Deliquescence of small particles. *Journal of Chemical Physics*, **116**: 311-321.
69. Biskos, G., Paulsen, D., Russell, L.M., Buseck, P.R., and Martin, S.T. 2007. Prompt deliquescence and efflorescence of aerosol nanoparticles. *Atmospheric Chemistry and Physics*, **6**: 4633-4642.
70. Biskos, G., Malinowski, A., Russell, L., Buseck, P., and Martin, S. 2006. Nanosize effect on the deliquescence and the efflorescence of sodium chloride particles. *Aerosol Science and Technology*, **40**: 97-106.
71. Martin, S.T. 2000. Phase transitions of aqueous atmospheric particles. *Chemical Reviews (Washington, D. C.)*, **100**: 3403-3453.
72. Parsons, M.T., Mak, J., Lipetz, S.R., and Bertram, A.K. 2004. Deliquescence of malonic, succinic, glutaric, and adipic acid particles. *Journal of Geophysical Research, [Atmospheres]*, **109**: D06212/1-D06212/8.
73. Chen, L.R., *Solid state behavior of pharmaceutical hydrates*. Ph.D dissertation. 1999.
74. Vippagunta, S.R., Brittain, H.G., and Grant, D.J.W. 2001. Crystalline solids. *Advanced Drug Delivery Reviews*, **48**: 3-26.
75. Burley, J.C., van de Streek, J., and Stephens, P.W. 2006. Ampicillin trihydrate from synchrotron powder diffraction data. *Acta Crystallographica, Section E: Structure Reports Online*, **E62**: o797-o799.
76. Zhu, H., Young, V.G., Jr., and Grant, D.J.W. 2002. Crystal structures and thermal analysis of nedocromil bivalent metal salt hydrates. *Journal of Chemical Crystallography*, **31**: 421-434.
77. Haleblian, J.K. 1975. Characterization of habits and crystalline modification of solids and their pharmaceutical applications. *Journal of Pharmaceutical Sciences*, **64**: 1269-1288.
78. Kim, Y.-s. and Rousseau, R.W. 2004. Characterization and Solid-State Transformations of the Pseudopolymorphic Forms of Sodium Naproxen. *Crystal Growth & Design*, **4**: 1211-1216.
79. Zhu, H. and Grant, D.J.W. 2001. Dehydration behavior of nedocromil magnesium pentahydrate. *International Journal of Pharmaceutics*, **215**: 251-262.
80. Zhu, H., Halfen, J.A., Young, V.G., Jr., Padden, B.E., Munson, E.J., Menon, V., and Grant, D.J.W. 1997. Physicochemical Characterization of Nedocromil Bivalent Metal Salt Hydrates: 3. Nedocromil Calcium. *Journal of Pharmaceutical Sciences*, **86**: 1439-1447.

81. Zhu, H., Khankari, R.K., Padden, B.E., Munson, E.J., Gleason, W.B., and Grant, D.J.W. 1996. Physicochemical Characterization of Nedocromil Bivalent Metal Salt Hydrates. 1. Nedocromil Magnesium. *Journal of Pharmaceutical Sciences*, **85**: 1026-1034.
82. Reutzel, S.M. and Russell, V.A. 1998. Origins of the Unusual Hygroscopicity Observed in LY297802 Tartrate. *Journal of Pharmaceutical Sciences*, **87**: 1568-1571.
83. Chen, L.R., Young, V.G., Jr., Lechuga-Ballesteros, D., and Grant, D.J. 1999. Solid-state behavior of cromolyn sodium hydrates. *Journal of Pharmaceutical Sciences*, **88**: 1191-200.
84. Cox, J.S.G., Woodard, G.D., and McCrone, W.C. 1971. Solid-state chemistry of cromolyn sodium (disodium cromoglycate). *Journal of Pharmaceutical Sciences*, **60**: 1458-1465.
85. Apperley, D.C., Basford, P.A., Dallman, C.I., Harris, R.K., Kinns, M., Marshall, P.V., and Swanson, A.G. 2005. Nuclear magnetic resonance investigation of the interaction of water vapor with sildenafil citrate in the solid state. *Journal of Pharmaceutical Sciences*, **94**: 516-523.
86. Te, R.L., Griesser, U.J., Morris, K.R., Byrn, S.R., and Stowell, J.G. 2003. X-ray Diffraction and Solid-State NMR Investigation of the Single-Crystal to Single-Crystal Dehydration of Thiamine Hydrochloride Monohydrate. *Crystal Growth & Design*, **3**: 997-1004.
87. Watanabe, A., Tasaki, S., Wada, Y., and Nakamachi, H. 1979. Polymorphism of thiamine hydrochloride. II. Crystal structure of thiamine hydrochloride hemihydrate and its stability. *Chemical & Pharmaceutical Bulletin*, **27**: 2751-9.
88. Bandyopadhyay, R., Erixon, K., Young, V.G., and Grant, D.J.W. *Effects of water activity on recrystallized L-lysine monohydrochloride*. in *World Congress on Particle Technology 3, Brighton, UK, July 6-9*. 1998.
89. Stephenson, G.A., Stowell, J.G., Toma, P.H., Pfeiffer, R.R., and Byrn, S.R. 1997. Solid-State Investigations of Erythromycin A Dihydrate: Structure, NMR Spectroscopy, and Hygroscopicity. *Journal of Pharmaceutical Sciences*, **86**: 1239-1244.
90. Stephenson, G.A., Groleau, E.G., Kleemann, R.L., Xu, W., and Rigsbee, D.R. 1998. Formation of isomorphic desolvates: creating a molecular vacuum. *Journal of Pharmaceutical Sciences*, **87**: 536-542.
91. Han, J., Gupte, S., and Suryanarayanan, R. 1998. Applications of pressure differential scanning calorimetry in the study of pharmaceutical hydrates. II. Ampicillin trihydrate. *International Journal of Pharmaceutics*, **170**: 63-72.
92. Chen, L.R., *Solid state behavior of pharmaceutical hydrates*. Ph.D dissertation. 1999 University of Minnesota, Minneapolis.
93. Griesser, U.J. and Burger, A. 1995. The effect of water vapor pressure on desolvation kinetics of caffeine 4/5-hydrate. *International Journal of Pharmaceutics*, **120**: 83-93.
94. Phadnis, N.V. and Suryanarayanan, R. 1997. Polymorphism in anhydrous theophylline--implications on the dissolution rate of theophylline tablets. *Journal of Pharmaceutical Sciences*, **86**: 1256-63.

95. Lin, C.T., Perrier, P., Clay, G.G., Sutton, P.A., and Byrn, S.R. 1982. Solid-state photooxidation of 21-cortisol tert-butylacetate to 21-cortisone tert-butylacetate. *Journal of Organic Chemistry*, **47**: 2978-81.
96. Katdare, A.V. and Bavitz, J.F. 1984. Hydrate related dissolution characteristics of norfloxacin. *Drug Development and Industrial Pharmacy*, **10**: 789-807.
97. Kahela, P., Aaltonen, R., Lewing, E., Anttila, M., and Kristoffersson, E. 1983. Pharmacokinetics and dissolution of two crystalline forms of carbamazepine. *International Journal of Pharmaceutics*, **14**: 103-12.
98. Khankari, R.K. and Grant, D.J.W. 1995. Pharmaceutical hydrates. *Thermochimica Acta*, **248**: 61-79.
99. Ticehurst, M.D., Storey, R.A., and Watt, C. 2002. Application of slurry bridging experiments at controlled water activities to predict the solid-state conversion between anhydrous and hydrated forms using theophylline as a model drug. *International Journal of Pharmaceutics*, **247**: 1-10.
100. Zhu, H., Yuen, C., and Grant, D.J.W. 1996. Influence of water activity in organic solvent + water mixtures on the nature of the crystallizing drug phase. 1. Theophylline. *International Journal of Pharmaceutics*, **135**: 151-160.
101. Murphy, D., Rodriguez-Cintron, F., Langevin, B., Kelly, R.C., and Rodriguez-Hornedo, N. 2002. Solution-mediated phase transformation of anhydrous to dihydrate carbamazepine and the effect of lattice disorder. *International Journal of Pharmaceutics*, **246**: 121-134.
102. O'Brien, L.E., Timmins, P., Williams, A.C., and York, P. 2004. Use of in situ FT-Raman spectroscopy to study the kinetics of the transformation of carbamazepine polymorphs. *Journal of Pharmaceutical and Biomedical Analysis*, **36**: 335-340.
103. Otsuka, M., Ishii, M., and Matsuda, Y. 2003. Effect of surface modification on hydration kinetics of carbamazepine anhydrate using isothermal microcalorimetry. *AAPS PharmSciTech*, **4**: E5.
104. Kelly, R.C. and Rodriguez-Hornedo, N. 2003. Directed nucleation and solution-mediated phase transformation of carbamazepine in aqueous and organic solutions. *Abstracts of Papers, 225th ACS National Meeting, New Orleans, LA, United States, March 23-27, 2003*, IEC-055.
105. Rodriguez-Hornedo, N. and Murphy, D. 2004. Surfactant-facilitated crystallization of dihydrate carbamazepine during dissolution of anhydrous polymorph. *Journal of Pharmaceutical Sciences*, **93**: 449-460.
106. Tanninen, V.P., Luhtala, S., and Yliruusi, J. 1992. X-ray powder diffraction line profile analysis in the study on the effect of surface active agent on the crystal properties of carbamazepine. *Acta Pharmaceutica Nordica*, **4**: 277-282.
107. Katzhendler, I., Azoury, R., and Friedman, M. 1998. Crystalline properties of carbamazepine in sustained release hydrophilic matrix tablets based on hydroxypropyl methylcellulose. *Journal of controlled release*, **54**: 69-85.
108. Jorgensen, A.C., Airaksinen, S., Karjalainen, M., Luukkonen, P., Rantanen, J., and Yliruusi, J. 2004. Role of excipients in hydrate formation kinetics of theophylline in wet masses studied by near-infrared spectroscopy. *European Journal of Pharmaceutical Sciences*, **23**: 99-104.

109. Yu, L. 2001. Amorphous pharmaceutical solids: preparation, characterization and stabilization. *Advanced Drug Delivery Reviews*, **48**: 27-42.
110. Gordon, M. and Taylor, J.S. 1952. Ideal copolymers and the second-order transitions of synthetic rubbers. I. Noncrystalline copolymers. *Journal of Applied Chemistry*, **2**: 493-500.
111. Andronis, V. and Zografi, G. 1998. The molecular mobility of supercooled amorphous indomethacin as a function of temperature and relative humidity. *Pharmaceutical Research*, **15**: 835-842.
112. Fitzpatrick, S., McCabe, J.F., Petts, C.R., and Booth, S.W. 2002. Effect of moisture on polyvinylpyrrolidone in accelerated stability testing. *International Journal of Pharmaceutics*, **246**: 143-151.
113. Schmitt, E.A., Law, D., and Zhang, G.G. 1999. Nucleation and crystallization kinetics of hydrated amorphous lactose above the glass transition temperature. *Journal of Pharmaceutical Sciences*, **88**: 291-6.
114. Carstensen, J.T. and Van Scoik, K. 1990. Amorphous-to-crystalline transformation of sucrose. *Pharmaceutical Research*, **7**: 1278-1281.
115. Zografi, G., Kontny, M.J., Yang, A.Y.S., and Brenner, G.S. 1984. Surface area and water vapor sorption of microcrystalline cellulose. *International Journal of Pharmaceutics*, **18**: 99-116.
116. Brunauer, S., Emmett, P.H., and Teller, E. 1938. Adsorption of gases in multimolecular layers. *Journal of the American Chemical Society*, **60**: 309-319.
117. Zografi, G. and kontony, M.J. 1986. The interactions of water with cellulose- and starch-derived pharmaceutical excipients. *Pharmaceutical research*, 187-194.
118. Stubberud, L., Arwidsson, H.G., Larsson, A., Graffner, C. 1996. Water solid interactions II. Effect of moisture sorption and glass transition temperature on compactibility of microcrystalline cellulose alone or in binary mixtures with polyvinyl pyrrolidone. *International Journal of Pharmaceutics*, **134**: 79-88.
119. Sun, C.C. 2008. Mechanism of moisture induced variations in true density and compaction properties of microcrystalline cellulose. *International Journal of Pharmaceutics*, **346**: 93-101.
120. Li, S., Wei, B., Fleres, S., Comfort, A., and Royce, A. 2004. Correlation and prediction of moisture-mediated dissolution stability for benazepril hydrochloride tablets. *Pharmaceutical Research*, **21**: 617-624.
121. Flory, P.J. 1942. Thermodynamics of high-polymer solutions. *Journal of Chemical Physics*, **10**: 51-61.
122. MacKenzie, A.P. and Rasmussen, D.H., *Interactions in the water-polyvinylpyrrolidinone system at low temperatures*, in *Water Struct. Water-Polym. Interface, Proc. Symp.* 1972. p. 146-172.
123. Hancock, B.C. and Zografi, G. 1993. The use of solution theories for predicting water vapor absorption by amorphous pharmaceutical solids: A test of the Flory-Huggins and Vrentas models. *Pharmaceutical Research*, **10**: 1262-1267.
124. Gupta, P. and Bansal, A.K. 2005. Molecular interactions in celecoxib-PVP-meglumine amorphous system. *Journal of Pharmacy and Pharmacology*, **57**: 303-310.

125. Andronis, V., Yoshioka, M., and Zografi, G. 1997. Effects of sorbed water on the crystallization of indomethacin from the amorphous state. *J Pharm Sci FIELD Full Journal Title:Journal of pharmaceutical sciences*, **86**: 346-51.
126. Fujita, H. 1961. Free diffusion in a two-component system in which there is a volume change on mixing. *Journal of the American Chemical Society*, **83**: 2862-2865.
127. Hageman, M.J. 1992. Water sorption and solid-state stability of proteins. *Pharmaceutical Biotechnology*, **2**: 273-309.
128. Kocherbitov, V., Arnebrant, T., and Soederman, O. 2004. Lysozyme-water interactions studied by sorption calorimetry. *Journal of Physical Chemistry B*, **108**: 19036-19042.
129. Kaneniwa, N., Yamaguchi, T., Watari, N., and Otsuka, M. 1984. Hygroscopicity of carbamazepine crystalline powders. *Yakugaku Zasshi*, **104**: 184-90.
130. Danesh, A., Connell, S.D., Davies, M.C., Roberts, C.J., Tendler, S.J., Williams, P.M., and Wilkins, M.J. 2001. An in situ dissolution study of aspirin crystal planes (100) and (001) by atomic force microscopy. *Pharmaceutical research*, **18**: 299-303.
131. Zhang, J., Ebbens, S., Chen, X., Jin, Z., Luk, S., Madden, C., Patel, N., and Roberts, C.J. 2006. Determination of the surface free energy of crystalline and amorphous lactose by atomic force microscopy adhesion measurement. *Pharmaceutical Research*, **23**: 401-407.
132. Ecke, S., Raiteri, R., Bonaccurso, E., Reiner, C., Deiseroth, H.-J., and Butt, H.-J. 2001. Measuring normal and friction forces acting on individual fine particles. *Review of Scientific Instruments*, **72**: 4164-4170.
133. Hu, J., Xiao, X.d., Ogletree, D.F., and Salmeron, M. 1995. Atomic scale friction and wear of mica. *Surface Science*, **327**: 358-70.
134. Cappella, B., Kaliappan, S.K., and Sturm, H. 2005. Using AFM force-distance curves to study the glass-to-rubber transition of amorphous polymers and their elastic-plastic properties as a function of temperature. *Macromolecules*, **38**: 1874-1881.
135. Schaer-Zammaretti, P. and Ubbink, J. 2003. Imaging of lactic acid bacteria with AFM - elasticity and adhesion maps and their relationship to biological and structural data. *Ultramicroscopy*, **97**: 199-208.
136. Carpick, R.W., Ogletree, D.F., and Salmeron, M. 1997. Lateral stiffness: a new nanomechanical measurement for the determination of shear strengths with friction force microscopy. *Applied Physics Letters*, **70**: 1548-1550.
137. Hansma, H.G., Kasuya, K., and Oroudjev, E. 2004. Atomic force microscopy imaging and pulling of nucleic acids. *Current Opinion in Structural Biology*, **14**: 380-385.
138. Hussain, M.A., Agnihotri, A., and Siedlecki, C.A. 2005. AFM Imaging of Ligand Binding to Platelet Integrin aIIbb3 Receptors Reconstituted into Planar Lipid Bilayers. *Langmuir*, **21**: 6979-6986.
139. Kendall, T.A. and Martin, S.T. 2007. Water-induced reconstruction that affects mobile ions on the surface of calcite. *Journal of Physical Chemistry A*, **111**: 505-514.

140. Cleaver, J.A.S. and Wong, P. 2004. Humidity-induced surface modification of boric acid. *Surface and Interface Analysis*, **36**: 1592-1599.
141. Sedin, D.L. and Rowlen, K.L. 2000. Adhesion forces measured by atomic force microscopy in humid air. *Analytical Chemistry*, **72**: 2183-2189.
142. Binggeli, M. and Mate, C.M. 1994. Influence of capillary condensation of water on nanotribology studied by force microscopy. *Applied Physics Letters*, **65**: 415-17.
143. Ducker, W.A., Senden, T.J., and Pashley, R.M. 1991. Direct measurement of colloidal forces using an atomic force microscope. *Nature (London, United Kingdom)*, **353**: 239-41.
144. Young, P.M., Price, R., Tobyn, M.J., Buttrum, M., and Dey, F. 2004. The influence of relative humidity on the cohesion properties of micronized drugs used in inhalation therapy. *Journal of Pharmaceutical Sciences*, **93**: 753-761.
145. Frisbie, C.D., Rozsnyai, L.F., Noy, A., Wrighton, M.S., and Lieber, C.M. 1994. Functional group imaging by chemical force microscopy. *Science*, **265**: 2071-2074.
146. Begat, P., Morton, D.A.V., Staniforth, J.N., and Price, R. 2004. The Cohesive-Adhesive Balances in Dry Powder Inhaler Formulations II: Influence on Fine Particle Delivery Characteristics. *Pharmaceutical Research*, **21**: 1826-1833.
147. van der Werf, K.O., Putman, C.A.J., de Grooth, B.G., and Greve, J. 1994. Adhesion force imaging in air and liquid by adhesion mode atomic force microscopy. *Applied Physics Letters*, **65**: 1195-7.
148. Allen, S., Connell, S.D.A., Chen, X., Davies, J., Davies, M.C., Dawkes, A.C., Roberts, C.J., Tendler, S.J.B., and Williams, P.M. 2001. Mapping the surface characteristics of polystyrene microtiter wells by a multimode scanning force microscopy approach. *Journal of Colloid and Interface Science*, **242**: 470-476.
149. Reich, G. 2005. Near-infrared spectroscopy and imaging: Basic principles and pharmaceutical applications. *Advanced Drug Delivery Reviews*, **57**: 1109-1143.
150. Giangiacomo, R. 2006. Study of water-sugar interactions at increasing sugar concentration by NIR spectroscopy. *Food Chemistry*, **96**: 371-379.
151. Duong, N.-H., Arratia, P., Muzzio, F., Lange, A., Timmermans, J., and Reynolds, S. 2003. A homogeneity study using NIR spectroscopy: Tracking magnesium stearate in bohle bin-blender. *Drug Development and Industrial Pharmacy*, **29**: 679-687.
152. Grant, A., Davies, A.M.C., and Bilverstone, T. 1989. Simultaneous determination of sodium hydroxide, sodium carbonate and sodium chloride concentrations in aqueous solutions by near-infrared spectrometry. *Analyst (Cambridge, United Kingdom)*, **114**: 819-22.
153. Jones, J.A., Last, I.R., MacDonald, B.F., and Prebble, K.A. 1993. Development and transferability of near-infrared methods for determination of moisture in a freeze-dried injection product. *Journal of Pharmaceutical and Biomedical Analysis*, **11**: 1227-31.
154. Reich, G. 2002. Potential of attenuated total reflection infrared and near-infrared spectroscopic imaging for quality assurance/quality control of solid pharmaceutical dosage forms. *Pharmazeutische Industrie*, **64**: 870-874.

155. Kramer, K. and Ebel, S. 2000. Application of NIR reflectance spectroscopy for the identification of pharmaceutical excipients. *Analytica Chimica Acta*, **420**: 155-161.
156. Ulmschneider, M., Barth, G., and Trenka, E. 2000. Building transferable cluster calibrations for the identification of different solid excipients with near-infrared spectroscopy. *Pharmazeutische Industrie*, **62**: 374-376.
157. Buning-Pfaue, H. 2003. Analysis of water in food by near infrared spectroscopy. *Food Chemistry*, **82**: 107-115.
158. Gergely, S. and Salgo, A. 2007. Changes in protein content during wheat maturation-what is measured by near infrared spectroscopy? *Journal of Near Infrared Spectroscopy*, **15**: 49-58.
159. Soller, B.R., Favreau, J., and Idwasi, P.O. 2003. Investigation of electrolyte measurement in diluted whole blood using spectroscopic and chemometric methods. *Applied Spectroscopy*, **57**: 146-151.
160. Zhou, X., Hines, P., and Borer, M.W. 1998. Moisture determination in hygroscopic drug substances by near infrared spectroscopy. *Journal of Pharmaceutical and Biomedical Analysis*, **17**: 219-225.
161. Zhou, G.X., Ge, Z., Dorwart, J., Izzo, B., Kukura, J., Bicker, G., and Wyvratt, J. 2003. Determination and differentiation of surface and bound water in drug substances by near infrared spectroscopy. *Journal of Pharmaceutical Sciences*, **92**: 1058-1065.
162. Cao, W., Mao, C., Chen, W., Lin, H., Krishnan, S., and Cauchon, N. 2006. Differentiation and quantitative determination of surface and hydrate water in lyophilized mannitol using NIR spectroscopy. *Journal of Pharmaceutical Sciences*, **95**: 2077-2086.
163. Al-Abadleh, H.A. and Grassian, V.H. 2003. Phase transitions in magnesium nitrate thin films: a transmission FT-IR study of the deliquescence and efflorescence of nitric acid reacted magnesium oxide interfaces. *Journal of Physical Chemistry B*, **107**: 10829-10839.
164. Ide, M., Yoshikawa, D., Maeda, Y., and Kitano, H. 1999. State of water inside and at the surface of poly(ethylene glycol) films examined by FT-IR. *Langmuir*, **15**: 926-929.
165. Kalutskaya, E.P. 1988. IR-spectroscopic study of the interaction of sorbed water and xylan. *Vysokomolekulyarnye Soedineniya, Seriya A*, **30**: 867-73.
166. Shen, Y. and Wu, P. 2003. Two-dimensional ATR-FTIR spectroscopic investigation on water diffusion in polypropylene film: water bending vibration. *Journal of Physical Chemistry B*, **107**: 4224-4226.
167. Kitano, H., Ichikawa, K., Ide, M., Fukuda, M., and Mizuno, W. 2001. Fourier transform infrared study on the state of water sorbed to poly(ethylene glycol) films. *Langmuir*, **17**: 1889-1895.
168. Gemmei-Ide, M., Motonaga, T., and Kitano, H. 2006. State of irremovable water in solid polymer films examined by Fourier transform infrared spectroscopy I: Poly(ethylene glycol) dimethyl ether. *Langmuir*, **22**: 2422-2425.

169. Shen, Y., Wang, H.-t., Zhong, W., and Wu, P.-y. 2006. Two-dimensional ATR-FTIR spectroscopic study on the water diffusion behavior in polyimide/silica nanocomposite. *Chinese Journal of Chemical Physics*, **19**: 481-484.
170. Chan, K.L.A. and Kazarian, S.G. 2004. Visualization of the heterogeneous water sorption in a pharmaceutical formulation under controlled humidity via FT-IR imaging. *Vibrational Spectroscopy*, **35**: 45-49.
171. Lemus, R. 2004. Vibrational excitations in H2O in the framework of a local model. *Journal of Molecular Spectroscopy*, **225**: 73-92.
172. Al-Abadleh, H.A. and Grassian, V.H. 2003. FT-IR study of water adsorption on aluminum oxide surfaces. *Langmuir*, **19**: 341-347.
173. Bouteiller, Y. and Perchard, J.P. 2004. The vibrational spectrum of (H2O)2: comparison between anharmonic ab initio calculations and neon matrix infrared data between 9000 and 90 cm-1. *Chemical Physics*, **305**: 1-12.
174. Ohno, K., Okimura, M., Akai, N., and Katsumoto, Y. 2005. The effect of cooperative hydrogen bonding on the OH stretching-band shift for water clusters studied by matrix-isolation infrared spectroscopy and density functional theory. *Physical Chemistry Chemical Physics*, **7**: 3005-3014.
175. Fornes, V. and Chaussidon, J. 1978. An interpretation of the evolution with temperature of the v2 + v3 combination band in water. *Journal of Chemical Physics*, **68**: 4667-71.
176. Wagner, R., Benz, S., Moehler, O., Saathoff, H., Schnaiter, M., and Schurath, U. 2005. Mid-infrared extinction spectra and optical constants of supercooled water droplets. *Journal of Physical Chemistry A*, **109**: 7099-7112.
177. Praprotnik, M., Janezic, D., and Mavri, J. 2004. Temperature dependence of water vibrational spectrum: A molecular dynamics simulation study. *Journal of Physical Chemistry A*, **108**: 11056-11062.
178. Schaefer, J. and Stejskal, E.O. 1976. Carbon-13 nuclear magnetic resonance of polymers spinning at the magic angle. *Journal of the American Chemical Society*, **98**: 1031-2.
179. Tishmack, P.A., Bugay, D.E., and Byrn, S.R. 2003. Solid-state nuclear magnetic resonance spectroscopy-pharmaceutical applications. *Journal of Pharmaceutical Sciences*, **92**: 441-474.
180. Harris, R.K. 2006. NMR studies of organic polymorphs & solvates. *Analyst (Cambridge, United Kingdom)*, **131**: 351-373.
181. Offerdahl, T.J. and Munson, E.J. 2004. Solid state NMR spectroscopy of pharmaceutical materials. *American Pharmaceutical Review*, **7**: 109-112.
182. Harris, R.K. 2004. NMR crystallography: the use of chemical shifts. *Solid State Science*, **6**: 1025-1037.
183. Reutzel-Edens, S.M. and Bush, J.K. 2002. Solid-state NMR spectroscopy of small molecules: from NMR crystallography to the characterization of solid oral dosage forms. *American Pharmaceutical Review*, **5**: 112-115.
184. Majolino, D., Corsaro, C., Crupi, V., Venuti, V., and Wanderlingh, U. 2008. Water diffusion in nanoporous glass: an NMR study at different hydration levels. *The Journal of Physical Chemistry. B*, **112**: 3927-30.

185. Soria, J., Sanz, J., Sobrados, I., Coronado, J.M., Maira, A.J., Hernandez-Alonso, M.D., and Fresno, F. 2007. FTIR and NMR study of the adsorbed water on nanocrystalline anatase. *Journal of Physical Chemistry C*, **111**: 10590-10596.
186. Benesi, A.J., Grutzeck, M.W., O'Hare, B., and Phair, J.W. 2004. Room temperature solid surface water with tetrahedral jumps of 2H nuclei detected in 2H2O-hydrated porous silicates. *Journal of Physical Chemistry B*, **108**: 17783-17790.
187. Yoshioka, S., Aso, Y., Osako, T., and Kawanishi, T. 2008. Wide-ranging molecular mobilities of water in active pharmaceutical ingredient (API) hydrates as determined by NMR relaxation times. *Journal of Pharmaceutical Sciences*, **4258-4268**.
188. Yoshioka, S., Aso, Y., Osako, T., and Kawanishi, T. 2008. Wide-ranging molecular mobilities of water in active pharmaceutical ingredient (API) hydrates as determined by NMR relaxation times. *Journal of Pharmaceutical Sciences*, **97**: 4258-4268.
189. Vogt, F.G., Dell'Orco, P.C., Diederich, A.M., Su, Q., Wood, J.L., Zuber, G.E., Katrincic, L.M., Mueller, R.L., Busby, D.J., and DeBrosse, C.W. 2006. A study of variable hydration states in topotecan hydrochloride. *Journal of Pharmaceutical and Biomedical Analysis*, **40**: 1080-1088.
190. Vogt, F.G., Brum, J., Katrincic, L.M., Flach, A., Socha, J.M., Goodman, R.M., and Haltiwanger, R.C. 2006. Physical, crystallographic, and spectroscopic characterization of a crystalline pharmaceutical hydrate: understanding the role of water. *Crystal Growth & Design*, **6**: 2333-2354.
191. Labuza, T.P. and Busk, G.C. 1979. An analysis of the water binding in gels. *Journal of Food Science*, **44**: 1379-1385.
192. Yoshioka, S. and Aso, Y. 2005. A quantitative assessment of the significance of molecular mobility as a determinant for the stability of lyophilized insulin formulations. *Pharmaceutical Research*, **22**: 1358-1364.
193. Masuda, K., Tabata, S., Sakata, Y., Hayase, T., Yonemochi, E., and Terada, K. 2005. Comparison of molecular mobility in the glassy state between amorphous indomethacin and salicin based on spin-lattice relaxation times. *Pharmaceutical Research*, **22**: 797-805.
194. Aso, Y., Yoshioka, S., and Terao, T. 1994. Effect of the binding of water to excipients as measured by 2H-NMR relaxation time on cephalothin decomposition rate. *Chemical & Pharmaceutical Bulletin*, **42**: 398-401.
195. Aso, Y., Yoshioka, s., and Kojima, S. 1996. Relationship between water mobility, measured as nuclear magnetic relaxation time, and the crystallization rate of amorphous nifedipine in the presence of some pharmaceutical excipients. *Chemical & Pharmaceutical Bulletin*, **44**: 1065-1067.
196. Yoshioka, S., Aso, Y., and Miyazaki, T. 2006. Negligible contribution of molecular mobility to the degradation rate of insulin lyophilized with poly(vinylpyrrolidone). *Journal of Pharmaceutical Sciences*, **95**: 939-943.
197. Xiang, T.-X. and Anderson, B.D. 2005. Distribution and effect of water content on molecular mobility in poly(vinylpyrrolidone) glasses: a molecular dynamics simulation. *Pharmaceutical Research*, **22**: 1205-1214.

198. Aso, Y., Yoshioka, S., Zhang, J., and Zografi, G. 2002. Effect of water on the molecular mobility of sucrose and poly(vinylpyrrolidone) in a colyophilized formulation as measured by 13C-NMR relaxation time. *Chemical & Pharmaceutical Bulletin*, **50**: 822-826.
199. Glasstone, S., *Textbook cf. Physical Chemistry. 2nd ed*. 1946 Van Nostrand, New York.
200. Carpick, R.W. and Salmeron, M. 1997. Scratching the surface: fundamental investigations of tribology with atomic force microscopy. *Chemical Reviews (Washington, D. C.)*, **97**: 1163-1194.
201. Finot, E., Lesniewska, E., Mutin, J.C., Hosain, S.I., and Goudonnet, J.P. 1996. Contact force dependence on relative humidity: investigations using atomic force microscopy. *Scanning Microscopy*, **10**: 697-708.
202. Berard, V., Lesniewska, E., Andres, C., Pertuy, D., Laroche, C., and Pourcelot, Y. 2002. Affinity scale between a carrier and a drug in DPI studied by atomic force microscopy. *International Journal of Pharmaceutics*, **247**: 127-137.

Chapter 2

1. Reutzel-Edens, S.M. and Newman, A.W., *Physical characterization of hygroscopicity in pharmaceutical solids*, in *Polymorphism in the Pharmaceutical Industry*, R. Hilfiker, Editor. 2006, Wiley-VCH: Weinheim, Germany. pp. 235-258.
2. Govindarajan, R. and Suryanarayanan, R., *Processing-induced phase transformations and their implications on pharmaceutical products quality*, in *Polymorphism in the Pharmaceutical Industry*, R. Hilfiker, Editor. 2006, Wiley-VCH: Weinheim, Germany. pp. 333-364.
3. Ewing, G.E. 2006. Ambient thin film water on insulator surfaces. *Chemical Reviews*, **106**: 1511-1526.
4. Verdaguer, A., Sacha, G.M., Luna, M., Ogletree, D.F., and Salmeron, M. 2005. Initial stages of water adsorption on NaCl (100) studied by scanning polarization force microscopy. *Journal of Chemical Physics*, **123**: 124703-124703.
5. Amado Ana, M., Nolasco Mariela, M., and Ribeiro-Claro Paulo, J.A. 2007. Probing pseudopolymorphic transitions in pharmaceutical solids using Raman spectroscopy: Hydration and dehydration of theophylline. *Journal of Pharmaceutical Sciences*, **96**: 1366-79.
6. Burnett, D.J., Thielmann, F., Sokoloski, T., and Brum, J. 2006. Investigating the moisture-induced crystallization kinetics of spray-dried lactose. *International Journal of Pharmaceutics*, **313**: 23-28.
7. Newman, A.W., Reutzel-Edens, S.M., and Zografi, G. 2008. Characterization of the "hygroscopic" properties of active pharmaceutical ingredients. *Journal of Pharmaceutical Sciences*, **97**: 1047-1059.

8. Ahlneck, C. and Zografi, G. 1990. The molecular basis of moisture effects on the physical and chemical stability of drugs in the solid state. *International Journal of Pharmaceutics*, **62**: 87-95.
9. Kontny, M.J. and Zografi, G. 1995. Water-solid interactions in pharmaceutical systems. *Drugs and the Pharmaceutical Sciences*, **70**: 387-418.
10. Faqih, A.M.N., Mehrotra, A., Hammond, S.V., and Muzzio, F.J. 2007. Effect of moisture and magnesium stearate concentration on flow properties of cohesive granular materials. *International Journal of Pharmaceutics*, **336**: 338-345.
11. Sun, C.C. 2008. Mechanism of moisture induced variations in true density and compaction properties of microcrystalline cellulose. *International Journal of Pharmaceutics*, **346**: 93-101.
12. Padmadisastra, Y., Kennedy, R.A., and Stewart, P.J. 1994. Solid bridge formation in sulfonamide-Emdex interactive systems. *International Journal of Pharmaceutics*, **112**: 55-63.
13. Cleaver, J.A.S., Karatzas, G., Louis, S., and Hayati, I. 2004. Moisture-induced caking of boric acid powder. *Powder Technology*, **146**: 93-101.
14. Rohrs, B.R., Thamann, T.J., Gao, P., Stelzer, D.J., Bergren, M.S., and Chao, R.S. 1999. Tablet dissolution affected by a moisture mediated solid-state interaction between drug and disintegrant. *Pharmaceutical Research*, **16**: 1850-1856.
15. Fassihi, A.R. and Persicaner, P.H.R. 1987. Solid state interaction of bromazepam with poly(vinylpyrrolidone) in the presence of moisture. *International Journal of Pharmaceutics*, **37**: 167-170.
16. Koizumi, N.A., T.; Kouji, M.; Itai, S. 1997. Effect of water content and temperature on the stability of lornoxicam tablets. *Drug Stability*, **1**: 202-208.
17. Zografi, G. 1991. Report of the advisory panel on moisture specifications. *Pharmacopeial Forum*, **1**: 1459-1474.
18. Zografi, G. 1988. States of water associated with solids. *Drug Development and Industrial Pharmacy*, **14**: 1905-1926.
19. Kontny, M.J. and Zografi, G. 1995. Sorption of water by solids. *Drugs and the Pharmaceutical Sciences*, **70**: 387-418.
20. El-Sabaawi, M. and Pei, D.C.T. 1977. Moisture isotherms of hygroscopic porous solids. *Industrial & Engineering Chemistry Fundamentals*, **16**: 321-326.
21. Krzyzaniak, J.F., Williams, G.R., and Ni, N. 2007. Identification of phase boundaries in anhydrate/hydrate systems. *Journal of Pharmaceutical Sciences*, **96**: 1270-1281.
22. Salameh, A.K. and Taylor, L.S. 2005. Deliquescence in Binary Mixtures. *Pharmaceutical Research*, **22**: 318-324.
23. Petit, S. and Coquerel, G., *The amorphous state*, in *Polymorphism in the Pharmaceutical Industry*, R. Hilfiker, Editor. 2006, Wiley-VCH: Weinheim, Germany. pp. 259-285.
24. Hancock, B.C. and Zografi, a.G. 1996. Effects of solid-state processing on water vapor sorption by aspirin. *Journal of Pharmaceutical Sciences*, **85**: 246-8.
25. Balbach, S. and Korn, C. 2004. Pharmaceutical evaluation of early development candidates "the 100 mg-approach". *International Journal of Pharmaceutics*, **275**: 1-12.

26. Callahan, J.C., Cleary, G.W., Elefant, M., Kaplan, G., Kensler, T., and Nash, R.A. 1982. Equilibrium moisture content of pharmaceutical excipients. *Drug Development and Industrial Pharmacy*, **8**: 355-69.
27. Thiel, P.A. and Madey, T.F. 1987. The interaction of water with solid surfaces: fundamental aspects. *Surface Science Reports*, **7**: 211-385.
28. Sheth, A.R., Brennessel, W.W., Young, V.G., Jr., Muller, F.X., and Grant, D.J.W. 2004. Solid-state properties of warfarin sodium 2-propanol solvate. *Journal of Pharmaceutical Sciences*, **93**: 2669-2680.
29. Ticehurst, M.D., Storey, R.A., and Watt, C. 2002. Application of slurry bridging experiments at controlled water activities to predict the solid-state conversion between anhydrous and hydrated forms using theophylline as a model drug. *International Journal of Pharmaceutics*, **247**: 1-10.
30. Muangsin, N., Prajaubsook, M., Chaichit, N., Siritaedmukul, K., and Hannongbua, S. 2002. Crystal structure of a unique sodium distorted linkage in diclofenac sodium pentahydrate. *Analytical Sciences*, **18**: 967-968.
31. Furuseth, S., Karlsen, J., Mostad, A., Roemming, C., Salmen, R., and Toennesen, H.H. 1990. N4-(7-Chloro-4-quinolinyl)-N1,N1-diethyl-1,4-pentanediamine. An X-ray diffraction study of chloroquine diphosphate hydrate. *Acta Chemica Scandinavica*, **44**: 741-745.
32. Preston, H.S. and Stewart, J.M. 1970. Crystal structure of the antimalarial chloroquine diphosphate monohydrate. *Journal of the Chemical Society [Section] D: Chemical Communications*, 1142-3.
33. Okabe, N., Fukuda, H., and Nakamura, T. 1993. Structure of hydralazine hydrochloride. *Acta Crystallographica, Section C: Crystal Structure Communications*, **C49**: 1844-5.
34. Griesser, U.J., *The importance of solvates*, in *Polymorphism in the Pharmaceutical Industry*, R. Hilfiker, Editor. 2006, Wiley-VCH: Weinheim, Germany. pp. 211-233.
35. Van Campen, L., Amidon, G.L., and Zografi, G. 1983. Moisture sorption kinetics for water-soluble substances. II: Experimental verification of heat transport control. *Journal of Pharmaceutical Sciences*, **72**: 1388-1393.
36. Van Campen, L., Amidon, G.L., and Zografi, G. 1983. Moisture sorption kinetics for water-soluble substances. I: Theoretical considerations of heat transport control. *Journal of Pharmaceutical Sciences*, **72**: 1381-1388.
37. Carstensen, J.T., *Physical characteristics of solids.*, in *Drug Stability: Principles and Practices*, J.T.R. Carstensen, C.T., Editor. 2000, Marcel Dekker: New York, NY. pp. 209-236.
38. Weast, R.C. and Selby, S.M., *Handbook of Chemistry and Physics*. 47th ed. 1966 The Chemical Rubber, Cleveland, OH.
39. Carvajal, M.T. and Staniforth, J.N. 2006. Interactions of water with the surfaces of crystal polymorphs. *International Journal of Pharmaceutics*, **307**: 216-224.
40. Grzesiak, A.L., Lang, M., Kim, K., and Matzger, A.J. 2003. Comparison of the four anhydrous polymorphs of carbamazepine and the crystal structure of form I. *Journal of Pharmaceutical Sciences*, **92**: 2260-2271.

41. Connolly, M.L. 1985. Computation of molecular volume. *Journal of the American Chemical Society*, **107**: 1118-24.
42. McMahon, L.E.T., P.; Williams, A.; York, P. 1996. Characterization of dihydrates prepared from carbamazepine polymorphs. *Journal of Pharmaceutical Sciences*, 1064-1069.
43. Krahn, F.U. and Mielck, J.B. 1987. Relations between several polymorphic forms and the dihydrate of carbamazepine. *Pharmaceutica Acta Helvetiae*, **62**: 247-254.
44. Murphy, D., Rodriguez-Cintron, F., Langevin, B., Kelly, R.C., and Rodriguez-Hornedo, N. 2002. Solution-mediated phase transformation of anhydrous to dihydrate carbamazepine and the effect of lattice disorder. *International Journal of Pharmaceutics*, **246**: 121-134.
45. Rodriguez-Hornedo, N. and Murphy, D. 2004. Surfactant-facilitated crystallization of dihydrate carbamazepine during dissolution of anhydrous polymorph. *Journal of Pharmaceutical Sciences*, **93**: 449-460.
46. Mitchell, A.G. 1984. The preparation and characterization of ferrous sulfate hydrates. *Journal of Pharmacy and Pharmacology*, **36**: 506-10.
47. Hough, E., Neidle, S., Rogers, D., and Troughton, P.G.H. 1973. Crystal structure of a-D-glucose monohydrate. *Acta Crystallographica, Section B: Structural Crystallography and Crystal Chemistry*, **29**: 365-7.
48. Roelofsen, G. and Kanters, J.A. 1972. Citric acid monohydrate, C6H8O7.H2O. *Crystal Structure Communications*, **1**: 23-6.
49. Al-Badr, A.A. and Muhtadi, F.J., *Atropine*, in *Analytical Profiles of Drug Substances*, K. Florey, Editor. 1985, Academic Press: New York, NY. pp. 325-390.
50. Ali, S.L., *Benzocaine*, in *Analytical Profiles of Drug Substances*, K. Florey, Editor. 1983, Academic Press: New York, NY. pp. 73-104.
51. Edwards, H.G.M., Lawson, E., de Matas, M., Shields, L., and York, P. 1997. Metamorphosis of caffeine hydrate and anhydrous caffeine. *Journal of the Chemical Society, Perkin Transactions 2*, **2**: 1985-1990.
52. Szulczewski, D. and Eng, F., *Chloramphenicol*, in *Analytical Profiles of Drug Substances*, K. Florey, Editor. 1975, Academic Press: New York, NY. pp. 47-90.
53. Eckhart, C.G. and McCorkle, T., *Chlorpheniramine maleate*, in *Analytical Profiles of Drug Substances*, K. Florey, Editor. 1978, Academic Press: New York, NY. pp. 43-80.
54. *The United States Pharmacopeia*. 2005, United States Pharmacopieal Convention: Rockville, MD.
55. Janicki, C.A. and Gilpin, R.K., *Droperidol*, in *Analytical Profiles of Drug Substances*, K. Florey, Editor. 1978, Academic Press: New York, NY. pp. 171-192.
56. Ali, S.L., *Ephedrine hydrochloride*, in *Analytical Profiles of Drug Substances*, K. Florey, Editor. 1986, Academic Press: New York, NY. pp. 233-282.
57. Orzech, C.E., Nash, N.G., and Daley, R.D., *Hydroflumethiazide*, in *Analytical Profiles of Drug Substances*, K. Florey, Editor. 1978, Academic Press: New York, NY. pp. 297-318.

58. Brewer, G.A., *Isoniazid*, in *Analytical Profiles of Drug Substances*, K. Florey, Editor. 1977, Academic Press: New York, NY. pp. 183-258.
59. Al-Badr, A.A. and Tariq, M., *Mebendazole*, in *Analytical Profiles of Drug Substances*, K. Florey, Editor. 1987, Academic Press: Orlando, FL. pp. 291-326.
60. Grubb, P.E., *Nalidixic Acid*, in *Analytical Profiles of Drug Substances*, K. Florey, Editor. 1979, Academic Press: New York, NY. pp. 371-398.
61. Hale, J.L., *Nortriptyline hydrochloride*, in *Analytical Profiles of Drug Substances*, K. Florey, Editor. 1972, Academic Press: New York, NY. pp. 233-248.
62. Hifnawy, M.S. and Muhtadi, F.J., *Analytical profile of papaverine hydrochloride*, in *Analytical Profiles of Drug Substances*, K. Florey, Editor. 1988, Academic Press: New York, NY. pp. 367-448.
63. Blessel, K.W., Rudy, B.C., and Senkowski, B.Z., *Phenazopyridine hydrochloride*, in *Analytical Profiles of Drug Substances*, K. Florey, Editor. 1974, Academic Press: New York, NY. pp. 465-482.
64. Daley, R.D., *Primidone*, in *Analytical Profiles of Drug Substances*, K. Florey, Editor. 1973, Academic Press: New York, NY. pp. 409-438.
65. Felder, E. and Pitre, D., *Pyrazinamide*, in *Analytical Profiles of Drug Substances*, K. Florey, Editor. 1983, Academic Press: New York, NY. pp. 433-462.
66. Loutfy, M.A. and Aboul-Enein, H.Y., *Pyrimethamine*, in *Analytical Profiles of Drug Substances*, K. Florey, Editor. 1983, Academic Press: New York, NY. pp. 463-482.
67. Gu, C.-H. and Grant, D.J.W. 2001. Estimating the relative stability of polymorphs and hydrates from heats of solution and solubility data. *Journal of Pharmaceutical Sciences*, **90**: 1277-1287.
68. Stober, H. and DeWitte, W., *Sulfadiazine*, in *Analytical Profiles of Drug Substances*, K. Florey, Editor. 1982, Academic Press: New York, NY. pp. 523-554.
69. Rudy, B.C. and Senkowski, B.Z., *Sulfamethoxazole*, in *Analytical Profiles of Drug Substances*, K. Florey, Editor. 1973, Academic Press: New York, NY. pp. 467-486.
70. Rudy, B.C. and Senkowski, B.Z., *Sulfisoxazole*, in *Analytical Profiles of Drug Substances*, K. Florey, Editor. 1973, Academic Press: New York, NY. pp. 487-506.
71. Hong, D.D., *Chloroquine phosphate*, in *Analytical Profiles of Drug Substances*, K. Florey, Editor. 1976, Academic Press: New York, NY. pp. 61-86.
72. Adeyeye, C.M. and Li, P.-K., *Diclofenac sodium*, in *Analytical Profiles of Drug Substances*, K. Florey, Editor. 1990, Academic Press: San Diego, CA. pp. 123-144.
73. Orzech, C.E., Nash, N.G., and Daley, R.D., *Hydralazine hydrochloride*, in *Analytical Profiles of Drug Substances*, K. Florey, Editor. 1979, Academic Press: New York, NY. pp. 283-314.
74. Blaton, N.M., Peeters, O.M., and De Ranter, C.J. 1980. 1-{1-[4-(4-Fluorophenyl)-4-oxobutyl]-1,2,3,6-tetrahydro-4-pyridyl}-1,3-dihydro-2H-benzimidazol-2-one dihydrate (dehydrobenzperidol). *Acta Crystallographica, Section B: Structural Crystallography and Crystal Chemistry*, **B36**: 2828-30.

75. Rodier, N., Chauvet, A., and Masse, J. 1978. Crystal structure of succinylsulfathiazole monohydrate. *Acta Crystallographica, Section B: Structural Crystallography and Crystal Chemistry*, **B34**: 218-21.
76. Alleaume, M. and Decap, J. 1968. Three-dimensional refinement of sulfanilamide monohydrate structure. *Acta Crystallographica, Section B: Structural Crystallography and Crystal Chemistry*, **24**: 214-22.
77. Holcombe, I.J. and Fusari, S.A., *Diphenhydramine hydrochloride*, in *Analytical Profiles of Drug Substances*, K. Florey, Editor. 1974, Academic Press: New York, NY. pp. 173-232.
78. Nakano, K. 1968. Kinetic studies on the decomposition of homochlorocyclizine in aqueous solution. *Yakugaku Zasshi*, **88**: 259-65.
79. Tsau, J. and DeAngelis, N., *Hydroxyzine dihydrochloride*, in *Analytical Profiles of Drug Substances*, K. Florey, Editor. 1978, Academic Press: New York, NY. pp. 319-342.
80. Al-Badr, A.A. and Tariq, M., *Neostigmine*, in *Analytical Profiles of Drug Substances*, K. Florey, Editor. 1987, Academic Press: Orlando, FL. pp. 403-444.
81. Chang, Z.L., *Sodium valproate and valproic acid*, in *Analytical Profiles of Drug Substances*, K. Florey, Editor. 1979, Academic Press: New York, NY. pp. 529-553.
82. Florey, K., *Triflupromazine hydrochloride*, in *Analytical Profiles of Drug Substances*, K. Florey, Editor. 1973, Academic Press: New York, NY. pp. 523-550.
83. Florey, K., *Fluphenazine hydrochloride*, in *Analytical Profiles of Drug Substances*, K. Florey, Editor. 1973, Academic Press: New York, NY. pp. 263-295.
84. Post, A., Warren, R.J., and Zarembo, J.E., *Trifluoperazine hydrochloride*, in *Analytical Profiles of Drug Substances*, K. Florey, Editor. 1980, Academic Press: New York, NY. pp. 543-582.
85. Henderson, M.A. 2002. The interaction of water with solid surfaces: fundamental aspects revisited. *Surface Science Reports*, **46**: 1-308.

Chapter 3

1. Lohani, S. and Grant, D.J.W., *Thermodynamics of polymorphs*, in *Polymorphism in the Pharmaceutical Industry*, R. Hilfiker, Editor. 2006, Wiley-VCH: Weinheim, Germany. pp. 21-42.
2. Griesser, U.J., Jetti, R.K.R., Haddow, M.F., Brehmer, T., Apperley, D.C., King, A., and Harris, R.K. 2008. Conformational polymorphism in oxybuprocaine hydrochloride. *Crystal Growth & Design*, **8**: 44-56.
3. Phadnis, N.V. and Suryanarayanan, R. 1997. Polymorphism in anhydrous theophylline--implications on the dissolution rate of theophylline tablets. *Journal of Pharmaceutical Sciences*, **86**: 1256-63.
4. Zhang, G.G.Z., Gu, C., Zell, M.T., Burkhardt, R.T., Munson, E.J., and Grant, D.J.W. 2002. Crystallization and transitions of sulfamerazine polymorphs. *Journal of Pharmaceutical Sciences*, **91**: 1089-1100.

5. Boldyreva, E.V., Drebushchak, V.A., Drebushchak, T.N., Paukov, I.E., Kovalevskaya, Y.A., and Shutova, E.S. 2003. Polymorphism of glycine. Thermodynamic aspects. Part I. Relative stability of the polymorphs. *Journal of Thermal Analysis and Calorimetry*, **73**: 409-418.
6. Bauer, J., Spanton, S., Henry, R., Quick, J., Dziki, W., Porter, W., and Morris, J. 2001. Ritonavir: an extraordinary example of conformational polymorphism. *Pharmaceutical Research*, **18**: 859-66.
7. Gu, C.H., Young, V., Jr., and Grant, D.J. 2001. Polymorph screening: influence of solvents on the rate of solvent-mediated polymorphic transformation. *Journal of Pharmaceutical Sciences*, **90**: 1878-90.
8. Yang, X., Lu, J., Wang, X.-J., and Ching, C.-B. 2008. Effect of sodium chloride on the nucleation and polymorphic transformation of glycine. *Journal of Crystal Growth*, **310**: 604-611.
9. Matsumoto, T., Ichikawa, J., Kaneniwa, N., and Otsuka, M. 1988. Effect of environmental temperature on the polymorphic transformation of phenylbutazone during grinding. *Chemical & Pharmaceutical Bulletin*, **36**: 1074-85.
10. Rankell, A.S., *Influence of compressional force on solid-state crystal conversion of succinylsulfathiazole*. Ph.D dissertation. 1969 University of Wisconsin, WI.
11. Ebian, A.R., Moustafa, M.A., Khalil, S.A., and Motawi, M.M. 1973. Effect of additives on the kinetics of interconversion of sulphamethoxydiazine crystal forms. *Journal of Pharmacy and Pharmacology*, **25**: 13-20.
12. Moustafa, M.A., Khalil, S.A., Ebian, A.R., and Motawi, M.M. 1972. Kinetics of interconversion of sulphamethoxydiazine crystal forms. *The Journal of Pharmacy and Pharmacology*, **24**: 921-6.
13. Paul, I.C. and Curtin, D.Y. 1973. Thermally induced organic reactions in the solid state. *Accounts of Chemical Research*, **6**: 217-25.
14. Beckham, G.T., Peters, B., Starbuck, C., Variankaval, N., and Trout, B.L. 2007. Surface-mediated nucleation in the solid-State polymorph transformation of terephthalic acid. *Journal of the American Chemical Society*, **129**: 4714-4723.
15. McMillan, P.F., Shebanova, O., Daisenberger, D., Cabrera, R.Q., Bailey, E., Hector, A., Lees, V., Machon, D., Sella, A., and Wilson, M. 2007. Metastable phase transitions and structural transformations in solid-state materials at high pressure. *Phase Transitions*, **80**: 1003-1032.
16. Klotz, S., Straessle, T., Nelmes, R.J., Loveday, J.S., Hamel, G., Rousse, G., Canny, B., Chervin, J.C., and Saitta, A.M. 2005. Nature of the polymorphic transition in ice under pressure. *Physical Review Letters*, **94**: 1-4.
17. Linol, J. and Coquerel, G. 2007. Influence of high energy milling on the kinetics of the polymorphic transition from the monoclinic form to the orthorhombic form of (+-)5-methyl-5-(4'-methylphenyl)hydantoin. *Journal of Thermal Analysis and Calorimetry*, **90**: 367-370.
18. Boldyrev, V.V. 2006. Mechanochemistry and mechanical activation of solids. *Russian Chemical Reviews*, **75**: 177-189.
19. Kuznetsov, P.N., Kuznetsova, L.I., Zhyzhaev, A.M., Kovalchuk, V.I., Sannikov, A.L., and Boldyrev, V.V. 2006. Investigation of mechanically stimulated solid

phase polymorphic transition of zirconia. *Applied Catalysis, A: General*, **298**: 254-260.
20. Kawakami, K. 2007. Reversibility of enantiotropically related polymorphic transformations from a practical viewpoint: thermal analysis of kinetically reversible/irreversible polymorphic transformations. *Journal of Pharmaceutical Sciences*, **96**: 982-989.
21. Byrn, S.R., Pfeffer, R.R., and Stowell, J.G., *Solid-State Chemistry of Drugs*, ed. 2nd. 1999 SSCI, West Lafayette, Indiana.
22. Okumura, T., Ishida, M., Takayama, K., and Otsuka, M. 2006. Polymorphic transformation of indomethacin under high pressures. *Journal of Pharmaceutical Sciences*, **95**: 689-700.
23. Boldyreva, E. 2007. High-pressure polymorphs of molecularsolids: when are they formed, and when are they not? Some examples of the role of kinetic control. *Crystal Growth & Design*, **7**: 1662-1668.
24. Senna, M. 1985. Problems on the mechanically induced polymorphic transformation. *Crystal Research and Technology*, **20**: 209-17.
25. Salameh, A.K. and Taylor, L.S. 2006. Role of deliquescence lowering in enhancing chemical reactivity in physical mixtures. *Journal of Physical Chemistry B*, **110**: 10190-10196.
26. Schmitt, E.A., Law, D., and Zhang, G.G. 1999. Nucleation and crystallization kinetics of hydrated amorphous lactose above the glass transition temperature. *Journal of Pharmaceutical Sciences*, **88**: 291-6.
27. Saltmarch, M. and Labuza, T.P. 1980. Influence of relative humidity on the physicochemical state of lactose in spray-dried sweet whey powders. *Journal of Food Science*, **45**: 1231-1236.
28. Chen, L., *Solid State Behavior of Pharmaceutical Hydrates*. Ph.D dissertation. 1999 University of Minnesota, Minneapolis.
29. Matsuo, K. and Matsuoka, M. 2007. Solid-State Polymorphic Transition of Theophylline Anhydrate and Humidity Effect. *Crystal Growth & Design*, **7**: 411-415.
30. Yoshinari, T., Forbes, R.T., York, P., and Kawashima, Y. 2002. Moisture induced polymorphic transition of mannitol and its morphological transformation. *International Journal of Pharmaceutics*, **247**: 69-77.
31. Matsuo, K. and Matsuoka, M. 2007. Kinetics of solid state polymorphic transition of caffeine. *Journal of Chemical Engineering of Japan*, **40**: 468-472.
32. Morris, K.R., Griesser, U.J., Eckhardt, C.J., and Stowell, J.G. 2001. Theoretical approaches to physical transformations of active pharmaceutical ingredients during manufacturing processes. *Advanced Drug Delivery Reviews*, **48**: 91-114.
33. *Patient Package Insert: Homoclomin Tablets (10mg)*. 2007, Eisai Co., Ltd.: Tokyo, Japan.
34. Hammersley, A.P., Svensson, S.O., Hanfland, M., Fitch, A.N., and Häusermann, D. 1996. Two-dimensional detector software: from real detector to idealised image or two-theta scan. *High Pressure Research*, 235-248.

35. Griesser, U.J., *The importance of solvates*, in *Polymorphism in the Pharmaceutical Industry*, R. Hilfiker, Editor. 2006, Wiley-VCH: Weinheim, Germany. pp. 211-233.
36. Tang, X.C., Pikal, M.J., and Taylor, L.S. 2002. A spectroscopic investigation of hydrogen bond patterns in crystalline and amorphous phases in dihydropyridine calcium channel blockers. *Pharmaceutical Research*, **19**: 477-483.
37. Volkmann, H., *Handbook of Infrared Spectroscopy*. 1972 Verlag Chemie, Weinheim, Germany.
38. Post, A., Warren, R.J., and Zarembo, J.E., *Trifluoperazine hydrochloride*, in *Analytical Profiles of Drug Substances*, K. Florey, Editor. 1980, Academic Press: New York, NY. pp. 543-582.
39. Burger, A. and Ramberger, R. 1979. On the polymorphism of pharmaceuticals and other molecular crystals. II. Applicability of thermodynamic rules. *Mikrochimica Acta*, **2**: 273-316.
40. Kitaigorodskii, A.I., *Organic Chemical Crystallography*. 1961 Consultants Bureau, New York, NY.
41. Stephenson, G.A. and Liang, C. 2006. Structural determination of the stable and meta-stable forms of atomoxetine HCl using single crystal and powder X-ray diffraction methods. *Journal of Pharmaceutical Sciences*, **95**: 1677-1683.
42. Jerry Workman, J. and Weyer, L., *Practical Guide to Interpretive Near-Infrared Spectroscopy*. Angewandte Chemie, International Edition. 2008 CRC Press, Boca Raton, FL.
43. Fornes, V. and Chaussidon, J. 1978. An interpretation of the evolution with temperature of the v2 + v3 combination band in water. *Journal of Chemical Physics*, **68**: 4667-71.
44. Nieuwmeyer, F.J.S., Damen, M., Gerich, A., Rusmini, F., Voort Maarschalk, K., and Vromans, H. 2007. Granule characterization during fluid bed drying by development of a near infrared method to determine water content and median granule size. *Pharmaceutical Research*, **24**: 1854-1861.
45. Zhou, G.X., Ge, Z., Dorwart, J., Izzo, B., Kukura, J., Bicker, G., and Wyvratt, J. 2003. Determination and differentiation of surface and bound water in drug substances by near infrared spectroscopy. *Journal of Pharmaceutical Sciences*, **92**: 1058-1065.
46. Derbyshire, H.M., Feldman, Y., Bland, C.R., Broadhead, J., and Smith, G. 2002. A study of the molecular properties of water in hydrated mannitol. *Journal of Pharmaceutical Sciences*, **91**: 1080-1088.
47. Giangiacomo, R. 2006. Study of water-sugar interactions at increasing sugar concentration by NIR spectroscopy. *Food Chemistry*, **96**: 371-379.
48. Cao, W., Mao, C., Chen, W., Lin, H., Krishnan, S., and Cauchon, N. 2006. Differentiation and quantitative determination of surface and hydrate water in lyophilized mannitol using NIR spectroscopy. *Journal of Pharmaceutical Sciences*, **95**: 2077-2086.
49. Grant, A., Davies, A.M.C., and Bilverstone, T. 1989. Simultaneous determination of sodium hydroxide, sodium carbonate and sodium chloride concentrations in

aqueous solutions by near-infrared spectrometry. *Analyst (Cambridge, United Kingdom)*, **114**: 819-22.
50. Hirschfeld, T. 1985. Salinity determination using NIRA. *Applied Spectroscopy*, **39**: 740-1.

Chapter 4

1. Ewing, G.E. 2005. H_2O on NaCl: from single molecule, to clusters, to monolayer, to thin films, to deliquescence. *Structure and Bonding (Berlin, Germany)*, **116**: 1-25.
2. Ghosal, S., Verdaguer, A., Hemminger, J.C., and Salmeron, M. 2005. In situ study of water-induced segregation of bromide in bromide-doped sodium chloride by scanning polarization force microscopy. *Journal of Physical Chemistry A*, **109**: 4744-4749.
3. Kendall, T.A. and Martin, S.T. 2007. Water-induced reconstruction that affects mobile ions on the surface of calcite. *Journal of Physical Chemistry A*, **111**: 505-514.
4. Usher, C.R., Baltrusaitis, J., and Grassian, V.H. 2007. Spatially resolved product formation in the reaction of formic acid with calcium carbonate: the role of step density and adsorbed water-assisted ion mobility. *Langmuir*, **23**: 7039-7045.
5. Xu, L., Lio, A., Hu, J., Ogletree, D.F., and Salmeron, M. 1998. Wetting and capillary phenomena of water on mica. *Journal of Physical Chemistry B*, **102**: 540-548.
6. Verdaguer, A., Sacha, G.M., Bluhm, H., and Salmeron, M. 2006. Molecular structure of water at interfaces: Wetting at the nanometer scale. *Chemical Reviews*, **106**: 1478-1510.
7. Dash, J.G. 1999. History of the search for continuous melting. *Reviews of Modern Physics*, **71**: 1737-1743.
8. Dash, J.G., Rempel, A.W., and Wettlaufer, J.S. 2006. The physics of pre-melted ice and its geophysical consequences. *Reviews of Modern Physics*, **78**: 695-741.
9. Ewing, G.E. 2006. Ambient thin film water on insulator surfaces. *Chemical Reviews*, **106**: 1511-1526.
10. Thiel, P.A. and Madey, T.F. 1987. The interaction of water with solid surfaces: fundamental aspects. *Surface Science Reports*, **7**: 211-385.
11. Rahaman, A., Grassian, V.H., and Margulis, C.J. 2008. Dynamics of water adsorption onto a calcite surface as a function of relative humidity. *Journal of Physical Chemistry C*, **112**: 2109-2115.
12. Vogt, R. and Finlayson-Pitts, B.J. 1994. A diffuse reflectance infrared Fourier transform spectroscopic study of the surface reaction of NaCl with gaseous NO_2 and HNO_3. *Journal of Physical Chemistry*, **98**: 3747-55.
13. Foster, M., D'Agostino, M., and Passno, D. 2005. Water on MgO(100). An infrared study at ambient temperatures. *Surface Science*, **590**: 31-41.

14. Foster, M.C. and Ewing, G.E. 2000. Adsorption of water on the NaCl(001) surface. II. An infrared study at ambient temperatures. *Journal of Chemical Physics*, **112**: 6817-6826.
15. Hucher, M., Oberlin, A., and Hocart, R. 1967. Adsorption of water vapor on the cleavage surfaces of some alkali metal halides. *Bulletin de la Societe Francaise de Mineralogie et de Cristallographie*, **90**: 320-32.
16. Dai, Q., Hu, J., and Salmeron, M. 1997. Adsorption of water on NaCl (100) surfaces: role of atomic steps. *Journal of Physical Chemistry B*, **101**: 1994-1998.
17. Kontny, M.J., Grandolfi, G.P., and Zografi, G. 1987. Water vapor sorption of water-soluble substances: studies of crystalline solids below their critical relative humidities. *Pharmaceutical Research*, **4**: 104-112.
18. Khankari, R.K. and Grant, D.J.W. 1995. Pharmaceutical hydrates. *Thermochimica Acta*, **248**: 61-79.
19. Phadnis, N.V. and Suryanarayanan, R. 1997. Polymorphism in anhydrous theophylline--implications on the dissolution rate of theophylline tablets. *Journal of Pharmaceutical Sciences*, **86**: 1256-63.
20. Herman, J., Visavarungroj, N., and Remon, J.P. 1989. Instability of drug release from anhydrous theophylline-microcrystalline cellulose formulations. *International Journal of Pharmaceutics*, **55**: 143-6.
21. Kahela, P., Aaltonen, R., Lewing, E., Anttila, M., and Kristoffersson, E. 1983. Pharmacokinetics and dissolution of two crystalline forms of carbamazepine. *International Journal of Pharmaceutics*, **14**: 103-12.
22. Matsuo, K. and Matsuoka, M. 2007. Solid-state polymorphic transition of theophylline anhydrate and humidity effect. *Crystal Growth & Design*, **7**: 411-415.
23. Amado Ana, M., Nolasco Mariela, M., and Ribeiro-Claro Paulo, J.A. 2007. Probing pseudopolymorphic transitions in pharmaceutical solids using Raman spectroscopy: Hydration and dehydration of theophylline. *Journal of Pharmaceutical Sciences*, **96**: 1366-79.
24. Rodriguez-Hornedo, N., Lechuga-Ballesteros, D., and Wu, H.J. 1992. Phase transition and heterogeneous/epitaxial nucleation of hydrated and anhydrous theophylline crystals. *International Journal of Pharmaceutics*, **85**: 149-162.
25. Rodriguez-Hornedo, N. and Murphy, D. 2004. Surfactant-facilitated crystallization of dihydrate carbamazepine during dissolution of anhydrous polymorph. *Journal of Pharmaceutical Sciences*, **93**: 449-460.
26. Maji, T.K., Uemura, K., Chang, H.-C., Matsuda, R., and Kitagawa, S. 2004. Expanding and shrinking porous modulation based on Pillared-layer coordination polymers showing selective guest adsorption. *Angewandte Chemie, International Edition*, **43**: 3269-3272.
27. Thallapally, P.K., Lloyd, G.O., Atwood, J.L., and Barbour, L.J. 2005. Diffusion of water in a nonporous hydrophobic crystal. *Angewandte Chemie, International Edition*, **44**: 3848-3851.
28. Connolly, M.L. 1985. Computation of molecular volume. *Journal of the American Chemical Society*, **107**: 1118-24.

29. Connolly, M.L. 1983. Solvent-accessible surfaces of proteins and nucleic acids. *Science (Washington, DC, United States)*, **221**: 709-13.
30. Binnig, G., Quate, C.F., and Gerber, C. 1986. Atomic force microscope. *Physical Review Letters*, **56**: 930-933.
31. Israelachvili, J.N. 1992. Adhesion forces between surfaces in liquids and condensable vapors. *Surface Science Reports*, **14**: 109-59.
32. Zhang, J., Ebbens, S., Chen, X., Jin, Z., Luk, S., Madden, C., Patel, N., and Roberts, C.J. 2006. Determination of the surface free energy of crystalline and amorphous lactose by atomic force microscopy adhesion measurement. *Pharmaceutical Research*, **23**: 401-407.
33. Davies, M., Brindley, A., Chen, X., Marlow, M., Doughty, S.W., Shrubb, I., and Roberts, C.J. 2005. Characterization of drug particle surface energetics and Young's modulus by atomic force microscopy and inverse gas chromatography. *Pharmaceutical Research*, **22**: 1158-1166.
34. Plassard, C., Lesniewska, E., Pochard, I., and Nonat, A. 2004. Investigation of the surface structure and elastic properties of calcium silicate hydrates at the nanoscale. *Ultramicroscopy*, **100**: 331-338.
35. Goles, F. 1961. The examination and calculation of thermodynamic data from experimental measurements. I. The numerical integration of the vapor-pressure curves of the system methanol-water. *Monatsh. Chem.*, **92**: 981-991.
36. Xu, L., Bluhm, H., and Salmeron, M. 1998. An AFM study of the tribological properties of NaCl(100) surfaces under moist air. *Surface Science*, **407**: 251-255.
37. Carpick, R.W. and Salmeron, M. 1997. Scratching the surface: fundamental investigations of tribology with atomic force microscopy. *Chemical Reviews (Washington, D. C.)*, **97**: 1163-1194.
38. Haugstad, G., Gladfelter, W.L., Weberg, E.B., Weberg, R.T., and Weatherill, T.D. 1994. Probing biopolymers with scanning force methods: adsorption, structure, properties, and transformation of gelatin on mica. *Langmuir*, **10**: 4295-306.
39. Butt, H.J. 1991. Measuring electrostatic, van der Waals, and hydration forces in electrolyte solutions with an atomic force microscope. *Biophysical Journal*, **60**: 1438-44.
40. Mate, C.M., Lorenz, M.R., and Novotny, V.J. 1989. Atomic force microscopy of polymeric liquid films. *Journal of Chemical Physics*, **90**: 7550-5.
41. Garcia, R. and Perez, R. 2002. Dynamic atomic force microscopy methods. *Surface Science Reports*, **47**: 197-301.
42. Cleveland, J.P., Anczykowski, B., Schmid, A.E., and Elings, V.B. 1998. Energy dissipation in tapping-mode atomic force microscopy. *Applied Physics Letters*, **72**: 2613-2615.
43. Zhu, H., Yuen, C., and Grant, D.J.W. 1996. Influence of water activity in organic solvent + water mixtures on the nature of the crystallizing drug phase. 1. Theophylline. *International Journal of Pharmaceutics*, **135**: 151-160.
44. Ticehurst, M.D., Storey, R.A., and Watt, C. 2002. Application of slurry bridging experiments at controlled water activities to predict the solid-state conversion between anhydrous and hydrated forms using theophylline as a model drug. *International Journal of Pharmaceutics*, **247**: 1-10.

45. Amado, A.M., Nolasco, M.M., and Ribeiro-Claro, P.J.A. 2007. Probing pseudopolymorphic transitions in pharmaceutical solids using Raman spectroscopy: hydration and dehydration of theophylline. *Journal of Pharmaceutical Sciences*, **96**: 1366-1379.
46. Otsuka, M., Kaneniwa, N., Kawakami, K., and Umezawa, O. 1990. Effect of surface characteristics of theophylline anhydrate powder on hygroscopic stability. *Journal of Pharmacy and Pharmacology*, **42**: 606-10.
47. Lehto, V.-P. and Laine, E. 2000. Simultaneous determination of the heat and the quantity of vapor sorption using a novel microcalorimetric method. *Pharmaceutical Research*, **17**: 701-706.
48. Vora, K.L., Buckton, G., and Clapham, D. 2004. The use of dynamic vapor sorption and near infra-red spectroscopy (DVS-NIR) to study the crystal transitions of theophylline and the report of a new solid-state transition. *European Journal of Pharmaceutical Sciences*, **22**: 97-105.
49. Otsuka, M., Kaneniwa, N., Otsuka, K., Kawakami, K., Umezawa, O., and Matsuda, Y. 1992. Effect of geometric factors on hydration kinetics of theophylline anhydrate tablets. *Journal of Pharmaceutical Sciences*, **81**: 1189-1193.
50. Heng, J.Y.Y., Thielmann, F., and Williams, D.R. 2006. The effects of milling on the surface properties of form I paracetamol crystals. *Pharmaceutical Research*, **23**: 1918-1927.
51. Ohta, M. and Buckton, G. 2004. Determination of the changes in surface energetics of cefditoren pivoxil as a consequence of processing induced disorder and equilibration to different relative humidities. *International Journal of Pharmaceutics*, **269**: 81-88.
52. Ebisuzaki, Y., Boyle, P.D., and Smith, J.A. 1997. Methylxanthines. I. Anhydrous theophylline. *Acta Crystallographica, Section C: Crystal Structure Communications*, **C53**: 777-779.
53. Allen, S., Connell, S.D.A., Chen, X., Davies, J., Davies, M.C., Dawkes, A.C., Roberts, C.J., Tendler, S.J.B., and Williams, P.M. 2001. Mapping the surface characteristics of polystyrene microtiter wells by a multimode scanning force microscopy approach. *Journal of Colloid and Interface Science*, **242**: 470-476.
54. Cappella, B. and Dietler, G. 1999. Force-distance curves by atomic force microscopy. *Surface Science Reports*, **34**: 1-104.
55. Israelachvili, J.N., *Intermolecular and Surface Forces*. 2 ed. 1991 Academic Press, San Diego, CA.
56. Frisbie, C.D., Rozsnyai, L.F., Noy, A., Wrighton, M.S., and Lieber, C.M. 1994. Functional group imaging by chemical force microscopy. *Science*, **265**: 2071-2074.
57. Green, J.-B.D., McDermott, M.T., Porter, M.D., and Siperko, L.M. 1995. Nanometer-scale mapping of chemically distinct domains at well-defined organic interfaces using frictional force microscopy. *Journal of Physical Chemistry*, **99**: 10965-10970.

58. Overney, R.M., Meyer, E., Frommer, J., Guentherodt, H.J., Fujihira, M., Takano, H., and Gotoh, Y. 1994. Force microscopy study of friction and elastic compliance of phase-separated organic thin films. *Langmuir*, **10**: 1281-1286.
59. Xiao, X., Hu, J., Charych, D.H., and Salmeron, M. 1996. Chain length dependence of the frictional properties of alkylsilane molecules self-assembled on mica studied by atomic force microscopy. *Langmuir*, **12**: 235-237.
60. Waizumi, K., Plomp, M., and van Enckevort, W. 2003. Atomic force microscopy studies on growing surfaces of bovine insulin crystals. *Colloids and Surfaces, B: Biointerfaces*, **30**: 73-86.
61. Kossel, W. 1934. The energy of surface processes. *Annalen der Physik (Berlin, Germany)*, **21**: 457-480.
62. Garcia, R., Martinez, R.V., and Martinez, J. 2006. Nanochemistry and scanning probe nanolithographies. *Chemical Society Reviews*, **35**: 29-38.
63. Amado, A.M., Nolasco Mariela, M., and Ribeiro-Claro Paulo, J.A. 2007. Probing pseudopolymorphic transitions in pharmaceutical solids using Raman spectroscopy: Hydration and dehydration of theophylline. *Journal of Pharmaceutical Sciences*, **96**: 1366-79.
64. Landman, U., Luedtke, W.D., Burnham, N.A., and Colton, R.J. 1990. Atomistic mechanisms and dynamics of adhesion, nanoindentation, and fracture. *Science (Washington, DC, United States)*, **248**: 454-461.
65. Dey, F.K., Cleaver, J.A.S., and Zhdan, P.A. 2000. Atomic force microscopy study of adsorbed moisture on lactose particles. *Advanced Powder Technology*, **11**: 401-413.
66. Forcada, M.L., Jakas, M.M., and Gras-Marti, A. 1991. On liquid-film thickness measurements with the atomic-force microscope. *Journal of Chemical Physics*, **95**: 706-708.
67. Kaneniwa, N., Yamaguchi, T., Watari, N., and Otsuka, M. 1984. Hygroscopicity of carbamazepine crystalline powders. *Yakugaku Zasshi*, **104**: 184-90.

Chapter 5

1. Newman, A.W., Reutzel-Edens, S.M., and Zografi, G. 2008. Characterization of the "hygroscopic" properties of active pharmaceutical ingredients. *Journal of Pharmaceutical Sciences*, **97**: 1047-1059.
2. Reutzel-Edens, S.M. and Newman, A.W., *Physical characterization of hygroscopicity in pharmaceutical solids*, in *Polymorphism in the Pharmaceutical Industry*, R. Hilfiker, Editor. 2006, Wiley-VCH: Weinheim, Germany. pp. 235-258.
3. Govindarajan, R. and Suryanarayanan, R., *Processing-induced phase transformations and their implications on pharmaceutical products quality*, in *Polymorphism in the Pharmaceutical Industry*, R. Hilfiker, Editor. 2006, Wiley-VCH: Weinheim, Germany. pp. 333-364.

4. Kontny, M.J., Grandolfi, G.P., and Zografi, G. 1987. Water vapor sorption of water-soluble substances: studies of crystalline solids below their critical relative humidities. *Pharmaceutical Research*, **4**: 104-112.
5. Giron, D., Goldbronn, C., Mutz, M., Pfeffer, S., Piechon, P., and Schwab, P. 2002. Solid state characterizations of pharmaceutical hydrates. *Journal of Thermal Analysis and Calorimetry*, **68**: 453-465.
6. Vippagunta, S.R., Brittain, H.G., and Grant, D.J.W. 2001. Crystalline solids. *Advanced Drug Delivery Reviews*, **48**: 3-26.
7. Lohani, S. and Grant, D.J.W., *Thermodynamics of polymorphs*, in *Polymorphism in the Pharmaceutical Industry*, R. Hilfiker, Editor. 2006, Wiley-VCH: Weinheim, Germany. pp. 21-42.
8. El-Sabaawi, M. and Pei, D.C.T. 1977. Moisture isotherms of hygroscopic porous solids. *Industrial & Engineering Chemistry Fundamentals*, **16**: 321-326.
9. Terakita, A. and Byrn, S.R. 2006. Structure and physical stability of hydrates and thermotropic mesophase of calcium benzoate. *Journal of Pharmaceutical Sciences*, **95**: 1162-1172.
10. Wunderlich, B. 1999. A classification of molecules, phases, and transitions as recognized by thermal analysis. *Thermochimica Acta*, **340**: 37-52.
11. Figueiredo Neto, A.M. and Salinas, S.R.A., *The Physics of Lyotropic Liquid Crystals: Phase Transitions and Structural Properties*. 2005 University Press, Oxford.
12. Suzuki, Y., Fukunaga, K., Baba, M., Taki, M., and Watanabe, S. 2005. Three-dimensional temperature measurement with micro-capsulated thermo-chromic liquid crystal for assessment of dielectric and insulation materials. *Annual Report - Conference on Electrical Insulation and Dielectric Phenomena*, 609-612.
13. Boyd, B.J., Khoo, S.-M., Whittaker, D.V., Davey, G., and Porter, C.J.H. 2007. A lipid-based liquid crystalline matrix that provides sustained release and enhanced oral bioavailability for a model poorly water soluble drug in rats. *International Journal of Pharmaceutics*, **340**: 52-60.
14. Farkas, E., Kiss, D., and Zelko, R. 2007. Study on the release of chlorhexidine base and salts from different liquid crystalline structures. *International Journal of Pharmaceutics*, **340**: 71-75.
15. Stevenson, C.L., Bennett, D.B., and Lechuga-Ballesteros, D. 2005. Pharmaceutical liquid crystals: The relevance of partially ordered systems. *Journal of Pharmaceutical Sciences*, **94**: 1861-1880.
16. Bunjes, H. and Rades, T. 2005. Thermotropic liquid crystalline drugs. *Journal of Pharmacy and Pharmacology*, **57**: 807-816.
17. Rades, T. and Mueller-Goymann, C.C. 1992. Structural investigations on the liquid crystalline phases of fenoprofen. *Pharmaceutical and Pharmacological Letters*, **2**: 131-4.
18. Rades, T. and Mueller-Goymann Christel, C. 1994. Melting behavior and thermotropic mesomorphism of fenoprofen salts. *European Journal of Pharmaceutics and Biopharmaceutics*, **40**: 277-82.
19. Atassi, F. and Byrn, S.R. 2006. General trends in the desolvation behavior of calcium salts. *Pharmaceutical Research*, **23**: 2405-2412.

20. Zhou, M., Nemade, P.R., Lu, X., Zeng, X., Hatakeyama, E.S., Noble, R.D., and Gin, D.L. 2007. New type of membrane material for wate desalination based on a cross-linked bicontinuous cubic lyotropic liquid crystal assembly. *Journal of the American Chemical Society*, **129**: 9574-9575.
21. Lechuga-Ballesteros, D., Abdul-Fattah, A., Stevenson, C.L., and Bennett, D.B. 2003. Properties and stability of a liquid crystal form of cyclosporine-the first reported naturally occurring peptide that exists as a thermotropic liquid crystal. *Journal of Pharmaceutical Sciences*, **92**: 1821-1831.
22. Goldsbury, C., Kistler, J., Aebi, U., Arvinte, T., and Cooper, G.J.S. 1999. Watching amyloid fibrils grow by time-lapse atomic force microscopy. *Journal of Molecular Biology*, **285**: 33-39.
23. Zeng, X., Liu, Y., and Imperor-Clerc, M. 2007. Hexagonal close packing of nonionic surfactant micelles in water. *Journal of Physical Chemistry B*, **111**: 5174-5179.
24. Kocherbitov, V. and Soederman, O. 2006. Hydration of dimethyldodecylamine-N-oxide: enthalpy and entropydriven processes. *Journal of Physical Chemistry B*, **110**: 13649-13655.
25. Milton, N. and Nail, S.L. 1996. The physical state of nafcillin sodium in frozen aqueous solutions and freeze-dried powders. *Pharmaceutical Development and Technology*, **1**: 269-277.
26. Cox, J.S.G., Woodard, G.D., and McCrone, W.C. 1971. Solid-state chemistry of cromolyn sodium (disodium cromoglycate). *Journal of Pharmaceutical Sciences*, **60**: 1458-65.
27. Vadas, E.B., Toma, P., and Zografi, G. 1991. Solid-state phase transitions initiated by water vapor sorption of crystalline L-660711, a leukotriene D4 receptor antagonist. *Pharmaceutical Research*, **8**: 148-55.
28. Umprayn, K. and Mendes, R.W. 1987. Hygroscopicity and moisture adsorption kinetics of pharmaceutical solids: a review. *Drug Development and Industrial Pharmacy*, **13**: 653-693.
29. McDowell, J.J.H. 1980. Trifluoperazine hydrochloride, a phenothiazine derivative. *Acta Crystallographica, Section B: Structural Crystallography and Crystal Chemistry*, **B36**: 2178-81.
30. Kocherbitov, V. and Alfredsson, V. 2007. Hydration of MCM-41 studied by sorption calorimetry. *Journal of Physical Chemistry C*, **111**: 12906-12913.
31. Caira, M.R., Bettinetti, G., and Sorrenti, M. 2002. Structural relationships, thermal properties, and physicochemical characterization of anhydrous and solvated crystalline forms of tetroxoprim. *Journal of Pharmaceutical Sciences*, **91**: 467-481.
32. Ghosh, S., Ojala, W.H., Gleason, W.B., and Grant, D.J.W. 1995. Relationships between crystal structures, thermal properties, and solvate stability of dialkylhydroxypyridones and their formic acid solvates. *Journal of Pharmaceutical Sciences*, **84**: 1392-9.
33. Marsh, K.N., *Recommended reference materials for the relization of physicochemical properties*. 1987 Oxford, Blckwell.

34. Hosokawa, T., Datta, S., Sheth, A.R., and Grant, D.J.W. 2004. Relationships between crystal structures and thermodynamic properties of phenylbutazone solvates. *CrystEngComm*, **6**: 243-249.
35. Kocherbitov, V. 2005. Driving forces of phase transitions in surfactant and lipid systems. *Journal of Physical Chemistry B*, **109**: 6430-6435.
36. Nieuwmeyer, F.J.S., Damen, M., Gerich, A., Rusmini, F., Voort Maarschalk, K., and Vromans, H. 2007. Granule characterization during fluid bed drying by development of a near infrared method to determine water content and median granule size. *Pharmaceutical Research*, **24**: 1854-1861.
37. Ward, H.W. and Sistare, F.E. 2007. On-line determination and control of the water content in a continuous conversion reactor using NIR spectroscopy. *Analytica Chimica Acta*, **595**: 319-322.
38. Iwamoto, R. and Matsuda, T. 2007. Infrared and near-infrared spectral evidence for water clustering in highly hydrated poly(methyl methacrylate). *Analytical Chemistry*, **79**: 3455-3461.
39. Ellis, J.W. and Bath, J. 1938. Modifications in the near infrared absorption spectra of protein and of light and heavy water molecules when water is bound to gelatin. *Journal of Chemical Physics*, **6**: 723-729.
40. Giangiacomo, R. 2006. Study of water-sugar interactions at increasing sugar concentration by NIR spectroscopy. *Food Chemistry*, **96**: 371-379.
41. Doglia, S.M., Martini, M., Spinolo, G., and Villan, A.M. 1992. The NIR absorption spectrum of water in iron(**II**) chloride tetrahydrate single crystals. *Journal of Physics and Chemistry of Solids*, **53**: 1237-43.
42. Lin, J. and Brown, C.W. 1992. Near-IR spectroscopic determination of sodium chloride in aqueous solution. *Applied Spectroscopy*, **46**: 1809-15.
43. Cheema, M.A., Siddiq, M., Barbosa, S., Castro, E., Egea, J.A., Antelo, L.T., Taboada, P., and Mosquera, V. 2007. Compressibility, isothermal titration calorimetry and dynamic light scattering analysis of the aggregation of the amphiphilic phenothiazine drug thioridazine hydrochloride in water/ethanol mixed solvent. *Chemical Physics*, **336**: 157-164.
44. Hashmi, S.A.N., Hu, X., Immoos, C.E., Lee, S.J., and Grinstaff, M.W. 2002. Synthesis and characterization of p-stacked phenothiazine-labeled oligodeoxynucleotides. *Organic Letters*, **4**: 4571-4574.
45. Florence, A.T. and Parfitt, R.T. 1971. Micelle formation by some phenothiazine derivatives. **II**. Nuclear magnetic resonance studies in deuterium oxide. *Journal of Physical Chemistry*, **75**: 3554-60.
46. Roseboom, H. and Perrin, J.H. 1977. Mechanism for phenothiazine oxidation. *Journal of Pharmaceutical Sciences*, **66**: 1395-8.

Chapter 6

1. Zhou, D., Zhang, G.G.Z., Law, D., Grant, D.J.W., and Schmitt, E.A. 2002. Physical stability of amorphous pharmaceuticals: importance of configurational thermodynamic quantities and molecular mobility. *Journal of Pharmaceutical Sciences*, **91**: 1863-1872.

2. Petit, S. and Coquerel, G., *The amorphous state*, in *Polymorphism in the Pharmaceutical Industry*, R. Hilfiker, Editor. 2006, Wiley-VCH: Weinheim, Germany. pp. 259-285.
3. Yu, L. 2001. Amorphous pharmaceutical solids: preparation, characterization and stabilization. *Advanced Drug Delivery Reviews*, **48**: 27-42.
4. Hilden, L.R. and Morris, K.R. 2004. Physics of amorphous solids. *Journal of Pharmaceutical Sciences*, **93**: 3-12.
5. Chono, S., Takeda, E., Seki, T., and Morimoto, K. 2008. Enhancement of the dissolution rate and gastrointestinal absorption of pranlukast as a model poorly water-soluble drug by grinding with gelatin. *International Journal of Pharmaceutics*, **347**: 71-78.
6. Shamblin, S.L., Hancock, B.C., and Pikal, M.J. 2006. Coupling between chemical reactivity and structural relaxation in pharmaceutical glasses. *Pharmaceutical Research*, **23**: 2254-2268.
7. Guo, Y., Byrn, S.R., and Zografi, G. 2000. Physical characteristics and chemical degradation of amorphous quinapril hydrochloride. *Journal of Pharmaceutical Sciences*, **89**: 128-143.
8. Aso, Y., Yoshioka, S., and Kojima, S. 2000. Relationship between the crystallization rates of amorphous nifedipine, phenobarbital, and flopropione, and their molecular mobility as measured by their enthalpy relaxation and ^{1}H NMR relaxation times. *Journal of Pharmaceutical Sciences*, **89**: 408-416.
9. Hancock, B.C. and Zografi, a.G. 1996. Effects of solid-state processing on water vapor sorption by aspirin. *Journal of Pharmaceutical Sciences*, **85**: 246-8.
10. Faqih, A.M.N., Mehrotra, A., Hammond, S.V., and Muzzio, F.J. 2007. Effect of moisture and magnesium stearate concentration on flow properties of cohesive granular materials. *International Journal of Pharmaceutics*, **336**: 338-345.
11. Burnett, D.J., Thielmann, F., Sokoloski, T., and Brum, J. 2006. Investigating the moisture-induced crystallization kinetics of spray-dried lactose. *International Journal of Pharmaceutics*, **313**: 23-28.
12. Sun, C.C. 2008. Mechanism of moisture induced variations in true density and compaction properties of microcrystalline cellulose. *International Journal of Pharmaceutics*, **346**: 93-101.
13. Stubberud, L., Arwidsson, H.G., Larsson, A., Graffner, C. 1996. Water solid interactions II. Effect of moisture sorption and glass transition temperature on compactibility of microcrystalline cellulose alone or in binary mixtures with polyvinyl pyrrolidone. *International Journal of Pharmaceutics*, **134**: 79-88.
14. Surana, R., Pyne, A., and Suryanarayanan, R. 2004. Effect of preparation method on physical properties of amorphous trehalose. *Pharmaceutical Research*, **21**: 1167-1176.
15. Graeser, K.A., Strachan, C.J., Patterson, J.E., Gordon, K.C., and Rades, T. 2008. Physicochemical properties and stability of two differently prepared amorphous forms of simvastatin. *Crystal Growth & Design*, **8**: 128-135.
16. Tsukushi, I., Yamamuro, O., and Suga, H. 1994. Heat capacities and glass transitions of ground amorphous solid and liquid-quenched glass of tri-O-methyl-b-cyclodextrin. *Journal of Non-Crystalline Solids*, **175**: 187-94.

17. Hancock, B.C., Shalaev, E.Y., and Shamblin, S.L. 2002. Polyamorphism: A pharmaceutical science perspective. *Journal of Pharmacy and Pharmacology*, **54**: 1151-1152.
18. Greaves, G.N., Meneau, F., Kargl, F., Ward, D., Holliman, P., and Albergamo, F. 2007. Zeolite collapse and polyamorphism. *Journal of Physics: Condensed Matter*, **19**: 415102/1-415102/17.
19. Demirjian, B.G., Dosseh, G., Chauty, A., Ferrer, M.-L., Morineau, D., Lawrence, C., Takeda, K., Kivelson, D., and Brown, S. 2001. Metastable solid phase at the crystalline-amorphous border: the glacial phase of triphenyl phosphite. *Journal of Physical Chemistry B*, **105**: 2107-2116.
20. Hedoux, A., Guinet, Y., Derollez, P., Hernandez, O., Lefort, R., and Descamps, M. 2004. Description and origin of the polyamorphism in triphenyl phosphite. *Recent Research Developments in Physics*, **5**: 887-902.
21. Hedoux, A., Guinet, Y., Derollez, P., Hernandez, O., Paccou, L., and Descamps, M. 2006. Micro-structural investigations in the glacial state of triphenyl phosphite. *Journal of Non-Crystalline Solids*, **352**: 4994-5000.
22. Kurita, R., Shinohara, Y., Amemiya, Y., and Tanaka, H. 2007. Microscopic structural evolution during the liquid-liquid transition in triphenyl phosphite. *Journal of Physics: Condensed Matter*, **19**: 152101/1-152101/8.
23. Kurita, R. and Tanaka, H. 2004. Critical-like phenomena associated with liquid-liquid transition in a molecular liquid. *Science*, **306**: 845-848.
24. Abdul-Fattah, A.M., Dellerman, K.M., Bogner, R.H., and Pikal, M.J. 2007. The effect of annealing on the stability of amorphous solids: chemical stability of freeze-dried moxalactam. *Journal of Pharmaceutical Sciences*, **96**: 1237-1250.
25. Abdul-Fattah, A.M., Truong-Le, V., Yee, L., Nguyen, L., Kalonia, D.S., Cicerone, M.T., and Pikal, M.J. 2007. Drying-induced variations in physico-chemical properties of amorphous pharmaceuticals and their impact on stability (I): stability of a monoclonal antibody. *Journal of Pharmaceutical Sciences*, **96**: 1983-2008.
26. Bhugra, C. and Pikal, M.J. 2008. Role of thermodynamic, molecular, and kinetic factors in crystallization from the amorphous state. *Journal of Pharmaceutical Sciences*, **97**: 1329-1349.
27. Moore, W.P., *Mechanical stress crystallization of thermoplastic polymers*. 2002, Agri-Nutrients Technology Group, Inc., USA: US.
28. Sahoo, K.L., Poddar, P., Das, G., and Kumar, B.R. 2007. Crystallization behaviour and mechanical properties of rapidly solidified amorphous alloy. *Journal of Materials Science*, **42**: 6665-6671.
29. Song, N.-K., Kim, M.-S., Han, S.-H., Kim, Y.-S., and Joo, S.-K. 2007. Effects of mechanical stress on the growth behaviors of metal-induced lateral crystallization. *Journal of the Electrochemical Society*, **154**: H370-H373.
30. Bates, S., Zografi, G., Engers, D., Morris, K., Crowley, K., and Newman, A. 2006. Analysis of amorphous and nanocrystalline solids from their X-ray diffraction patterns. *Pharmaceutical Research*, **23**: 2333-2349.

31. Sheth, A.R., Bates, S., Muller, F.X., and Grant, D.J.W. 2005. Local structure in amorphous phases of piroxicam from powder X-ray diffractometry. *Crystal Growth & Design*, **5**: 571-578.
32. Andronis, V. and Zografi, G. 2000. Crystal nucleation and growth of indomethacin polymorphs from the amorphous state. *Journal of Non-Crystalline Solids*, **271**: 236-248.
33. Shalaev, E. and Zografi, G. 2002. The concept of 'structure' in amorphous solids from the perspective of the pharmaceutical sciences. *Special Publication - Royal Society of Chemistry*, **281**: 11-30.
34. Winkel, K., Hage, W., Loerting, T., Price, S.L., and Mayer, E. 2007. Carbonic acid: from polyamorphism to polymorphism. *Journal of the American Chemical Society*, **129**: 13863-13871.
35. Sheth, A.R., Bates, S., Muller, F.X., and Grant, D.J.W. 2004. Polymorphism in Piroxicam. *Crystal Growth & Design*, **4**: 1091-1098.
36. Post, A., Warren, R.J., and Zarembo, J.E., *Trifluoperazine hydrochloride*, in *Analytical Profiles of Drug Substances*, K. Florey, Editor. 1980, Academic Press: New York, NY. pp. 543-582.
37. McDowell, J.J.H. 1980. Trifluoperazine hydrochloride, a phenothiazine derivative. *Acta Crystallographica, Section B: Structural Crystallography and Crystal Chemistry*, **B36**: 2178-81.
38. Ghormley, J.A. 1968. Enthalpy changes and heat-capacity changes in the transformations from high-surface-area amorphous ice to stable hexagonal ice. *Journal of Chemical Physics*, **48**: 503-8.
39. Mahlin, D., Berggren, J., Alderborn, G., and Engstroem, S. 2004. Moisture-induced surface crystallization of spray-dried amorphous lactose particles studied by atomic force microscopy. *Journal of Pharmaceutical Sciences*, **93**: 29-37.
40. Searles, J.A., Carpenter, J.F., and Randolph, T.W. 2001. The ice nucleation temperature determines the primary drying rate of lyophilization for samples frozen on a temperature-controlled shelf. *Journal of Pharmaceutical Sciences*, **90**: 860-871.
41. Milton, N. and Nail, S.L. 1996. The physical state of nafcillin sodium in frozen aqueous solutions and freeze-dried powders. *Pharmaceutical Development and Technology*, **1**: 269-277.
42. Nail, S.L., Jiang, S., Chongprasert, S., and Knopp, S.A. 2002. Fundamentals of freeze-drying. *Pharmaceutical Biotechnology*, **14**: 281-360.
43. Zeng, X., Liu, Y., and Imperor-Clerc, M. 2007. Hexagonal close packing of nonionic surfactant micelles in water. *Journal of Physical Chemistry B*, **111**: 5174-5179.
44. Fong, C., Wells, D., Krodkiewska, I., Weerawardeena, A., Booth, J., Hartley, P.G., and Drummond, C.J. 2007. Diversifying the solid state and lyotropic phase behavior of nonionic uea-based surfactants. *Journal of Physical Chemistry B*, **111**: 10713-10722.
45. Griesser, U.J., *The importance of solvates*, in *Polymorphism in the Pharmaceutical Industry*, R. Hilfiker, Editor. 2006, Wiley-VCH: Weinheim, Germany. pp. 211-233.